ISBM 2024

XVIth Congress of the International Society of Bone Morphometry

MaRS Centre • Toronto, ON, Canada
Sept 30th to Oct 3rd, 2024

ISBM 2026

Get Ready!

London, England
Late June 2026

Join your community for scientific sessions, travel award programs, workshops, and more

http://www.bonemorphometry.org/isbm-2026/

Saravana Ramasamy, PhD
Local Organizing Chair

Aline Bozec, PhD
Program Organizing Chair

Stefaan Verbruggen, PhD
Fundraising Chair

Michelle McDonald, PhD
ISBM President

Table of Contents

Welcome to ISBM 2024

Dear Colleagues,

It is our pleasure to welcome you to the XVIth meeting of the International Society of Bone Morphometry. Thank you all for your participation in this congress, where we will bring together more than 200 clinicians and scientists from 25 different countries who are all interested in bone morphometry.

This meeting would not have been possible without the support of our sponsors, including the National Institutes of Health, as well as the biotech, biopharma, and provincial support listed on the next pages. ISBM is proud to announce inaugural awards to support early career researchers created by generous donations from leaders and founders of the ISBM, including Hartmut Malluche, Juliet Compston, David Dempster, and Webster Gee. The last day of the conference features Open Science & Training Workshops supported by funding from the Canadian Institutes of Health Research. We are also very grateful to the American Society of Bone and Mineral Research for promoting and assisting in the organization of ISBM 2024 as well as their generous support for the early career investigator awards.

We have an exciting program featuring Keynote Speaker, Dr. Christopher Hernandez, 8 dynamic sessions spanning established and new topics in bone morphometry, a special session on Open Science in Musculoskeletal Imaging, and 9 Workshops that will integrate approaches to data sharing and open science. Our program features 13 Award Presentations, 19 Invited Speakers, 19 Abstract Talks, 26 Poster Teasers, and 101 Posters. The program is designed to support students, fellows, and early career scientists to develop communication and collaborations with senior investigators. Take advantage of formal and informal networking opportunities to engage with each other during the scientific sessions, poster sessions, networking breaks, and social events.

Thank you for your interest and support of the ISBM. We look forward to many engaging discussions. Enjoy the meeting!

Sincerely,

Erica L Scheller
Washington University in St. Louis
President of ISBM

Elizabeth A Zimmermann
McGill University
Chair of organizing committee for ISBM 2024

Joel Boerckel
University of Pennsylvania
Chair of programming committee for ISBM 2024

Frank Ko
Rush University
Chair of finance committee for ISBM 2024

ISBM 2024 Sponsors

Platinum Level Sponsor

Micro Photonics Inc.
Helping Researchers Change the World

Gold Level Sponsor

Miltenyi Biotec

SCANCO MEDICAL

Scintica

Silver Level Sponsor

angitia

INVENTIA LIFE SCIENCE

OsteoMetrics

Federal Grant Support

National Institutes of Health (USA) - R13-AR084338

Canadian Institutes of Health Research - CIHR PCS-190957

Volunteers

Thank you to all the volunteers contributing to the 2024 Congress of the ISBM 2024.

Abstract book curator
Sarah Ford

Award emcee
Ralph Müller PhD

Photos and twitter posts
Mohamed Hassan DDS, PhD
Martina Jolic
Anika Shimonty PhD

Session moderators
Ahmed Al Saedi PhD
Tom Ambrosi PhD
Diana Athonvarangkul MD, PhD
Andrei Chagin PhD
Mary Beth Cole PhD
David Cooper PhD
Marta Diaz del Castillo PhD
Jodi Dowthwaite PhD
Xenia Goldberg Borggaard PhD
Koji Ishikawa MD, PhD
Christa Maes PhD
Quentin Meslier
Christina Moeller Andreasen PhD
Emily Quarato PhD
Natalie Sims PhD
Lisbeth Thomsen MS
Rachana Vaidya PhD
Matthias Walle PhD
Lidan You, PhD

Walk leaders
Pelumi Adedigba
Mahdi Hosseinitabatabaei PhD
Melia Matthews

ISBM 2024 Awards

ASBMR Hartmut H. Malluche Early Career Investigator Award

Dr. Hartmut H. Malluche

Dr. Hartmut H. Malluche is a past president and founder of the ISBM. The purpose of this program is to promote the professional and technical development of exceptional early career basic, translational, and clinical researchers in skeletal biology. Support for this award was generously provided by the ASBMR and Dr. Hartmut Malluche.

2024 ASBMR Hartmut H. Malluche Early Career Investigator Awardees:

Marta Diaz del Castillo, University of Aarhus

Matthias Walle University of Calgary

Lisbeth Thomsen, University of Southern Denmark

Emily Quarato, University of Rochester

Tom Ambrosi, University of California Davis

Rachel Surowiec, Purdue University

Diana Athonvarangkul, Yale University

Quentin Meslier, Northeastern University

Koji Ishikawa, Duke University; Showa University

Xenia Goldberg Borggaard, Osense Universite Hospital

ISBM 2024 Awards

Juliet Compston Travel Award for Clinical Research in Morphometry

Dr. Juliet Compston

Dr. Juliet Compston is a physician scientist and the 9th President of the ISBM (1999-2002). Her work has substantially advanced our understanding of the pathophysiology and treatment of osteoporosis and metabolic bone disorders. This competitive award, created by Dr. Compston in partnership with the ISBM, honors talented early- to mid-career physicians that are actively pursuring clinical research related to bone morphometry and bone health.

2024 Juliet Compston Travel Award for Clinical Research in Morphometry Awardees:

Liza Das,
PGIMER, Chandigarh

Keita Nagira,
Tottori University

Patricia and David Dempster Rising Star Award for Excellence in Bone Metabolism Research

Dr. David Dempster and Patricia Dempster

Dr. David Dempster was the first non-clinician to serve as the President of the ISBM (1996-1999), ushering in an era of partnership between basic/translational and clinical scientists. He and his wife Patti organized the 8th ISBM Congress in Arizona in 1999. They remain committed to supporting emerging leaders in the field and have created this award in partnership with the ISBM to honor rising stars in the field of bone morphometry that are actively contributing to the advancement of cutting-edge quantitative imaging techniques and training of new members of the field.

2024 Patricia & David Dempster Rising Star Award for Excellence in Bone Metabolism Research Awardees:

Chao Liu,
Southern University of Science and Technology

Karl Lewis,
Cornell University

ISBM 2024 Awards

Webster S.S. Jee Travel Award for Research in Bone Histomorphometry

Dr. Webster S. S. Jee

Dr. Jee was a pioneer in bone histomorphometry, and as an inspirational mentor, instilled an enthusiasm for this important technique in graduate students, postdocs, and junior investigators who trained with him. This award was created in his name by ISBM Past President Dr. Tom Wronski (2009 to 2012) and Dr. Donald Kimmel to honor a member of the ISBM that exemplifies and continues this important mission.

2024 Webster S.S. Jee Travel Award for Research in Bone Histomorphometry Awardee:

Christina Mœller Andreasen,
University of Southern Denmark

RiSBOd Best Abstract Awards

RiSBOd
Réseau intersectoriel en santé buccodentaire et osseuse durable

RiSBOd is an intersectorial network in Quebec, Canada for sustainable oral and bone health research funded by the Fonds de Recherche du Québec. This award from the RiSBOd recognizes trainees at the graduate student level that submitted top ranking abstracts.

2024 RiSBOd Best Abstract Awardees:

Zachary Haverfield
Martina Jolic
Naomi Jung
Natalie Koh
Francisco Correia Marques

About ISBM

Celebrating 50 years

ISBM is celebrating over 50 years as a society! ISBM originated from a series of workshops on bone morphometry, the first of which was held in Ottawa in 1973 and entitled 'First Workshop on Bone Morphometry.' Since its founding, the society seeks to advance research, education, and clinical practice through the development and refinement of tools for quantitative imaging and analysis of bone. Indeed, the first workshops focused on radiological and histological aspects of bone morphometry. Today, the methodologies used to investigate bone morphometry span histological, tomographical, and other advanced imaging modalities for basic, translational, and clinical studies in skeletal tissues.

Our core mission has four elements:
1. Educate and train clinicians and scientists in all aspects of bone morphometry,
2. Provide a forum for experts to share and to develop their research,
3. Set standards within the field for skeletal imaging and morphometry, and
4. Advance novel therapies to support lifelong skeletal health.

To find out more about the history of the society, read our article *'Celebrating 50-years: the history and future of the International Society of Bone Morphometry*' in JBMR Plus (https://doi.org/10.1093/jbmrpl/ziae070).

As an attendee of ISBM 2024, **your are now a full member of ISBM**.
We encourage you to get involved in the life of the society; please visit bonemorphometry.org or keep up to date on Twitter (@ISBM_Society) for more information.

Article on ISBM history

ISBM website

Enjoy ISBM 2024, the XVIth Congress of the International Society of Bone Morphometry!

ISBM Leadership

ISBM 2022 - 2024 Board of Directors

President
Erica L. Scheller, DDS, PhD
Washington University in St. Louis

President Elect
Michelle McDonald, PhD
The Garvan Institute of Medical Research

Working Group Coordinator
Thomas L. Andersen, PhD
University of Southern Denmark

Treasurer
J. Ignacio Aguirre, DVM, PhD
University of Florida

Board Member and Scientific Leadership Committee Chair
Ralph Mueller, PhD
ETH Zurich

Board Member
Sarah L. Dallas, PhD
University of Missouri Kansas City

Board Member and Young Investigator Initiatives
Lilian I. Plotkin, PhD
Indiana University School of Medicine

Board Member and ISBM 2024 Local Organizing Committee Chair
Elizabeth A. Zimmermann, PhD
McGill University

Board Member and ISBM 2024 Programming Committee Chair
Joel Boerckel, PhD
University of Pennsylvania

Scientific Leadership Committee (SLC)

ISBM 2022 - 2024 Scientific Leadership Committee

Special thanks to the Scientific Leadership Committee, who in addition to the Board, scored the abstracts submitted to the conference. Thank you to all abstract reviewers for their time and contributions to the scientific programming of ISBM 2024.

SLC Chair
Ralph Muller, PhD
ETH Zurich

SLC Co-Chair
Randee L. Hunter, PhD
The Ohio State University

SLC Member
Farzin M. Takyar, MD, PhD
The University of Minnesota Research Institute for Endocrine Sciences

SLC Member
Frank Ko, PhD
Rush University

SLC Member
Furqan A. Shah, PhD
University of Gothenburg

SLC Member
Xiao-Hua Qin, PhD
ETH Zurich

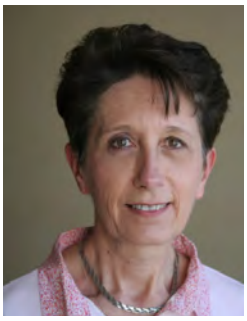

SLC Member
Pascale Chavassieux, MD
INSERM Unit 1033

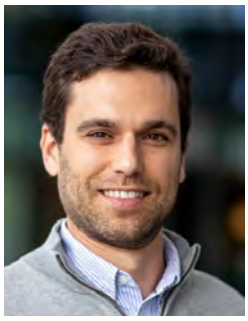

SLC Member
Miguel Castilho, PhD
Eindhoven University of Technology

SLC Member
Saravana Ramasamy, PhD
Imperial College London

SLC Member
Aline Bozec, PhD
Friedrich-Alexander-University

ISBM Early Career Investigators (ECI) Comittee

ISBM 2022 - 2024 Early Career Investigator Committee

The Early Career Investigator (ECI) Committee was created in 2022. Over the past two years, the ECI Committee coordinated numerous virtual scientific seminars to engage ISBM members and create opportunities to discuss bone morphometry. Thank you for your contributions to the society.

Lejla Emini,
Chair
Technische Universität Dresden (TUD), Germany

Ahmed Al Saedi,
Co-chair
Harvard Medical School, MA, USA

Marta Diaz-delCastillo,
Co-chair,
University of Aarhus, Denmark

Julián Balanta Melo,
Member
Indiana University, Indianapolis, IN USA

Sebastian Zanner,
Member
University of Southern Denmark

Yaser Peymanfar,
Member
Forsyth/ Harvard School of Dental Medicine, USA

Ankita Agrawal,
Member
Copenhagen University Hospital, Denmark

Matthias Walle,
Member
Institute for Biomechanics, Switzerland

Ali Ghasem-Zadeh,
Member
The University of Melbourne Australia

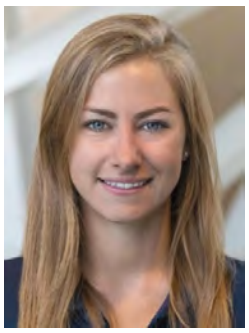

Danielle Whittier,
Member
Institute for Biomechanics, Switzerland

Lisbeth Koch Thomsen,
Member
University of Southern Denmark

Biagio Palmisano,
Member
Sapienza University of Rome

Hanne Skou Jørgensen,
Member
Aarhus University Hospital, Denmark

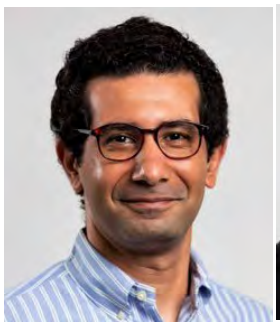

Mohamed Hassan,
Member
Washington University School of Medicine, USA

Martina Jolic,
Member
University of Gothenburg, Sweden.

Invited Speakers

Keynote Address

Christopher Hernandez, Ph.D.

Professor
Department of Orthopedic Surgery
Department of Bioengineering and Orthopedic Sciences
University of California, San Francisco, CA, USA

Beyond Bone: How bone will inspire the next generation of materials

Abstract: To scientists and clinicians, understanding bone morphology and microstructure is necessary to address bone disease. Bone is also a useful material: it was among the first materials used as tools by early humans and was the first material used to illustrate the concepts of mechanical stress and strain that are fundamental to engineering. Here I argue that the skills and techniques behind histomorphometry are not only useful for understanding bone, but are also key to solving some of the greatest challenges in engineering. I discuss work showing how the biomechanics of bone can inspire new ways of making materials and how the lacunar canalicular network may provide the basis for the next generation of engineering materials.

Special session: Open science in musculoskeletal imaging

Serena Bonaretti, Ph.D.

Senior Research Scientist
Balgrist Campus, Zurich, Switzerland

Why and how to do open and reproducible MSK imaging research

Abstract: Openness and reproducibility have progressively gained attention within scientific research communities as means to assess the validity of scientific claims, build upon existing findings, and strengthen collaborations. In recent years, funding agencies and institutions have increasingly supported open and reproducible research to enhance trustworthiness and optimize allocation of resources. However, many researchers still have doubts about the necessity of working openly and face uncertainties regarding the implementation of open and reproducible practices. In this talk, we will elucidate the fundamental importance of openness and reproducibility for the accelerated advancement of musculoskeletal imaging. We will also explore state-of-the-art tools designed for open research practices. Finally, we will introduce the Open and Reproducible Musculoskeletal Imaging Research (ORMIR) community, who develops computational tools, guidelines, and templates to promote standardization and homogenization in musculoskeletal imaging research.

Invited Speakers

Session I: Osteocyte dynamics

Chelsea Heveran, PhD
Montana State University

The impact of aging on osteocyte lacunar-canalicular bone turnover

Karl Lewis, PhD
Cornell University

In vivo observation of osteocyte endocytosis

Session II: Spatial transcriptomics in bone

Erica L. Scheller, DDS, PhD
Washington University in St. Louis

Optimizing spatial transcriptomics in mouse bone from the single gene to the whole transcriptome identifies regional changes in response to applied load

Zhaoyang Liu, Ph.D.
University of Southern California

Spatial transcriptomics reveals the role of a G protein-coupled receptor in growth plate homeostasis through regulation of IHH signaling

Session III: Multiscale bone structure and function

Mariana Kersh, Ph.D.
University of Illinois

From muscle to molecule: bone response to exercise

Ottman Tertuliano, Ph.D.
University of Pennsylvania

Resolving history in fibril-mediated fatigue in 3D at the nanoscale with synchrotron X-rays

Invited Speakers

Session IV: Clinical bone imaging

Steven Boyd, PhD
University of Calgary

HR-pQCT: State-of-the-art and prospects for clinical use

Session V: Bone marrow and adipocytes

Anjali Kusumbe, PhD
University of Oxford

Advanced Light sheet imaging techniques for high-resolution visualization of bone and bone marrow microenvironments

Daniel Coutu, Ph.D.
University of Ottawa

Self-renewing Sox9+ osteochondral stem cells in the postnatal skeleton

SessionVI: Mechanoregulation of bone development & regeneration

Elazar Zelzer, Ph.D.
Weizmann Institute of Science

From feedback to function: understanding proprioception's role in musculoskeletal biology

Chao Liu, Ph.D.
Southern University of Science and Technology

Mechanical regulation of angiogenesis-osteogenesis coupling during bone regeneration

Invited Speakers

Session VII: Emerging paradigms in bone research

Tadahiro Iimura, PhD
Hokkaido University

Pharmacological effects of PTH on bone pain

Lilian Plotkin, PhD
Indiana University School of Medicine

Role of gonadal and chromosomal sex in the musculoskeletal system

Thomas L. Nickolas, MD
Columbia University

Opening Pandora's box: Using deep phenotyping to assess drivers of renal osteodystrophy

Session VIII: Preclinical bone imaging

Warren Grayson, Ph.D.
Johns Hopkins

Neurovascular imaging in the murine calvarium

Nat Dyment, Ph.D.
University of Pennsylvania

Imaging at the interface: how hedgehog signaling integrates tendon and bone

Workshop Descriptions

Workshop IA: Histomorphometry basics: starting off on the right track

Deborah Veis, MD, PhD
Washington University in St. Louis

Workshop aims:

- Understand common histomorphometry terms
- Understand common challenges in histomorphometry
- Understand appropriate metrics for data reporting
- Transparency in data reporting for histomorphometry

Workshop IB: Intravital Imaging in Calcified Tissues

Karl Lewis, PhD
Cornell University

Workshop aims:

- Basics considerations for designing intravital imaging experiments
- State of the art approaches for intravital imaging in MSK tissues
- Highlight protocols available online for different in vivo imaging approaches
- Challenges/limitations to intravital imaging approaches and making raw datasets open access

Workshop IC: Basic Micro-CT(Quantitative Basics of Bone Microstructure Analysis Using Micro-CT)

Ali Ghasem-Zadeh, PhD
University of Melbourne

Randee Hunter, PhD
The Ohio State University

Workshop aims:

- Principals of Micro-CT imaging
- Selection of ROI scanning
- Basics of Image analysis
- Guidelines and clarity in reporting of micro-CT data

Workshop Descriptions

Workshop IIA: AI-assisted image analysis

Cari Whyne, PhD & Michael Hardisty, PhD
University of Toronto

Workshop aims:

- Understand differences between Artificial Intelligence, Machine Learning and Deep Learning
- Analyze applications of AI in bone image analysis
- Learn about open access AI resources to facilitate musculoskeletal image analysis

Workshop IIB: Tissue clearing & 3D imaging

Christa Maes, PhD
KU Leuven

Workshop aims:

- Get an overview of different methodological options for bone microscopy applications, and their advantages and limitations
- Understand the basics of tissue processing, staining, and clearing for 3D microscopy
- Get introduced to quantitative analysis of microscopy images

Workshop IIC: Multiplexed, fluorescent cryohistomorphometry of mineralized tissues

Nat Dyment, PhD
University of Pennsylvania

Workshop aims:

- Learn techniques for processing undecalcified tissues for multiplexed cryohistological assessment through multiple rounds of imaging on the same section
- See examples of how to use this multiplexed technology to quantitate cell and tissue dynamics
- Discussion of how to openly share these data with the scientific community

Workshop Descriptions

Workshop IIIA: Spatially resolved transcriptomics

Zhaoyang Liu, PhD
University of Southern California

Xenia Borggaard, PhD,
Odense University Hospital

Workshop aims:

- Understand the special considerations when performing spatially resolved transcriptomics on bone and cartilage.
- Explore the available methodologies and their respective strengths and weaknesses.
- Learn about data sharing and open science opportunities.

Workshop IIIB: Advances in bone histomorphometry

Chistina Moeller Andreasen, PhD & Lisbeth Koch Thomsen, MS
University of Southern Denmark

Workshop aims:

- Decoding intracortical bone remodeling: Insights from pore structure analysis
- Exploring dynamics in the development of intracortical vascular networks
- Understanding the relevance of osteopontin staining – our new best friend in detecting bone structural units
- Using Bone Structural Units (BSU's) to detect changes in bone remodeling over time
- Quantifying bone formation: The significance of modeling vs. remodeling
- Current and future perspectives for data sharing

Workshop IIIC: Advanced CT analysis for pre-clinical and clinical applications

David Cooper, PhD
University of Saskatchewan

Steven Boyd, PhD
University of Calgary

Workshop aims:

- Synchrotron imaging of mineralized tissues: techniques and access
- Online tool for calculating normative data
- A distributed method for accessing machine learning tools for segmentation of HR-pQCT images at the radius/tibia and knee (i.e., making inference by machine learning available to the community)

Scientific Sessions Agenda

Agenda Summary - *XVIth Congress of the International Society of Bone Morphometry*
September 30th – October 3rd, 2024 • MaRS Centre, Toronto, Canada

MONDAY, SEPTEMBER 30TH	
18:00 - 20:00	Registration open - *MaRS Centre Auditorium Concourse*
18:30 - 19:30	Welcome reception - *MaRS Centre Auditorium Concourse* Get registered, greet your colleagues, and relax with drinks and hors d'oeuvres that you are welcome to bring with you into the keynote session
19:30 - 20:45	Welcome and Keynote Address – *MaRS Centre Auditorium* Moderator: **Joel Boerckel, PhD**, University of Pennsylvania ○ *Welcome and highlights of ISBM 2024:* **Erica L Scheller DDS, PhD**, Washington University in St. Louis ○ *Keynote address:* **Christopher Hernandez, PhD**, University of California, San Francisco *Beyond Bone: How bone will inspire the next generation of materials*
20:45 - 22:00	Welcome reception continued - *MaRS Centre Auditorium Concourse* Wrap out the night with additional post-keynote networking with colleagues and friends as we continue to offer a range of beverages and snacks. We encourage you to find your ISBM buddies to say hello.

TUESDAY, OCTOBER 1ST		
7:30 - 17:00	Registration open - *MaRS Centre Auditorium Concourse*	
7:30 - 8:30	Poster setup - *MaRS Centre Atrium*	
7:30 - 8:30	Continental breakfast - *MaRS Centre Auditorium Concourse*	
8:30 - 9:45	Session I: Osteocyte Dynamics Moderators: **Lidan You, PhD**, University of Toronto **Xenia Borggaard, PhD**, Odense University Hospital Location: *MaRS Centre Auditorium*	
	8:30 - 8:50	○ *Invited speaker:* **Chelsea Heveran, PhD**, Montana State University *Abstract S1-1: The impact of aging on osteocyte lacunar-canalicular bone turnover*
	8:50 - 9:10	○ *Dempster Awardee:* **Karl Lewis, PhD**, Cornell University *Abstract S1-2: In vivo observation of osteocyte endocytosis*
	9:10 - 9:20	○ *Malluche Awardee:* **Diana Athonvarangkul, MD, PhD**, Yale University *Abstract S1-3: Functional osteoclasts regulate osteocytic osteolysis during lactation*
	9:20 - 9:27	○ Short talks selected from abstracts: 1. **Mathilde Palmier, PhD**, University of Southern Denmark, *Abstract S1-4: Bone mass gain during maturation occurs despite the loss of osteocytes and blood vessels in mouse cortical bone*
	9:27 - 9:34	2. **Naomi Jung, PhD**, University of British Columbia, *Abstract S1-5: We don't talk anymore: Lacunocanalicular network disruptions in prostate cancer bone metastasis*
	9:34 - 9:43	3. **Sarah Dallas, PhD**, University of Missouri Kansas City, *Abstract S1-6: Tissue expression of GFP-tagged collagen in transgenic mice and live cell imaging of osteoblast collagen assembly and bone collagen resorption*
9:45 - 11:15	Concurrent coffee break, poster orals, and poster session	
	9:45 - 11:15	○ **Coffee break** Location: *MaRS Centre Auditorium Concourse*
	9:50 - 10:30	**Poster oral session I:** *PO-1 through PO-24 odd numbers* ○ Moderators: **Emily Quarato, PhD**, University of Rochester **Ahmed Al Saedi, PhD**, Boston Children's Hospital; Harvard Medical School Location: *MaRS Centre Auditorium*
	10:30 - 11:15	○ **Poster session I:** *PO-1 through P-101 odd numbers* Location: *MaRS Centre Atrium*
11:15 - 12:30	Session II: Spatial Transcriptomics in Bone Moderators: **Christina Moeller Andreasen**, PhD, University of Southern Denmark **Thomas Ambrosi**, PhD, University of California Davis Location: *MaRS Centre Auditorium*	
	11:15 - 11:35	○ *Invited speaker:* **Erica L Scheller DDS, PhD**, Washington University in St. Louis *Abstract S2-1: Optimizing spatial transcriptomics in mouse bone from the single gene to the whole transcriptome identifies regional changes in response to applied load*
	11:35 - 11:55	○ *Invited speaker:* **Zhaoyang Liu, PhD**, University of Southern California *Abstract S2-2: Spatial transcriptomics reveals the role of a G protein-coupled receptor in growth plate homeostasis through regulation of IHH signaling*
	11:55 - 12:05	○ *Malluche Awardee:* **Xenia Goldberg Borggaard, PhD**, Odense University Hospital *Abstract S2-3: Spatial transcriptional profiling of osteoprogenitors proximate to osteoclasts in human bone remodeling*
	12:05 - 12:15	○ *Malluche Awardee:* **Quentin Meslier,** Northeastern University *Abstract S2-4: WISH-BONE: Whole-mount in situ histology, to label osteocyte mRNA and protein in 3D adult mouse bones*
	12:15 - 12:22	○ Short talks selected from abstracts: 1. **Peter Maye, PhD**, University of Connecticut Health, *Abstract S2-5: A method to perform spatial transcriptomics on human articular cartilage*

	12:22 - 12:29	2. **Francisco Correia Marques**, ETH Zurich, *Abstract S2-6: Multiscale mechanoregulation analysis using super-resolution spatial transcriptomics data and multimodal imaging*
12:30 - 12:40	Group Photo - *MaRS Centre Auditorium Concourse*	
12:40 - 13:45	Networking lunch break - *MaRS Centre Auditorium Concourse and Auditorium* Please join your assigned table to meet your buddy group for a lightly structured discussion about open science.	
13:45 - 15:00	Session III: Multiscale Bone Structure and Function Moderators: **Natalie Sims, PhD**, St. Vincent's Institute of Medical Research **Marta Diaz del Castillo, PhD**, University of Aarhus Location: *MaRS Centre Auditorium*	
	13:45 - 14:05	○ *Invited speaker:* **Mariana Kersh, PhD**, University of Illinois *Abstract S3-1: From muscle to molecule: bone response to exercise*
	14:05 - 14:25	○ *Invited speaker:* **Ottman Tertuliano, PhD**, University of Pennsylvania *Abstract S3-2: Resolving history in fibril-mediated fatigue in 3D at the nanoscale with synchrotron X-rays*
	14:25 - 14:35	○ *Malluche Awardee:* **Koji Ishikawa, MD, PhD**, Duke University, Showa University *Abstract S3-3: Age-related changes in immune and endothelial response impair bone repair*
	14:35 - 14:42	○ Short talks selected from abstracts: *1.* **Natalie Koh**, St. Vincent's Institute of Medical Research, *Abstract S3-4: Inducing STAT3 hyperactivation in osteoblasts and osteocytes in the adult murine skeleton increases cortical porosity*
	14:42 - 14:49	*2.* **Martina Jolic**, University of Gothenburg, *Abstract S3-5: An in vivo multiscale and multimodal analysis of the impact of mechanical overload on osseointegration*
	14:49 - 14:56	*3.* **Dilara Yilmaz**, ETH Zurich, *Abstract S3-6: Spatially resolved age- and sex-specific alterations in bone mechanomics and mechanoregulation in prematurely aging PolgA mice*
15:00 - 15:30	Coffee break: *MaRS Centre Auditorium Concourse*	
15:30 - 17:00	Session IV: Clinical Bone Imaging Moderators: **David Cooper, PhD**, University of Saskatchewan **Matthias Walle, PhD**, University of Calgary Location: *MaRS Centre Auditorium*	
	15:30 - 15:50	○ *Invited speaker:* **Steven Boyd, PhD**, University of Calgary *Abstract S4-1: HR-pQCT: State-of-the-art and prospects for clinical use*
	15:50 - 16:00	○ *Malluche Awardee:* **Lisbeth Thomsen, MS,** Odense University Hospital *Abstract S4-2: Intermittent treatment with parathyroid hormone overactivates intratrabecular tunneling, a previously overlooked mode of remodeling: A randomized clinical trial in patients with hypoparathyroidism and pre-clinical rabbit model*
	16:00 - 16:10	○ *Compston Awardee:* **Liza Das, MD**, Postgraduate Institute of Medical Education and Research, Chandigarh, *Abstract S4-3: Oral semaglutide, weight loss, and alterations in bone microarchitecture, vBMD, and bone turnover in obese T2DM patients with metabolic dysfunction associated with steatotic liver disease*
	16:10 - 16:17	○ Short talks selected from abstracts: *1.* **Zachary Haverfield**, Ohio State University, *Abstract S4-4: Sex-specific relationships in femoral neck bone mineral content and volumetric density*
	16:17 - 16:24	*2.* **Farhan Sadik**, Purdue University, *Abstract S4-5: Physics-driven motion simulation and motion correction pipeline for HR-pQCT bone imaging*
	16:24 - 16:31	*3.* **Alyssa Williams**, McMaster University, *Abstract S4-6: 3D visualization of nanoscale features including, mineral ellipsoids and collagen fibrils in mineralized human bone tissue*
	16:32 - 17:00	*Industry speaker:* **Raj Manoharan**, Micro Photonics*, Abstract S4-7: Dual Energy X-Ray Absorptiometry (DEXA) Applications in Small Lab Animals (even in outer space!)*
18:00	Meet at MaRS Centre to walk together to Chefs Hall for Dinner (open food hall, paid by attendees) Walk Leaders: Mahdi Hosseinitabatabaei, Melia Matthews, and Pelumi Adedigba *Meet us to walk with the group or make your own way to 111 Richmond St W, Toronto, ON* Highly rated Beer Hall, Chef's Lounge, Main Hall, Coffee Bar, and Outdoor Patio Space with 16 vendors to choose from - https://www.chefshall.com/food-drink	

WEDNESDAY, OCTOBER 2nd		
7:30 - 17:30	Registration open - *MaRS Centre Auditorium Concourse*	
7:30 - 8:30	Continental breakfast - *MaRS Centre Auditorium Concourse*	
8:30 - 9:45	Session V: Bone Marrow and Adipocytes Moderators: **Erica Scheller, DDS, PhD,** Washington University in St. Louis **Koji Ishikawa, MD, PhD,** Duke University, Showa University Location: *MaRS Centre Auditorium*	
	8:30 - 8:50	○ *Invited speaker:* **Anjali Kusumbe, PhD**, University of Oxford *Abstract S5-1: Advanced Light sheet imaging techniques for high-resolution visualization of bone and bone marrow microenvironments*
	8:50 - 9:10	○ *Invited speaker:* **Daniel Coutu, PhD**, University of Ottawa *Abstract S5-2: Self-renewing Sox9+ osteochondral stem cells in the postnatal skeleton*
	9:10 - 9:20	○ *Malluche Awardee:* **Emily Quarato, PhD**, University of Rochester *Abstract S5-3: Enhanced engulfment of apoptotic targets by bone marrow stromal cells increases their senescence, decreases bone, and causes myeloid skewing*
	9:20 - 9:30	○ *Malluche Awardee:* **Marta Diaz del Castillo, PhD**, University of Aarhus *Abstract S5-4: Multiple myeloma induces angiogenesis and neuronal degeneration in the human hematopoietic bone marrow*
	9:30 - 9:37	○ Short talks selected from abstracts: *1.* **Johanna Besold**, KU Leuven, *Abstract S5-5: Skeletal stem/progenitor cells (SSPCs) contribute to the anabolic actions of intermittent PTH through PDGF receptor signaling*
	9:37 - 9:44	*2.* **Natalie Sims, PhD**, St. Vincent's Institute of Medical Research, *Abstract S5-6: Immature neutrophils in bone marrow inhibit osteoclast differentiation in vivo and in vitro*
9:45 - 11:15	Concurrent coffee break, poster orals, and poster session	
	9:45 - 11:15	○ **Coffee break** Location: *MaRS Centre Auditorium Concourse*
	9:50 - 10:30	**Poster oral session II:** *PO-1 through PO-24 even numbers* ○ Moderators: **Diana Athonvarangkul, MD, PhD**, Yale University **Rachana Vaidya, PhD**, Washington University in St. Louis Location: *MaRS Centre Auditorium*
	9:45 - 11:15	○ **Poster session II:** *PO-1 through P-101 even numbers* Location: *MaRS Centre Atrium*
11:15 - 12:30	Session VI: Mechanoregulation of Bone Development & Regeneration Moderators: **Andrei Chagin, PhD,** Karolinska Institute **Quentin Meslier**, Northeastern University Location: *MaRS Centre Auditorium*	
	11:15 - 11:35	○ *Invited speaker:* **Elazar Zelzer, PhD**, Weizmann Institute of Science *Abstract S6-1: From feedback to function: understanding proprioception's role in musculoskeletal biology*
	11:35 - 11:55	○ *Dempster Awardee:* **Chao Liu, PhD**, Southern University of Science and Technology *Abstract S6-2: Mechanical regulation of angiogenesis-osteogenesis coupling during bone regeneration*
	11:55 - 12:05	○ *Malluche Awardee:* **Thomas Ambrosi, PhD**, University of California Davis *Abstract S6-3: Decoding niches of developing human skeletal stem cell lineages*
	12:05 - 12:15	○ *Malluche Awardee:* **Matthias Walle, PhD,** University of Calgary *Abstract S6-4: Investigating the time-dependent recovery of spaceflight-induced bone resorption in astronauts*
	12:15 - 12:25	○ *Compston Awardee:* **Keita Nagira, MD, PhD**, Tottori University *Abstract S6-5: Effects of lunar gravity on calcaneal bone metabolism and the microstructure of osteochondral unit in the calcaneocuboid joint*

	12:25 - 12:32	○ Short talks selected from abstracts: **Christopher Panebianco, PhD**, University of Pennsylvania, *Abstract S6-6: YAP and TAZ regulate fetal growth plate chondrocyte hypertrophy and maturation*
12:30 - 13:30	Lunch break: *MaRS Centre Auditorium Concourse* Open seating and discussion	
13:30 - 15:05	Session VII: Emerging Paradigms in Bone Research Moderators: **Jodi Dowthwaite, PhD**, SUNY Upstate Medical University **Lisbeth Thomsen, MS**, University of Southern Denmark Location: *MaRS Centre Auditorium*	
	13:30 - 13:50	○ *Invited speaker:* **Tadahiro Iimura, PhD**, Hokkaido University *Abstract S7-1: Pharmacological effects of PTH on bone pain*
	13:50 - 14:10	○ *Invited speaker:* **Lilian Plotkin, PhD**, Indiana University School of Medicine *Abstract S7-2: Role of gonadal and chromosomal sex in the musculoskeletal system*
	14:10 - 14:30	○ *Invited speaker:* **Thomas Nickolas, MD**, Columbia University *Abstract S7-3: Opening Pandora's Box: Using Deep Phenotyping to Assess Drivers of Renal Osteodystrophy*
	14:30 - 14:40	○ *Jee Awardee:* **Christina Moeller Andreasen, PhD**, University of Southern Denmark *Abstract S7-4: Exploring the bone microenvironment in relation to bone remodeling activity in metastatic breast cancer patients*
	14:40 - 14:47	○ Short talks selected from abstracts: *1.* **Roger Valle-Tenney, PhD**, KU Leuven, *Abstract S7-5: Pharmacological activation of the hypoxia signaling pathway alleviates the metabolic and skeletal consequences of diet-induced obesity and type-2 diabetes in mice*
	14:47 - 15:04	*2.* **Zoe Herdman**, Rush University, *Abstract S7-6: Postn deletion impairs intramembranous bone regeneration in mice*
15:05 - 15:30	Coffee break: *MaRS Centre Auditorium Concourse*	
15:30 - 16:00	Special Session: Open Science in Musculoskeletal Imaging Location: *MaRS Centre Auditorium* ○ *Introduction:* **Elizabeth Zimmermann, PhD**, McGill University ○ *Invited speaker:* **Serena Bonaretti, PhD**, Balgrist Campus *Why and how to do open and reproducible MSK imaging research*	
16:00 - 17:15	Session VIII: Preclinical Bone Imaging Moderators: **Christa Maes, PhD**, KU Leuven **Mary Beth Cole, PhD**, The Ohio State University Location: *MaRS Centre Auditorium*	
	16:00 - 16:20	○ *Invited speaker:* **Warren Grayson, PhD**, Johns Hopkins *Abstract S8-1: Neurovascular imaging in the murine calvarium*
	16:20 - 16:40	○ *Invited speaker:* **Nat Dyment, PhD**, University of Pennsylvania *Abstract S8-2: Imaging at the interface: how hedgehog signaling integrates tendon and bone*
	16:40 - 16:50	○ *Malluche Awardee:* **Rachel Surowiec, PhD**, Purdue University *Abstract S8-3: Preclinical bone MRI using a novel 3D dual echo rosette (PETALUTE) K-space trajectory: comparison to 3D radial ultrashort-and zero echo time approaches*
	16:50 - 16:57	○ Short talks selected from abstracts: *1.* **Satvika Bharadwaj**, Emory/Georgia Tech, *S8-4: Machine-learning driven automation for digital phenotyping and morphological texture analysis of bone biopsy images*
	16:57 - 17:04	*2.* **Anushka Gerald**, Washington University in St. Louis, *Abstract S8-5: Mapping and function of P75-NTR+ periosteal cells in the regeneration of craniofacial bone*
	17:04 - 17:11	*3.* **Talayah Johnson**, University of Pennsylvania, *Abstract S8-6: Reduced loading after sciatic nerve resection impairs hindlimb growth*
17:15 – 17:30	Poster removal - *MaRS Centre Atrium*	
18:00 - 21:30	Gala dinner - Location: Hart House at University of Toronto (7 Hart House Circle, Toronto, ON M5S 3H3) Room: Great Hall (Opening cocktails 18:00-19:00; Seated Dinner and Award Presentations 19:00-21:00) *Featuring Jazz/Pop Quartet from the University of Toronto, Faculty of Music, and Student Musicians* Award Presenters: **Ralph Müller, PhD**, ETH Zürich and **Erica Scheller, DDS, PhD**, Washington University	

Open Science & Training Workshops

THURSDAY, OCTOBER 3rd	
7:30 - 8:30	Continental breakfast - *Outside rooms CR2 and CR3*
8:30 - 9:45	Concurrent Training Workshops I ○ **Workshop Ia: Histomorphometry basics: starting off on the right track** Deborah Veis, MD, PhD, Washington University in St. Louis Location: Cafe ○ **Workshop Ib: Intra vital imaging in calcified tissues** Karl Lewis, PhD, Cornell University Location: CR2 ○ **Workshop Ic: Quantitative basics of bone microstructure analysis using micro-CT** Ali Ghasem-Zadeh, PhD, University of Melbourne Randee Hunter, PhD, The Ohio State University Location: CR3
9:45 - 11:00	Concurrent Training Workshops II ○ **Workshop IIa: AI-assisted image analysis** Cari Whyne, PhD, University of Toronto, Sunnybrook Research Institute Michael Hardisty, PhD, University of Toronto, Sunnybrook Research Institute Location: CR3 ○ **Workshop IIb: Tissue clearing & 3D imaging** Christa Maes, PhD, KU Leuven Location: Cafe ○ **Workshop IIc: Multiplexed, fluorescent cryohistomorphometry of mineralized tissues** Nat Dyment, PhD, University of Pennsylvania Location: CR2
11:00 - 11:30	Coffee break - *Outside rooms CR2 and CR3*
11:30 - 12:45	Concurrent Training Workshops III ○ **Workshop IIIa: Spatially resolved transcriptomics** Zhaoyang Liu, PhD, University of Southern California Xenia Borggaard, PhD, Odense University Hospital Location: Cafe ○ **Workshop IIIb: Advances in bone histomorphometry** Christina Moeller Andreasen, PhD, University of Southern Denmark Lisbeth Thomsen, MS, University of Southern Denmark Location: CR2 ○ **Workshop IIIc: Advanced CT analysis for pre-clinical and clinical applications** David Cooper, PhD, University of Saskatchewan Steven Boyd, PhD, University of Calgary Location: CR3
12:45 - 13:00	Concluding remarks - *Outside rooms CR2 and CR3*

Poster Orals and Posters

POSTER ORALS (PO) AND POSTERS (P)

All odd numbered posters are presented at Poster Session I (Tuesday, October 1st). All even numbered posters are presented at Poster Session II (Wednesday, October 2nd). Poster Orals (PO) also give a three-minute oral presentation in the corresponding Poster Orals session.

Poster Number	Presenter Name, Affiliation, Poster title
PO-001	**Melissa Bevers, PhD**, VieCuri Medical Center, *Romosozumab Improves Areal BMD at the Axial Skeleton but not Areal and Volumetric BMD, Microarchitecture, and Strength at the Peripheral Skeleton in a Real-World Cohort*
PO-002	**Babatunde Ayodele, PhD**, The University of Melbourne, *Increased subchondral bone resorption in the proximal sesamoids of racehorses is associated with accumulation of bone microdamage*
PO-003	**Michael David, PhD**, University of Colorado Anshutz Medical Campus, *Generalizability of Deep Learning Segmentation of the Trabecular Compartment in Mouse Vertebral Body Across Micro-Computed Tomography Image Resolutions*
PO-004	**Ananya Goyal**, Stanford University, *The aging knee: changes in bone metabolic activity measured using [F18]NaF PET-MR Imaging*
PO-005	**Kim Harrison, PhD**, University of Saskatchewan*, Multi-Time Point Tracking of Cortical Bone Remodeling Events in the Rabbit Using Serial Time-Lapsed Synchrotron Micro-CT Scans*
PO-006	**Melissa Bevers, PhD**, VieCuri Medical Center*, Impaired Cortical and Trabecular Microarchitecture in Female Elite Cyclists as Assessed using HR-pQCT*
PO-007	**Cayetano Galera-Martinez**, Vall d'Hebron Institute of Oncology (VHIO), *Elucidating Leukemia Inhibitory Factor (LIF) on Prostate Cancer Bone Metastasis Microenvironment*
PO-008	**Samantha Bratcher**, Cornell University, *Characterizing the Limits of 3-Photon Microscopy as a Tool for Deep Imaging of Whole, Cortical Bone Tissue*
PO-009	**Tengteng Tang, PhD**, University of Virginia, *Advancements in 3D Correlative Multiscale and Multimodal Microscopy: Revealing New Insights into Vertebrate Tissue Biomineralization*
PO-010	**Brittany Wilson, PhD**, Rush University, *Early Postnatal Bone Structure in a Pig Model of Preterm Birth*
PO-011	**Abigail Coffman**, The City College of New York, *Bisphosphonate treatment leads to rapid increases in bone microdamage content and extensive osteocyte death around microcracks following in vivo fatigue*
PO-012	**David Barreto**, Perelman School of Medicine, *Osteoporotic Fracture Prediction Using Opportunistic MR Imaging and Deep Learning*
PO-013	**Hoomin Lee, PhD**, Rush University, *Examining Endothelial-Mesenchymal Transition in Intramembranous Bone Regeneration*
PO-014	**Kenna Brown**, Montana State University, *High-Fat Diet and Aging Each Reduce Fracture Toughness and Matrix Properties in C57BL/6 Mice*
PO-015	**Pelumi Adedigba**, Indiana University School of Medicine, *Fructooligosaccharide Promotes Bone Formation and Mineralization Coincident with Alterations in PPARγ/WNT Signaling, Calcium Homeostasis and T-cell Biology*
PO-016	**Marie-Josée Bégin, MD**, Centre hospitalier de l'Université de Montréal, Canada, *Histomorphometric Evaluation of TRAcP in Bone Biopsies of Patients with Renal Osteodystrophy: Assessment of Trabecular and Endocortical Surfaces*
PO-017	**Mohamed Hassan, DDS, PhD**, Washington University in Saint Louis, *The role of macrophases in the superior regenerative capacity of neural crest-derived bone_3D insights into craniofacial healing*
PO-018	**Vishal Gokani**, Texas Scottish Rite Hospital, *Automated Quantitative Histomorphometric Analysis of Osteonecrosis of the Femoral Head: A Deep Learning Approach*
PO-019	**Anastasiia Sadetskaia**, Aarhus University, *The Mystery of Cement Lines in Bone Structure: Spatial Distribution of Zn and Changes in Surrounding Matrix Mapped by Synchrotron-Radiation Experiments*
PO-020	**Atousa Moayedi**, University of Portsmouth, *Investigating the alterations in enthesis lacunae morphometry under mechanical loading*
PO-021	**Hongzhi Liu**, Southern University of Science and Technology, *Macrophages Regulate Angiogenesis-Osteogenesis Coupling Induced by Mechanical Loading through the Piezo1 Pathway*

Poster Number	Presenter Name, Affiliation, Poster title
PO-022	**Xuan Wei**, University of Saskatchewan, *3D Morphological Analysis of Age and Sex-Related Changes in Human Cortical Bone Remodeling Spaces Using Micro-CT*
PO-023	**Cindy Cruz**, University of Florida, *In Vivo Sequential MicroCT-based Radiographic Features of the Pre-Clinical Osteonecrosis of the Jaw (ONJ) prodrome in rice rats*
PO-024	**Brett Mattingly**, Indiana University School of Medicine, *Conditional Loss of CaMKK2 in Osterix-Positive Osteoprogenitors Enhances Osteoblast Function in a Sex-Divergent Manner*
P-025	**Ahmed Al Saedi, PhD**, Boston Children's Hospital, Harvard Medical School**,** *A novel role of CXXC Finger Protein1 in osteoblast differentiation during the early stages of bone development*
P-026	**Kim Harrison, PhD**, University of Saskatchewan, *Cortical Remodeling Dynamics in the Rabbit: Does Alendronate Reduce Longitudinal Erosion Rate?*
P-027	**Yixia Xie, PhD**, University of Missouri Kansas City, *Expression of GFP-Tagged Collagen in Craniofacial Tissues in GFP-Collagen Transgenic Mice*
P-028	**Tor Hildebrand, PhD**, Lucid concepts AG, *Volumetric Quantification of Plates, Rods, and Junctions in Trabecular Bone with the Local SMI – A New Approach*
P-029	**Elizabeth Zimmermann, PhD**, McGill University, *Bone density and microarchitecture in ambulatory children with spastic diplegic cerebral palsy*
P-030	**Yener Yeni, PhD**, Henry Ford Health, *Textural and geometric measures derived from digital tomosynthesis discriminate patients with vertebral fracture from those without*
P-031	**Sneha Korlakunta, PhD**, University of Texas Southwestern, *Elucidating the mechanism of fibrosis in clubfoot recurrence*
P-032	**Jodi Dowthwaite, PhD**, SUNY Upstate Medical University, *Circum-menarcheal Exercise Loading and gSOS Polygenic Risk Score Independently Predict Variance in Distal Radius Bone Properties in Post-menarcheal Girls*
P-033	**Jodi Dowthwaite, PhD**, SUNY Upstate Medical University, *Contrasting Physical Activity and Energy Availability Patterns from Childhood to Adulthood: A Comparison of Height, Body Composition, and Bone Mass Growth Curves Relative to Menarche*
P-034	**Rachel Klassen**, Unversity of Calgary, *Comparing In Vivo HR-pQCT Against Ex Vivo Histological Methods to Assess Remodeling in Knee Osteoarthritis Bone Marrow Lesions*
P-035	**Galateia Kazakia, PhD**, University of California San Francisco, *The Effect of Laplace-Hamming Segmentation on Micro-Finite Element Bone Mechanics Estimations Is Cohort- and Skeletal Site-specific*
P-036	**Stephane Blouin, PhD**, Ludwig Boltzmann Institute of Osteology, *Abnormally Low Bone Matrix Mineralization in a Boy with a Pathogenic SATB2 Variant*
P-037	**Kaja Laursen, PhD**, Institut for Retsmedicin, *Development of a 7-plex Immunofluorescent Protocol for Cellular and Molecular Characterization of the Bone Marrow Microenvironment in Muliple Myeloma*
P-038	**Flavia Kiweewa Matovu, PhD**, Makerere University-Johns Hopkins University Research Collaboration, *High Hypovitaminosis D prevalence among Women with Normal Bone Mass in an African Setting*
P-039	**Heithem Ben Amara, PhD**, University of Gothenburg, *Bone regeneration around biodegradable magnesium-based biomaterials: Diferential efects on osteopromotion and adiposity accumulation as a function of material composition*
P-040	**Eugenie Macfarlane, PhD**, The University of Sydney, *Rhythmic circulating glucocorticoid levels play a critical role in osteoarthritis driven by chronic disruption of circadian rhythms*
P-041	**Mahdi Hosseinitabatabaei, PhD**, McGill University, *Natural history of the peripheral bones in children with osteogenesis imperfecta and age- and sex-matched healthy controls using longitudinal HR-pQCT analysis*
P-042	**Ali Ghasem-Zadeh, PhD**, University of Melbourne, *Bone's microarchitechtural spatial configuration determines its own remodelling and susceptibility to becoming fragile*
P-043	**Gurpreet Baht, PhD**, Duke University, *Targeting circulating apolipoprotein E to improve aged bone healing*
P-044	**Michael Wan, PhD**, Northeastern University, *NOISe: Nuclei-Aware Osteoclast Instance Segmentation for Mouse-to-Human Domain Transfer*
P-045	**Krittikan Chanpaisaeng, PhD**, Chulalongkorn University, *Cannabidiol does not ameliorate ovariectomy-induced bone loss in skeletally mature rats*
P-046	**Mitchell Froemming, PhD**, Mayo Clinic, *Spatial Mapping of Senescent Cells in the Bone Microenvironment*
P-047	**Gabriel Ramirez**, Indiana University School of Medicine, *Sex-Dependent Changes in Body Composition and Bone Mineral Density in Wild Type Mice and the APP-SAA Alzheimer's Disease Mouse Model*

Poster Number	Presenter Name, Affiliation, Poster title
P-048	**Xiao-Hua Qin, PhD**, ETH Zurich, *Laser-printed Hydrogel Niches to Grow 3D Cell Networks for Miniaturized Bone Organoids*
P-049	**Mary Beth Cole, PhD**, Ohio State University, *Preliminary Comparison of Cortical Volumes and Cortical Cross-Sections as Predictors of Human Rib Structural Bending Response*
P-050	**Furqan Ali Shah, PhD**, University of Gothenburg, *Rethinking the validity of Ca/P ratio as a measure of bone mineral stoichiometry*
P-051	**Lindsay Loundagin, PhD**, University of Saskatchewan, *Balanced Basic Multicellular Unit Activity in a Rabbit Model of Osteoporosis*
P-052	**Lindsay Loundagin, PhD**, University of Saskatchewan, *Fusing 2D histological and 3D imaging techniques: a novel apporach to investigate spatio-temporal organizaiton of basic multicellular units in the rabbit*
P-053	**Maja Ostergaard, PhD**, Aarhus University, *Changes in Osteocyte Lacunar Properties Are Due to New Bone Formation in Patients with Hypoparathyroidism Treated with Parathyroid Hormone*
P-054	**Manabu Tsukamoto, PhD**, University of Occupational and Environmental Health, *Impact of Pulmonary Emphysema on Bone Quality*
P-055	**Nikolas Knowles, PhD**, University of Waterloo, *Image Based Finite Element Model Stiffness and vBMD by Single and Dual Energy CT Reconstruction Kernel*
P-056	**Sirion Aksornthong**, McGill University, *Osteoclast indices in Osteogenesis Imperfecta: systematic review and meta-analysis*
P-057	**Jianguo Tao**, Westlake University, *Multi-omics Integration Reveals Candidate Determinants of Bone Mineral Density and the Role of AZIN1 in Bone Homeostasis*
P-058	**Melia Matthews**, Cornell University, *Intravital Perturbation of Osteocyte Nanoparticle Uptake with Dynamin and Cholesterol Inhibitors*
P-059	**Anika Shimonty, PhD**, Brigham & Women's Hospital, Harvard Medical School, *Mutation in CLCN7 Results in Impaired Osteoclast Resorption and Puzzle-like Bone Structural Units in ADOII Mice*
P-060	**Jan Hughes-Austin, PhD**, University of California, San Diego, *Femoral Head Bone Marrow Fat Fraction by Computed Tomography is Associated with Higher Bone Turnover in Patients Experiencing Hip Fractures*
P-061	**Adam Yiu-chung Lau, MBBS**, Chinese University of Hong Kong, *Lower CYP27B1 Expression in Osteocytes Increases the Risk of Curve Progression in a New Mouse Model of Scoliosis*
P-062	**Adam Yiu-chung Lau, MBBS**, Chinese University of Hong Kong, *Preventing Curve Progression to Bracing Threshold in Early Adolescent Idiopathic Scoliosis (AIS) Using Calcium Plus Vitamin D Supplementation – An Initiated Randomized Double-blinded Placebo-controlled Trial*
P-063	**Xiangjiao Yi, PhD**, Westlake University, *Multi-omics Integration Uncovers Atrazine Induces Skeletal Muscle Atrophy by Disturbing Satellite Cell Fate, Energy Metabolism and Proteostasis*
P-064	**Hang Zhou**, Southern University of Science and Technology, *Hyperbaric oxygen promotes bone regeneration by activating the mechanosensitive Piezo1 pathway in osteogenic progenitors*
P-065	**Abhayavarshini Sridhar**, Rush University, *In utero and Lactation Exposure to Dolutegravir-based Combination Antiretroviral Therapy Reduced Trabecular Bone but not Cortical Bone Mass in Rats*
P-066	**Christopher Hernandez, PhD**, University of California San Francisco, *Staphylococcus Aureus does not use durotaxis to penetrate osteocyte canaliculi-like channels*
P-067	**Anders Palmquist, PhD**, University of Gothenburg, *Correlative HAADF STEM-EDX tomography of bone*
P-068	**Mathieu Simon**, University of Bern, *Automatic Segmentation of Cortical Bone Microstructure: analysis of three proximal femur sites*
P-069	**Martina Dzubanova**, Charles University, *Revealing a role of NADPH oxisase 4 (NOX4) in bone homeostasis and sex dimorphism*
P-070	**Christopher Panebianco, PhD**, University of Pennsylvania, *Maternal exercise enhances fetal bone development*
P-071	**Noemy Vergara Vera**, Eindhoven University of Technology, *Influence of macromolecular crowding on collagen fibrillogenesis and fiber alignment in 3D printed collagen constructs*
P-072	**Natasha Sanz**, Rosario National University, *Assessing offspring tooth and mandibular histomorphometric parameters and bone property changes due to caffeinated beverage (Yerba Mate) consumption during gestation and lactation*

Poster Number	Presenter Name, Affiliation, Poster title
P-073	**Ruban Dhaliwal, MD**, University of Texas Southwestern Medical Center, *PEN and CML Associate Differently with Bone Loss in Type 2 Diabetes: the Health, Aging, and Body Composition Study*
P-074	**Patrick Bidros**, University of Kentucky, *Perioperative Use of Anabolic Agents in Three Young Adult Patients with Developmental Hip Dysplasia*
P-075	**Choiselle Marius**, Duke University, *Yolk Sac Erythromyeloid Progenitors in Fracture Healing and Regeneration*
P-076	**Yuwen Zheng, PhD**, University of Saskatchewan, *Early Sign of Bone Loss at Femoral Neck: Fifteen Years of Bone Accrual from Peak Bone Mass*
P-077	**Yasaman Moharrer**, University of Pennsylvania, *YAP and TAZ mediate mechanical load-induced bone adaptation*
P-078	**Annabel Bugbird**, University of Calgary, *Quantifying morphometric defects in clinical computed tomography*
P-079	**Malene Nielsen, PhD**, University of Southern Denmark; Aarhus University, *Combined cyro and paraffin bone histomorphometry: a quick and novel approach opening new opportunities*
P-080	**Amirreza Haghighi, PhD**, Harvard University, *A Genome-Wide Association Study on Patients with Atypical Femur Fractures*
P-081	**Darrah Condino**, Brock University, *Maternal Supplementation of Red Rooibos Tea on Mandible Bone Mineral Following Pregnancy and Lactation*
P-082	**Fatima Sandmann-Afonso, MD and Carolina Aguiar Moreira, MD, PhD**, Federal University of Parana, *Bone histomorphometry in female Wistar rats treated with different doses of Melatonin*
P-083	**Haydee Torres, PhD**, Mayo Clinic, *PHLPP inhibitors reduce sensory neuron joint knee innervation during OA progression in mice*
P-084	**Erica Clinkenbeard, PhD**, Indiana University School of Medicine, *Interplay of polyamines on mineralization during iron deficiency and CKD-MBD*
P-085	**Michael Friedman, PhD**, Virginia Commonwealth University, *Genetics, sex, and body weight affect the musculoskeletal response to disuse in mice*
P-086	**Miryoung Lee, PhD**, University of Texas Health Science Center at Houston, *Adverse Effects of Metabolic Dysfunction-Associated Steatotic Liver Disease on Skeletal Health in Mexican Americans*
P-087	**Kimberly Denman**, Ohio State University, *Ablation of Discoidin Domain Receptor 1 (Ddr1) Alters Collagen and Mineral in Murine Bone Matrix*
P-088	**Shilpa Shree Kuduva Ramesh Babu, DDS**, University of North Carolina at Chapel Hill, *Establishing Age-related Normative Bone Strength Data for C3 vertebra using Cone Beam Computed Tomography*
P-089	**Jing Zhang, PhD**, McMaster University, *Exploring collagen mineralization by liquid-phase transmission electron microscopy*
P-090	**Farzin Takyar, MD, PhD**, University of Minnesota, *Differential Effect of High Versus Moderate Intensity Statin Therapy on Bone Density: A Substudy of a Randomized Controlled Trial*
P-091	**Sami Alsabri**, Osteoarthritis Research Unit Centre de Recherche du Centre Hospitalier de l'Université de Montréal (CRCHUM), *Role of DNA methylation on 15-Lipoxygenase-1 gene expression in Osteoarthritis*
P-092	**Sarah Ford**, McGill University, *Bone formation by osteoid-osteocytes and osteocytes in C57Bl/6 mice*
P-093	**Rachana Vaidya, PhD**, Washington University in St. Louis, *Impact Microindentation Accurately Predicts Hip and Wrist Fracture Susceptibility in Aging Females*
P-094	**Patricia Clark, MD, PhD**, Universidad Nacional Autonoma de Mexico, *Effect Of Tibolone On Cortical and Trabecular Bone In Postmenopausal Women Compared With Estrogen Therapy*
P-095	**MD Selim Reza, PhD**, Tulane University, *A Multi-Task Learning Framework Discovers Potential Drug-Repurposing Targets for Sarcopenia*
P-096	**Yi-An Hsieh, MS**, University of Pennsylvania, *A Deep Learning Pipeline for Bullet Fragment Detection in Gunshot Wound Patients for Enhanced Orthopaedic Assessment in Emergency Care*
P-097	**Naoki Tsuji, PhD**, University of Tokyo, *Functional Bone Organoids Unveil Osteoblast-Driven Engulfment of Apoptotic Osteoclasts as a Key Contributor to Bone Remodeling*
P-098	**Eun Jung Lee, PhD**, Korea University College of Medicine, *Enhancing the Responsiveness of Immune Checkpoint Inhibitors in Breast Cancer Through PTHrP Blockade*

Poster Number	Presenter Name, Affiliation, Poster title
P-099	**Kazette Yuen Yu Chan**, University of Alberta, *Characterization of Two Novel KIF22 Variants and Their Association with A Rare Neonatal-Onset Disease*
P-100	**Andrew Jayarajah**, Sunnybrook Health Sciences Centre, *Clinical Impact of New AI Tool that Predicts Low Bone Mineral Density from X-Ray: Experience at Sunnybrook Health Sciences Centre*
P-101	**Kyra Hunsberger**, University of Arizona, *The Relationship Between Age at Menarche and Osteoporosis: A Systematic Review and Meta-Analysis*

Speaker Abstracts

Session 1: Osteocyte Dynamics

S1-1 Chelsea Heveran, PhD

The impact of aging on osteocyte lacunar-canalicular bone turnover

Osteocytes engage in bone resorption and mineralization surrounding their expansive lacunar-canalicular system (LCS) through LCS turnover. However, fundamental questions persist about where, when, and how often osteocytes engage in LCS turnover and how these processes change with aging. To address these questions, we utilized confocal scanning microscopy, immunohistochemistry, and scanning electron microscopy to quantify osteocyte LCS turnover in the cortical (mid-diaphysis) and cancellous (metaphysis) femurs from young (5 mo) and early-old-age (22 mo) female C57BL/6JN mice. LCS bone mineralization was measured by the presence of perilacunar fluorochrome labels. LCS bone resorption was measured by immunohistochemical markers of bone resorption. The dynamics of LCS turnover were estimated from serial fluorochrome labeling, where each mouse was administered two labels between 2 days and 16 days before euthanasia. Osteocyte participation in mineralizing their surroundings is highly abundant in both cortical and cancellous bone of young adult mice but significantly decreases with aging. LCS bone resorption also decreases with aging. Aging has a greater impact on LCS turnover dynamics in cancellous bone than in cortical bone. Lacunae with recent LCS turnover have larger lacunae in both age groups. The impact of aging on decreasing LCS turnover may have significant implications for bone quality and mechanosensation.

Session 1: Osteocyte Dynamics

S1-2 Karl Lewis, PhD

In Vivo Observation of Osteocyte Endocytosis

The imaging limitations imposed by the dense optical scattering matrix of bone can now be overcome using intravital imaging with multiphoton microscopy (MPM). A novel way to reach subcellular resolution with MPM osteocyte imaging involves surface functionalized fluorescent silica core-shell nanoparticles known as Cornell Prime Dots (C'Dots). These extremely bright nanoparticles can be functionalized in many ways, including to target integrins via surface RGD motifs (RGD-C'Dots). Fluorescent C'Dots are a novel method to study osteocytes and integrins in vivo, allowing for investigation of a range of structural, functional, and mechanobiological questions. This new tool offers an alternative to genetically modified mouse lines, reducing time and expense in the study of osteocyte/integrin mechanobiology, and could be translated to different species as well. Additionally, C'Dots can be used to visualize osteocyte subcellular localization in vivo and interrogate biologically relevant topics in osteocytes such as endocytosis and potentially integrin dynamics.

Session 1: Osteocyte Dynamics

S1-3 Diana Athonvarangkul, MD, PhD

Functional osteoclasts regulate osteocytic osteolysis during lactation

Increased bone turnover leads to a net bone loss during lactation. Our group previously presented that osteoclastic surface bone resorption is coupled to osteocytic osteolysis during lactation[1]. Inhibition of osteoclasts by recombinant osteoprotegerin or bisphosphonate treatment resulted in suppression of lactation-induced activation of resorptive gene programs in osteocytes and enlargement of osteocyte lacunae.

We applied an unbiased approach to identify potential clastokines involved in the crosstalk between osteoclasts and osteocytes during lactation. We treated 10 week-old lactating CD1 mice with recombinant osteoprotegerin (OPG, 10mg/kg) to block RANKL signaling, zoledronic acid (ZA,100 ug/kg) to inhibit osteoclasts, or vehicle, from delivery through mid-lactation (day 12). We performed bulk RNA sequencing from bone marrow depleted, osteocyte enriched tibial samples from these mice. Using gene set enrichment analysis, we identified significant upregulation in osteoclast differentiation, calcium signaling, and regulation of actin cytoskeleton pathways in lactation compared with virgin groups; and these pathways were downregulated with osteoclast inhibition compared with lactation controls.

In addition, our preliminary data show that osteoclast inhibition with osteoprotegerin during lactation downregulates transforming growth factor beta (TGFb) pathways compared to lactation control. By ploton silver staining, we observe disruptions to the integrity and area of the osteocyte lacunar network, which is consistent with previous reports [2-4]. Our working theory is that during lactation, osteoclast resorption liberates TGFb from the bone matrix, which in turn, activates TGFb signaling pathways in osteocytes to upregulate the resorptive gene program as well as calcium signaling and cytoskeletal rearrangements for increased bone turnover.

1. Athonvarangkul, D., Z. Salloot, R. Baron and J. Wysolmerski, Coupling of osteocytic osteolysis to functional osteoclasts during lactation. J Bone Miner Res, 2023. 38.
2. Dole, N.S., C.S. Yee, C.M. Mazur, C. Acevedo and T. Alliston, TGFβ Regulation of Perilacunar/Canalicular Remodeling Is Sexually Dimorphic. Journal of Bone and Mineral Research, 2020. 35(8): p. 1549-1561.
3. Dole, N.S., C.M. Mazur, C. Acevedo, J.P. Lopez, D.A. Monteiro, T.W. Fowler, et al., Osteocyte-Intrinsic TGF-β Signaling Regulates Bone Quality through Perilacunar/Canalicular Remodeling. Cell Rep, 2017. 21(9): p. 2585-2596.
4. Kegelman, C.D., J.C. Coulombe, K.M. Jordan, D.J. Horan, L. Qin, A.G. Robling, et al., YAP and TAZ Mediate Osteocyte Perilacunar/Canalicular Remodeling. J Bone Miner Res, 2020. 35(1): p. 196-210.

Session 1: Osteocyte Dynamics

S1-4 Mathilde Palmier, PhD

Bone Mass Gain During Maturation Occurs Despite the Loss of Osteocytes and Blood Vessels in Mouse Cortical Bone

Mathilde Palmier 1, Marlène Maître 2, Hélène Doat 2, Thierry Lesté-Lasserre 2, Claudine Boiziau 1+, Delphine Maurel 1+
(1) Inserm, University of Bordeaux, BioTis Laboratory UMR 1026, Bordeaux, France. (2)Inserm, University of Bordeaux, Neurocentre Magendie UMR 1215, Bordeaux, France. +both authors equally contributed

During maturation, bone mass increases until peak bone mass is reached. The higher the peak, the less risks there are to obtain weak bones while aging. During long bone maturation, cortical bone is consolidated to support the body weight. Understanding the physiological conditions that lead to peak bone mass would help to understand the dysregulations that might occur under pathological conditions, and to identify them years before the onset of bone loss. Blood vessels (BVs) and osteocytes (OCys) form two networks within cortical bone supporting its functions. The aim of this study was to analyze these networks and compare their morphologies in growing and mature bones. As there are evidence of interactions between BVs and Ocys, we hypothesized that a change in blood vessel network would impact osteocyte access to oxygen and that they would react through VEGFA regulation.

We studied the femurs of male Flk1-GFP mice in which the GFP is expressed in endothelial cells making BVs fluorescent. We compared two groups: growing (5 weeks old) and mature (5 to 8 months old). We assessed the changes in bone using microCT imaging, and quantified the blood vessel network using the GFP on thick sections, or tissue clearing after injection of lectin. We characterized the osteocyte network in 3D using phalloidin staining. We also analyzed Ocy gene expression (Pdpn, VegfA) using previously optimized laser microdissection protocol. Finally, we compared the Ocy access to oxygen between the two groups using immuno-fluorescence labeling. We measured a 75% bone gain during maturation. Conversely, the number of GFP-positive BVs decreased by 88%, and the blood vessel volume over the bone volume measured after tissue clearing was divided by 2. The mature bone presented 29% less OCys than the growing bone, less dendrite per OCy and a down-regulation of Pdpn. Consequently, for a given bone volume, the number of OCy per BV was higher in the mature group than in the growing group. Surprisingly, the VegfA expression levels and the percentage of VEGFA-positive OCys were similar in both groups, and OCy access to oxygen was reduced in the growing animals. These results suggest that Ocy VegfA expression and access to oxygen do not depend on the density of the blood vessel network during maturation. A decreased number of OCys and BVs is often associated with bone loss during aging. In this study, it appears to be concomitant with bone gain through mechanisms that remain to be determined.

Session 1: Osteocyte Dynamics
S1-5 Naomi Jung, PhD

We don't talk anymore: Lacunocanalicular network disruptions in prostate cancer bone metastasis

Naomi Jung 1, 2, Qiong Wang 3, Felipe Y Eltit 1, 2, Doris Liang 4, 5, Marina Eckermann 6, Samuel Xu 1, 2, Danmei Liu 5, Alexandra Pacureanu 7, Peter Cloetens 6, Eva Corey 8, Colm Morrissey 8, Lawrence True 9, Rizhi Wang 3, 4, 5 and Michael Edward Cox 1, 2
(1) Department of Urologic Sciences, University of British Columbia, Vancouver, BC, Canada (2) Vancouver Prostate Centre, Vancouver, BC, Canada (3) Department of Materials Engineering, University of British Columbia, Vancouver, BC, Canada (4) School of Biomedical Engineering, University of British Columbia, Vancouver, BC, Canada (5) Centre for Aging SMART at VCH, Vancouver, BC, Canada (6) Division of Experiments, European Synchrotron Radiation Facility, Grenoble, France (7) Neuroimaging Unit, European Synchrotron Radiation Facility, Grenoble, France (8) Department of Urology, University of Washington, Seattle, WA, USA (9) Department of Pathology and Laboratory Medicine, University of Washington, Seattle, WA, USA

Prostate cancer (PC) is the most prevalent male cancer with about 1.5 million new diagnoses each year. 20% of patients develop metastatic disease and greater than 90% of whom will have bone metastases (BM). PCBM increase mortality risk, cause intractable pain and result in high risk of fracture. Bone homeostasis is dysregulated in PCBM, with lesions defined as being predominantly osteoblastic with increased bone deposition on residual trabeculae (RT). Osteocytes are mechanosensitive cells embedded in the bone matrix in voids called lacunae, and interface with other osteocytes, vasculature and the marrow milieu through a web of fine processes called canaliculi that regulate bone homeostasis. How PCBM affects osteocytes, and this lacunocanalicular network (LCN) is not well understood, especially in trabecular bone. We hypothesize that the disruption of LCN is integral to the loss of homeostasis and contributes to excess and disorganized matrix deposition, and increased fracture risk.

In order to describe how the LCN is impacted in PCBM, we performed synchrotron nanoCT imaging on 4 cadaveric vertebral trabecular bone samples (2 cancer-free, 2 PCBM) at 50 nm resolution (5 images, field of view of 160x160x102 µm, 32-bit). Canalicular structures were identified using a Frangi 3D filter and lacunae were manually segmented to train a U-Net based convolutional neural network in Dragonfly software. The model was then applied to the image sets, and quantitative parameters were used to describe shape, volume, and density of LCN.
The LCN in osteoblastic bone lacks the anisotropic organization seen in the RT and control bone (Figure 1). The lacunae in osteoblastic bone are: at increased density, not aligned to a common axis, and lack canalicular connections between lacunae in the RT bone and the osteoblastic bone. Our observations demonstrate that increased lacunar density and canalicular volume in PCBMs results in increased voids in the osteoblastic bone. These changes suggest altered osteocyte mechanosensitivity, irregular interstitial fluid flow, and a reduced ability to resist crack propagation during fracture in osteoblastic PCBM bone.

Session 1: Osteocyte Dynamics
S1-5 Naomi Jung

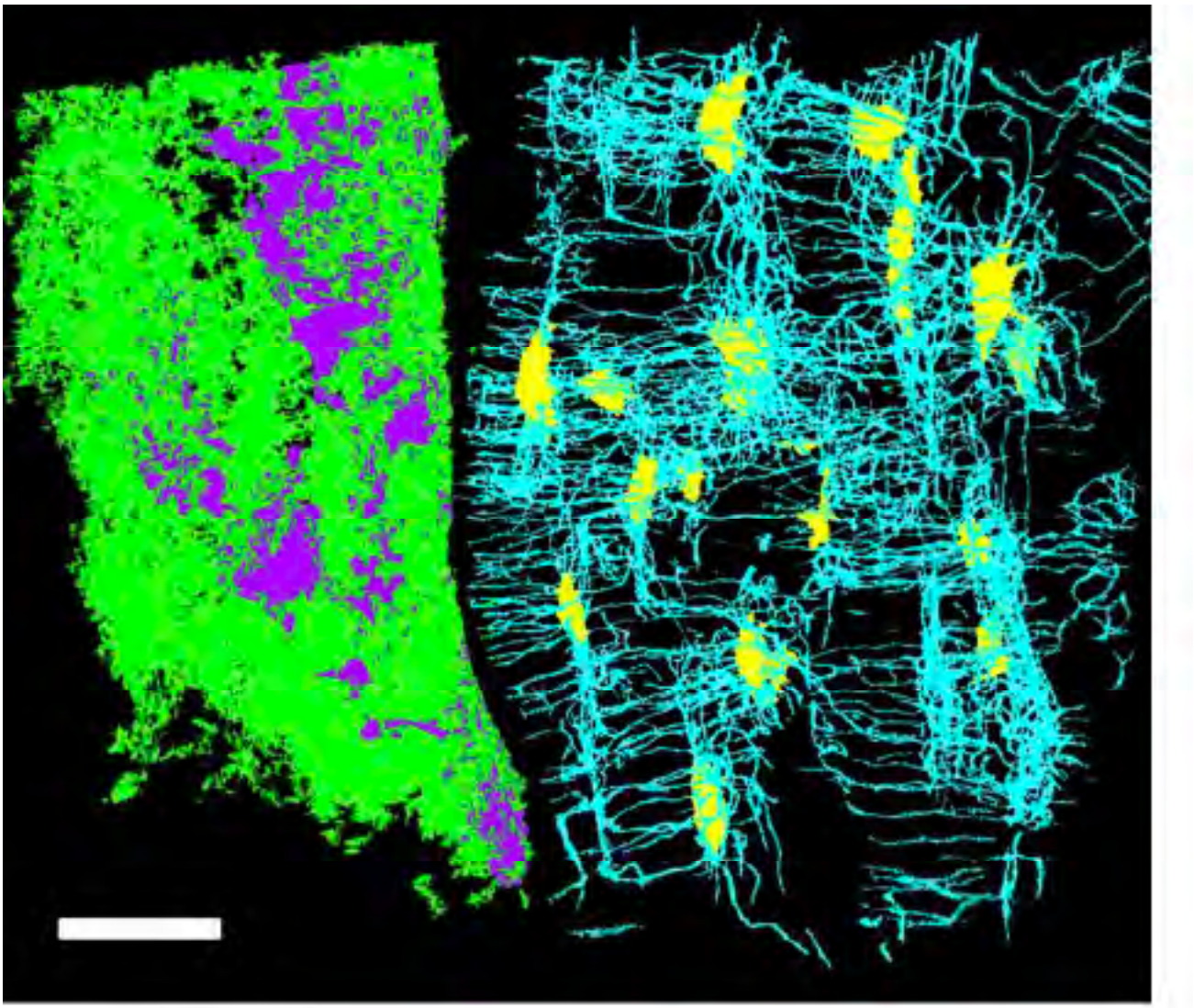

Figure 1: LCN segmentation from a synchotron nanoCT image of a mixed PCBM vertebral trabecular bone sample (50 nm voxel size). Residual trabecular bone (right) with lacunae in yellow and canaliculi in blue and osteoblastic bone (left) with lacunae in purple and canaliculi in green. The boundary between the two types of bone has limited canalicular connectivity. Scale bar = 20 µm

Session 1: Osteocyte Dynamics

S1-6 Sarah Dallas, PhD

Tissue Expression of GFP-Tagged Collagen in Transgenic Mice and Live Cell Imaging of Osteoblast Collagen Assembly and Bone Collagen Resorption

Kun Wang*1, Yixia Xie1, David Moore1, Claire Houchen1, Yongbo Lu1,2, Eleanor Ray1, Mark Dallas3 and Sarah L. Dallas1
(1) University of Missouri Kansas City, Kansas City, MO, USA, (2) Texas A&M University, Dallas, TX, USA, (3) UMKC School of Dentistry, Kansas City, MO, USA

Type I collagen, the major bone matrix protein, is a heterotrimer of two α1(I) chains and one α2(I) chain, encoded by the COL1A1 and COL1A2 genes. Although the collagen biosynthetic pathway is well understood, the dynamic process by which collagen is assembled into extracellular fibrillar networks is less well defined. We previously generated transgenic mice expressing GFP-tagged α2(I) collagen driven by the 3.6kb-COL1A1 promoter. Immortalized osteoblast (OBL) cell lines were made from these mice as well as mice co-expressing GFP-collagen and a membrane-targeted TdTomato reporter (mTmG). Here, we report on further characterization of the GFP-collagen distribution in these mice and real-time imaging of collagen assembly and turnover. GFP-collagen was expressed in bone, tendon, ligament, intervertebral disc, skin dermis, cornea and sclera of the eye, heart valve, and connective tissue septae/fasciae of muscle and soft tissue organs. Fluorescence imaging of GFP-collagen in cryosections of the vertebrae and femur, revealed detailed substructure, with cement lines from cycles of bone formation visible and collagen in newly deposited bone appearing brighter vs. mature bone. New collagen around osteocyte lacunae or vascular channels was brighter and cycles of bone formation appeared as concentric rings. Live-cell imaging was done on primary OBL from GFP-collagen mice and GFP-collagen/mTmG mice using a scoreline wounding model to visualize collagen repair dynamics. Cells migrated directionally, dragging the front of pre-existing collagen ~100μm into the wounded area. Collagen assembly was cell density-dependent and highly dynamic, with cell motions stretching, contracting and physically reshaping fibers to form meshworks, generate holes, and form thick fiber bundles via compaction of finer fibrils. Cells moved in waves depositing collagen, with other cells moving in adding to the already existing collagen. Individual OBL could be observed to deposit a “trail” of collagen as they migrated. Live imaging of GFP-collagen/mTmG OBL seeded at low density onto wild-type OBL suggested an active cell placement mechanism, with no collagen deposited distant from the cell body or processes. Live cell imaging in calvarial bone explants from GFP-collagen/LysM-Cre/TdTomato mice showed real-time osteoclast resorption of collagen via scalloping on exposed bone surfaces and formation of shallow resorption trenches. Larger volumes were resorbed cooperatively via deeper excavation by osteoclasts and coalescence of multiple resorption lacunae. These data show the power of the GFP-collagen transgenic mice for real-time imaging of collagen assembly and resorption and suggest that collagen assembly is driven by tissue-level and local cell motions and physical reshaping via cell-generated forces.

Session 2: Spatial Transcriptomics in Bone

S2-1 Erica L. Scheller, DDS, PhD

Optimizing spatial transcriptomics in mouse bone from the single gene to the whole transcriptome identifies regional changes in response to applied load

Spatial transcriptomics allows for resolution of gene expression in the spatial dimension from the single-gene to the whole transcriptome. However, methods are not well optimized for bone, which limits current applications. To overcome this, we optimized protocols for single gene RNAscope prior to adaptation for whole transcriptome analysis (WTA) using the NanoString GeoMx platform. This workflow was used to analyze gene expression in the periosteum and cortical bone after biomechanical loading of the mouse tibia. Specifically, 5-month old C57Bl/6 mice were loaded unilaterally to -2200 με for 5-days and sacrificed 4-hours after the final loading bout. Non-loaded and loaded tibias were harvested and transverse paraffin sections from the mid-diaphysis were prepared for analysis. Spatial capture tools were used to subdivide each section into regions of maximum tensile and compressive strain, resulting in four areas of interest (AOIs) per section (max compressive-bone; max compressive-periosteum; max tensile-bone; max tensile-periosteum). Periosteal and cortical bone AOIs expressed gene profiles in accordance with tissue type, providing evidence of successful AOI selection (ex. Postn, Bglap, Sparc, and Aspn enriched in periosteum; Mepe, Dmp1, and Dkk1 enriched in bone). The resulting spatial transcriptomic datasets were also validated against prior bulk tissue RNAseq. This identified 128 overlapping DEGs between gene sets ($p<0.05$, Log2FC $>|0.5|$) including known responders such as Bglap, Col1a1, Gja1, and Phospho1. Regression analysis of overlapping genes revealed relatively high concordance in fold change between techniques ($r2=0.556$, $p<0.001$). AOI-based subanalysis of the spatial data in bone vs periosteum identified 224 vs 809 significant DEGs with loading, respectively. Gene ontology analysis revealed an upregulation of genes associated with collagen fibril organization and mineralization in bone, while key genes and pathways associated with collagen biosynthesis, vesicle transport, osteoblast differentiation, and angiogenesis were more prominent in the periosteum. Further characterization based on FEA-determined stress maps identified a spectrum of loading-induced gene changes with maximal upregulation of osteoanabolic genes and pathways at sites of maximum compression. Overall, this novel workflow substantially expands our capabilities for spatial WTA in bone tissues while clarifying the relationship between applied stress and regional skeletal adaptation.

Session 2: Spatial Transcriptomics in Bone

S2-2 Zhaoyang Liu, PhD

Spatial Transcriptomics Reveals the Role of a G Protein-Coupled Receptor in Growth Plate Homeostasis through Regulation of IHH Signaling

The cartilage growth plate is essential for maintaining skeletal growth; however, the mechanisms governing postnatal growth plate homeostasis are still poorly understood. Using approaches of molecular mouse genetics and spatial transcriptomics applied to formalin-fixed, paraffin-embedded (FFPE) tissues, we show that ADGRG6/GPR126, a cartilage-enriched adhesion G protein-coupled receptor (GPCR), is required for postnatal growth plate homeostasis. Ablation of Adgrg6 with Col2a1Cre leads to a short resting zone, formation of cell clusters, and an elongated hypertrophic growth plate, marked by limited expression of PTHrP but increased IHH signaling. Attenuation of Smoothened (SMO)-dependent HH signaling restored the Adgrg6 deficiency-induced expansion of hypertrophic chondrocytes, confirming that IHH signaling can promote chondrocyte hypertrophy in a PTHrP-independent manner. Our findings elucidate the essential role of a cartilage-enriched adhesion GPCR in regulating cell differentiation by regulation of PTHrP/IHH signaling, maintenance of slow-cycle resting zone chondrocytes, and safeguarding chondrocyte homeostasis in postnatal mouse growth plates.

Session 2: Spatial Transcriptomics in Bone

S2-3 Xenia Goldberg Borggaard, PhD

Spatial transcriptional profiling of osteoprogenitors proximate to osteoclasts in human bone remodeling

Xenia Borggaard*1,2, Malene Hykkelbjerg Nielsen1,2, Ching-Hsin Huang2,3, Kristine Edvardsen3, Sam Khac Dinh3, Christina Moeller Andreasen2,3, Julia F. Charles4,5 and Thomas Levin Andersen2,3,6
(1) Molecular Bone Histology Lab, Research Unit of Pathology, Department of Clinical Research, University of Southern Denmark, Denmark, (2) Danish Spatial Imaging Consortium, Odense, Denmark, (3) Molecular Bone Histology Lab, Research Unit of Pathology, Department of Clinical Research, University of Southern Denmark, Odense, Denmark, (4) Brigham & Women's Hospital, BOSTON, MA, USA, (5) Harvard Medical School, Boston, MA, USA, (6) Department of Forensic Medicine, Aarhus University, Aarhus, Denmark

Crosstalk between bone cells is essential in remodeling. Reversal cells (Rv.Cs) are osteoprogenitors in close proximity to osteoclasts (OC) that may play an overlooked central role in remodeling. In human trabecular bone these Rv.Cs express early osteoblastic markers and collagenases like MMP13, consistent with a catabolic function in cleaning the eroded surface from OC debris. However, Rv.Cs also express receptors for coupling factors, indicating a pro-formative role too. In this study, we aim to extend the characterization of Rv.Cs and their partnership with OCs in human intracortical bone remodeling events.

Decalcified paraffin-embedded cortical bone samples from adolescents (aged 12-15 yr) were subjected to spatial transcriptional profiling of the whole transcriptome using GeoMXTM digital spatial profiling (GeoMx) and RNA in situ hybridization (ISH) combined with TRAcP immunostaining. A TRAcP/CD34 immunofluorescence staining guided the DSP of spatially defined cell populations: Rv.Cs, bone-forming osteoblasts, and OCs (TRAcP+).

GeoMx analysis of one bone sample included 12 active and 4 inactive remodeling events. In the active remodeling events, bone-forming osteoblasts expressed typical genes like IBSP, COL1A1, and BGLAP, while TRAcP+ OCs expressed genes like MMP9, ACP5, TCIRG1 and CTSK. DEGs identified when comparing Rv.Cs to bone-forming osteoblasts included IGFBP5, TNC, BGLAP, and MMP13 whereas DEGs identified between Rv.Cs and OCs included BGN, FN1, and SPARC. Histological analysis of MMP13 expression of 7596 cells in intracortical pores from 6 bone samples was evaluated. 16% of the analyzed cells were MMP13+. Evaluating the spatial location of MMP13+ supported the initial findings from GeoMx. Rv.Cs on eroded surfaces (n=1154) had significantly higher MMP13-expression than osteoblasts (n=743, p=<0.0001) and bone lining cells (n=428, p=<0.0001). Moreover, Rv.Cs proximate to OCs (< 25 µm) had significantly higher expression of MMP13 compared to those further away (> 25 µm). Interestingly, by evaluating ISH of RANKL and TRAcP immunostaining, RANKL appeared to be expressed in the same pattern with higher expression of RANKL near OCs. Co-expression of MMP13 and RANKL is consistent with published scRNA-seq data from mice and remains to be evaluated in a larger scale in human.
GeoMx appears to be an informative method for investigation of Rv.Cs, and we hope that addition of more samples will reveal more about this interesting cell population.
physical reshaping via cell-generated forces.

Session 2: Spatial Transcriptomics in Bone

S2-4 Quentin Meslier

WISH-BONE: Whole-Mount In Situ Histology, To Label Osteocyte mRNA And Protein In 3D Adult Mouse Bones

Quentin A. Meslier 1,3, Timothy J. Duerr 2,4, Brian Nguyen3, James R. Monaghan 1,2,4, Sandra J Shefelbine 1,4
(1) Department of Bioengineering, Northeastern University, Boston, MA, United States. (2) Department of Biology, Northeastern University, Boston, MA, United States (3) LifeCanvas Technologies, Cambridge, MA, United States (4) Institute for Chemical Imaging of Living Systems, Northeastern University, Boston, MA, United States

Introduction: Osteocytes sense external forces and initiate the bone mechanoadaptation response by regulating their molecular expression. This response depends on the cells 3D mechanical environment. However, current methods to investigate bone molecular biology do not preserve 3D spatial information. In this work, we present WISH-BONE, methods for 3D investigation of molecular expression in osteocytes in their spatially preserved location. We demonstrate the use of WISH-BONE for investigation of bone mechanoadaptation.

Methods: The right tibia of adult mice was loaded using a uniaxial compression model. The applied triangular loading profile is known to induce bone formation in adult mouse bone (10N, 4Hz, 72N/s, 100cycles, rest period of 1 second). Left tibiae were kept as controls. Following loading, tibiae were collected, fixed, and decalcified. mRNA labeling: We used HCR-FISH to label Sost mRNA transcripts (Fig1.A &B), a mechanosensitive gene that is down-regulated with loading. Protein labeling: samples were preserved using SHIELD (LifeCanvas Technologies), an epoxy-based solution that has been shown to protect tissue structure. Then, a collagenase matrix permeabilization step was performed to enable antibody penetration. Sclerostin, the protein regulated by Sost, was labeled via immunolabeling. In addition, connexin 43, MMP9, osteopontin, and osteocalcin were labeled as a demonstration of potential application of the method. Imaging: Samples were made optically transparent via incubation in a solution with a refractive index of 1.52. 3D images were acquired using lightsheet microscopy. A custom neural network was used to detect cells in 3D.

Results: mRNA labeling: ~300,000 cells were detected in the cortical bone. Sost-positive cells decreased in loaded legs compared to control (n=5) (Fig.1.D). The largest decreases in Sost-positive cells were in the posterior-lateral region, where the mechanical stimulus is the highest (Fig.1.E). Protein labeling: Matrix permeabilization was critical for optimal antibodies penetration through the cortical thickness (Fig1.F). SHIELD preserved sample integrity during permeabilization. Preliminary results suggest a decrease of sclerostin-positive cells at 35% of the bone length.

Significance: This is the first whole-mount mRNA and protein labeling protocol for osteocytes in 3D mouse bones. This method could be applied to various bone biology research fields in which the 3D environment influences the cells response.

Session 2: Spatial Transcriptomics in Bone

S2-4 Quentin Meslier

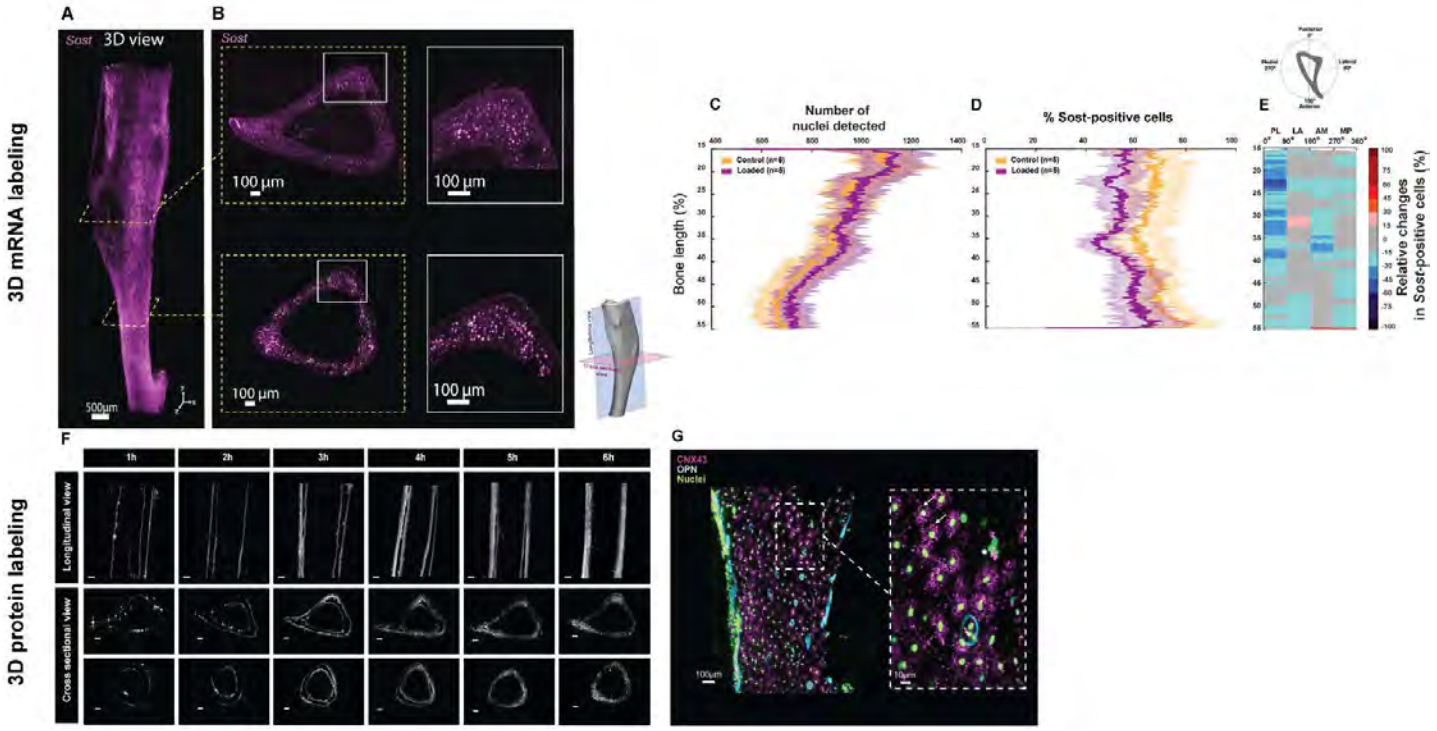

Figure 1: A) 3D mRNA labeling of Sost in 3D mouse tibia. B) Cross sectional views showing osteocytes expressing Sost mRNA. C) Total number of cell nuclei detected in the cortical bone in 3D. D) Percentage of Sost-positive cells along the bone length in loaded and control legs. E) 2D map showing relative changes in percentage of Sost-positive cells along the bone length and around the bone cross-section. PL: Posterior-Lateral; LA: Lateral-Anterior; AM: Anterior-Medial; MP: Medial-posterior. F) Effect of collagenase permeabilization on anti-sclerostin antibodies penetration throughout the cortical bone. G) 3D protein labeling of Connexin 43 in mouse tibia.

Session 2: Spatial Transcriptomics in Bone
S2-5 Peter Maye, PhD

A Method to Perform Spatial Transcriptomics on Human Articular Cartilage

Peter Maye*1, Mejeong Lee1, Li Chen1, David W. Rowe1, Honglin Wang2, Pujan Joshi2, Dong-Guk Shin2, Jeffrey Moffitt3, Ji Yu4, Merissa Olmer5, Hannah Swahn5 and Martin Lotz5,
(1) Regenerative Medicine and Skeletal Development, Department of Reconstructive Sciences, School of Dental Medicine, University of Connecticut Health, Farmington, CT, USA, (2) Computer Science & Engineering, School of Engineering,University of Connecticut, Storrs, CT, USA, (3) Program in Cellular and Molecular Medicine, Boston Children's Hospital; Department of Microbiology, Harvard Medical School, Boston, MA, USA, (4) Center for Cell Analysis and Modeling, University of Connecticut Health, Farmington, CT, USA, (5) Departments of Molecular and Cell Biology and Molecular Medicine, Scripps Research, La Jolla, CA, USA

Developing experimental methods to determine the potential molecular pathways that contribute to degenerative joint disease is a major challenge that needs to be solved. As part of the Human Biomolecular Atlas Project, our group has been developing applications to gain insight into the normal physiology of human articular cartilage. Imaging based spatial transcriptomics approaches can provide insight into the cellular and molecular composition of tissues at subcellular resolution. However, performing this technique on skeletal tissues is fraught with challenges. Here we present a sequential in situ hybridization approach that has been successfully tested on human articular cartilage. Thirty biomarkers obtained from the clustering of single cell RNA (scRNA) sequencing datasets were selected for spatial mapping. Sequential in situ hybridization was performed, based on the principles of MERFISH, on 3mm3 tissue blocks obtained from the distal femur. A process of tissue preservation and permeabilization was developed that, in conjunction with microfluidics and imaging, allows for the sequential detection of different RNA transcripts. Existing and customized software applications were used to establish an image processing workflow that allowed for the quantitation of gene expression on a per cell basis. Cell by gene matrices were used for cluster analysis and the subsequent mapping of clusters back to tissue sections. Consistent with recent scRNA sequencing studies performed on human articular cartilage, our preliminary studies suggest the cellular complexity of normal articular cartilage is greater than expected and extends beyond the three zonal model. Ongoing work will continue to build out a molecular map of normal articular cartilage that includes the integration of scRNA sequencing datasets. The development of a spatial atlas of normal human articular cartilage will serve as an important reference for understanding the cellular and molecular changes that take place under various disease conditions.

Session 2: Spatial Transcriptomics in Bone
S2-6 Francisco Correia Marques

Multiscale Mechanoregulation Analysis Using Super-Resolution Spatial Transcriptomics Data and Multimodal Imaging

Francisco Manuel Correia Marques*1, Amit Singh1, Neashan Mathavan1, Dilara Yilmaz1, Denise Günther1, Gisela A. Kuhn1, Esther Wehrle1,2 and Ralph Mueller1
(1) Institute for Biomechanics, ETH Zürich, Zürich, Switzerland, (2) AO Research Institute Davos, Davos, Switzerland

Local tissue mechanics play a crucial role in bone mechanobiology, as formulated in the Mechanostat Theory by Frost, which describes a monotonic response of bone adaptation based on tissue strains. While this regulation also affects gene expression, we hypothesised that it does not necessarily follow a similar linear or monotonic response given, for example, the complex interactions between different pathways. To test this, we have developed Spatial μProBe, a tool for multimodal correlation of in vivo micro-CT images with ex vivo histological sections from the same bone. Notably, it can integrate gene expression from 2D spatial transcriptomics (ST) data with the corresponding 3D mechanical strains computed in the local in vivo environment (LivE) using micro-finite element analysis (micro-FE). While ST technologies such as Visium (10x Genomics) do not yet reach single-cell resolution, recent in silico methods (iStar) can produce super-resolution ST data at near single-cell scale. In this study, we used Spatial μProBe to link local gene expression and tissue mechanics to evaluate bone mechanoregulation during fracture healing. We used time-lapsed in vivo micro-CT images (10.5 μm) from one adult female mouse femur to co-register paraffin sections (FFPE, 5 μm thickness) prepared for Visium ST. Bone in the section was manually segmented and 2D-3D registered to the corresponding in vivo micro-CT scan (Fig 1A). ST data analysed with Squidpy revealed the spatial expression for selected mechanically regulated genes such as Col1a1, encoding the pro-alpha1 chains of type I collagen, an abundant structural protein in bone (Fig 1B). Micro-FE analysis yielded the local mechanical signal as effective strain (με) (Fig 1B-C). Since micro-FE provides a highly resolved mechanical environment, we used iStar to obtain super-resolution ST data at micro-CT resolution (Fig 1C). This approach described gene expression at each tissue strain with improved precision compared to the data obtained from sparse Visium spots (Fig 1D). Remarkably, Col1a1 showed a sinusoidal-like response, supporting our hypothesis, while also suggesting a very stable control of gene expression including well-defined strain intervals of high and low expression. These could help identify functionally and therapeutically relevant strain targets supported by mechanical loading to control the expression of selected genes. In conclusion, Spatial μProBe using super-resolution ST data can investigate the mechanical regulation of thousands of genes provided by Visium to explore multiscale bone mechanobiology in ageing, disease and treatment.

Session 2: Spatial Transcriptomics in Bone
S2-6 Francisco Correia Marques

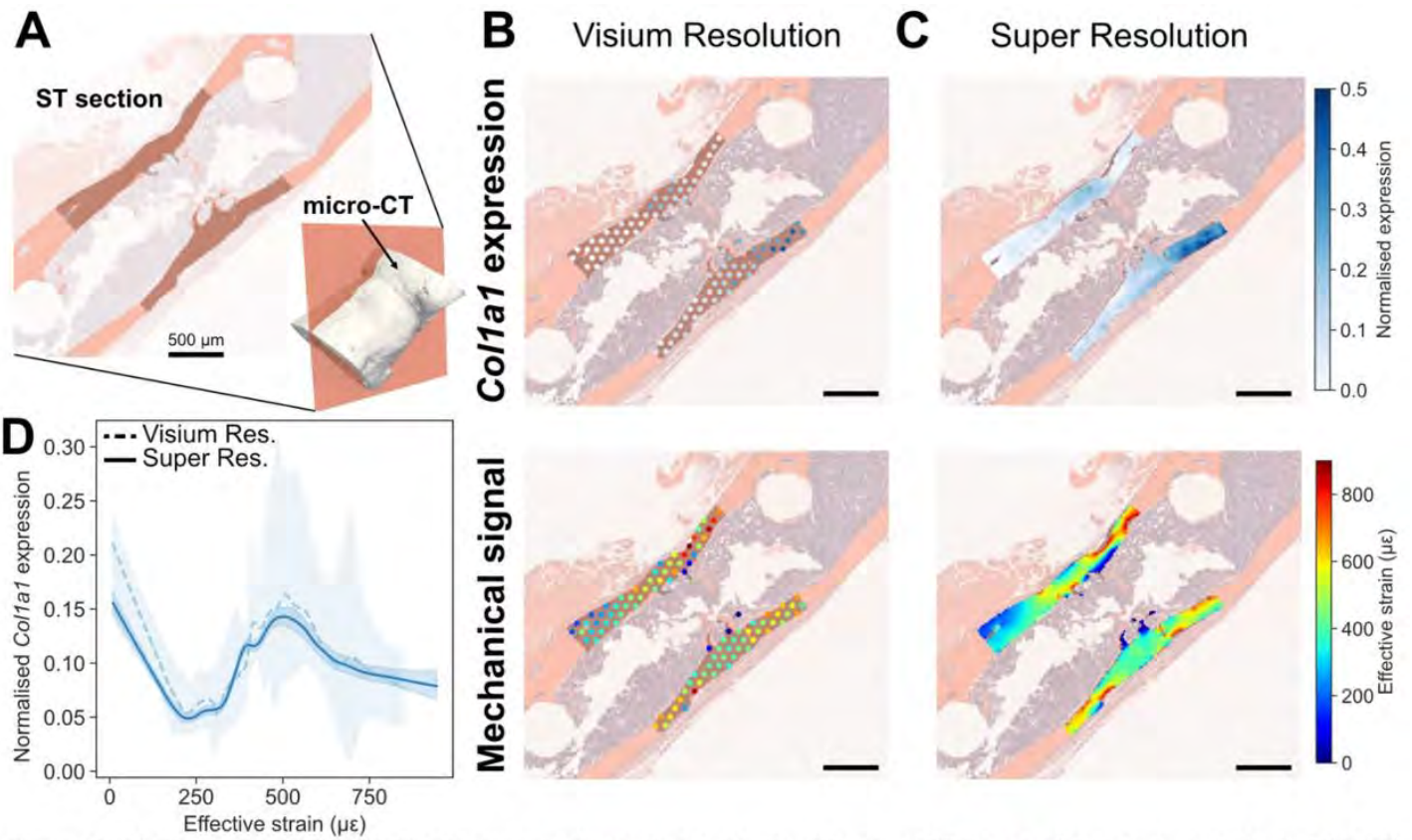

Figure 1: A) Rendering of the 2D histological section registered to the 3D micro-CT image of the same sample and 2D-2D overlay of the 2D-3D registration outcome. **B)** Expression map of *Col1a1* for spots on the Visium slide overlapping with the registered micro-CT section and mechanical signal (effective strain) computed with micro-FE at the Visium spots. **C)** Super-resolution expression map of *Col1a1* predicted using iStar at the resolution of the micro-CT image (normalised to the interval 0-1) and mechanical signal (effective strain) mapped to the registered section. **D)** Comparison between the normalised gene expression for *Col1a1* from sparse Visium spots and the super-resolution map. Plots show the mean expression curves after bootstrapped LOWESS and their 95% confidence intervals.

Session 3: Multiscale Bone Structure and Function

S3-1 Mariana Kersh, PhD

From muscle to molecule: bone response to exercise

For most individuals, the musculoskeletal system sustains thousands of mechanical loading cycles every day with remarkable resilience. Yet, increased loading cycles is a known risk factor for tissue dysfunction. This talk will explore the benefits and risks of mechanical loading for bone in the context of exercise. The interactions of macroscopic loading from muscle on bone, subsequent response at the meso-scale, and molecular level changes will be discussed.

Session 3: Multiscale Bone Structure and Function

S3-2 Ottman Tertuliano, PhD

Resolving history in fibril-mediated fatigue in 3D at the nanoscale with synchrotron X-rays

Fatigue is uniquely difficult to quantify in bone due to cell-driven remodeling and limitations in situ volumetric imaging during deformation. Developing a context in which we can quantify deformation under cyclic loading is a critical factor in understanding fracture risk under non-traumatic physiological conditions. Here, we demonstrate the use of synchrotron X-ray radiography coupled with nanoscale three-point bend fracture experiments on lamellae excised from human trabeculae. We provide a fibril-centric context for understanding fatigue crack growth mitigation in bone at these scales prior, covering fracture from the slow to the fast crack growth regimes.

Session 3: Multiscale Bone Structure and Function
S3-3 Koji Ishikawa, MD, PhD

Age-related changes in immune and endothelial response impair bone repair

Koji Ishikawa1.2, Choiselle Marius1, Eijiro Shimada1, Mahoko Ishikawa1, Savanna Ma1, Puvi Nadesan1, Tuyet Nguyen1, Asjah Wallace1, Jing Xie1, Makoto Nakagawa1, Vijitha Puvindran1, Tomasa Barrientos De Renshaw1, Benjamin Alman1
(1) Department of Orthopaedic Surgery, Duke University, North Carolina, USA (2) Department of Orthopaedic Surgery, Showa Medical University, Japan

Age-related decline in bone regenerative capacity is multifactorial, and specifically the dyscoordination of the immune response contributing to regenerative failure remains poorly understood. Here, we thought to identify aging-associated immune subpopulations and investigate their contribution to bone healing. Our single-cell RNA sequencing (scRNA-seq) revealed age-related changes in immune cells and identified expanding subclusters with aging following bone injury. These subclusters highly express the chemokine receptor genes Cx3cr1, and their transcriptional programs shift towards pro-inflammatory phenotypes, suggesting a contribution to age-related physiological changes in bone metabolism. Further validation at the protein level confirmed that CX3CR1+ immune cells, but not CX3CR1- immune cells, exhibit an age-related increase under both homeostatic and injury conditions (Figure A). Additionally, circulating cells also displayed age-related changes, leading to increased migration of CX3CR1+ monocytes/macrophages to injury sites in older mice, as determined by parabiosis models (Figure B). The diphtheria toxin-mediated ablation of CX3CR1+ cells fast bone repair by reducing osteoclasts and resolving chronic inflammation (Figure C). To explore the mechanism behind the accumulation of CX3CR1+ cells in aging, we examined CX3CL1, the specific ligand for CX3CR1. CX3CL1 is predominantly expressed in fibrotic areas by endothelial cells, including CD157+ vessel stem cells and type H vessels after injury, with limited co-localization with CX3CR1 expressing cells (Figure D and E). Notably, higher CX3CL1 expression in young mice suggests an age-associated decrease owing to alterations in basic tissue remodeling architecture. rmCX3CL1 promotes osteoblastogenesis in vitro, leading us to assess the functional role of CX3CL1. The conditional local deletion of Cx3cl1 using adenovirus-Cre recombinase injection in Cx3cl1flox/flox mice delayed the pace of repair by accumulating of CX3CR1+ cells and inhibiting osteoblastogenesis. Conversely, local rm-CX3CL1 administration around the injury site promotes osteoblastogenesis, resulting in fast repair in old mice. Our findings reveal age-related alterations in immune and endothelial responses, highlighting a potential therapeutic target for enhancing bone repair.

Session 3: Multiscale Bone Structure and Function

S3-3 Koji Ishikawa, MD, PhD

Figure

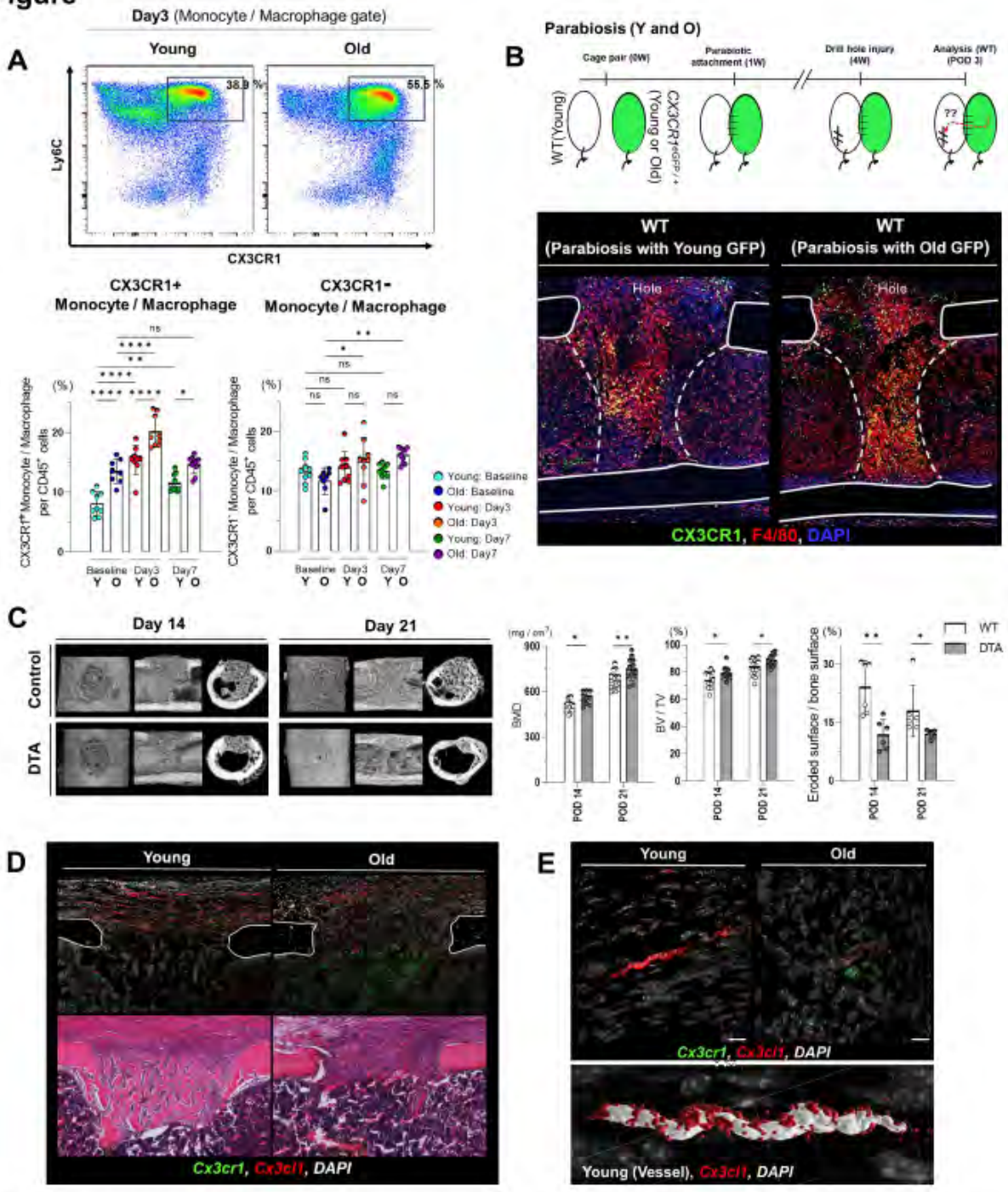

A. FACS was used to quantify CX3CR1+ and CX3CR1- monocyte/macrophage based on surface expression of CD45+CD11b+ and/or F4/80+ following drill hole injury (n=6-8 per group). (Young:2-3 months, Old: 21-24 months).
B. Schematic of the parabiosis experimental procedure (Upper). Representative confocal images showing eGFP expression on injured femurs immunostained for F4/80 in young WT mice (Lower).
C. Representative micro-CT images of femurs from *CX3CR1^{creER}; DTA* mice at Day 14 and 21 post-injury (n=10-14 per group)(Left). Quantification of Bone mass and bone histomorphometric analysis at injury site (Right).
D. RNAScope images of *Cx3cr1* and *Cx3cl1*(Upper) and HE staining (Lower) of femur at Day7 post injury (n=6/Groups).
E. Enlarge area of FigureD at *Cx3cl1 expressing* cells, depicting newly formed vessels in young mice (Upper: white scale bars, 5 μm) (Lower: 3D image)

Session 3: Multiscale Bone Structure and Function

S3-4 Natalie Koh

Inducing STAT3 hyperactivation in osteoblasts and osteocytes in the adult murine skeleton increases cortical porosity

Natalie Yu Ying Koh*1,2, Narelle E. McGregor3, Natalie Kah Yun Wee1,2, Christa Maes4 and Natalie A. Sims5,6
(1) St. Vincent's Institute of Medical Research, Fitzroy, VIC, Australia, (2) Department of Medicine at St. Vincent's Hospital, The University of Melbourne, VIC, Australia, (3) St. Vincent's Institute of Medical Research, Melbourne, Australia, (4) Laboratory of Skeletal Cell Biology and Physiology (SCEBP), Skeletal Biology and Engineering Research Center (SBE), Department of Development and Regeneration, KU Leuven, Leuven, Belgium, (5) Department of Medicine at St. Vincent's Hospital, The University of Melbourne, Melbourne, Australia, (6) St. Vincent's Institute of Medical Research and Department of Medicine at St. Vincent's Hospital, Fitzroy, VIC, Australia

Cortical bone degenerates with ageing, including by aberrant expansion of cortical pores, but the signals responsible are not known. Previous work has shown that elevated signal transducer and activator of transcription 3 (STAT3) signalling caused by suppressor of cytokine signalling 3 (SOCS3) deletion within osteoblasts and osteocytes led to high cortical porosity in the developing skeleton. We here sought to determine whether adult-onset STAT3 hyperactivation in osteoblasts and osteocytes would also lead to increased cortical porosity in a healthy skeleton.
We generated 10kbDmp1-CreERt2-driven conditional SOCS3-deficient mice (iDMPCre+.Ai9. Socs3f/f) and controls (iDMPCre+.Ai9), all harbouring the Ai9/tdTomato reporter allele. Gene recombination was induced in female mice with 4 doses of 20mg/kg tamoxifen suspended in corn oil, given between 12- and 13.5-weeks of age.

First, we validated the model. Tamoxifen-induced recombination was assessed in cryosections of control iDMPCre+.Ai9 femora at 14- and 26-weeks of age. At both ages, ~80% of metaphyseal cortical osteocytes were tdTomato+, indicating persistently high recombination. At the diaphysis this was ~50%, suggesting region-biased iDMPCre-induced recombination. Compared with mice that received vehicle (corn oil), metaphyseal trabecular bone volume and cortical porosity, each detected by micro-CT, were both nearly doubled in tamoxifen-treated mice at 14-weeks, but the bones fully normalized by 26-weeks. This transient bone mass comprised mainly low- and mid-density bone. Next, we investigated the impact of the SOCS3 mutation introduced by the same tamoxifen regimen (also applied to controls). Micro-CT scanning of iDMPCre+.Ai9. Socs3f/f femora at 16-, 20-, 26- and 32-weeks of age revealed development of profound cortical porosity. Highly porous cortical bone was detected near the growth plate at 16 weeks, which expanded towards the diaphysis with age, but the mid-diaphysis remained unaffected. Histology revealed greater levels of both bone resorption and formation in the metaphysis, indicating increased remodelling of the cortex in the presence of elevated STAT3 signalling.

These data indicate that inducing SOCS3 deletion in osteoblasts and osteocytes in a young adult skeleton prematurely increases remodelling in the cortex, leading to high metaphyseal cortical porosity. This finding suggests that suppression of STAT3 signalling in osteoblasts and osteocytes may limit age-induced cortical porosity.

Session 3: Multiscale Bone Structure and Function

S3-5 Martina Jolic

An in vivo multiscale and multimodal analysis of the impact of mechanical overload on osseointegration

M. Jolic1, C. Primeau2, M.A. Williams2, P. Thomsen1, F.A. Shah1, A. Palmquist1
(1) Department of Biomaterials, University of Gothenburg, Sweden, (2) WMG, University of Warwick, Coventry, United Kingdom

Osseointegration, the direct contact between living bone and metal implant surface, offers a reliable solution for bone reconstruction and restoration of function [1]. Although rare, implant failures can occur, especially in conditions of low bone quality, bone volume, or mechanical overload [2]. Interestingly, intentional disruption of the bone-implant interface can lead to improved implant stability [3]. With increasing reliance on metal implants, it is crucial to understand the consequences of implant overload on peri-implant bone. This study introduces an in vivo model to investigate the effects of mechanical overload on peri-implant bone, utilizing a correlative approach for multiscale and multimodal analysis of bone healing and remodelling.

Commercially pure titanium implants were micro-roughened with 5M NaOH and placed in the tibiae of female Sprague Dawley rats (n=9). After 28 days, one implant per tibia underwent mechanical overload by a 90° clockwise snap-disruption of the bone-implant interface, followed by an equal counterclockwise rotation. The undisrupted implant served as a control. For both implants, peri-implant bone healing was allowed for additional 28 d. Calcium-binding fluorescent dyes, calcein and alizarin red, were injected 3 d before and 21 d after disruption, respectively. Biomechanical anchorage was evaluated at endpoint. Implants with adjacent bone were collected for X-ray micro-computed tomography, histomorphometry, electron microscopy, and Raman spectroscopy (n=6). In bisected resin-embedded samples, bone within implant threads was used to determine bone areas formed prior and after the disruption, evaluate microarchitecture, chemical composition, and degree of bone mineralization.

After 28 d of healing, disruption of the bone-implant interface neither impaired the stability nor the level of osseointegration of previously osseointegrated, then disrupted, implants. Within implant threads, comparable stability (9.4 ± 2.9 and 8.7 ± 1.7 Ncm), bone volume (41.2 ± 6.9 and 37.1 ± 5.7%), bone-implant contact (~80%), and bone area (~60%) were measured. Our correlative analysis pipeline revealed that bone formed prior to disruption remains in close proximity to the implant surface, suggesting that mechanical disruption occurs at a distance. Moreover, a higher degree of bone mineralization and carbonate substitution, as measured by quantitative backscattered electron imaging and Raman spectroscopy, correlated to bone formed prior to the mechanical overload (Figure 1).

REFERENCES: 1F.A. Shah et al (2018) Acta Biomater, 84:1-15. 2M. Esposito et al (1998) Eur J Oral Sci, 106(3):721-64. 3C-J. Ivanoff et al (1997) Int J Oral Maxillofac Implants, 26(4):310-5.

Session 3: Multiscale Bone Structure and Function
S3-5 Martina Jolic

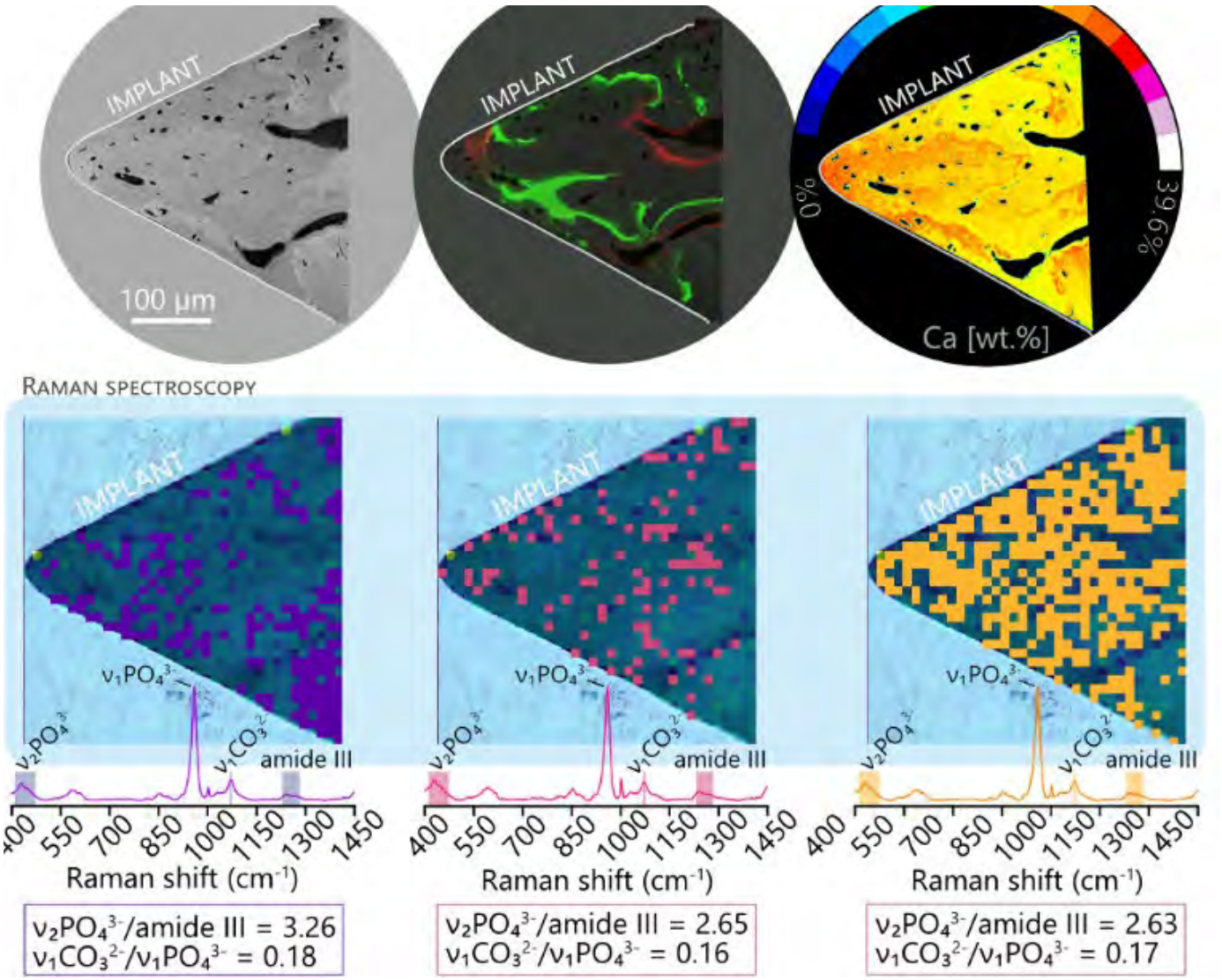

Session 3: Multiscale Bone Structure and Function

S3-6 Dilara Yilmaz

Spatially Resolved Age- and Sex-Specific Alterations in Bone Mechanomics and Mechanoregulation in Prematurely Aging PolgA Mice

Dilara Yilmaz*1, Neashan Mathavan1, Francisco Manuel Correia Marques1, Charles Ledoux1, Daniele Boaretti1, Danielle Whittier1, Esther Wehrle2, Gian N. Schädli1, Amit Singh1, Gisela A. Kuhn1 and Ralph Mueller1
(1) Institute for Biomechanics, ETH Zürich, Zürich, Switzerland, (2) AO Research Institute Davos, Davos Platz, Switzerland

Aging leads to a decline in physiological function, increasing vulnerability to frailty and osteoporosis. Bone adaptation is a key factor in maintaining skeletal integrity; however, it becomes compromised with age. The molecular mechanisms underpinning bone adaptation to mechanical stimuli, and how these processes are affected by age and sex, remain unclear.
To investigate the age- and sex-specific bone adaptation responses to mechanical stimuli, we used prematurely aging PolgA (PolgAD257A/D257A) mice to map the corresponding gene expression changes through spatial transcriptomics analysis.
Mechanical loading (either 8-10N or sham, 5 min, 3x/week) was applied to the 6th caudal vertebra (CV6) of PolgA mice for 4 weeks in young/aged females (n=14/18) and young/aged males (n=19/24). Time-lapsed in vivo micro-CT imaging (10.5 µm resolution) was used to evaluate static and dynamic morphometry. Spatially resolved transcriptomics were performed on excised vertebrae (n = 1/group) using Visium CytAssist (10x Genomics) for formalin-fixed paraffin-embedded (FFPE) sections registered to the corresponding in vivo micro-CT images. Sequencing data were analyzed with SpaceRanger followed by post-processing in Seurat in R.
Mechanical loading significantly increased net remodeling rate in young males ($p<0.01$) and females ($p<0.001$), measured as the difference between bone formation rate (BFR) and bone resorption rate (BRR). In contrast, the net remodeling rate declined in aged PolgA females, indicating negative remodeling, while aged PolgA males did not exhibit a change in the net remodeling rate compared to the sham (Fig 1A). Spatial transcriptomics analysis in the trabecular and cortical bone post-loading demonstrated most prominently an increase in Bglap (bone formation) and a decrease in Ctsk (bone resorption) expression in young PolgA mice. Aged PolgA mice, however, displayed downregulation of these genes with loading for both males and females (Fig 1B-C). In conclusion, young PolgA mice, particularly females, exhibited a robust response to mechanical loading, while this adaptive response was absent in aged PolgA mice of both sexes. Spatial transcriptomics analysis further revealed increased bone formation and resorption indicative of an enhanced osteogenic response and balanced remodeling in young loaded PolgA mice. Conversely, aged PolgA mice showed reduced formation and resorption with loading, suggesting imbalanced remodeling and reduced osteogenic activity with age.

Session 3: Multiscale Bone Structure and Function

S3-6 Dilara Yilmaz

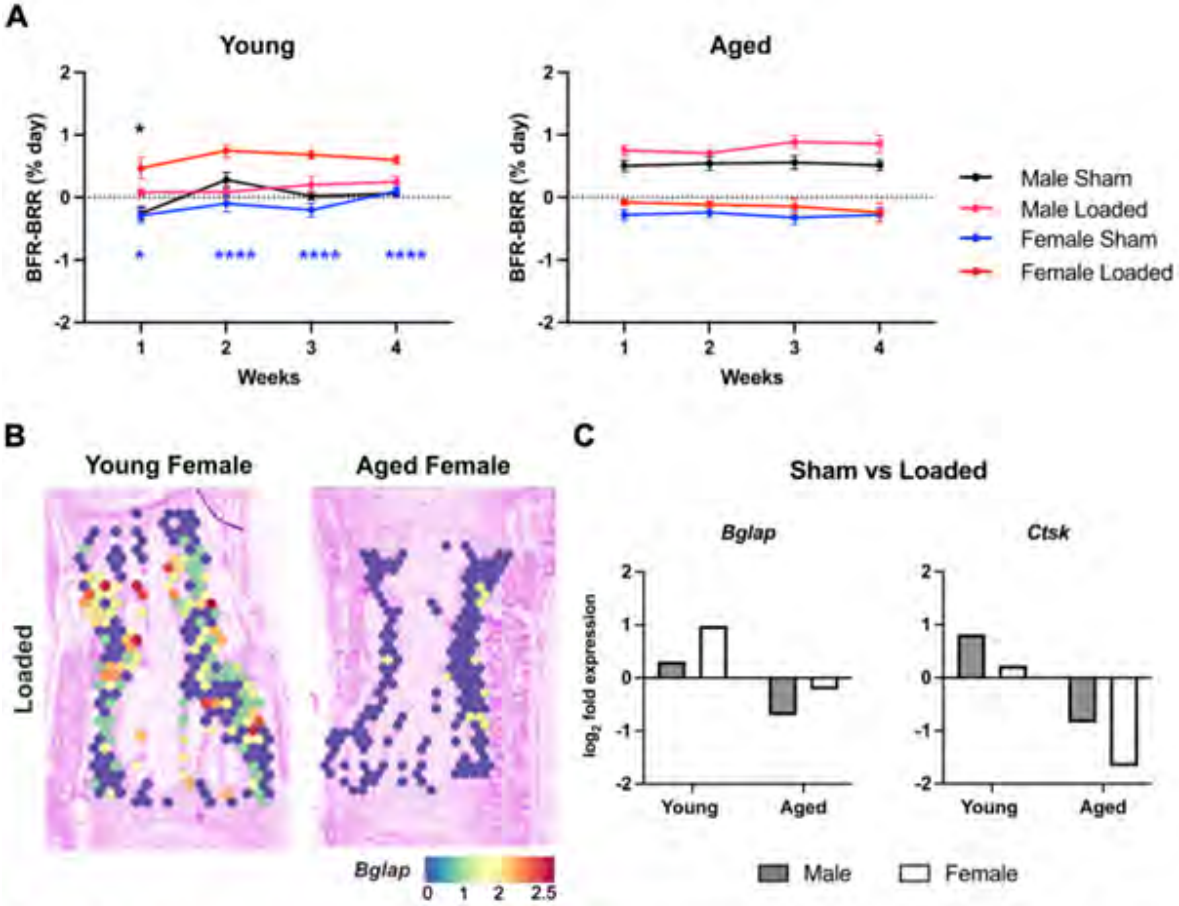

Figure 1: A) Net remodeling rate over the 4-week loading period in male and female PolgA mice. Data are presented as mean ± s.e.m. (n= 6-14 mice/group). *≤0.05, **≤0.01, ***≤0.001, ****≤0.0001determined by two-way ANOVA with Šídák's multiple comparison and significance was indicated as black for males, blue for females B) Visualization of the spatial expression patterns of *Bglap* on H&E-stained sections of young and aged female loaded PolgA mice with the scale bar indicating the the normalized expression levels. C) Gene expression profiling in sham vs loaded vertebra indicating *Bglap*, linked to bone formation and *Ctsk* associated with bone resorption.

Session 4: Clinical Bone Imaging
S4-1 Steven Boyd, PhD

HR-pQCT: State-of-the-art and prospects for clinical use

Twenty years have passed since the introduction of high-resolution peripheral quantitative computed tomography (HR-pQCT) for the assessment of human bone microarchitecture. In that time, it has emerged as an important research tool used by clinicians and scientists to learn about the pathophysiology of bone adaptation in the context osteoporosis and many other bone-affected conditions. Its rich three-dimensional data is well-suited for precise longitudinal monitoring of bone microarchitecture and associated patient-specific estimated bone strength. However, uptake as a clinical diagnostic tool has been limited, in part due challenges such as availability, regulatory approvals and demonstrated cost effectiveness. New research suggests fracture risk assessment based on HR-pQCT is comparable to current standards based on traditional bone densitometry, but its contribution to clinical care is best suited to two areas. First, leveraging microarchitectural information to assist in treatment decisions for the large subset of patients who lie in the ‘grey zone’ by current fracture risk assessment. Second, longitudinal monitoring that establishes highly refined trajectories of bone adaptation and to inform decisions to initiate treatment, monitor treatment effects, and inform cessation. This talk will provide an overview of some of the latest innovations for HR-pQCT and discuss the strengths and weaknesses for its application to clinical use.

Session 4: Clinical Bone Imaging
S4-2 Lisbeth Thomsen, MS

Intermittent Treatment with Parathyroid Hormone Overactivates Intratrabecular Tunneling, a Previously Overlooked Mode of Remodeling: A Randomized Clinical Trial in Patients with Hypoparathyroidism and Pre-Clinical Rabbit Model

Lisbeth Koch Thomsen*1,2, Kaja Søndergaard Laursen3, Ali R Rizvi4, KIM Harrison4, Lindsay Loundagin5, Xuan Wei5, Tanja Tvistholm Sikjaer6,7, Jesper Skovhus Thomsen8, Christina Moeller Andreasen1,2, Lars Rejnmark6, David Michael Lane Cooper5 and Thomas Levin Andersen 2,3,9, (1) Department of Pathology, Odense University Hospital, Odense, Denmark, (2) Molecular Bone Histology Lab, Research Unit of Pathology, Department of Clinical Research, University of Southern Denmark, Odense, Denmark, (3) Department of Forensic Medicine, Aarhus University, Aarhus, Denmark, (4) Department of Anatomy Physiology and Pharmacology, College of Medicine, University of Saskatchewan, Saskatoon, SK, Canada, (5) Department of Anatomy, Physiology and Pharmacology, College of Medicine, University of Saskatchewan, Saskatoon, SK, Canada, (6) Department of Endocrinology and Internal Medicine, Aarhus University Hospital, Aarhus, Denmark, (7) Department of Internal Medicine, Horsens Regional Hospital, Horsens, Denmark, (8) Department of Biomedicine, Aarhus University, Aarhus, Denmark, (9) Odense University Hospital, Odense, Denmark

Intratrabecular tunneling – resorption of bone within the trabeculae – has been observed in patients with hyperparathyroidism, renal osteodystrophy and patients treated with intermittent parathyroid hormone (rhPTH). However, the phenomenon has rarely been systematically quantified and may reflect an overlooked mode of trabecular remodeling.
We applied our intracortical classification scheme to trabecular bone of 68 iliac crest biopsies collected from 50 patients with hypoparathyroidism randomized to receive either placebo (PLB6; n=25) or 100 µg/day rhPTH(1–84) s.c. (PTH6; n=25) for 6 months as an add-on to conventional treatment. Additional biopsies were collected 24 months later from 18 patients who had continued open-labeled treatment with either i) conventional treatment (CON30; n=5), ii) continued rhPTH-treatment (PTH30; n=5), or iii) were withdrawn from rhPTH treatment (PTHw30; n=8). Each biopsy underwent µCT and was sectioned for histomorphometry of the intratrabecular tunneling (fig. A). For comparison, intratrabecular tunneling was investigated with µCT in vivo and ex vivo in the calcanei of ovariohysterectomized rabbits (n=4) treated with daily rhPTH(1–34) for 4 weeks.
Trabecular porosity originating from intratrabecular tunneling increased 18-fold in PTH6 compared with PLB6 ($p<0.001$), and while reduced in PTH30, intratrabecular porosity remained significantly higher than in CON30 ($p<0.05$). Trabecular pore density increased 2.5-fold in PTH6 relative to PLB6 ($p<0.001$), and further increased 1.8-fold in PTH30 relative to PTH6 ($p=0.055$), whereas mean pore diameter was only significantly increased in PTH6 (2.5-fold relative to PLB; $p<0.001$). Intratrabecular tunneling of existing pores increased 10-fold in PTH30 compared to PTH6 ($p<0.01$), and its contribution to intratrabecular porosity was significantly increased in PTH30 (30-fold relative to PTH6, $p<0.05$; 190-fold relative to CON30, $p<0.05$). Porosity from non-quiescent pores was increased in PTH6 and PTH30 compared to PLB6 (7.6-fold)/CON30 (95.4-fold), but not in PTHw30 (3.6-fold lower than PTH6; $p<0.001$). Intratrabecular tunneling was evident in rabbit calcanei after as little as 4 weeks of rhPTH(1–34) treatment (fig. B). Preliminary observations suggest similar intratrabecular remodeling patterns as those seen in human biopsies.

Session 4: Clinical Bone Imaging
S4-2 Lisbeth Thomsen, MS

Collectively, this study suggests that intratrabecular tunneling is an overlooked mode of intratrabecular remodeling, which is significantly increased with rhPTH treatment, accumulated with treatment-time, and time-lapsed imaging provides an in vivo platform for investigation of the generation of intratrabecular tunnels in the rabbit model.

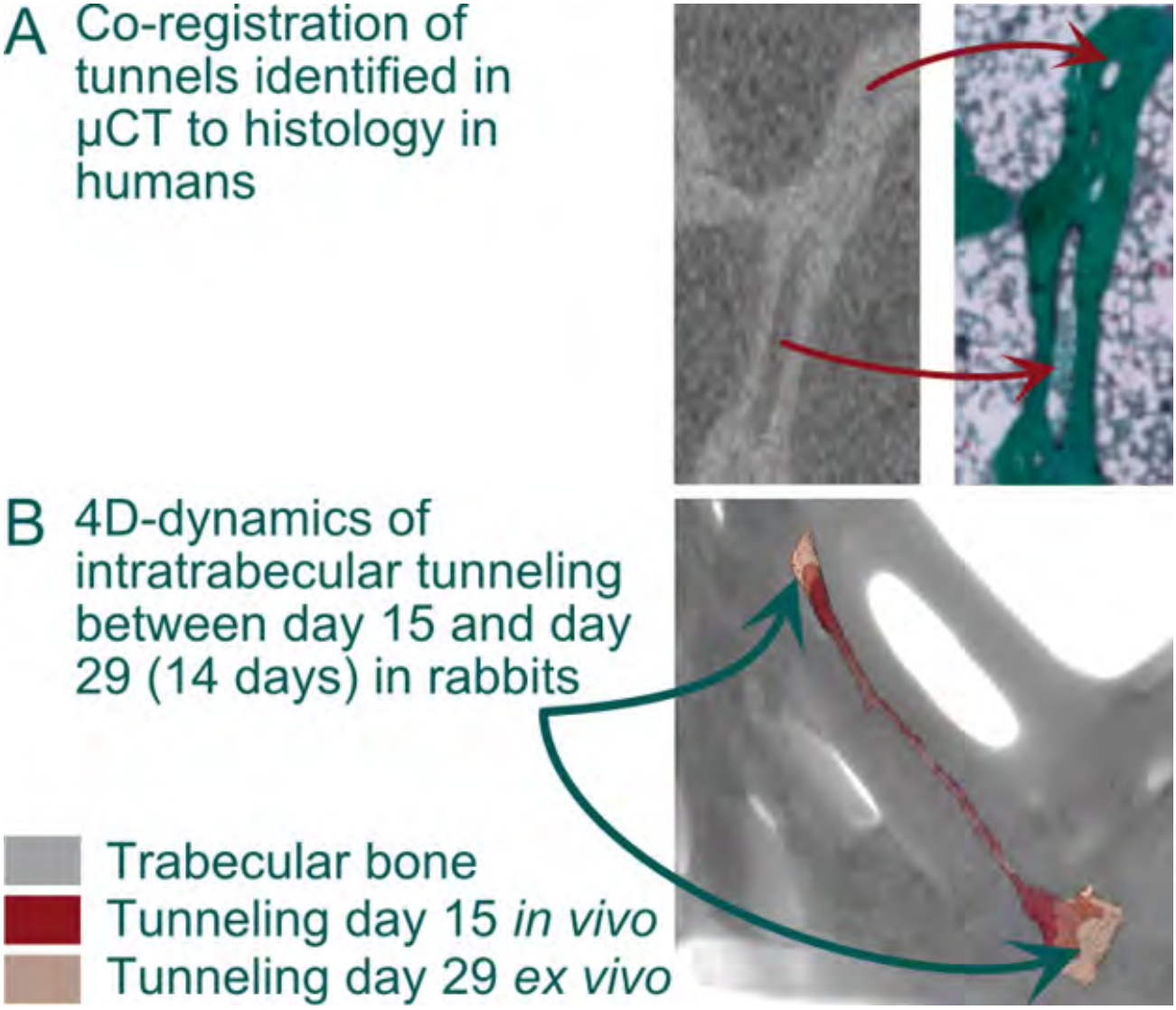

Session 4: Clinical Bone Imaging
S4-3 Liza Das, MD

Oral semaglutide, weight loss, and alterations in bone microarchitecture, vBMD, and bone turnover in obese T2DM patients with metabolic dysfunction associated with steatotic liver disease

Introduction: Diabetes, obesity and metabolic-dysfunction associated steatotic liver disease (MASLD) all predispose to impaired bone microarchitecture. However, the effect of therapeutic weight loss intended to treat obese T2DM individuals with MASLD, on bone microarchitecture is not known and evidence on the beneficial effect of semaglutide on skeletal health is predominantly preclinical. The objective of the current study was to assess bone microarchitectural alterations with oral semaglutide in obese type 2 diabetes mellitus (T2DM) with MASLD.

Methods: Obese T2DM patients with MASLD [steatosis defined as controlled attenuation parameter (CAP) > 248dB/m with/without fibrosis [defined as liver stiffness measurement (LSM)] were recruited. Oral semaglutide was initiated at 3mg daily dose, followed by 4-weekly increments to 7mg and 14mg till 52 weeks of follow-up. Those on chronic glucocorticoids (>3 months), thiazolidinediones, phenytoin, tamoxifen, estrogen, eGFR<30ml/min/1.73m2, contraindication to GLP1 agonist or with known endocrinopathy were excluded. Bone microarchitecture including volumetric BMD (vBMD) was assessed by second generation high-resolution peripheral quantitative CT. Body composition by DXA and BTMs (P1NP, CTX) were assessed at baseline and 52 weeks.

Results: There were 45 patients (49% males) with mean (± SD) age 49.4± 9.3 years, mean BMI 35.9± 6.1kg/m2 and median duration of T2DM 7 (IQR 2-10) years. All patients had hepatic steatosis (95% severe) and 70% had clinically relevant fibrosis. At 52 weeks, there was significant reduction in body weight [-7.0% (IQR 3.5 to 11.8), p=0.002] and HbA1c [-1.1% (0.7 to 2.3), p=0.001]. There was significant improvement in trabecular volumetric BMD at both radius (147.7 ± 46.5 vs 154.0 ± 47.8, p=0.00) and tibia (154.7 ± 29.4 vs 157.7 ± 32.3, p=0.00) as well as cortical volumetric BMD at tibia (908.6 ± 73.8 vs 938.2 ± 75.1, p = 0.00). Cortical microarchitecture improved in terms of increase in cortical thickness and perimeter at both sites (p<0.05). Trabecular bone volume fraction and thickness also increased at both radius and tibia (p<0.05). Tibial trabecular volumetric BMD at 52 weeks was correlated with radial trabecular volumetric BMD (Pearson co-efficient r=0.895, p=0.00), change in visceral adipose mass (r 0.483, p=0.08) and lean mass (r 0.515, p=0.05). Tibial cortical volumetric BMD was correlated with change in fat mass (r 0.461, p=0.09). Cortical thickness at radius showed a strong positive correlation with cortical thickness at tibia (r 0.633, p=0.006) and with change in HbA1c (r 0.442, p=0.09). Serum CTX (pg/ml) (335.1 ± 190.9 vs 329.8 ± 151.4, p = 0.16), and P1NP (ng/ml) (32.5 ± 13.5 vs 37.6 ± 24.1, p = 0.20) were non-significantly higher with semaglutide use.

Conclusion: Oral semaglutide resulted in significant weight loss in obese patients with T2DM and MASLD. This was associated with improvement in vBMD especially trabecular, as well as cortical and trabecular thickness and trabecular bone volume fraction.

Session 4: Clinical Bone Imaging
S4-4 Zachary Haverfield

Sex-specific Rela1onships in Femoral Neck Bone Mineral Content and Volumetric Density

Zachary. A Haverfield, Lauren E. Hayden, Amanda M. Agnew, Randee L. Hunter
The Ohio State University, Injury Biomechanics Research Center

Representations of femoral neck (Fem-N) bone quality and resulting assumptions of fracture risk typically use bone mineral density (BMD) as a proxy measure for mineralization [1]. Measures of areal/volumetric BMD (aBMD/vBMD) are normalized by size which can obscure the influence of sex-linked differential skeletal morphometry on bone strength [2,3]. Accounting for size through bone mineral content (BMC) highlights some sex-specific variations in coupled Fem-N morphometry2 and mineralization, but has yet to be explored volumetrically using quanitiative computed tomography (QCT) in specific bone compartments. Therefore, the aim of this study is to isolate sexspecific relationships between BMC and vBMD across the Fem-N including the superior and inferior cortices. Whole-body clinical QCT scans of one-hundred and forty-six female (n=70) and male (n=76) post-mortem human subjects (24-102 years) were analyzed. The resulting Fem-N Total volume of interest (VOI), including both trabecular and cortical voxels, was further segmented into VOIs for the superior (Sup) and inferior (Inf) cortex. BMC and vBMD were then calculated for all three VOIs and were compared between sexes using Kruskal Wallis tests and Pearson correlations.
Female vBMD was significantly larger than male vBMD in Fem-N Inf and Total, but males had greater mineral density at Fem-N Sup ($p<0.05$). In contrast, BMC was significantly larger in males than females at all VOIs ($p<0.05$) suggesting that size normalization of vBMD may present contrasting assump1ons of bone strength between sexes.
The rela1onship between BMC and vBMD (Fig.1) was also sex-specific where the Fem-N Inf and Sup had stronger correlations in females than males ($p<0.05$), suggesting similar representations of bone quality between the two measures in females. Conversely, there were weak relationships between BMC and vBMD at Fem-N Total VOIs in both sexes, indicating that both measures capture distinct aspects of bone structure that may differentially contribute to bone strength. Additionally, these results support previous findings [2] that size normalization obscures sex-specific relationships and differing mechanisms of maintenance for bone mass/density in the Fem-N. As the relationships between Fem-N BMC and vBMD are inconsistent across VOIs/sexes, these measures reflect different but complementary components of bone quality that would be advantageous when integrating traits that capture multiple aspects into assessments of bone quality.

References:
1. Kanis JA. Diagnosis of osteoporosis and assessment of fracture risk. World Health Organiza1on Summary Report. 2004;359(9321):1929-1936. doi:10.1016/S0140-6736(02)08761-5
2. Jepsen KJ, Bigelow EMR, Goulet RW, et al. Structural differences contribu1ng to sex-specific associa1ons between FN BMD and whole-bone strength for adult White women and men. JBMR Plus. 2024;8(4). doi:10.1093/jbmrpl/ziae013
3. Jepsen KJ, Kozminski A, Bigelow EMR, et al. Femoral Neck External Size but not aBMD Predicts Structural and Mass Changes for Women Transitioning Through Menopause. Journal of Bone and Mineral Research. 2017;32(6):1218-1228. doi:10.1002/jbmr.3082

Session 4: Clinical Bone Imaging
S4-4 Zachary Haverfield

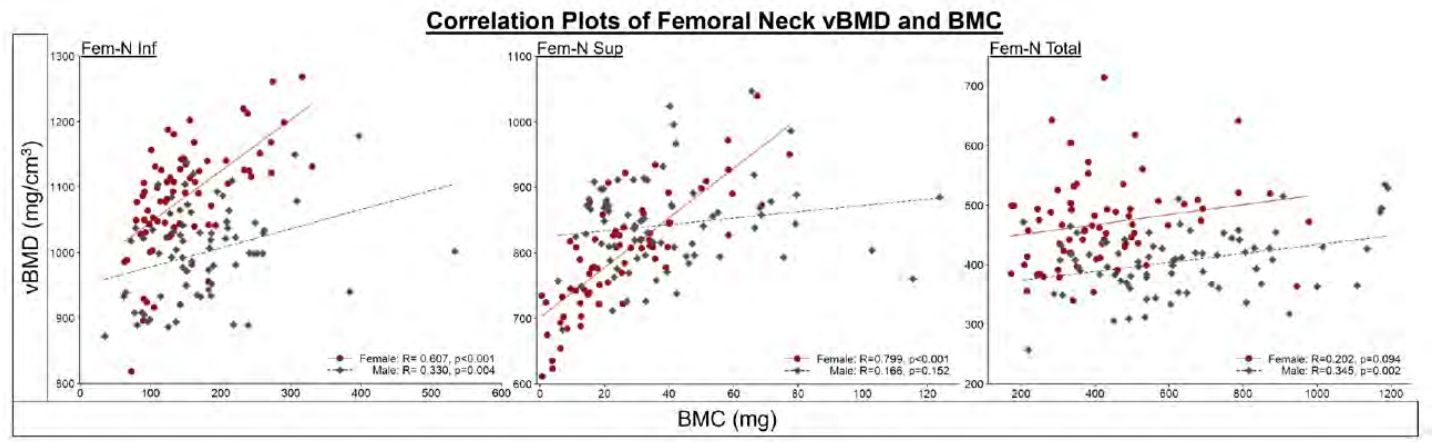

Figure 1

Session 4: Clinical Bone Imaging

S4-5 Farhan Sadik

Physics-driven Motion Simulation and Motion Correction Pipeline for HR-pQCT Bone Imaging

Farhan Sadik*1, Christopher Newman2, Stuart J. Warden3 and Rachel Kathleen Surowiec4
(1) Purdue University, West Lafayette, IN, USA, (2) Indiana University School of Medicine, Indianapolis, IN, USA, (3) Department of Physical Therapy, Indiana University School of Health & Human Sciences, Indianapolis, IN, USA, (4) Weldon School of Biomedical Engineering, Purdue University, West Lafayette, IN, USA

Introduction: High-resolution peripheral quantitative computed tomography (HR-pQCT) enables the assessment of cortical and trabecular microarchitecture at peripheral sites with nominal radiation (~0.025 mSv). However, HR-pQCT's high-resolution (voxel size ~61–82 μm) makes it extremely sensitive to motion artifacts, where even slight motion can severely impact microstructural information. The current protocol for managing subject-specific motion includes re-scanning patients, which might not be feasible within a busy workflow or for specific populations (e.g., pediatrics and individuals suffering from tremors, twitches, and spasms). While retrospective motion grading using deep learning has been described1,2, retrospective motion correction has been identified as a critical need requiring a solution.

Despite deep learning's successful application in MRI and CT motion correction3, it has not been employed in HR-pQCT due to the lack of proper patient motion models, resulting in the absence of appropriate ground truth. This study aims to address this gap by simulating physics-constrained motion scenarios to replicate actual patient movement, thereby creating training pairs that lay the necessary foundation for the widespread utilization of supervised deep learning methods where the ground truth is absolutely necessary to correct motion.

Methods: We modeled the patient motion as rotation and translation of the object, followed by retrospectively corrupting the sinograms to create motion artifacts from ground truth images. Fig.1A depicts the motion model equation, Fig.1B presents the corresponding sinogram equation resulting from motion; the consequential changes in sinograms are illustrated in Fig.1C, with simulated HR-pQCT images shown in Fig.1D, compared against real-world motion-corrupted data.

Results: The findings shown in Fig.1D are compared with genuine motion-corrupted data, revealing a qualitative similarity in streaking artifacts, indicative of our assumption that motion is caused by the rotation of the imaged object.

Conclusions and future work: The synthesized motion-corrupted data will be utilized to generate training pairs for data-driven and deep learning for motion correction without additional hardware constraints, which is currently in progress.

References link:
https://purdue0-my.sharepoint.com/personal/fsadik_purdue_edu/_layouts/15/onedrive.

Session 4: Clinical Bone Imaging

S4-5 Farhan Sadik

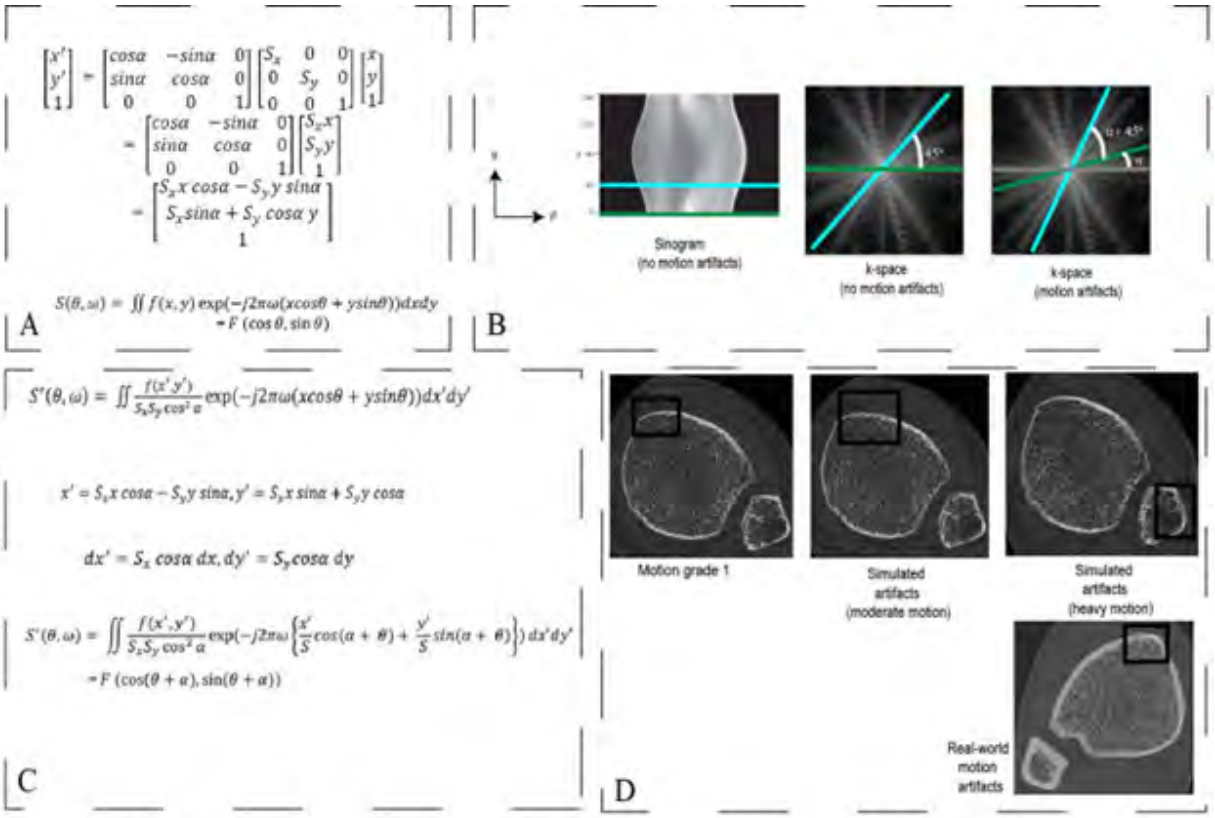

Figure 1: A simulated sinogram is created from an HR-pQCT image assuming a fan beam geometry (for 2D data processing) using ASTRA toolbox[a]. The patient motion equation is shown in "**A**", where α is the subject rotation angle and S_x, S_y is a translation in the X and Y direction respectively. From the Fourier Slice theorem, the 1D Fourier transform of the projection signal in fan-beam geometry must represent a spoke in that specific angle in the k-space. According to the Fourier Slice theorem, 1D Fourier Transform of the projection signal, without motion, $S(\theta, \omega)$ and with motion $S'(\theta, \omega)$ is shown in "**A**" and "**C**", where θ is the projection angle, ω is the angular frequency and α is the rotation angle. Therefore, we can see that additional rotation caused by patient movement rotates some spokes in the k-space to the rotation angle as shown in "**B**". Using this principle, we took multiple rotation angles and multiple projections of the sinogram where it is corrupted by motion to simulate HR-pQCT motion artifacts which are shown in "**D**". Two parameters, the rotation angle and the number of spokes to be adjusted, can be manipulated to attain different levels of motion.

Session 4: Clinical Bone Imaging
S4-6 Alyssa Williams

3D visualization of nanoscale features, including mineral ellipsoids and collagen fibrils in mineralized human bone tissue

Alyssa Williams1,2*, Tengteng Tang3, Aurélien Gourrier4,5, Michael W. Phaneuf2, Nabil Bassim1,3,6, Kathryn Grandfield1,3
(1) School of Biomedical Engineering, McMaster University, Hamilton, Ontario, Canada (2) Fibics Incorporated, Ottawa, Ontario, Canada (3) Department of Materials Science and Engineering, McMaster University, Hamilton, ON, Canada (4) Univ. Grenoble Alpes, LIPHY, F-38000, Grenoble, France (5) CNRS, LIPHY, F-38000, Grenoble, France (6) Canadian Centre for Electron Microscopy, McMaster University, Hamilton, ON, Canada

Understanding the nanoscale organization of mineral and organic components of bone tissue is crucial to understanding biomineralization processes. The fundamental building blocks of this process include mineralized type 1 collagen fibrils and ellipsoidal-shaped mineral aggregates (“mineral ellipsoids”) [1–3]. Due to the nanoscale imaging requirements and the mineralized environment, visualizing these structures requires advanced tools to characterize their arrangement. Performing high-resolution and large 3D volume imaging is accomplished in this investigation using focused ion beam scanning electron microscopy (FIB-SEM) nanotomography to image collagen fibrils and mineral ellipsoids. A transverse section of the posterior-lateral section of human tibial bone tissue was fixed and dehydrated using a graded series of ethyl acetate and embedded in EMBED 812 resin [1]. FIB-SEM nanotomography imaging was performed in the mid-cortex region of the cortical bone tissue using the Atlas 3D Nanotomography program (Fibics Inc) on a Zeiss Crossbeam 540. Imaging parameters were optimized to improve visualization of the collagen fibril banding and mineral ellipsoids. Tools, including u-net segmentation, fast Fourier transform (FFT) and inverse fast Fourier transform (iFFT) analysis, were implemented to enhance the identification of the collagen fibril organization. FIB-SEM data revealed clear visualization of type 1 collagen fibril D-banding in all orthogonal planes. 3D segmentation tools reveals the abundant presence of collagen fibrils in and around mineral ellipsoids, as well as their coalignment with mineral ellipsoids. FFT and iFFT processing reveals the presence of collagen fibrils in both high and low-mineralized regions of tissue. This study is the first segment collagen fibrils throughout the entire bone tissue volume to elucidate the interwoven structure of collagen and mineral ellipsoids. The novel iFFT workflow proposed provides a technique to enhance the visualization of collagen fibrils at the nanoscale level using FIB-SEM data. This study provides insight into the structure of collagen fibrils and mineral ellipsoids while proposing an advanced technique to improve the visualization of collagen fibrils.

Session 4: Clinical Bone Imaging
S4-6 Alyssa Williams

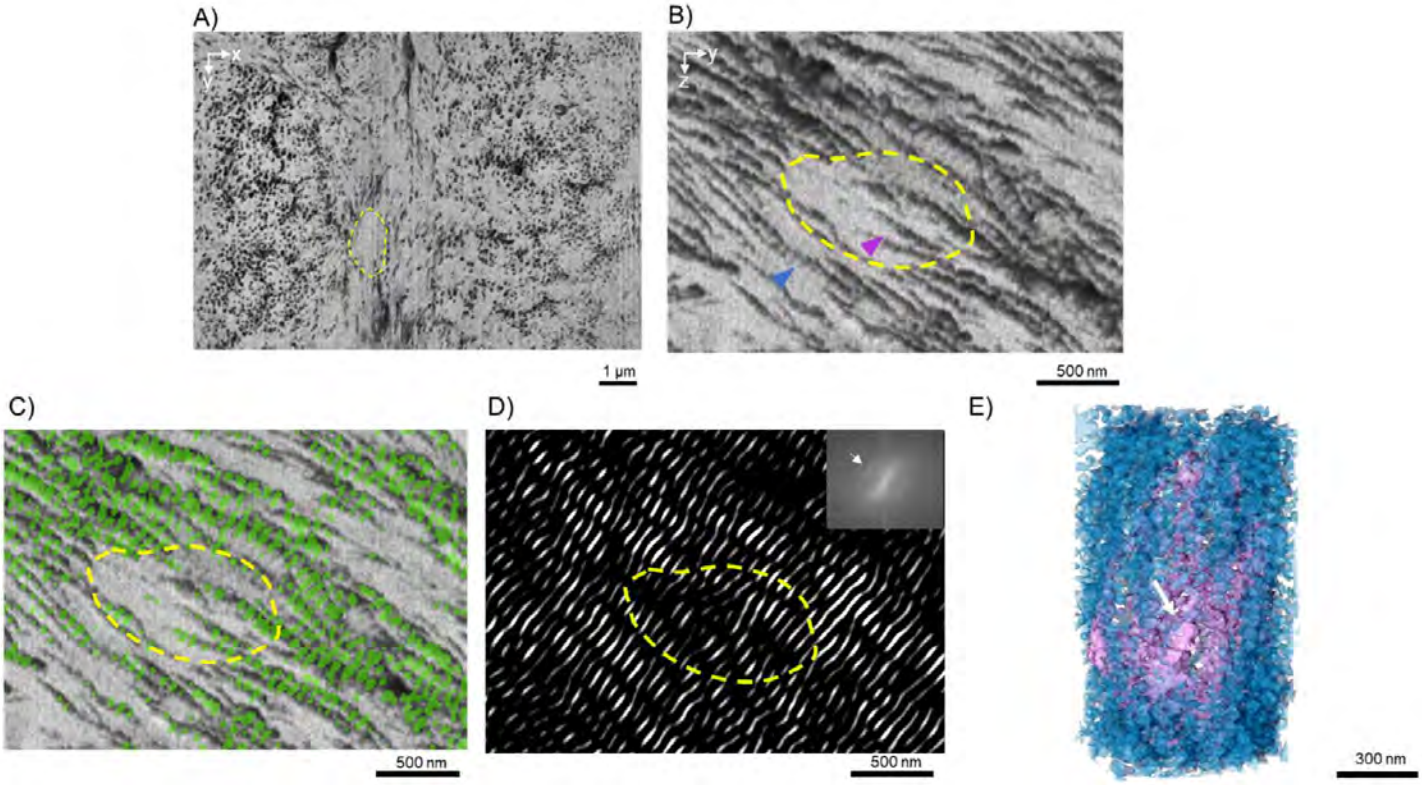

Figure 1: A) FIB-SEM cross-section with mineral ellipsoids present (yellow outline). B) Mineral ellipsoid structure with collagen fibrils visible in (pink arrowhead) and outside (blue arrowhead) of the mineral ellipsoid. C) Segmentation of collagen fibrils. D) Inverse fast Fourier transform processing analyzing collagen fibril periodicity in bone tissue. E) 3D view of mineral ellipsoid with collagen fibrils in (pink) and outside (blue) of the mineral ellipsoid including collagen fibrils crossing from the periphery to the center of the mineral ellipsoid (white arrow).

References

[1] Binkley et al. J Struct Biol (2020) 107615.
[2] Buss et al. J Struct Biol 212 (2020) 107603.
[3] Katz et al. Connect Tissue Res 21 (1989) 149–158.
[4] Raguin et al. Ssrn Electron J (2020).

Session 4: Clinical Bone Imaging
S4-7: Raj Manoharan, Micro Photonics

Dual Energy X-Ray Absorptiometry (DEXA) Applications in Small Lab Animals (even in outer space!)

Dual Energy X-Ray Absorptiometry (DEXA) is a precise, fast, and low-cost imaging modality for assessing longitudinal changes in body composition, including bone density, in mammals. Modern systems provide researchers with the ability to quantify percentages of body fat, lean tissue, and bone mineral content in laboratory animals in very short periods of time. Longitudinal changes in variables that result from dietary, genetic, or medicinal experiments can be visualized graphically with color-coded images in an easy to obtain method. A NASA study involving mice sent to the ISS used Medikors' InAlyzer2 DEXA to compare pre-space flight and post-flight changes in mice over a 28 day period to explore the effects of partial and zero gravity on body composition and bone health. DEXA was chosen over other imaging modalities such as in-vivo micro-CT or MRI due to lower radiation exposure to mice, ease of software use, instrument cost, and scan speed.

Session 5: Bone Marrow and Adipocytes

S5-1 Anjali Kusumbe, PhD

Advanced Light Sheet Imaging Techniques for High-Resolution Visualization of Bone and Bone Marrow Microenvironments

This talk will present a new and efficient pipeline for clearing and immunolabeling intact calcified tissues, allowing for superfast, single-cell resolution, and quantitative 3D imaging of skeletal elements and discovery of lymphatic vessels in bones. The application of this rapid imaging technique revealed unexpected lymphatic vascular networks in bones, challenging the conventional belief that bones lack lymphatic vessels. Using high-resolution light-sheet imaging and cell-specific mouse genetics, demonstrated the presence of lymphatic vessels in both mouse and human bones. Furthermore, this research uncovers that lymphatic vessel expand in response to genotoxic stress, driven by VEGF-C/VEGFR-3 signaling and stress-induced IL6. During lymph angiogenesis, the secretion of CXCL12 from proliferating lymphatic endothelial cells emerged as a crucial factor for hematopoietic and bone regeneration. Additionally, lymphatic vessel derived CXCL12 induced the expansion of mature Myh11+ CXCR4+ pericytes, which differentiate into bone cells and contribute to both bone and hematopoietic regeneration. The study suggests that targeting bone lymphatics could serve as a therapeutic strategy to stimulate hematopoietic and bone regeneration, particularly in the context of stress and injury, with implications for age-related impairment of bone regeneration.

Session 5: Bone Marrow and Adipocytes

S5-2 Daniel Coutu, PhD

Self-renewing Sox9+ osteochondral stem cells in the postnatal skeleton

Postnatal skeletal growth, homeostatic maintenance, and regeneration is driven by skeletal stem cells. In addition, it is well established that skeletal tissues lose their regenerative potential with age, comorbidities, and repeated trauma, possibly through stem cell exhaustion or loss of function. However, it is largely unknown where these cells reside in skeletal tissues, what molecular mechanisms regulate their self-renewal and fate decisions, and how to isolate, purify, and expand them ex vivo. Therefore, there is an urgent need for a deeper understanding of postnatal skeletal stem cells. Here, we used genetic lineage tracing, thymidine analogues retention, whole bone microscopy, imaging cytometry, in vitro assays, and single cell transcriptomics and provide the first experimental evidence for the existence of self-renewing osteochondral stem cells in the postnatal skeleton in both males and females. We also show direct comparisons between adult, fetal, mouse, and human skeletal stem cells at the transcriptome level.

Session 5: Bone Marrow and Adipocytes

S5-3 Emily Quarato, PhD

Enhanced Engulfment of Apoptotic Targets by Bone Marrow Stromal Cells Increases Their Senescence, Decreases Bone, and Causes Myeloid Skewing.

Emily R. Quarato1,4,5, Noah A. Salama4,6, Adam Tyrlik4,6, Roman Eliseev4,5, and Laura M. Calvi3,4,5
(1) Department of Environmental Medicine, University of Rochester Medical Center, Rochester, NY; (2) Department of Pathology and Laboratory Medicine, University of Rochester Medical Center, Rochester, NY; (3) Department of Medicine, University of Rochester Medical Center, Rochester, NY; (4) Wilmot Cancer Institute, University of Rochester Medical Center, Rochester, (5) Center for Musculoskeletal Research, University of Rochester Medical Center, Rochester, NY (6) Department of Microbiology and Immunology, University of Rochester Medical Center, Rochester, NY

Bone marrow stromal cell (BMSC) dysfunction impacts age-induced bone loss and alters support for hematopoietic stem cells (HSCs). One hallmark of BMSC dysfunction is senescence however, the mechanisms inducing BMSC senescence remains unclear. Previously we demonstrated during aging that bone marrow macrophages become deficient in their ability to clear apoptotic cells, a process known as efferocytosis. While macrophages act as the primary efferocytic cells, we've shown that BMSCs can contribute to efferocytic clearance. Thus we hypothesized that excess efferocytosis may contribute to BMSC dysfunction, and represent a novel mechanism of senescence, bone loss and initiation of hematopoietic malignancy. Using in vitro and in vivo functional assays and scRNA sequencing in young (3m) and aged (24m) mice we found that BMSCs increase their efferocytic burden during aging. Additionally, efferocytic BMSC had increased markers of senescence (p53 & p21) compared to non-efferocytic counterparts. To confirm that increased efferocytic burden induced BMSC senescence, we developed a mouse model of enhanced efferocytosis by BMSCs (Bai1xPrxCre). We confirmed increased rates of efferocytosis (1.2x fold) and senescence via βgal (2x fold) in vitro. Consistent with increased senescence, Bai1xPrxCre mice had a 20% decrease in CFU-F/OB formation, and an 8% reduction in cortical thickness at 3 months, which declined significantly with age (12m). Consistent with BMSC dysfunction we found decreased HSC support via a 40% reduction in colony formation. Analysis of bone marrow from Bai1xPrxCre mice found premature myeloid skewing, a common phenotype of aging. As high levels of efferocytic activity are associated with BMSC dysfunction, we aimed to block BMSC efferocytic activity. Using pharmacological and transcriptional data we identified Axl as the primary efferocytic receptor on BMSCs. In mice with global loss of Axl, BMSCs had decreased efferocytic efficiency in vitro (-1.27x fold) and in vivo (-1.6x fold). In concordance, we found Axl mice had a 25% increase in CFU-F/OB formation, and a 9% gain in cortical thickness at 3 months, which remained significantly higher than WT with aging. To determine if the increased bone was due to a reduction in BMSC senescence, we measure BMSC senescence in vivo via β-gal and found a significant reduction at 24m of age (3x fold). Collectively, our data support the idea that excess BMSC efferocytosis is a novel mechanism to induce senescence and may be an underappreciated mechanism associated with bone loss and hematopoietic malignancy in settings of defective macrophages, as seen in aging, obesity, and diabetes-induced bone loss. Given the unique reliance of BMSC efferocytosis on Axl, a molecule that can be pharmacologically targeted, this novel mechanism may be leveraged for the treatment of bone loss in aging and in other diseases caused, in part, by BMSC efferocytic excess.

Session 5: Bone Marrow and Adipocytes

S5-4 Marta Diaz del Castillo, PhD

Multiple myeloma induces angiogenesis and neuronal degeneration in the human hematopoietic bone marrow.

Martin SJ Christensen1,2, Rebecca E. Andrews3,4, Aritri Mandal4, Andrew D. Chantry3,5, Thomas L Andersen1,2,6,7, Anne-Marie Heegaard8 and Marta Diaz del Castillo*1,2,
(1) Molecular Bone Histology (MBH) team, Department of Forensic Medicine, University of Aarhus, Aarhus, Denmark, (2) The Danish Spatial Imaging Consortium (DanSIC), Denmark, (3) Sheffield Myeloma Research Team, Department of Oncology and Metabolism, Mellanby Centre for Bone Research, University of Sheffield Medical School, Sheffield, United Kingdom, (4) Department of Haematology, Sheffield Teaching Hospitals NHS Foundation Trust, Royal Hallamshire Hospital, Sheffield, United Kingdom, (5) Sheffield Myeloma Research Team, Department of Oncology and Metabolism, Mellanby Centre for Bone Research, University of Sheffield Medical School, Sheffield, UK, Sheffield, United Kingdom, (6) Department of Clinical Research, University of Southern Denmark, Odense, Denmark, (7) Department of Clinical Pathology, Odense University Hospital, Odense, Denmark, (8) Department of Drug Design and Pharmacology, University of Copenhagen, Copehangen, Denmark

Multiple myeloma (MM) is a plasma cell cancer of the bone marrow that is always preceded by the premalignant conditions monoclonal gammopathy of undetermined significance (MGUS) and smoldering MM (SMM). Patients with MGUS/SMM present <10% plasma cell infiltration and 1-10% yearly risk of progression to MM. While the effect of MM on the bone marrow microenvironment is becoming increasingly studied, nothing is known about bone marrow innervation in this patient population. Here, we collected diagnostic iliac crest bone biopsies from 20 newly diagnosed MM patients and 17 MGUS/SMM patients to characterize the distribution of CD138+ plasma cells, CD34+ blood vessels, PGP9.5+ nerve profiles and tyrosine hydroxylase (TH)+ sympathetic nerve profiles. Formalin-fixed, paraffin-embedded bone biopsies were sectioned at 3.5µm thickness, immunostained and analyzed by artificial intelligence assisted histology. We found that biopsies from patients with MM presented higher CD138+ plasma cell burden compared with MGUS/SMM ($p<0.001$), along with decreased bone marrow PGP9.5+ nerve profile density ($p<0.05$). The density of TH+ nerve profiles was similar between groups, suggesting cancer-induced neurotoxicity of non-sympathetic nerve fibers. Spatial dissection of these results demonstrated that the decrease in PGP9.5+ nerve profile density was restricted to the hematopoietic niche (>100 µm from bone surfaces). In contrast, the density of CD34+ blood vessels was significantly higher in the hematopoietic marrow of patients with MM compared with MGUS/SMM ($p<0.05$). As MM, but not MGUS/SMM, presented increased density of CD138+ plasma cells in the hematopoietic niche compared with the endosteal ($p<0.0001$), the tumor-induced angiogenesis and neurotoxicity may be directly mediated by the increased presence of cancer cells. Indeed, the density of CD34+ blood vessels significantly correlated with tumor burden in MM. In contrast, PGP9.5+ nerve density was only associated with tumor burden in MGUS/SMM patients, while we encountered neuronal degeneration with plasma cell densities >1,000 CD138+ cells/mm2. In addition, the percentage of PGP9.5+ nerve profiles associated (<25µm) with blood vessels was <50% in all patients, compared

to previous reports of >80% association in non-cancer patients, indicating profound neuronal remodeling even during the premalignant MGUS/SMM conditions. We propose that MM induces a profound cell type dependent reprogramming of the bone marrow microenvironment, including angiogenesis and degeneration of non-sympathetic nerve fibers.

Session 5: Bone Marrow and Adipocytes

S5-5 Johanna Besold

Skeletal stem/progenitor cells (SSPCs) contribute to the anabolic actions of intermittent PTH through PDGF receptor signaling

Johanna Besold*1, Chloë Goossens1, Nicolas Peredo1, Dana Trompet1, Natalie A. Sims2,3 and Christa Maes1,
(1) Laboratory of Skeletal Cell Biology and Physiology (SCEBP), Skeletal Biology and Engineering Research Center (SBE), Department of Development and Regeneration, KU Leuven, Leuven, Belgium, (2) Department of Medicine at St. Vincent's Hospital, The University of Melbourne, Melbourne, Australia, (3) St. Vincent's Institute of Medical Research, Melbourne, Australia

Trabecular osteoblasts in adult life derive from skeletal stem/progenitor cells (SSPCs), which are generally quiescent reticular and perivascular stromal cells residing in the bone marrow. Although increased osteoblast numbers are a hallmark of intermittent parathyroid hormone (iPTH) osteoporosis treatment, the contribution of SSPC-activation to its bone-building actions is unclear, and insights in the molecular mechanisms are lacking. Based on previous work, we here investigated the roles of SSPCs marked by expression of platelet-derived growth factor receptors (PDGFRs), vascular interplay, and PDGFR signaling in the anabolic actions of iPTH in mice.
Firstly, qPCR revealed significantly elevated expression of PDGF ligands (-B,-C,-D) and receptors (PDGFRα/β), and related angiogenic signals (VEGF, MMP9), upon iPTH-treatment in vitro and in vivo, suggesting potential stromal-vascular involvement. Indeed, secondly, 3D confocal image analysis of cleared bone sections showed a 40% increase in trabecular bone surfaces immediately (<5µm) juxtaposed by endomucin+ blood vessels (27.3 ± 10.5% in vehicle-treated vs 44.7 ± 5.4% after 2 wks daily iPTH; $P<0.05$, n=4-5). Vessels in iPTH-treated mice had significantly less coverage by pericytic Prrx1-Cre;Ai9/tdTom+ SSPCs and a greater number of short branches, consistent with a proangiogenic state. Thirdly, flow cytometry after 10 days of iPTH in young adult mice revealed significantly lower (-17%) SSPC numbers (CD45/Ter119/ Tie2− CD51+Thy−6C3−CD105−CD200+), along with a 30% increase in more committed progenitor fractions ($P<0.001$ vs vehicle, n=6/group). Concomitantly, iPTH increased osteoblast differentiation (2.8-fold higher osteocalcin mRNA levels, qPCR), trabecular bone volume (+24%, µCT) and thickness (+16%). Preliminary flow cytometry and lineage tracing data suggest an early decrease of PDGFRα- (-47%, $P<0.001$) and PDGFRβ-expressing SSPCs (-30%, $P<0.01$) after 3 days of iPTH, followed by an expansion of PDGFRβ-lineage descendants, and differentiation into Col1-GFP+ osteoblasts. Altogether, these data suggest that iPTH may recruit PDGFR+ SSPCs for osteoblastogenesis by stimulating their release from perivascular niches.
To test whether PDGFR signaling is functionally required for the iPTH response, we generated mice lacking both PDGFRs in SSPCs using the Prrx1-Cre strain. In control mice, iPTH-treatment (80 µg/kg, 4 wks) significantly increased osteoblast number (3.5-fold more than vehicle controls, n=3-6, histomorphometry), trabecular thickness (+38%, µCT), and mineralized surface (+60%, calcein labeling), whereas loss of PDGFRα/β blocked all these effects (n=5-8; 2-way ANOVA).
In conclusion, this work uncovers that PDGFR+ SSPCs respond to iPTH and that PDGF-PDGFR signaling mechanistically contributes to the anabolic effect, likely by mediating SSPC expansion and differentiation into osteoblasts.

Session 5: Bone Marrow and Adipocytes
S5-6 Natalie Sims, PhD

Immature neutrophils in bone marrow inhibit osteoclast differentiation in vivo and in vitro

Tsuyoshi Isojima*1,2, Blessing Crimeen-Irwin1, Narelle E. McGregor1, Ingrid Poulton1, Emma C Walker1 and Natalie A. Sims1,3,
(1) St. Vincent's Institute of Medical Research, Melbourne, Australia, (2) Toranomon Hospital, Tokyo, Japan, (3) Department of Medicine at St. Vincent's Hospital, The University of Melbourne, Melbourne, Australia

Neutrophils differentiate in the bone marrow before egressing to the circulation, where they can stimulate osteoclast formation during inflammation by releasing cytokines. Despite the proximity of marrow-resident neutrophil progenitors to bone, they have no known role in regulating bone resorption and formation. We recently reported that mice lacking G-CSFR (Granulocyte Colony Stimulating Factor Receptor) in addition to osteoblast-targeted deletion of SOCS3 (Suppressor of Cytokine signalling 3) lack of cortical bone formation due to exceptionally high levels of trabecular bone resorption and formation. Since G-CSFR null mice have very few neutrophil progenitors in the marrow and this phenotype was restricted to marrow-facing bone surfaces, we hypothesized that neutrophil progenitors in the marrow inhibit osteoclast formation, at least when bone remodelling is high.

To test this, we treated 6 week old male control (Dmp1Cre) and SOCS3-deficient (Dmp1Cre.Socs3f/f) mice with anti-Ly6G 1A8 antibody or rat IgG isotype control for 2 weeks. This significantly increased immature neutrophils in the marrow by 25%. This short treatment had no effect on femoral bone mass. However, in SOCS3-deficient mice which have elevated bone resorption, their mRNA levels of osteoclast markers (Dcstamp, Acp5 (TRAP), both ~3x control) and the osteoblast marker Col1a1 (2x control) were lowered to control levels. This was not observed in control mice, suggesting that immature neutrophils inhibit osteoclast formation and bone formation, but only when they are at high levels.

Next, 6 week old female C57BL/6 mice, control (Dmp1Cre) and SOCS3-deficient (Dmp1Cre. Socs3f/f) mice were treated for 6 weeks with rat IgG (control) or anti-Ly6G 1A8 antibody plus anti-IgG2A. Unlike the previous protocol, this significantly reduced marrow pre-neutrophils (by 50%). The treatment reduced femoral trabecular bone mass (by 50%) in all three strains. It also reduced total femoral bone mass with no change in cross-sectional area. The lower bone mass was restricted to a reduction in high density bone content, particularly in the metaphysis. This was associated with a doubling in trabecular osteoclast surface, but no change in osteoblast surface, suggesting that marrow pre-neutrophils inhibit osteoclast formation.

Finally, since pre-neutrophils, unlike mature neutrophils, survive in culture, we co-cultured RAW264.7 cells with FACS-purified pre-neutrophils from C57BL/6 mice. Addition of pre-neutrophils dose-dependently inhibited osteoclast differentiation. This effect was halved by preventing cell-cell contact of the two populations with a membrane, suggesting that close proximity is needed.

In summary, this work identifies a novel mechanism where bone marrow neutrophil progenitors inhibit osteoclast differentiation, thereby limiting trabecular and endocortical bone resorption in vivo.

Session 6: Mechanoregulation of Bone Development and Regeneration

S6-1 Elazar Zelzer, PhD

From feedback to function: understanding proprioception's role in musculoskeletal biology

Proprioception, often referred to as the "sixth sense," is crucial for our ability to move and maintain posture without conscious thought. This complex sensory system provides feedback about body position, movement, and balance by detecting changes in muscle length, tension, and joint angle. In musculoskeletal biology, proprioception plays a pivotal role in coordinating movements, ensuring joint stability, and maintaining postural equilibrium. Research into proprioception can lead to significant insights into various conditions, such as scoliosis and hip dysplasia, and contribute to developing therapeutic strategies for improving mobility and quality of life, especially as the body ages and proprioceptive functions naturally decline.

Session 6: Mechanoregulation of Bone Development and Regeneration

S6-2 Chao Liu, PhD

Mechanical regulation of angiogenesis-osteogenesis coupling during bone regeneration

Bone repair is sensitive to the external mechanical environment. Controlled mechanical loading prior to matrix deposition inhibits functional regeneration, while loading during or after this phase supports angiogenesis and bone regeneration. Blood vessels are also mechanosensitive to loads on the extracellular matrix. A unique blood vessel type in bone, Type H vessels, is defined by high expression of CD31 and Endomucin, and is tightly coupled with osteogenesis. However, how externally applied controlled mechanical loading regulates Type H vessels during bone regeneration is still unclear. Using deep tissue imaging to visualize and quantify the blood vessels and surrounding cells during bone defect repair, we found new mechanisms in distinct cell types that contribute to the mechanosensitivity of bone regeneration.

Session 6: Mechanoregulation of Bone Development and Regeneration

S6-3 Thomas Ambrosi, PhD

Decoding niches of developing human skeletal stem cell lineages

As the impact of skeletal disorders resulting from aging continues to increase and reliable treatments remain sparce, new and innovative approaches are required to prevent bone loss and restore skeletal tissues. Understanding developmental processes of the musculoskeletal system could provide powerful clues for the development of new translational remedies. Skeletal stem cells (SSCs) present a promising therapeutic option, but progress has been hindered by a lack of understanding regarding the identity and function of homogeneous SSC populations in humans. To address this, a study was conducted using a combination of prospective flow cytometric isolation and SmartSeq2 single cell RNA-sequencing (scRNAseq) to analyze the human SSC lineage tree in fetal long bones, vertebral tissue and calvarium. This revealed unique SSC subtypes with distinct clonal dynamics. To reconstruct their spatial distribution and specific niches in situ, we used scRNAseq-guided RNAscope, confirming anatomical localization and functional associations. We then optimized Nanostring's CosMX platform for spatial transcriptomic readouts of skeletal tissues on the single cell level. Growth plate and vertebral fetal bones were enriched for osteochondral genes, while periosteal and suture tissues expressed more stromal and fibrogenic markers. SSC variants in subregions with high bone-forming activity at different skeletal sites associated with either endochondral or intramembranous ossification showed unique enrichment for genes of disparate signaling pathways. We also observed various areas of early hematopoiesis with distinct skeletal-immune cell crosstalk. Overall, this research provides novel approaches to interrogate skeletal tissues using spatial transcriptomic methods that have not been previously feasible with available technology.

Session 6: Mechanoregulation of Bone Development and Regeneration

S6-4 Matthias Walle, PhD

Investigating the time-dependent recovery of spaceflight-induced bone resorption in astronauts

Matthias Walle1 , Leigh Gabel1 , Danielle E. Whi4er1 , Anna-Maria Liphardt2 , Paul A. Hulme1 , Martina Heer3 , Sara R. Zwart4 , Scott M. Smith5 , Jean D. Sibonga5 , Steven K. Boyd1
(1) University of Calgary, Calgary, Alberta, Canada (2) University Hospital Erlangen, Friedrich-Alexander-Universität Erlangen-Nürnberg, Erlangen, Germany (3) University of Bonn, Bonn, Germany (4) University of Texas Medical Branch, Galveston, USA (5) NASA Lyndon B. Johnson Space Center, Houston, USA

Bone remodelling is a mechanically regulated process whereby osteoblastic formation is coupled biochemically to osteoclastic resorption. While disuse is known to cause bone loss, it is unknown if disuse-induced changes to bone microarchitecture are permanent or can be recovered through coupling mechanisms upon reloading. This study investigated bone recovery in 17 astronauts (14 male, 3 female) using spaceflight as a model for disuse and reloading.

High-resolution peripheral quantitative computed tomography (HR-pQCT, XtremeCT II, Scanco Medical AG, 60.7 µm)scans of the distal tibia were performed before and after 4-7 months in microgravity, on return (R) at R+0, R+6 and R+12 months. Bone turnover markers assessed metabolism. Image registratin in 3D identified local bone formation(Tt.F) and resorption (Tt.R) sites in vivo. Mechanical stimuli were quantified using micro-finite element analysis. Odds ratios determined the likelihood of bone formation (ORF) and resorption (ORR) with strain. Recovery of resorption sites was assessed by quantifying the fraction of bone formation at locations previously resorbed during spaceflight.

We evaluated early (R+0—R+6) and late (R+6—R+12) recovery phases to determine the time-dependent nature of coupling between unloading-induced resorption and subsequent formation during recovery. In microgravity, resorption was 4.5 times higher than formation, followed by targeted formation post-flight (Figure 1A). Remodelling correlated between tibiae (R=0.87) and with turnover markers. Mechanoregulation was weaker in-flight (ORF=2.3±0.5, ORR=2.0±0.7) than post-flight (ORF=5.5±3.2, ORR=6.5±2.7, Figure 1B). Notably, 31±10% of bone formed in the first six months of recovery occurred at sites resorbed during spaceflight, higher than months 6-12 (2.5±2.7%), suggesting a limited capacity to reverse loss aeer 6 months of reloading (Figure 1C). The strong relationship between remodelling sites and mechanics, along with the identified time limits for recovery, suggests that bone remodelling is jointly controlled by mechanical stimuli and coupling factors. Over time, unloading-induced resorption sites may become arrested, rendering the recovery process ineffective despite mechanical stimulation. This research has implications for long-duration spaceflight and elucidates fundamental mechanisms of bone adaptation to mechanical loads, relevant beyond microgravity.

Session 6: Mechanoregulation of Bone Development and Regeneration

S6-4 Matthias Walle, PhD

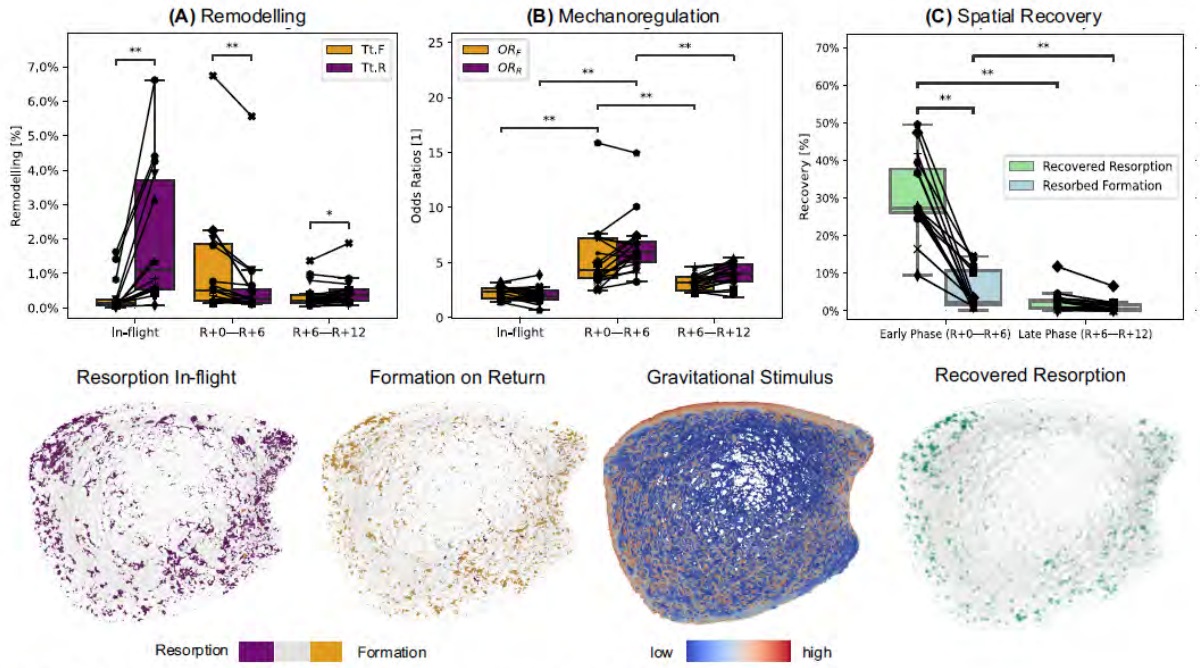

Figure 1: Bone remodelling and recovery in astronauts assessed by HR-pQCT.

Session 6: Mechanoregulation of Bone Development and Regeneration

S6-5 Keita Nagira, MD, PhD

Effects of lunar gravity on calcaneal bone metabolism and the microstructure of osteochondral unit in the calcaneocuboid joint

BACKGROUND: The microstructural changes of the osteochondral unit (OCU) in the calcaneocuboid joint due to lunar gravity are unknown. OBJECTIVE: To evaluate the effects of lunar gravity on calcaneal bone metabolism and the microstructure of osteochondral unit in the calcaneocuboid joint.

METHODS: The hind legs of the following two groups of mice provided in collaboration with the Japan Aerospace Exploration Agency (JAXA) were used. 1. flight group (1/6G); 24 legs of 12 mice reared in lunar gravity for approximately 4 weeks in an on-orbit cage of JAXA's Kibo launched at 9 weeks of age. 2. ground group (1G); mice of the same age and week as 1 reared on the ground as control. Except for three mice in the 1/6G group that lost more than 10% body weight, non-decalcified specimens were prepared and bone morphometry of the cancellous bone of the calcaneus, cortical bone of calcaneal bottom, and the OCU of the calcaneocuboid joint were measured, then compared between groups. The subchondral bone plate in the OCU was divided into two layers, the non-osteocyte layer following the articular cartilage and the osteocyte layer underneath it.

RESULTS: In 1/6G group, cortical bone of calcaneal bottom was thinning, the number of osteocytes in the cortical bone was significantly reduced, and the number of empty lacuna of osteocytes was significantly increased. Markedly increased bone resorption and decreased bone formation occurred both in cortical and trabecular bone, with thinning of the total cortical bone thickness and a 50.5% reduction in trabecular bone volume. Further, in 1/6G group, OCU in calcaneocuboid joint, the number of osteocytes in osteocyte layer in subchondral bone plate was significantly reduced ($p<0.01$). The thickness both of osteocyte layer and articular cartilage were thicker, while non-osteocyte layer was 62.5% thinner ($p<0.01$).

CONCLUSION: The reduction of mechanical stress due to lunar gravity induced osteocyte apoptosis which led osteoporosis both of calcaneal cortical and cancellous bone, while suppressed endochondral ossification of the articular cartilage, resulting in marked structural changes.

Session 6: Mechanoregulation of Bone Development and Regeneration

S6-5 Keita Nagira, MD, PhD

A. Phots of calcaneus and calcaneocuboid joint of each group (non-decalcified specimen)

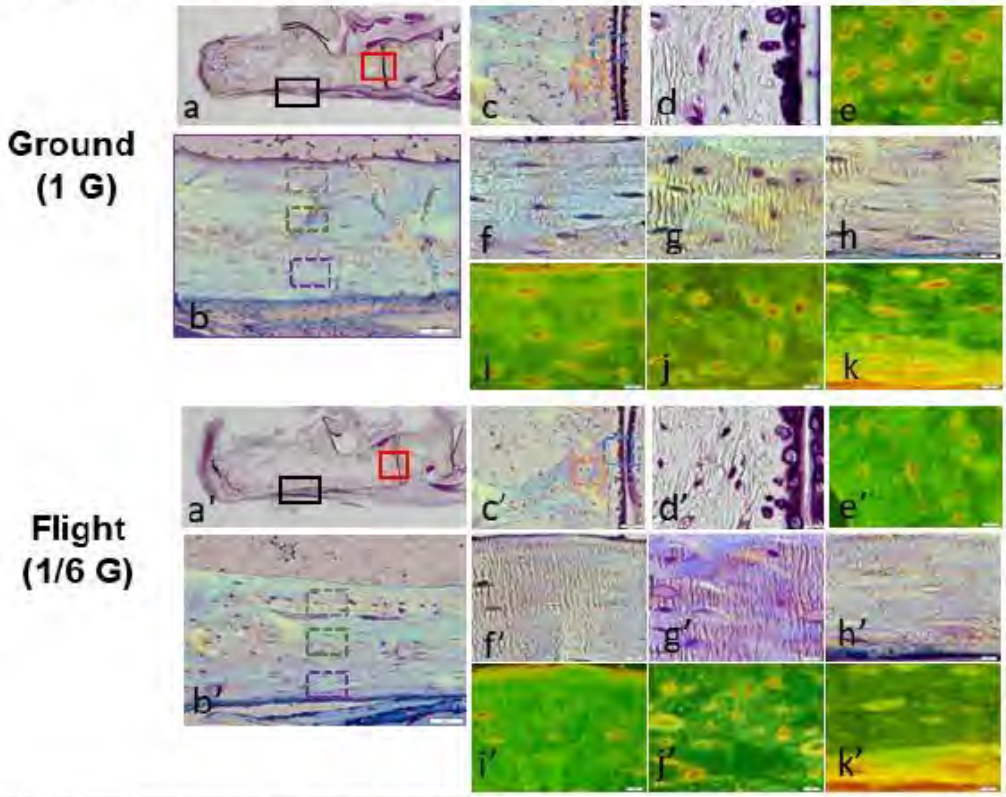

a. overview, b. cortical bone of the calcaneus (black line in a), c. osteochondral unit (OCU) of calcaneocuboid joint (red line in a), d) blue dotted line in c, e) orange dotted line in c, f & i. inner circumferential plate (grey dotted line in b), g & j. interstitial plate (green dottoed line in b), h & k. outer circumferential plate (purple dotted line in b) . * The apostrophe is each figure of flight control group corresponding to ground control group.

B. Cortical bone thickness of the calcaneal bottom

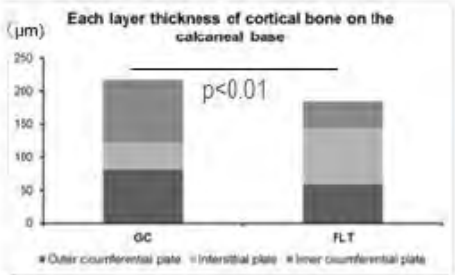

C. Osteocyte morphometry of the each layer in calcaneus

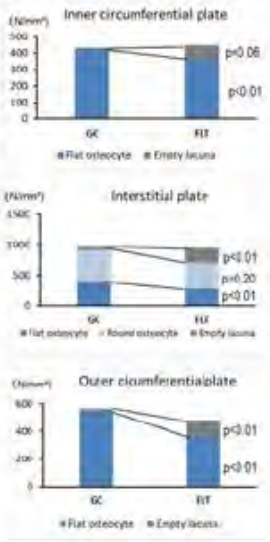

D. Each layer thickness of OCU in the calcaneocuboid joint

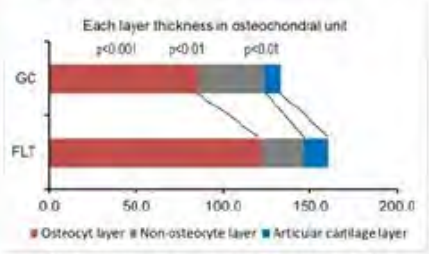

D. Osteocyte morphometry of the subchondral bone plate in OCU

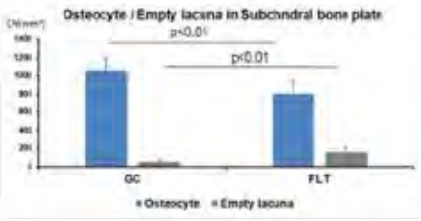

In fright control group; B) cortical bone of calcaneal bottom was thinning; C) the number of osteocytes in each layer was significantly reduced; D) the thickness of osteocyte layer of subchondral bone plate was thickening; E) the number of osteocyte was significantly reduced.

Session 6: Mechanoregulation of Bone Development and Regeneration

S6-6 Christopher Panebianco

YAP and TAZ regulate fetal growth plate chondrocyte hypertrophy and maturation

Christopher Panebianco* and Joel D. Boerckel, University of Pennsylvania, Philadelphia, PA, USA

Long bone growth occurs through continued expansion and remodeling of growth plate cartilage, via chondrocyte proliferating and hypertrophy; however, the transcriptional mechanisms are poorly understood. The transcriptional regulators yes-associated protein (YAP) and transcriptional co-activator with PDZ-binding motif (TAZ) control the development of many organs, including bone. Deleting YAP/TAZ from Col2a1-lineage chondrocytes impaired bone growth, but surprisingly did not alter proliferating chondrocytes.1 Recently, our group showed that deleting YAP and TAZ from Osterix-expressing (Osx) osteoprogenitors and hypertrophic chondrocytes (HCs) also impaired bone development.2 Together, these findings suggest HC-intrinsic roles of YAP/TAZ signaling, but how they regulate hypertrophy and bone growth is unknown.

In wildtype (WTfl/fl) growth plates, YAP and TAZ immunostaining was minimal in proliferating chondrocytes, but abundant in HCs (Fig 1A). We therefore deleted YAP and TAZ from HCs using a Col10a1-Cre mouse (YAP/TAZ cKOCol10), and analyzed hypertrophic cartilage at E17.5. Cre-mediated recombination reduced the percentage of YAP+ and TAZ+ HCs in the distal femur hypertrophic zone (HZ) by 60% and 50%, respectively, and did not alter YAP/TAZ expression in the proliferating zone (Fig 1A). YAP/TAZ deletion elongated the HZ and caused precocious hypertrophy initiation (Fig 1B). HZ elongation was characterized by expansion of pre-hypertrophic and calcified hypertrophic regions, but did not alter the morphology of the transverse cartilage septum (Fig 1C). Together, these findings demonstrate that HC-intrinsic YAP/TAZ signaling regulates both hypertrophy initiation and maturation. Previously, we showed that YAP/TAZ deletion from Osx+ HCs and osteprogenitors caused both growth plate expansion and disordered remodeling of the cartilage septum.2 Here we show that YAP/TAZ cKOCol10 phenocopied Col2a1-cKO mice,1 with hypertrophic expansion, but normal transverse cartilage septum. Thus, YAP and TAZ act intrinsically in HCs to control hypertrophy without altering recruitment of remodeling capillaries and septoclasts to the chondro-osseous junction. Future studies will mechanistically explore how HC-intrinsic YAP/TAZ signaling controls endochondral ossification, but our data shows that HC-intrinsic YAP/TAZ signaling is necessary for proper endochondral ossification.

Refs: [1] Vanyai+ Development 2020; [2] Collins+ Dev Cell 2024

Session 7: Emerging Paradigms in Bone Research
S7-1 Tadahiro Iimura, PhD

Pharmacological effects of PTH on bone pain

Clinical studies have reported that teriparatide (TPTD), a human parathyroid hormone (PTH) analog, reduces back pain in osteoporotic patients. However, the mechanistic insights of this pharmacological action remain elusive. We investigated the antinociceptive effect of TPTD mainly on primary sensory neurons in ovariectomized (OVX) rats. The plantar test showed thermal hyperalgesia in the OVX rats, which was significantly, but not fully, recovered immediately after the initial TPTD administration. The von Frey test also demonstrated reduced withdrawal threshold in the OVX rats. This was partially recovered by TPTD. Consistently, the number and size of spinal microglial cells were significantly increased in the OVX rats, while TPTD treatment significantly reduced the number of these cells. RNA sequencing-based bioinformatics of the dorsal root ganglia (DRG) demonstrated that changes in neuro-protective and inflammatory genes were involved in the pharmacological effect of TPTD. Most neurons in the DRG expressed substantial levels of parathyroid hormone 1 receptor. These findings suggest that TPTD targets neuronal cells as well as bone cells to exert its pharmacological action. Several published studies with other skeletal pain models also demonstrated pain-relieving effects of TPTD, which will be introduced and discussed.

Session 7: Emerging Paradigms in Bone Research
S7-2 Lilian Plotkin, PhD

Role of gonadal and chromosomal sex in the musculoskeletal system

Sexual dimorphism is often attributed to the hormones produced by the testes or ovaries. However, evidence suggests that sex chromosomes (XX or XY) also play a significant role. To separate the effects of these two factors on bone health, this work used a unique mouse model known as the Four-Core Genotypes (FCG). The FCG model allows us to manipulate the expression of the Sry gene, which determines testis development, resulting in four groups: XX mice with ovaries (XXO), XX mice with testes (XXT), XY mice with ovaries (XY-SryO), and XY mice with testes (XY-SryT). We have shown that the influence of sex chromosomes on the development of body weight, fat and lean/skeletal muscle mass, and bone mass becomes evident in an age-dependent manner, specifically after sexual maturity. Our evidence suggests that there are distinct differences in musculoskeletal development between mice with XX or XY chromosomes. We conclude that our findings uncovered sex chromosomes as a previously unacknowledged factor contributing to the sexual differences observed in musculoskeletal health.

Session 7: Emerging Paradigms in Bone Research
S7-3 Thomas Nickolas, MD

Opening Pandora's Box: Using Deep Phenotyping to Assess Drivers of Renal Osteodystrophy

LRenal osteodystrophy (ROD) is a complex disorder of bone metabolism that affects the majority of patients with chronic kidney disease (CKD). ROD is associated with adverse clinical outcomes including bone loss, abnormalities in bone mineralization and turnover, skeletal deformities, fractures, cardiovascular events, and death. Despite current therapies, fracture incidence is 2- to 100-fold higher in adults with compared to those without CKD. Limited knowledge of ROD pathogenesis impedes development of therapeutics aimed at reducing morbidity and mortality of patients with CKD. The lack of bone-tissue based deep-phenotyping obtained from patients with ROD highly contributes to this critical knowledge gap.To deepen our understanding of gene expression and regulation across both cell-types and kidney disease stages, we performed a preliminary study to assess the variability, rigor, and reliability of single nuclei sequencing in bone-tissue by profiling the transcriptome (using 10X 3' gene expression and Parse Biosciences Evercode technologies). Our long-term goal is to create the fundamental infrastructure to facilitate high-impact novel hypothesis-driven clinical and translational research in ROD by building a large-scale data and tissue biorepository integrating clinical, bone quality, and transcriptomic data along with stored urine, blood, and bone samples. We found that osteoblast and osteocyte alterations occur early in the course of CKD and worsen with disease severity. Compared to a kidney-healthy osteoporotic reference group: (1) in CKD stage 3, we found profound changes in genes encoding pro-inflammatory proteins, cell metabolism, and cell differentiation/maturation; and (2) in CKD stage 4 and CKD stage 5 on dialysis, we found an abundance of alterations in genes involved in chronobiology and in cell survival/apoptosis and necrosis. In aggregate, these data demonstrated that molecular changes in osteoblast and osteocytes occurred in the early phases of kidney function decline and continued to have profound effects on cell function and survival as kidney function worsened. This developing resource will provide the underpinnings for future research leading to the elucidation of the pathogenesis of ROD in CKD patients with and without dialysis. These results will contribute to efforts to redefine our understanding of ROD pathogenesis and pathophysiology and the development of disease targeted prevention strategies.

Session 7: Emerging Paradigms in Bone Research
S7-4 Christina Moeller Andreasen, PhD

Exploring the bone microenvironment in relation to bone remodeling activity in metastatic breast cancer patients

Melisa Kalkan Uguz1, Emma Bengtsson1, Nichole Pedersen1, Malene Hykkelbjerg Nielsen2, Bilal MOHAMAD EL-Masri1, Thomas Levin Andersen3,4, Anne Marie Bak Jylling5 and Christina Moeller Andreasen*1,5,
(1) Molecular Bone Histology lab, Department of Clincal Research, University of Southern Denmark, Odense M, Denmark, (2) Molecular Bone Histology Lab, Research Unit of Pathology, Department of Clinical Research, University of Southern Denmark, Denmark, (3) University of Southern Denmark, Odense M, Denmark, (4) Aarhus University, Aarhus, Denmark, (5) Department of Pathology, Odense University Hospital, Odense C, Denmark

Introduction: Bone is one of the major targets for breast cancer metastases and the interaction between cancer cells and bone cells is crucial for the establishment of a tumor-supportive bone microenvironment.

Aim: In this study, we aim to investigate the density and location of osteoclasts, cancer cells, adipocytes, and blood vessels in biopsies from metastatic breast cancer patients (MBC), in relation to the bone remodeling activity at the bone surface.

Methods: Bone marrow biopsies from 10 MBC-treated (MBC-T: radiation + chemotherapy, zoledronic acid, aged 51–92 years) and 10 MBC-treatment naïve (MBC-TN: newly diagnosed or cancer free >2 years, aged 38–87 years) were included. The paraffin-embedded biopsies were cut into 3.5-µm-thick sections and the bone remodeling activity was assessed on Masson Trichrome stained sections. Additionally, the neighboring section was multiplex immunofluorescent stained for CK7/19, TRAcP, perilipin, CD34, and DAPI to identify cancer cells, osteoclasts, adipocytes, blood vessels, and nuclei, respectively. The cell densities were quantified in a zone of 0–100 µm from the bone surface using HALO software.

Results: MBC-TN patients had higher bone volume ($p<0.025$), and fewer cancer cells ($p<0.047$) than MBC-T. As expected, both groups had more eroded than quiescent bone surfaces (MBC-T: $p<0.02$; MBC-TN: $p<0.002$), but with no evidence of bone formation. MBC-T patients had more cancer cells above eroded surfaces than MBC-TN ($p<0.005$), and mainly in the 25–100 µm marrow zone. Blood vessel density was higher in MBC-TN near the bone surface (0–25 µm), but similar in the 25–100 µm zone irrespectively of remodeling stage. Both groups had osteoclasts at the bone surface (0–25 µm), with no significant difference. Notably, some patients had a high osteoclast density in the marrow distant from bone surfaces. Ongoing studies utilizing GeoMX digital spatial profiling, investigate the gene expression pattern in populations of fibroblasts and cancer cells in the bone microenvironment and their impact on the bone remodeling activity.
Conclusion: Despite treated with anti-resorptive therapy the cancer patients had a high prevalence of eroded bone surfaces, and with no ongoing bone formation suggesting a prolonged reversal-resorption phase. A subset of the anti-resorptive-treated MBC patients still displayed a significant number of osteoclasts, even distant from bone surfaces.

Session 7: Emerging Paradigms in Bone Research
S7-5 Roger Valle-Tenney, PhD

Pharmacological activation of the hypoxia signaling pathway alleviates the metabolic and skeletal consequences of dietinduced obesity and type-2 diabetes in mice

Roger Valle-Tenney1, Seppe Melis1, Nicolas Peredo1, Karen De Samblancx1, Ruben Cardoen1, Elena Nefyodova1, Farlay Delphine2, and Christa Maes1
(1) Laboratory of Skeletal Cell Biology and Physiology (SCEBP), Skeletal Biology and Engineering Research Center (SBE), Department of Development and Regeneration, KU Leuven, Leuven, Belgium
(2) INSERM, UMR 1033, Univ Lyon, Université Claude Bernard Lyon 1, F-69008 Lyon, France

Obesity and diabetes commonly associate with poor bone quality, high fracture risk, and impaired repair. The causes are not yet resolved, but likely relate to impaired global glucose homeostasis, bone mass and material properties, and/or skeletal vascularization. All these features are impacted by hypoxia-inducible factor (HIF) signaling, suggesting that HIF-modulation might improve both energy metabolism and bone health in diabetes.

In our current work, we found that HIF-activation by administration of FG-4592 (Roxadustat) prevented high-fat diet (HFD)-induced body weight gain, hyperglycemia, and glucose intolerance in mice. Here, we investigated the impact of HFD and FG-4592 on bone, using various morphometric techniques. First, nanoCT showed that a 4-month HFD regimen led to a 20% reduced tibial trabecular bone mass (BV/TV, $p<0.05$ vs normal diet (ND), n=8). This was linked to impaired bone formation, as static and dynamic histomorphometry evidenced significantly reduced osteoid deposition and bone mineralization (MAR -30%, $p<0.05$; BFR -48%, $p<0.01$; n=9). Most of the HFD impact on trabecular bone was unaffected by FG-4592. In the cortex, nCT analysis showed no alterations in the classical parameters (Ct.Th, Pm). Yet, in-depth 3D exploration of the cortical porosity, with segmentation into lacunar porosity (structures with diameter <8 µm) and intracortical channels (>8 µm Ø), revealed that HFD significantly lowered the volume and connectivity of the channels, suggesting damage of the intracortical vasculature in diabetic conditions. Fourier-transform infrared micro-spectroscopy (FTIRM) further uncovered lower collagen maturity and mineral-to-matrix ratios after HFD, indicating alterations in cortical bone matrix composition and structural organization. The HFD-induced cortical changes showed no or minimal impact of FG-4592.

As a key focus though, we thoroughly examined the marrow vasculature, using computational 3D image analysis methods. Thick femur sections were stained for endomucin, cleared, and imaged by highresolution, deep-tissue, confocal microscopy (100µm). We developed a processing pipeline including supervised machine-learning pixel segmentation, denoising, and manual post-correction, to obtain quantifiable binary skeletonized maps of the vascular network. HFD-fed mice displayed decreases in vascular volume, vessel surface, and vascular branches and junctions ($p<0.001$, vs ND, n=4). Interestingly, FG-4592 prevented the vascular decline and rescued its complexity and topology. Furthermore, HFD also induced accumulation (2.6-fold, $p<0.01$) and hypertrophy of marrow adipocytes, which, remarkably, was also fully prevented by FG-4592 treatment. In summary, our data show that pharmacological HIF-activation protects against skeletal vascular damage and prevents excessive marrow adiposity in a mouse model of HFD-induced obesity and type-2 diabetes.

Session 7: Emerging Paradigms in Bone Research
S7-6 Zoe Herdman

Postn deletion impairs intramembranous bone regeneration in mice

Zoe Herdman1*, Hoomin Lee1, Mukundan Attur2, Rick Sumner1, Frank Ko1
(1) Department of Anatomy & Cell Biology, Rush University Medical Center, (2) Division of Rheumatology, Department of Medicine, NYU Grossman School of Medicine

Despite playing an integral role in dental or orthopaedic procedures such as implant placement, fracture healing, or distraction osteogenesis, the molecular basis of intramembranous bone regeneration has been relatively underexplored compared to endochondral-mediated bone repair. We previously examined transcriptomic profiles of regenerating bone from rats that underwent bone marrow ablation surgery, a model of intramembranous bone regeneration that keeps the cortical bone intact, and interestingly found a dramatic increase in Periostin (Postn). Postn is a matricellular protein expressed on the periosteal surface and has been demonstrated to be important in promoting endochondral-mediated fracture repair but has not been explored during intramembranous bone regeneration in the medullary space. To further determine the necessity of Postn in intramembranous bone regeneration, we used a mouse model of bone marrow ablation surgery. We first verified that Postn was detected in the regenerating bone marrow following surgery using immunofluorescence and RNAscope. Cells expressing Postn were also present in the regenerating bone marrow using a reporter mouse line (PostncreERT2;tdTM). We then performed bone marrow ablation surgery in Postn global knockout (KO) mice, and found that regenerating bone BV/TV measured by microCT was 43% lower in Postn KO mice compared to littermate wildtype controls ($p = 0.019$). In addition, osteogenic genes were significantly lower in Postn KO, including Runx2 (65%, $p = 0.021$) and Bglap (47%, $p = 0.048$). Since the global KO of Postn causes dwarfism and decreased bone, we then sought to conditionally delete Postn in bone marrow stromal cells postnatally. We generated PdgfracreERT2;tdTM;Postnfl/fl mice and performed bone marrow ablation surgery to induce intramembranous bone regeneration. Daily tamoxifen was administered during the time frame when an increase in Postn occurs (pre-operative day 1 to postoperative day 2) and examined regenerating bone by microCT at postnatal day 7. We discovered that the conditional deletion of Postn in PdgfracreERT2 cells reduced regenerating bone BV/TV by 68% ($p = 0.048$, Figure 1A). Immunofluorescence staining for osterix also showed decreased osteogenic cells in the regenerating bone marrow due to Postn conditional deletion (Figure 1B). Our study demonstrates that while Postn is exclusively expressed on the periosteal surface of intact bone, intramembranous bone regeneration from marrow ablation surgery induces Postn expression in bone marrow stromal cells, which is crucial to promoting bone regeneration in mice.

Session 7: Emerging Paradigms in Bone Research
S7-6 Zoe Herdman

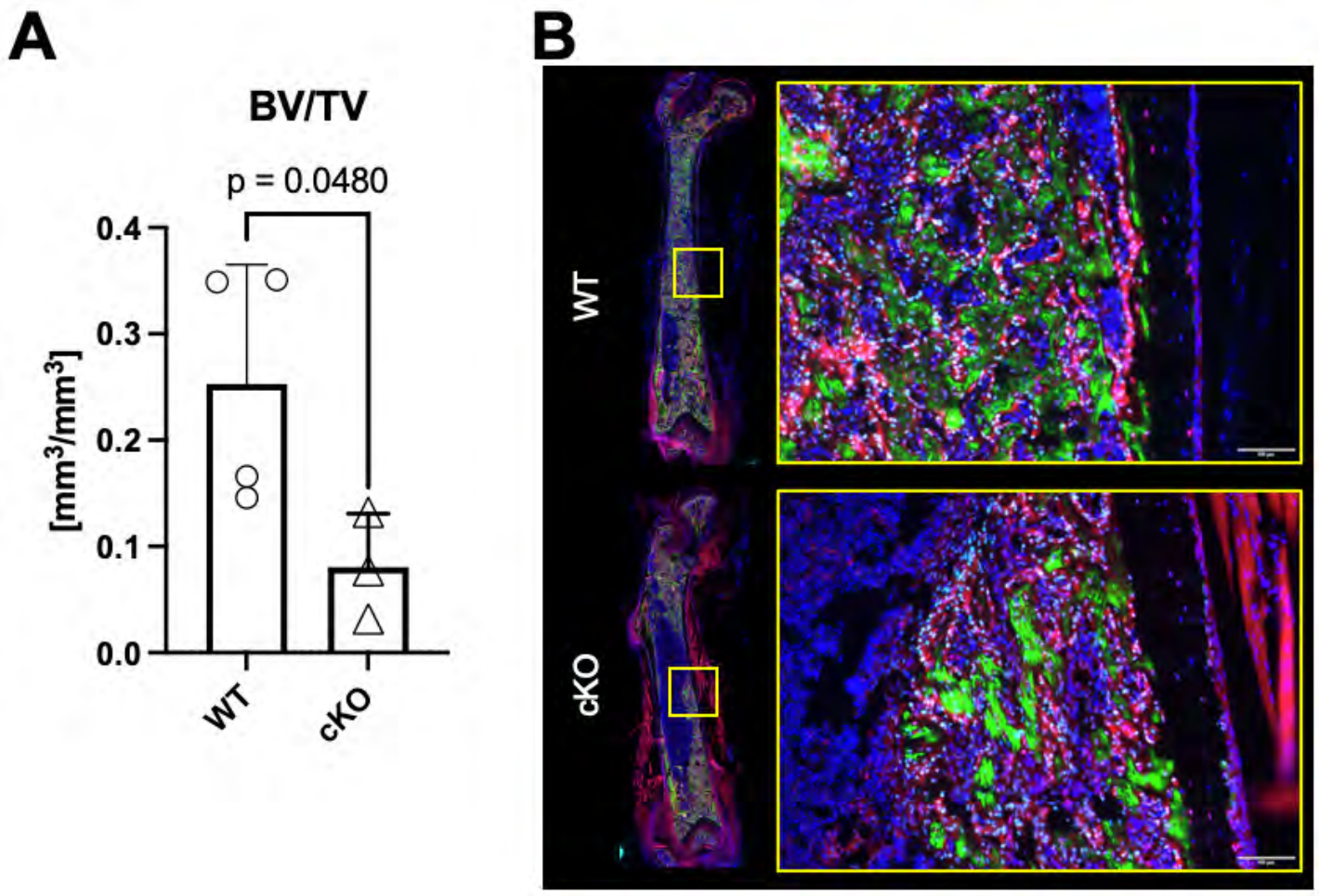

Figure 1. (A) Regenerating BV/TV measured by microCT in WT (Pdgfra^{creERT2};tdTM) and cKO (Pdgfra^{creERT2};tdTM;Postn$^{fl/fl}$) mice. (B) Immunofluroescence for osterix in WT in cKO mice. Blue = DAPI positive nuclei; green = calcein; red = tdTomato; cyan = osterix

Session 8: Pre-Clinical Bone Imaging

S8-1 Warren Grayson, PhD

Neurovascular imaging in the murine calvarium

Peripheral nerves are known to innervate bone tissue, however, a complete understanding of bone nerve distributions and patterning – particularly following injury – remains limited. Nerves play complex roles in coordinating bone development and maturation, thus, we sought to understand changes in nerve distributions and patterns throughout a mouse lifespan to provide insight into changes in the bone microenvironment that occur during development and aging. We imaged the pan-neural marker, TUBB3, and mapped its expression in the various regions of the calvaria throughout the mouse lifespan, including neonatal P0 to 80 weeks of age. Using this approach to evaluate neural responses to bone injuries, we also found that in healing injuries, early nerve infiltration is followed by nerve retraction to baseline levels. However, in non-healing injuries, nerves do not retract, suggesting that nerves and nerve factor persistence may have a negative impact on bone healing. To further understand the roles of calvarial nerves in coordinating bone formation, we developed a novel high throughput method to identify the transcriptional signatures of nerves that innervate calvarial defects using both retrograde tracing and scRNA-seq. The goal of these studies is to identify potential targets to modulate the healing environment and develop therapies for improved bone formation.

Session 8: Pre-Clinical Bone Imaging
S8-2 Nat Dyment, PhD

Imaging at the interface: how hedgehog signaling integrates tendon and bone

Despite extensive research aimed at improving surgical outcomes of enthesis injuries, re-tears remain a common problem, as the repairs often lead to fibrovascular scar as opposed to a zonal enthesis. Zonal enthesis formation involves anchoring collagen fibers to bone, synthesizing proteoglycan-rich fibrocartilage, and mineralizing this fibrocartilage. During development, the hedgehog signaling pathway promotes the formation and maturation of fibrocartilage within the zonal tendon-to-bone enthesis. However, whether this pathway has a similar role in adult zonal tendon-to-bone repair is not known. Therefore, we developed a murine anterior cruciate ligament (ACL) reconstruction model to better understand the zonal tendon-to-bone integration process. We activated the hedgehog signaling pathway using both genetic and pharmacological approaches, which promoted the formation of zonal attachments and tunnel integration strength. These improved outcomes were due in part to hedgehog signaling's positive role in proliferation of the bone marrow stromal cell (bMSC) progenitor pool and subsequent fibrocartilage production by bMSC progeny cells that produced the tendon-to-bone attachments. These results suggest that, similar to growth and development, hedgehog signaling promotes the production and maturation of fibrocartilage during tendon-to-bone integration in adults.

Session 8: Pre-Clinical Bone Imaging

S8-3 Rachel Surowiec, PhD

Preclinical bone MRI using a novel 3D dual echo rosette (PETALUTE) K-space trajectory: comparison to 3D radial ultrashort-and zero echo time approaches

1Farhan Sadik, 1Mohseu R. Subah, 2 Ali C. Ozen, 3 Stephen Sawiak, 4Mark Chiew, 1,5Uzay E. Emir, 1Rachel K. Surowiec
(1)Weldon School of Biomedical Engineering, Purdue University; (2) Dept. of Radiology, University of Freiburg; (3) Dept. of Clinical Neurosciences, University of Cambridge; (4) Wellcome Centre for Integrative Neuroimaging, University of Oxford; 5School of Health Sciences, Purdue University

Ultrashort echo time (UTE) and zero echo time (ZTE) magnetic resonance imaging (MRI) have significantly enhanced bone imaging and characterization1 by exploiting bone's ultrashort T2* components (water, collagen)2. However, UTE can suffer from low signal-to-noise ratio (SNR), lower resolution, and long scan time. Radial k-space trajectories have been the prevailing sampling trajectory in UTE but have several notable limitations3,4. The development of rosette k-space trajectories allows for increased sampling efficiency per rosette petal compared to radial spoke trajectories5. Compressed sensing (CS) reconstruction, a paradigm-shifting method for accelerating acquisition through undersampling, performs better when kspace is incoherently sampled using rosette trajectories. We implemented a 3D dual-echo novel rosette k-space trajectory (PETALUTE) for preclinical bone imaging and compared SNR and resolution to ZTE and radial UTE at 7T. The excised femoral diaphysis from two rats (2-month-old, Sprague-Dawley) were scanned in a 7T small animal MRI (BioSpec, 70/30; Bruker) equipped with a gradient insert (max gradient: 660 mT/m; max slew rate: 4570 T/m/s/) using a volume transmit/receive 1H 23-mm coil. 3D ZTE parameters included matrix:128x128x128, FOV: 40 mm3, 51896 radial spokes, TR: 2.5 ms, FA: 1.6°, and total acquisition time (TA) 2:16 [min:sec]. 3D radial UTE was acquired with a nominal 0.008 ms echo time (TE), matrix: 128x128x128, FOV: 23 mm3, 51360 radial spokes, TR: 3 ms, FA: 5°, and TA:10:27. PETALUTE was acquired with the first TE (0.016 ms) second (7.9 ms), matrix: 302x302x302, FOV: 32 mm3, 147456 petals, FA: 6.5°, TR 12 ms, and TA: 29:50. UTE and ZTE reconstructions were performed in Paravision 6.0.1, and dual-echo PETALUTE reconstruction was performed in MATLAB. In addition, a CS approach was used for the reconstruction of PETALUTE. SNR was calculated in the cortical bone, bone marrow and skeletal muscle. High-quality bone images (Fig.1B) with higher SNR in the cortical bone (Fig.1C) and higher resolution were obtained with PETALUTE vs. 3D ZTE and radial UTE and were even further enhanced with CS. PETALUTE resulted in substantial SNR improvements in the cortical bone and higher resolution over other acquisition strategies at preclinical (7T) field strength. The CS reconstruction further improved SNR. Future directions include evaluating quantitative MRI bone biomarkers using PETALUTE and assessing further accelerations with CS and deep learning.

References: 1. Ma YJ et al. 2020. Front Endocrinol, 11: 567417. 2. Surowiec RK et al. 2022. Bone Rep, 16: 101161. 3. Wan L et al. 2019. Magn Reson Med. 82: 225-236. 4. Weiger M et al. 2011. Magn Reson Med. 66: 379-389. 5. Shen X et al. 2023. Magn Reson Med. 89: 508-521. 6

Session 8: Pre-Clinical Bone Imaging

S8-3 Rachel Surowiec, PhD

A.

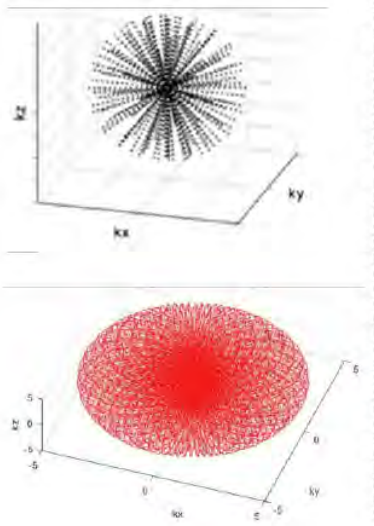

B.

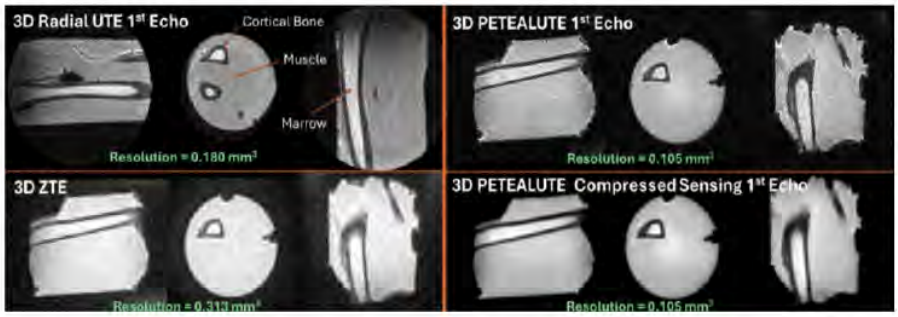

C.

Region	Signal to Noise Ratio (SNR) UTE	ZTE	PETALUTE	PETALUTE CS
Cortical Bone (*diaphysis*)	2.91	2.89	4.41	15.54
Bone Marrow (*prox. diaphysis*)	13.03	9.70	9.79	36.94
Muscle (*ant. to cortical*)	7.92	8.87	9.25	34.67

Optimization of PETALUTE- a novel 3D UTE sequence with Rosette K-space sampling for cortical bone imaging. A) example of the k-space sampling trajectory used for conventional 3D radial UTE MRI (top) and the PETALUTE k-space trajectory (bottom), which makes use of a rosette pattern that has increased sampling at the central k-space region resulting in less 'lost' data. B) High-resolution data and reconstruction were obtained with the PETALUTE compared to the conventional ZTE and 3D radial UTE. Images are from a rat tibia midshaft with soft tissues left intact. The resolution is listed in the figure. Compressed sensing further improved the bone signal of PETALUTE. C) Depicts signal-to-noise (SNR) ratio of the cortical bone, bone marrow, and muscle for each of the four MRI acquisitions. For cortical bone (our primary research focus), PETALUTE outperforms both ZTE and 3D radial UTE. The addition of compressed sensing during reconstruction resulted in a 434.021% SNR increase in the cortical bone from conventional UTE and a 252.381% increase in the same region compared to PETALUTE without compressed sensing.

Session 8: Pre-Clinical Bone Imaging
S8-4 Satvika Bharadwaj

Machine-learning driven automation for digital phenotyping and morphological texture analysis of bone biopsy images

Background: Static histomorphometric (HM) analysis of undecalcified bone biopsy images provides a quantitative assessment of bone volume, microstructure, and cellularity in metabolic bone disease (MBD). Standard quantification approaches use manual annotation and tracing of relevant tissue structures, a time-intensive process subject to inter-operator variability. This study implements an automated pipeline for digital phenotyping, to quantify static HM parameters such as bone and osteoid area, osteoclasts and osteoblasts count, and bone marrow adipose tissue (BMAT) area. The study also presents exploratory application of Morphological Texture Analysis (MTA), that measures relative pixel patterns, not visually discernible, that could represent texture features unique to diverse tissue conditions.
Methods: We used bone histology images from biopsies in 29 patients diagnosed with osteoporosis, osteomalacia or hyperparathyroid states to train Deep Learning (DL) models and generate feature maps for static HM analysis. The DL models were trained with a set of 443bone histology images at a magnification of 20X extracted from 29 image areas selected for feature identification and annotated by two experienced operators.
Results: The DL models rapidly generated up to 20 tissue or cell maps in less than a minute. Comparing DL-generated annotation pixels with manual annotations, we observed Spearman correlation coefficients of ρ=0.99 for both mineralized bone and osteoid, and ρ=0.94 for BMAT. For osteoclast and osteoblast counts, the cell types displaying heterogeneity, using only brightfield microscopic images without additional staining, we noted ρ=0.60 and 0.69, respectively (inter-operator correlation: ρ=0.62 for osteoclasts and 0.84 for osteoblasts). The clinical diagnostic categorization of the biopsies as low and high turnover was used to explore the classification ability of MTA for mineralized bone, osteoid, and BMAT features. The AUC-ROC obtained for BMAT MTA as a classifier was 0.87 compared to 0.72 and 0.79 from bone and osteoid MTA features.
Conclusions: An automated DL pipeline for static HM significantly improves the efficiency of evaluating tissue and cellular components in bone biopsies for MBD with rapid generation of precise tissue and cell maps. Exploratory MTA computer-extracted features could potentially classify tissue states and holds promise for future investigation. Integration of this pipeline into clinical routines would improve workflows and contribute to diagnostic insights into bone biopsy.

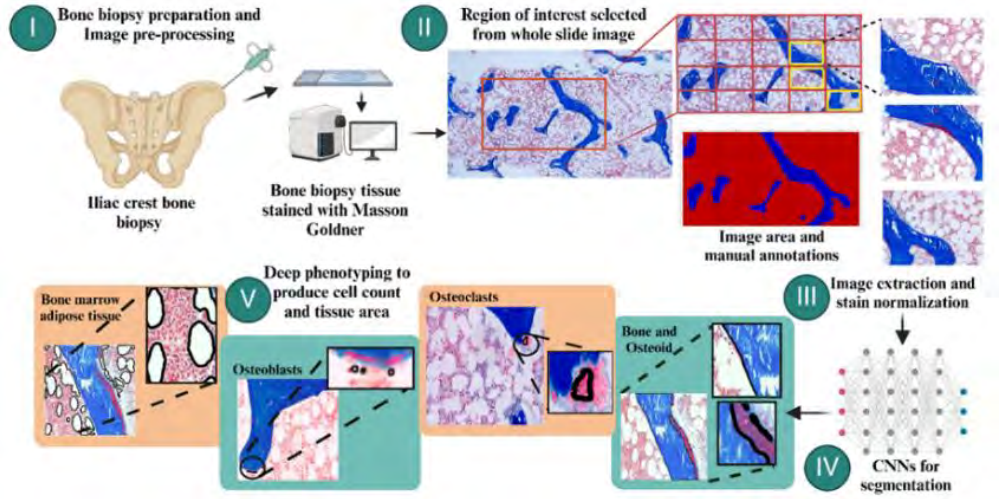

Session 8: Pre-Clinical Bone Imaging
S8-5 Anushka Gerald

Mapping and function of P75-NTR+ periosteal cells in the regeneration of craniofacial bone

Skeletal defects can greatly affect a patient's quality of life, but treatment is challenging due to limited spontaneous bone regeneration. Better understanding of the fundamental molecular and cellular mechanisms regulating bone healing, particularly in regions of accelerated skeletal regeneration such as neural crest-derived craniofacial bone could improve treatment options. The p75 neurotrophin receptor (p75-NTR) has been identified as an important regulator of skeletal regeneration and marker of neural crest stem cells and nerve-supporting glial cells. We hypothesize that p75-NTR+ cells contribute to the accelerated healing of neural crest-derived bone by directly differentiating into cells such as osteoblasts. To test this hypothesis, we created a p75-CreERT2 mouse model to perform lineage tracing (p75-CreERT2-Ai6) and conditional ablation (p75-CreERT2-DTA) of p75-expressing cells. Initial baseline mapping with p75-CreERT2-Ai6 reporter mice identified a dense web of p75-NTR+ Schwann- and fibroblast-like cells selectively covering the external periosteal surface of the calvaria in adult mice, with greater density on the neural crest-derived frontal bone. FACS sorting demonstrated that these cells make up a small portion of all cells in the calvaria (<1%). Preliminary assessment of calvarial regeneration in p75-CreERT2-DTA mice suggests that functional ablation of p75-NTR+ cells impairs healing and new bone formation in the neural crest-derived frontal bone. We expect that the future characterization of these cells and their mechanism of action will inform methods to enhance skeletal regeneration throughout the body.

Session 8: Pre-Clinical Bone Imaging

S8-6 Talayah Johnson

Reduced loading after sciatic nerve resection impairs hindlimb growth

Talayah Johnson*1, Nathaniel Dyment1, Natalie Fogarty2, Xi Jiang1, Alisia Lin1, Joel D. Boerckel1, Robert Mauck3, Josh Baxter1, Eiki Koyama2 and Lin Han4,
(1) University of Pennsylvania, Philadelphia, PA, USA, (2) Children's Hospital of Philadelphia, Philadelphia, PA, USA, (3) University of Pennsylvania, philadelphia, PA, USA, (4) Drexel University, Philadelphia, PA, USA

Mechanical forces influence the growth and maintenance of musculoskeletal tissues. By understanding the role of mechanical loading on developmental processes of load bearing tissues, specifically the mechanosignaling events that drive tissue formation and maturation, we can potentially leverage this knowledge to guide new regenerative strategies. We performed unilateral sciatic nerve resection (SNR) in both neonatal (surgery performed on postnatal day 1) and adult (surgery performed at 22 weeks of age) mice to explore how reductions in loading differentially impact the growth and maintenance of hindlimb load bearing tissues. We used video gait analysis to assess limb kinematics, μCT to access trabecular and cortical bone parameters, and cryohistology to assess tendon morphology. SNR limbs exhibited sustained gait abnormalities compared to contralateral limbs, including reduced paw print width (a hallmark of sciatic denervation), increased ankle dorsiflexion and reduced hock height ($p < 0.01$). SNR yielded marked alterations in bone parameters at both ages with neonatal limbs having reduced tibial length, trabecular BV/TV, trabecular thickness, and cortical area ($p<0.05$), and adult limbs having reduced trabecular BV/TV, BMD, trabecular number, and trabecular thickness ($p<0.05$). As expected, SNR did not alter tibial length in adults. Interestingly, SNR did not alter cortical bone parameters at 14 days post-surgery (D14) but did result in reduced cortical area and cortical thickness by D42 ($p<0.05$) in the adult group. The differences in the onset of bone loss between trabecular and cortical bone corroborate trabecular bone being more sensitive to altered loading. The differential effects of loading on tissues were also exemplified in tendons where neonatal SNR significantly decreased Achilles tendon cross sectional area (CSA) at postnatal day P14 and P42 ($p<0.05$, $p<0.01$), but SNR had much less of an effect on adult tendons. SNR reduced the growth rates of the affected limb in the neonates, resulting in reduce bone and tendon sizes. In contrast, the decrease in bone volume in the adult SNR group appears to be the result of disturbed remodeling processes and increased bone resorption, which is currently being analyzed. Thus, we provide a useful model for understanding the role of mechanical loading in the development of load-bearing tissues, and our data shed light on the mechanisms by which mechanical forces control postnatal hindlimb development and growth.

Poster Abstracts

PO-001 Melissa Bevers, PhD

Romosozumab Improves Areal BMD at the Axial Skeleton but not Areal and Volumetric BMD, Microarchitecture, and Strength at the Peripheral Skeleton in a Real-World Cohort

Melissa Bevers*1,2,3, Caroline Wyers1,2, Marsha van van Oostwaard1,2, Sophie Popma1, Marian Bouts1, Robert van der Velde1, Bert van Rietbergen2,3 and Joop van den Bergh1,2,
(1) VieCuri Medical Center, Venlo, Netherlands, (2) Maastricht University, Maastricht, Netherlands, (3)Eindhoven University of Technology, Eindhoven, Netherlands

Romosozumab (ROMO) treatment has been associated with large increases in areal bone mineral density (aBMD) at the lumbar spine (LS), total hip (TH), and femoral neck (FN) in postmenopausal women, but data on the effect on peripheral BMD, microarchitecture, and strength are sparse. In a real-world cohort study, we assessed the effect of ROMO on the axial and peripheral skeleton using dual-energy X-ray absorptiometry (DXA) and high-resolution peripheral quantitative CT (HR-pQCT). According to Dutch guidelines, ROMO treatment is recommended in postmenopausal women with a TH aBMD T-score ≤-2.0 and ≥2 grade 2 or 3 vertebral fractures (VF) or a TH T-score ≤-2.5 and ≥1 grade 2 or 3 VF. As part of regular care, DXA scans (hip, lumbar spine) and HR-pQCT scans (distal radius, distal tibia) were taken at the start (T0) and after the 12th month of ROMO treatment (T1). Follow-up data were available for 24 women (71.7±7.8 yrs.; 58.3% treatment naive). At T0, mean aBMD T-scores were -2.4±0.8 (TH), -2.8±0.6 (FN), and -2.4±1.3 (LS). At T1, changes in TH, FN, and LS aBMD were +4.6±7.2% (p=0.005), +1.6±5.6% (p=0.171), and +11.2±6.9% (p<0.001), respectively (Fig.1). At the distal radius (N=16), significant changes were found in total volumetric BMD (-2.0%; [IQR: -4.3, 0.6]; p=0.020; Fig.1) and trabecular volumetric BMD (-2.2%; [-3.8, 0.2]; p=0.013) but not cortical volumetric BMD. Significant changes were also found in trabecular number (-1.2%, [-2.4, 0.8]; p=0.049) and cortical thickness (-1.6%; [-2.9, 0.5]; p=0.015). Changes at the distal tibia (N=21) were not significant for total, trabecular, and cortical volumetric BMD (all p>0.05; Fig.1), but they were for trabecular number (-0.8%; [-1.7, 0.4]; p=0.046), separation (+1.1±2.0%; p=0.022), and heterogeneity (+1.8±3.3%; p=0.022). Changes in radial and tibial stiffness and failure load were not significant. Changes and significances in radial and tibial aBMD estimated from HR-pQCT in the axial, coronal, and sagittal plane were similar as those in total volumetric BMD. To conclude, one-year treatment with ROMO increased aBMD at the axial skeleton in postmenopausal women with osteopenia or osteoporosis and VFs but did not change or decreased volumetric BMD, bone microarchitecture, and strength at the peripheral skeleton. Together with similar changes in aBMD at the distal radius and tibia estimated from HR-pQCT as in volumetric BMD at these peripheral bones, it suggests skeletal-site dependent effects more than effects of the use of different imaging modalities at both skeletal regions.

PO-002 Babatunde Ayodele, PhD

Increased subchondral bone resorption in the proximal sesamoids of racehorses is associated with accumulation of bone microdamage

Babatunde A Ayodele1, Charles N Pagel1, Eleanor J Mackie1, Peta L Hitchens1, R Chris Whitton1
1Melbourne Veterinary School, Faculty of Science, University of Melbourne, Melbourne, Australia

Fracture of the proximal sesamoid bones (PSB) is a common musculoskeletal injury that may cause racehorse fatality. Fatigue fractures in racehorses occur due to repetitive high magnitude loads in focal bone sites during exercise but this process is not fully understood in PSB. Understanding how PSB respond to training and racing can inform management approaches to prevent PSB fractures. We have previously shown, by µCT imaging that the subchondral bone (SCB) underlying the articular surface in PSB had greater BV/TV, calcified microcracks and focal resorptive lesions than other bone regions indicating that the SCB is the primary site of mechanical loading. The aim of the current study was to further investigate the adaptation of the sesamoid SCB using higher resolution scanning electron microscopy to better understand the local response to training and racing exercise.

Proximal sesamoid bones (n=100) collected from 61 Thoroughbred horses were embedded in polymethyl methacrylate and sectioned along a sagittal plane. Bone surfaces were polished and imaged using scanning electron microscopy fitted with a back-scattered detector. Whole sesamoid bone area fraction (BAr/TAr) was determined and SCB microcracks were counted. Histomorphometry was performed on medial sesamoids (n=30) and bone resorption (eroded perimeter) and bone formation (mineralising surface) in the SCB were determined. Associations between bone parameters and the racing factors were determined using generalised linear regression models.

The number of SCB microcracks were greater in medial compared with lateral PSB ($P<0.001$), in older horses ($P <0.001$), in horses with greater number of races ($P<0.004$), those that had been in training for longer ($P<0.01$), and in geldings compared to entires and females ($P=0.03$). Eroded perimeter in sesamoid SCB was higher in horses that had been training for longer ($P=0.003$) and raced more often in the previous 30 days ($P=0.03$), and in bones with higher BAr/TAr ($P=0.001$) and more microcracks ($P<0.001$). Mineralising surface in the SCB was lower in older horses ($P=0.038$), horses that started racing at an older age ($P=0.037$), horses with more career starts ($P=0.043$), horses in training for a longer period ($P<0.001$), that raced more in the last 30 days ($P=0.039$) and in horses in training compared with resting horses ($P=0.027$).
Higher mineralising surface in the SCB of horses in training with more races suggests a bone modelling response to intensive exercise. Higher eroded perimeter in sesamoid SCB with higher BAr/TAr and more microcracks suggests targeted repair of bone microdamage by remodelling. These findings are consistent with bone fatigue response associated with fatal fractures in racehorses.

PO-003 Michael David, PhD

Generalizability of Deep Learning Segmentation of the Trabecular Compartment in Mouse Vertebral Body Across Micro-Computed Tomography Image Resolutions

Michael A. David* and Douglas J. Adams, Department of Orthopedics, University of Colorado Anschutz Medical Campus, Aurora, CO, USA

The generalizability of deep learning (DL) models for micro-computed tomography (microCT) image segmentation, particularly the trabecular compartment within the rodent vertebral body, is challenged by both anatomical variation and image resolution. We previously developed a DL segmentation (DL-Seg) model for the trabecular compartment based on the anatomical variation of the 4th vertebral body (L4) from Diversity Outbred (DO) mice and the 8 founder inbred strains comprising the DO. In this study, we tested the robustness of our DL-Seg model developed for L4 at high resolution (HR) when applied to L3, L4, and L5 from an additional set of DO mice (n = 14; male and female with and without parathyroid hormone) that were imaged via microCT (70 kVp, 200 μA) at low resolution (LR; 1000 projections, 20 μm discretization, 1 frame average) as well as HR (2000 projections, 10 μm discretization, 3 frame average). An additional set of synthetic HR images (HRs) was produced from the LR image sets using our previously developed and separate DL model. Paired transverse images (541/lumbar) were imported into Python for testing our existing DL-Seg model based on HR images for the LR and HRs image sets (Fig. 1A). Qualitatively, reduced accuracy of the DL-Seg model occurred in anomalous regions of vertebral anatomy and when applied to images acquired with LR (Fig. 1B). Notably, model accuracy was challenged by regions of sparse trabecular architecture and within the irrelevant posterior regions. As expected, HR and HRs image segmentations were nearly identical. Bone area/total area (BA/TA) quantified for each transverse image demonstrated similar BA/TA for HR vs HRs, with less agreement for LR vs HR (Fig. 1C). Our findings confirm that the HR and HRs, which are closer in resolution, result in largely similar accuracy of the DL-segmented trabecular compartment, but are both challenged by certain anatomical locations. The DL-Seg model on the HR test set of DO mice mirrors previous findings during DL-Seg model development, suggesting our model generalizes with both good and poor accuracies. Our DL-Seg model yields comparatively poor accuracy on the LR regardless of anatomical variation. Taken together, these results suggest the limited ability to apply the DL-Seg model to LR images, requiring researchers to either manually segment or train a separate LR-specific model. Nevertheless, these findings warrant the exploration of steps to enhance the accuracy of DL-based segmentation by increasing the number of training HR images around problematic anatomical regions. Overall, testing our DL-Seg model across varying microCT spatial resolutions provides a foundational understanding for enhancing DL models in order to implement an automated high-throughput segmentation pipeline for the vertebral trabecular network in mice or other species.

PO-004 Ananya Goyal

The aging knee: changes in bone metabolic activity measured using [F18]NaF PET-MR Imaging

Ananya Goyal1, Yael Vainberg1, Feliks Kogan1
(1) Department of Radiology, Stanford University

Osteoarthritis (OA) is the most common cause of chronic disability in older adults. Aging-related changes contribute to the development of OA by making joints more susceptible to the effects of abnormal biomechanics, injury, obesity, etc. Further, aging is known to impact bone turnover, which may also contribute to OA progression. Understanding the basic mechanisms by which aging affects joints may help detect early disease and provide new targets for slowing or preventing OA. Currently, many methods can evaluate long-term impacts of bone adaptation; however, the acute response of bone to loading remains poorly understood, largely due to a lack of methods to directly measure immediate changes in bone physiology and function in vivo. The radiotracer [18F]sodium fluoride ([18F]NaF) interrogates areas of newly mineralizing bone, providing information about bone metabolic activity. Further, [18F]NaF uptake changes after exercise, thus showing its sensitivity to changes in bone physiology resulting from acute bone loading. Here we evaluate whether a [18F]NaF PET-MRI 'stress test', imaging before and after a stair-climbing exercise, can detect and characterize changes in joint function associated with age and their spatial nature.

20 volunteers aged 22-67 years with no previous knee injuries were included. Subjects underwent two bilateral 30-min [18F]NaF PET/MRI knee scans using a 3T GE hybrid PET/MRI system at baseline and subsequently after a stair-climbing exercise (112 steps, up and down). Subchondral bone metabolic activity was quantified using maximum standardized uptake values (SUVmax), and kinetic parameters of bone perfusion (K1) and total tracer uptake into bone (Ki) were fit to the Hawkins 3-compartment model using COMKAT [Muzic, 2001]. Pre- and post-exercise changes were compared to measure the loading-induced response in both knees.

At baseline, a weak positive correlation was observed for values of SUVmax, K1 and Ki with age in the whole joint. After exercise, the change in SUVmax and K1 showed positive correlation with age, while the change in Ki showed a negative correlation with age. Representative PET-MR images from five subjects are shown in Figure 1.

Our preliminary results show that in a healthy aging cohort, there is increased bone remodeling activity in the knee joint as observed using [18F]NaF PET-MRI. Further work is needed to understand the differences due to loading in the metabolic joint response with age. Studying acute molecular markers of bone turnover in aging can help shed light on pathophysiologic variations that may occur in OA.

PO-005 Kim Harrison, PhD

Multi-Time Point Tracking of Cortical Bone Remodeling Events in the Rabbit Using Serial Time-Lapsed Synchrotron Micro-CT Scans

Kim Harrison*1, Xuan Wei1, Lindsay Loundagin1, Arash Panahifar2,3, James Johnston4 and David Cooper1,
(1) Department of Anatomy, Physiology and Pharmacology, College of Medicine, University of Saskatchewan, Saskatoon, SK, Canada, (2) BioMedical Imaging and Therapy Beamline, Canadian Light Source, Saskatoon, SK, Canada, (3) Department of Medical Imaging, College of Medicine, University of Saskatchewan, Saskatoon, SK, Canada, (4) Department of Mechanical Engineering, College of Engineering, University of Saskatchewan, Saskatoon, SK, Canada

We recently reported a novel experimental platform for time-lapsed tracking of remodeling events (i.e., basic multicellular units (BMUs)) in the distal tibial diaphysis of rabbits using a single in vivo synchrotron micro-CT scan followed 14 days later by an ex vivo conventional micro-CT scan. While this approach yielded the first direct dynamic tracking of BMU rate of advance (i.e., longitudinal erosion rate (LER)), the single in vivo scan limits experimental design possibilities. Here we report the first implementation of multiple in vivo scans (n=3; 5 day interval). Our objective was to demonstrate proof of principle both in terms of experimental logistics and the potential data obtained. Remodeling was elevated in seven New Zealand White Rabbits (6-month females) via daily dosing of parathyroid hormone 1-34 (30 µg/kg/day) for 15 days. Synchrotron micro-CT scans of the distal tibiae were acquired at the BioMedical Imaging and Therapy facility of the Canadian Light Source: 1) in vivo at 13 µm voxel size (37.5 keV; 2 Gy surface dose) on PTH dosing days 0, 5 and 10; 2) ex vivo at 6 µm voxel size on dosing day 15. The sequential datasets were co-registered in 3D and individual remodeling events were isolated to reveal progression over time (see Figure). Preliminary qualitative analysis has confirmed the ability of this approach to track remodeling events with sufficient change occurring over 5 days to be detectable at this scan resolution. Changes in form and trajectory of the osteoclastic cutting cones are readily evident and osteoblastic activity can be inferred from the progressive infilling of the remodeling spaces. Newly arising spaces are detectable in the sequential scans and create a novel opportunity to directly and volumetrically assess activation frequency (new remodeling events per bone volume per unit time). Similarly, the cessation of remodeling events between timepoints was observed and may elucidate how BMU activity terminates. This approach also enables assessment of LER over time, creating the possibility of probing how speed varies during the initiation and termination of remodeling events, with the caveat that we have yet to explore the question of potential impact on LER due to the radiation dose of the repeated scans. While logistically complex, serial in vivo synchrotron-based imaging holds great potential for establishing baseline characteristics of remodeling events and the immediate impacts of experimental interventions.

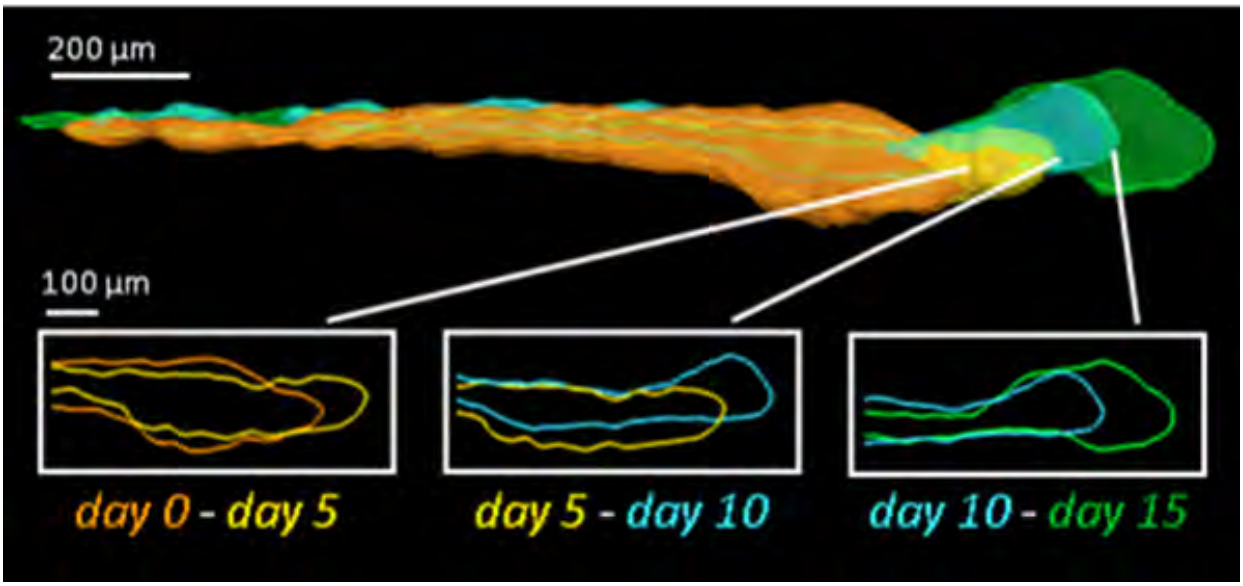
200 µm
100 µm
day 0 - day 5
day 5 - day 10
day 10 - day 15

PO-006 Melissa Bevers, PhD

Impaired Cortical and Trabecular Microarchitecture in Female Elite Cyclists as Assessed using HR-pQCT

Melissa Bevers*1,2,3, Luuk Hilkens2,4, Caroline Wyers1,2, Luc van Loon2,4, Joop van den Bergh1,2 and Jan-Willem van Dijk4, (1) VieCuri Medical Center, Venlo, Netherlands, (2) Maastricht University, Maastricht, Netherlands, (3) Eindhoven University of Technology, Eindhoven, Netherlands, (4)HAN University of Applied Sciences, Nijmegen, Netherlands

Increasing evidence suggests that elite road-race cyclists may have low areal bone mineral density (aBMD) as assessed using dual-energy X-ray absorptiometry (DXA). Data about bone structure at the micrometer level in this group are scarce but may give a more comprehensive understanding of any structural impairment of the bone. In an ongoing cross-sectional study, we assessed bone microarchitecture and strength in elite road-race cyclists using high-resolution peripheral quantitative CT (HR-pQCT). Twenty female athletes (21.5±2.4 yrs.) had DXA and HR-pQCT scans, from which aBMD (DXA), and bone geometry, volumetric BMD, and bone microarchitecture (all HR-pQCT) were assessed. Additionally, micro-finite element analysis was used to estimate bone strength from HR-pQCT in terms of failure load (FL). Z-scores were determined for all parameters using reference data, and a Z-score <-1 was considered impaired. aBMD Z-scores were -0.2±1.0, -0.3±0.9, and -0.9±1.1 at the hip, femoral neck, and lumbar spine, respectively, and they were <-1 in 20%, 25%, and 35% of the female cyclists. The mean Z-scores were also within ±1 for all HR-pQCT parameters at the distal radius and tibia (Figure 1), except for cortical thickness at the tibia (Z-score: -1.02±0.96). At the individual level at the distal radius, Z-scores were <-1 for total and trabecular area in 2 (10%) women and 1 (5%) woman, respectively. Larger proportions had Z-scores <-1 for cortical area (25%) as well as for total BMD (45%), trabecular BMD (15%), trabecular number (20%), trabecular separation (15%), cortical BMD (40%), cortical thickness (25%), and cortical porosity (15%). Proportions of female cyclists with HR-pQCT Z-scores <-1 at the tibia tended to be higher for trabecular BMD (25%), trabecular number (30%), trabecular separation (20%), and cortical area (45%) but not significantly (all p>0.05, one-sided) and were significantly higher for trabecular thickness (40%; p=0.010) and cortical thickness (60%; p=0.027). FL was normal at the group level (radius: -0.1±1.0; tibia: 0.04±1.0); however, Z-scores were <-1 in 3 (15%, radius) and 4 (20%, tibia) women. In conclusion, one-third to nearly half of the female elite road-race cyclists had low areal and volumetric BMD compared to age- and gender-matched reference data. Similar proportions had impaired trabecular microarchitecture (mainly at the tibia) and cortical microarchitecture (at the radius and tibia), reflected by fewer and thinner trabeculae and a thinner cortex. *Melissa Bevers and Luuk Hilkens have equal contribution and share first authorship.

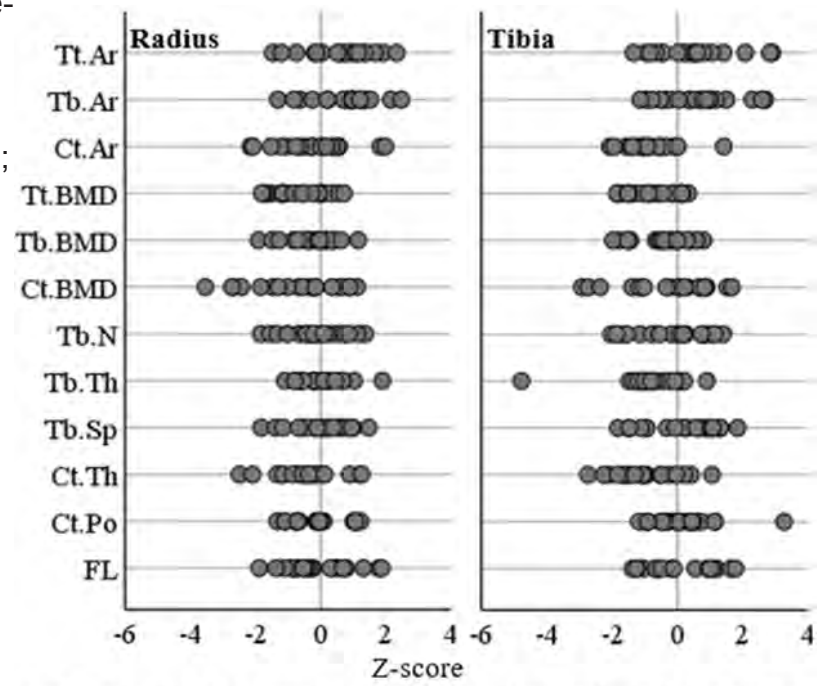

Fig.1: HR-pQCT Z-scores at the distal radius (left) and tibia (right).

PO-007 Cayetano Galera-Martinez

Elucidating Leukemia Inhibitory Factor (LIF) on Prostate Cancer Bone etastasis Microenvironment

Cayetano Galera-Martínez*1, Isabel Cuartas1 and Joan Seoane1,2
1) Vall d'Hebron Institute of Oncology (VHIO), Barcelona, Spain, (2) Vall d'Hebron University Hospital, CIBERONC, Universitat Autònoma de Barcelona, ICREA, Barcelona, Spain

Bone metastasis predominates in certain cancer types, notably originating from the prostate (85%). While Leukemia Inhibitory Factor (LIF) stands as a key player in bone remodeling, LIF role in bone metastasis remains poorly studied. Data from Stand Up To Cancer (2019) shows a substantial difference in survival outcomes among bone metastatic prostate cancer patients based on LIF expression. Patients in the highest LIF expression quartile exhibit a greater than 50% decrease in median overall survival compared to those in the lowest quartile ($p<0.05$; $n=12$) as well as a higher expression of osteoclast-related genes through an unbiased approach (log2-ratio>1). Thus, we hypothesized that LIF secreted by tumor cells could generate an aberrant bone remodeling. This would lead to the release of growth factors stored in bone, benefiting tumor growth. In this study, we assessed the involvement of LIF in the niche of prostate cancer bone metastasis using in vitro, ex vivo and in vivo methods. Also, we compared its effects with those of Receptor Activator of Nuclear Factor Kappa-B Ligand (RANKL), main target of currently approved therapies. Hence, bone marrow cells obtained from the long bones of C57BL/6j mice ($n=4$) were treated with recombinant mouse LIF or RANKL (20 ng/mL) for one week. Both cytokines upregulated the expression of osteoclast-related genes by qPCR. However, RANKL:OPG mRNA ratio only increased upon treatment with LIF. Flow cytometry analysis revealed a comparable increase in the CD68+CD265+CD11BLow- population following both treatments. TRAP staining was consistent with these findings. Moreover, ex vivo coculture of RM1 prostate cancer cells with 2 mm calvaria discs from C57BL/6j mice revealed a more than two-fold increase in tumor growth following LIF treatment after 4 weeks ($p<0.05$, $n=6$). These results made us perform a pilot syngeneic in vivo were RM1 cells were inoculated per 7-week-old C57BL/6j male mouse (HE for tumor area). Upon 2 doses of treatment with anti-LIF (15 mg/kg) in 12 days ($n=4$), RANKL:OPG mRNA decreased to less than half ($p<0.05$). Same setting treating with anti-RANKL (10 mg/kg, $n=5$) decreased mRNA expression of MMP9 ($p=0.05$), CTSK and ACP5 ($p<0.001$ both) but increased RANKL:OPG ($p<0.01$). In conclusion, these findings unveil the role of LIF in regulating RANKL:OPG dynamics within the bone metastatic niche offering promising prospects on therapeutically targeting LIF.

PO-008 Samantha Bratcher

Characterizing the Limits of 3-Photon Microscopy as a Tool for Deep Imaging of Whole, Cortical Bone Tissue

Samantha Bratcher*, Nicole Chernvasky, Chris Schaffer and Karl J Lewis, Cornell University, Ithaca, NY, USA

Osteocytes have emerged as the primary mechanosensors in bone, with a rising need to study their mechanobiology within the context of their in vivo microenvironment. Two-photon (2P) fluorescence microscopy enables observation of osteocyte signaling in vivo in mouse cortical bone but has depth limitations that prevent imaging through full cortical thickness1. Three-photon (3P) microscopy is a novel imaging platform with increased depth penetration in other tissues compared to 2P2. It also gives rise to third harmonic generation (THG) which fluorescently indicates material interfaces without exogenous labeling and has been used to observe osteocyte lacunae in mouse calvaria in vivo1. Here, we offer further characterization of this approach in long bone cortices ex vivo. We hypothesized that 3P microscopy has better imaging depth and quality compared to 2P in mouse long bones ex vivo.

Bilateral third metatarsals (MT3s), tibiae, femora, and humeri of 16-20 week old mice expressing osteocyte-targeted GCaMP6f were dissected, fixed in zinc formalin, and soaked overnight in 1mM CaCl2. Images were collected with a 25x objective (Olympus) at 920nm for 2P excitation and 1320nm for 3P excitation. Z-stacks were taken at the diaphysis while power was exponentially adjusted through depth. Stacks were cropped to a 200μm wide rectangle centered on the bone to avoid variations in depth due to the curved periosteal surface, and slices beyond the endocortical surface in the MT3 were excluded. Automated 3D segmentation was used to create ROIs around cells/lacunae in FIJI, and intensities were normalized to the background. The signal-to-noise ratio (SNR) and signal-to-power ratio (SPR) were calculated in MATLAB. T-tests, kolmogorov-smirnov tests, and linear regressions were calculated in R.

There was no significant difference in the average maximum depth at which fluorescent signal was collected by 2P or 3P, and in the femur 3P captured fewer cell ROIs (Fig A-B). THG did not reach equivalent depths but collected similar lacunae ROI quantities (Fig C-D). The distribution of ROIs through the depth was different in the tibia, femur, and humerus, with 3P shifted deeper (Fig E-H). SNR and SPR showed stable or increasing trends over depth in 3P while 2P generally decreased (Fig I-L). THG signal was as bright or brighter than 3P fluorescent signal with stable SPR in all bones except humerus (Fig M-P).

While similar quantities of data are collected by 2P and 3P fluorescence, differences in data quality become apparent as cortical depth increases with 3P performing similarly. THG brightly captures lacunae and adds valuable data on the osteocyte microenvironment. These data suggest 3P may be used to advance in vivo observation of osteocytes.

REFERENCES: 1) Lewis+ PNAS (2017). 2) Xu+ Nature Photon (2013). 3) Wu+ Optics Comm. (2018).

PO-008 Samantha Bratcher

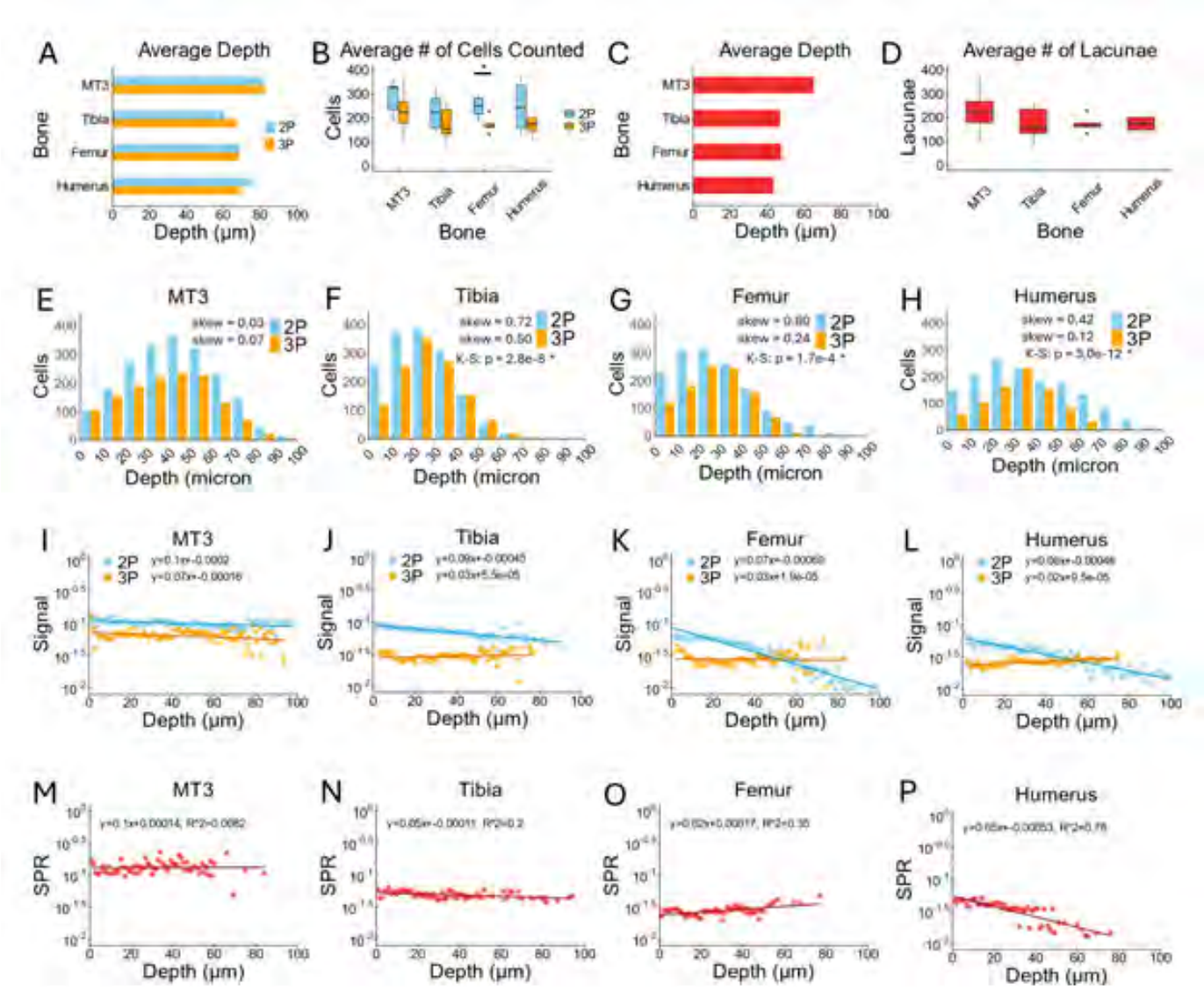

PO-009 Tengteng Tang, PhD

Advancements in 3D Correlative Multiscale and Multimodal Microscopy: Revealing New Insights into Vertebrate Tissue Biomineralization

Tengteng Tang*1, Travis Casagrande1, Pardis Mohammadpour1, William J. Landis2, Brent Lievers3 and Kathryn Grandfield1
(1) McMaster University, Hamilton, ON, Canada, (2) University of California at San Francisco, San Francisco, CA, USA, (3) Laurentian University, Sudbury, ON, Canada

Understanding the 3D organization of bone at multiple length scales across the hierarchy is essential for understanding its biological and mechanical functions. With the recent advances in 3D volume electron microscopy, notably focused ion beam-scanning electron microscopy (FIB-SEM), we probed the architecture of biomineralizing tissues more deeply than ever before—revealing novel sub-cellular nanochannels (10 times smaller than osteocyte canaliculi) in bone, mineralizing tendon and cartilage. This nanochannel system was shown to contribute to the mineral heterogeneity of bone at the nanoscale. Additionally, it may provide alternative pathways for mineral ions and small molecule diffusion throughout the tissue extracellular matrix in a manner that is complementary to the well-known lacunocanalicular network (LCN).

To build on these findings, we introduce a new correlative workflow combining X-ray microscopy (XRM), femtosecond laser (LaserFIB) ablation, and plasma FIB-SEM to provide a comprehensive 3D view of human trabecular bone across various length scales (Figure 1). LaserFIB was utilized to pattern a customer-designed micrometric grid on the bone specimen, enabling precise image alignment and registration across different imaging modalities. Subsequent XRM imaging provided overview of the specimen and revealed details of the trabecular bone architecture, including the fine cement lines and the individual osteocyte lacunae embedded within the tissue. With the tomographic information provided by XRM imaging and the guidance of the patterned grid, a single bone trabecula buried deep within the bulk of the bone tissue was identified and located. Through a correlative workspace system, the XRM data was directly overlaid with the SEM images of the sample surface which enabled us to accurately locate the chosen bone trabecula for further processing. LaserFIB was then employed for site-specific preparation, ablating excessive material and exposing the cross-section of the targeted trabecula. Finally, the as-prepared bone tissue section was examined using plasma FIB-SEM, revealing a 3D representation of the trabecular bone ultrastructure at nanometer-level resolution.
The correlative approach we have developed prov
ides a continuum of analysis, seamlessly transitioning from macroscopic examination down to the nanoscale details in 3D. This methodology not only offers a more complete view of the hierarchical organization of bone but is also versatile to be applied to a wide range of biological materials. The insights gained from this detailed structural analysis are important, especially where the structure-function relationships are central to the material application and performance.

PO-009 Tengteng Tang, PhD

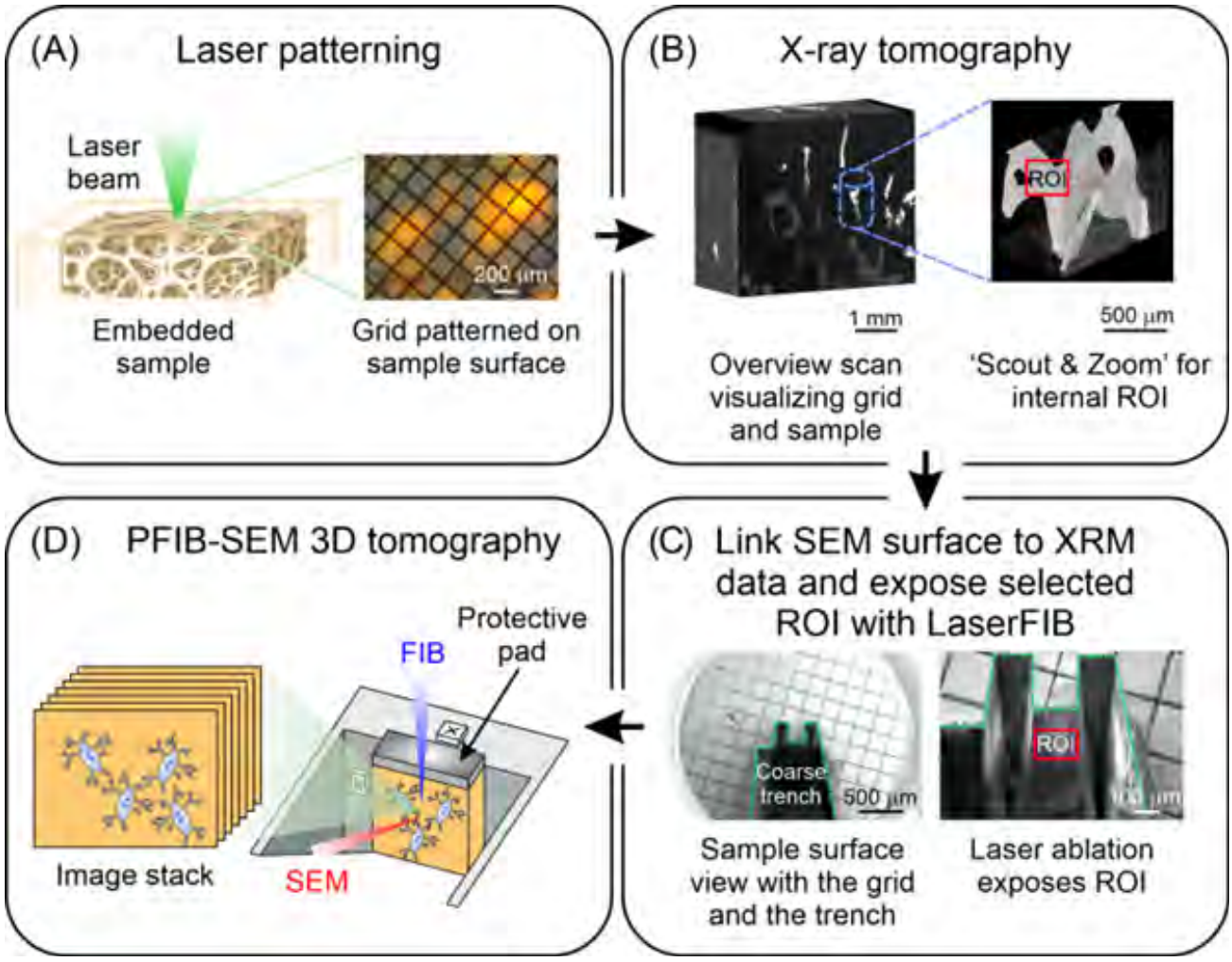

PO-010 Brittany Wilson, PhD

Early Postnatal Bone Structure in a Pig Model of Preterm Birth

Brittany Wilson*1, Frank Ko1, Anastasija Rudan1, Dawn Nix2, Autumn Sanderson2, Randal Buddington2 and D. Rick Sumner1
(1) Rush University Medical Center, Chicago, IL, USA, (2) Louisiana State University Health Science, Shreveport, LA, USA

Preterm birth disrupts skeletal development since mineralization predominantly occurs during the final gestational trimester. This puts preterm infants at increased risk for metabolic bone disease of prematurity, among other health challenges. Recently, the pig has been used to model preterm birth. The aims of this study were to determine the magnitude of skeletal deficits associated with preterm birth and to determine if the expected deficits resolved by term-corrected age in the pig model. Preterm pigs (Landrace x Yorkshire) were delivered by Cesarean section from two sows after about 105 of 115 days of gestation (i.e. ~90% of term). The preterm pigs were housed individually in incubators and transitioned by 48 hours from total parenteral nutrition to full enteral nutrition. Term control pigs of the same lineage were delivered vaginally from four sows on a farm and obtained within 12 hours after birth. Tissues and body mass data were collected from preterm and term pigs on the day of birth (i.e., postnatal day 0; n=8 and n=12, respectively) and from preterm pigs at term-corrected age (i.e., postnatal day 10; n=4). Right humeri and femora were measured with calipers for total bone lengths and mid-point widths in the anterior-posterior and medial-lateral directions. Bones were then scanned using micro-computed tomography to investigate cortical bone structure at the midshaft. Data were analyzed by one-way analysis of variance, using Tukey's honestly significant differences in post-hoc analyses ($p<0.05$ for significance).

Preterm pigs had 35% less body mass and about 17% shorter and thinner humeri and femora than term pigs on postnatal day 0. Deficits in body mass and bone lengths and widths in preterm pigs were resolved by term-corrected age (postnatal day 10), suggesting catch-up growth had occurred postnatally. Both cortical bone area and total cross-sectional area at the humeral mid-diaphysis were reduced by 29% and 25%, respectively, in preterm compared to term pigs on postnatal day 0, and these properties did not fully rebound by term-corrected age. Humerus cortical thickness and polar moment of inertia were each reduced (10% and 50%, respectively) in preterm compared to term pigs on postnatal day 0 and remained lower on average in preterm pigs on postnatal day 10. Similar patterns were observed for bone structure of the femora, but the deficits appeared to more fully recover.

While overall body mass and bone size tended to recover by term-corrected age in preterm pigs, other bone structural properties, particularly in the humerus, did not fully recover to the level observed in term pigs at birth. This suggests that catch-up bone growth occurs during the early postnatal period in preterm pigs, but decrements in cross-sectional properties may indicate that preterm bones are at increased risk for fracture.

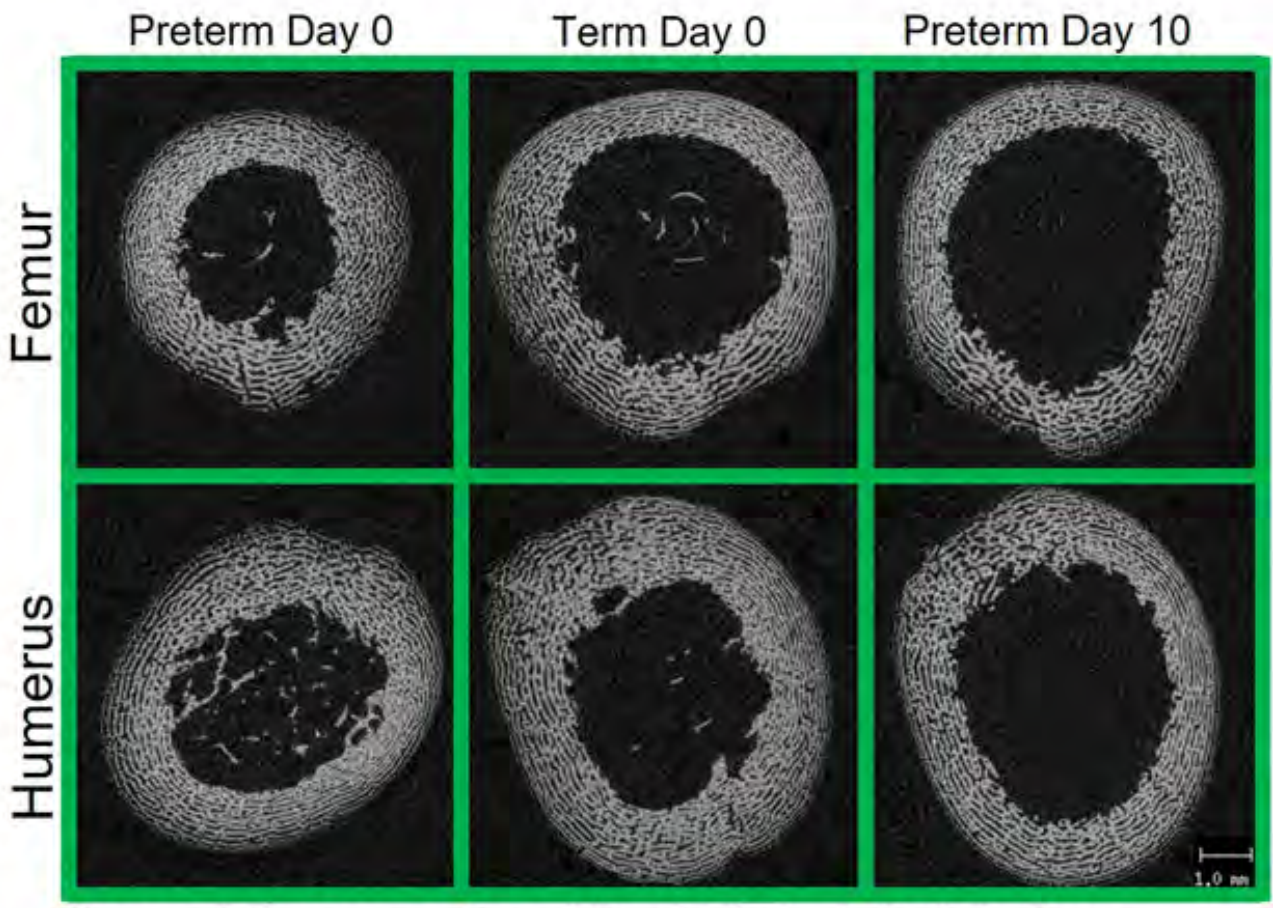

Representative cross-sections at the mid-diaphysis. Scale bar 1mm.

PO-011 Abigail Coffman

Bisphosphonate treatment leads to rapid increases in bone microdamage content and extensive osteocyte death around microcracks following in vivo atigue

Abigail Coffman*, The City College of New York, New York, NY, USA

PURPOSE: Bone microcracks (µcracks) and bisphosphonates (BPs) are implicated in atypical femoral fractures, though the nature of their interactions is not fully understood. µcrack accumulation has been reported in canine and human bone after years of BPs use, but these are endpoint studies and provide little insight into mechanisms of these interactions [1,2] In the current studies, we introduced µcracks in BP-treated bone in vivo to assess the cause-and-effect relationships between antiresorptive use and changes in pre-existing µcracks and changes in osteocyte integrity.
METHODS: µcracks were induced in ulnar diaphyses of adult SD rats (n=48) by fatigue (FAT) loading.[3] Rats were treated with either ALN (2.4µg/kg), NE58025 (200 µg/kg) or PBS vehicle starting 1 wk before loading. ALN high mineral binding has been speculated to directly influence bone mineral. Thus, comparison to low mineral affinity 58025 [4] allowed us to assess differential effects on µcracks. Baseline FAT ulnae were obtained immediately after loading. Survival rats were treated for 4 mo. Control ulnae were not fatigue-loaded (NoFAT). µcrack number, length and osteocyte integrity (% Empty lacunae) were measured, with Empty lacunae measured in damage regions or equivalent areas of NoFAT bone. Data shown as mean±SD and analyzed using ANOVA. Studies were IACUC approved.
RESULTS: µcrack number and length in FAT+PBS ulnae decreased, consistent with normal bone remodeling (Fig 1 A,B). In contrast, both BPs led to a nearly two-fold increase in µcrack number vs FAT-Base, but no change in µcrack length (Fig 1A, B). Remodeling suppression led to extensive osteocyte loss, with ~40% Empty lacunae in microdamaged bone (Fig 2).
DISCUSSION: This study reveals that in bone which was initially “seeded” with small amounts of bone microdamage in vivo, remodeling suppression led to a rapid increase in additional µcracks. Moreover, there was an unexpectedly large accumulation of dead bone around µcracks, likely due to failure to resorb and remove apoptotic osteocytes that normally occur acutely at new µcrack sites [3]. Critically, both µcracks and osteocyte loss each independently compromise bone mechanical properties. Finally, bone lacking osteocytes will not typically undergo remodeling. Thus, these results raise the critical question of whether osteocyte-depleted bone areas and the µcracks within would be remodeled if BP treatment is suspended, as suggested for a “drug holiday.”
REFERENCES: 1)Starr+ 2018; 2)Allen+ 2006; 3)Cardoso+2014; 4)Coffman+ 2021

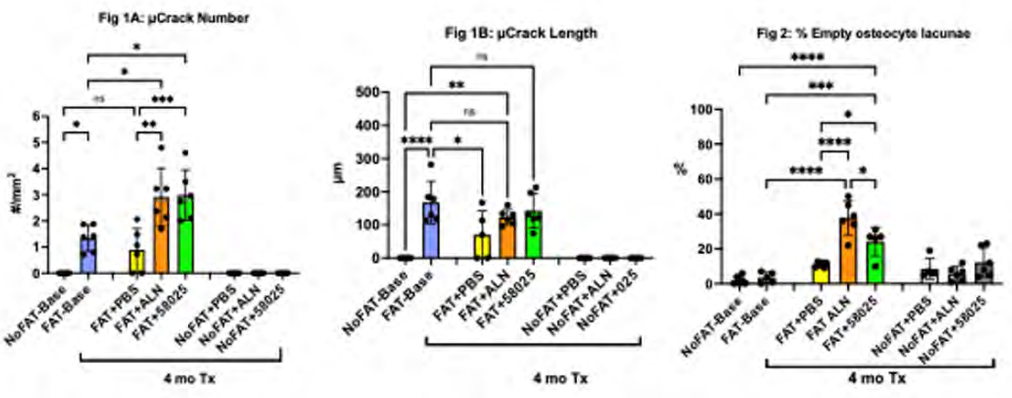

PO-012 David Barreto

Osteoporotic Fracture Prediction Using Opportunistic MR Imaging and Deep Learning

Albi Domi1, David Barreto*1, Enrie Gan1, Lihini Ranaweera1, Austin Vu1, Jianna Kim1, Vachan Patel1, Frank Pham1, Amber Lan1, Thamarie Pinnaduwage1, Makayla Clark1, Nilan Nandish1, Elaina Truong1, Angelina Diaz1, Harry Shi1, Sarem Khan1, Eva Gonzalez-Whitehouse1, Ethan Che1, Hannah Rosenblatt1, Sarah Bargamian1, Gregory Chang2, David Casper3 and Chamith S. Rajapakse1
(1) Perelman School of Medicine, Philadelphia, PA, USA, (2) Division of Muskuloskeletal Imaging, NYU Langone, NYC, NY, USA, (3) Department of Clinical Orthopaedic Surgery,Perelman School of Medicine, Philadelphia, PA, USA

Purpose: As the US population ages, spinal degeneration poses a growing challenge. Surgeries like decompression and spinal fusion carry risks, especially with factors like poor bone quality, increasing patient complications. Advanced surgical planning tools and predictive models are crucial. We utilized a 3D U-Net model to predict spinal fracture risk due to osteoporotic degeneration, streamlining manual segmentation and enhancing post-operative outcomes analysis.
Our study aimed to develop a non-invasive method for predicting spine fractures by automating the lumbar vertebrae segmentation in MR scans using a 3D U-Net model, followed by a discriminatory analysis between spine health measures derived between patients experiencing spine incidence fractures and a no-fracture reference group.

Methods: This research utilized retrospectively collected spine MR images from 732 patients (ages 28 to 93). Spine and hip DXA scores from 614 of these patients were collected and 104 patients experienced at least 1 fracture post-scan and post-DXA (0.72 +/- 2.65 years after). The cohort predominantly comprised females (92.3%), chosen due to a higher prevalence of osteoporosis in women. These scans, using T1-weighted spin-echo sequences, were sourced from the Hospital of the University of Pennsylvania with Institutional Review Board approval. Digital Imaging and Communications in Medicine (DICOM) series were manually segmented by trained annotators using ITK-SNAP. Each 2D slice in a single case underwent independent manual segmentation, with individual vertebrae being uniquely labeled for semantic segmentation.

These segmented images underwent augmentations and padding as model training inputs. A 3D U-Net model was trained for 100 epochs on an NVIDIA V100 GPU. The loss function was a combination of the Tversky loss (with parameter $\alpha=0.3$) and the Categorical Cross Entropy. The segmented predictions were overlaid onto the scan volume to generate vertebral volumes. ANOVA analysis was performed on fractures with vertebral mean intensities and separately with DXA values.
Results: Incidence spine fracture patients had significantly higher intensity mean vertebral values across all lumbar vertebrae ($p < 0.0001$). Interestingly, DXA values were not able to predict fractures, except for hip T-score ($p < 0.0001$). The trained model obtained an average Dice Score of 0.88 across all vertebrae (L5-T11) and a score of 0.89 for lumbar vertebrae (Fig. 1).

Conclusion: Our 3D U-Net efficiently segments lumbar vertebrae in MR scans, which is vital for analyzing fractures with complex anatomical structures. Fracture patients exhibited high intensity values due to soft tissue inside vertebral regions, which appears bright in MR scans. The correlation between fractures and mean vertebral intensity surpassed that of fractures and DXA, suggesting that MR scans are a superior predictor of spine fractures.

PO-012 David Barreto

Fig. 1) Workflow of extracting vertebral body intensities using the 3D U-Net. Model performance for each lumbar vertebra is shown in the upper table. The p values are shown to compare performance of lumbar intensities to DXA scores in predicting spine incidence fractures.

PO-013 Hoomin Lee, PhD

Examining Endothelial-Mesenchymal Transition in Intramembranous Bone Regeneration

Hoomin Lee*1, D. Rick Sumner2 and Frank Ko1
(1) Rush University Medical Center, USA, (2) Rush University Medical Center, Chicago, IL, USA

Intramembranous bone regeneration plays an important role in fracture healing, joint replacement, dental implant surgery, and distraction osteogenesis. The regenerative processes are composed of the initial inflammation following surgery, followed by blood vessel formation and subsequent new bone formation. The importance of blood vessel formation is well-known, such as a conduit for supplying necessary nutrients and growth factors to promote bone regeneration. However, potential de-differentiation or transdifferentiation of endothelial cells, such as Endothelial-mesenchymal transition (EndMT), have not been fully explored.

While not been explored in bone previously, EndMT has been observed during embryonic development of the heart, cardiac and renal fibrosis, wound healing and cancer progression, triggered by TGFβ, HIF1α, Notch, or Wnt. The key characteristics of EndMT are the loss of original endothelial cell markers (CD31, endomucin, etc.) and production of mesenchymal-specific proteins, including alpha-smooth muscle actin (αSMA) or collagen I, in endothelial cells. We therefore examined if EndMT is observed during intramembranous bone regeneration in mice.
We used fluorescent reporter mice (Cdh5-creERT2;tdTomato) that underwent mechanical bone marrow ablation surgery at 28 days old to examine EndMT on intramembranous bone regeneration. tdTomato was used as a marker for endothelial cells, and αSMA was used as a mesenchymal-specific marker. To label Cdh5+ endothelial cells, mice were administered with 10 μg/g of tamoxifen at 7 days old (T7) or 28 days old (T28). The two different tamoxifen induction strategies were used examine EndMT on only Cdh5+ descendants (T7) or both the Cdh5+ cells and their descendants (T28). Femurs were harvested post-operative days 7 (P7) or 10 (P10) and stained for aSMA and osterix.

In both tamoxifen induction strategies, we found EndMT to be present based on the number of cells that are positive for both tdTomato and aSMA. At 7 days after surgery, double positive cells in bone marrow were 2.04% (T7) and 3.65% (T28) of all tdTomato positive cells, respectively. Similarly, at 10 days after surgery, the double positive cells were 2.42% (T7) and 3.22% (T28) of all tdTomato-positive cells. However, no tdTomato positive cells were also positively stained for osterix in bone marrow for both 7 and 10 days after surgery. This suggests that while a subset of Cdh5 expressing cells acquire mesenchymal-like state, EndMT is likely transient and does not directly lead endothelial cells to bone forming cells. Future studies will further examine the necessity EndMT on intramembranous bone regeneration.

PO-014 Kenna Brown

High-Fat Diet and Aging Each Reduce Fracture Toughness and Matrix Properties in C57BL/6 Mice

Kenna Brown*1, Steven Watson1, Brady Hislop2, Ghazal Vahidi1, Ramina Behzad3, Ronald June2, Lamya Karim3 and Chelsea Marie Heveran1
(1) Montana State University, USA, (2) Montana State University, Bozeman, MT, USA, (3) Department of Bioengineering, University of Massachusetts, Dartmouth, Dartmouth, MA, USA

High fat diets (HFD) are common in Western countries, especially among the elderly (65+). Both aging and HFD increase fracture risk and reduce bone quality. Our data show that aging and HFD both reduce fracture toughness in C57BL/6 mice (Fig. A), suggesting that matrix properties are compromised by both. We hypothesized that aging and HFD differently impact bone matrix. Female and male C57BL/6 mice were fed low fat diet (LFD, 10% fat) or HFD (45% fat) for 8 weeks and euthanized at 5 or 22 months of age (n = 7-11/group). A fluorometric assay quantified advanced glycation end products (fAGEs) from the flushed cortical bone of humeri. Hydrated Raman spectroscopy was performed at the periosteal surface and the area near the endocortical surface of the femur diaphysis (0-30% cortical thickness, 7 μm spacing between rows). At both sites, medians were measured for matrix structure (I1670/I1640, I1670/I1610), mineral:matrix ratio (v1phos:amideIII), and mineral maturity (carbonate:phosphate, crystallinity). For endocortical measures, the gradient (slope of data linear fit) and heterogeneity (data root mean square deviation) were also calculated. 3-way ANOVA was used to analyze all measures. Clustering by absolute correlation identified matrix properties most strongly correlated with fracture toughness for males. At the periosteal surface, sex and age differences were found. Males had lower median mineral:matrix than females (-12%, $p < 0.001$) and aging increased mineral maturity (median carbonate:phosphate ratio, +12%, $p < 0.001$). At the endocortical region, sex and diet effects were pronounced. HFD impacted several matrix measures for females and less for males. Compared to LFD, HFD females had a lower median mineral crystallinity (-15%, $p = 0.017$) and matrix structure heterogeneity (I1670/I1610, -85%, $p < 0.001$). Males did not have significant differences with HFD. Nonetheless, for males, fracture toughness strongly correlated with median matrix structure (I1670/I1610), matrix structure heterogeneity (I1670/I1610), and median mineral:matrix ratio. fAGEs were not significantly different between groups or strongly correlated with fracture toughness (Fig. B). We show that age and diet both contribute to the loss of fracture toughness and matrix quality. HFD and aging both decrease fracture toughness, but the contributing changes to bone matrix properties differ. Our data advances understanding of how matrix properties vary with different causes of bone fragility and could lead to the development of improved therapies.

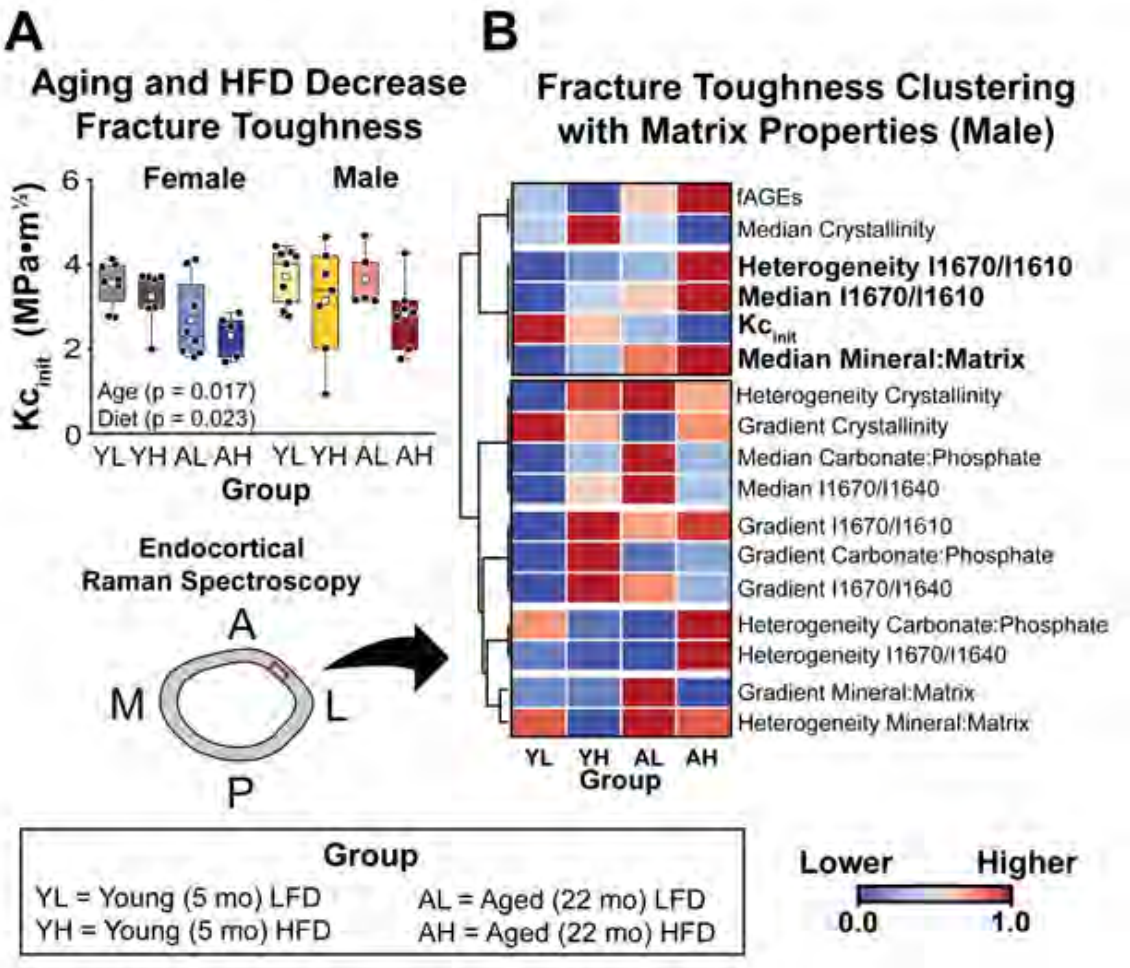
A
Aging and HFD Decrease Fracture Toughness
Female
Male
Kc_{init} (MPa•m^{½})
6
4
2
0
Age (p = 0.017)
Diet (p = 0.023)
YL YH AL AH YL YH AL AH
Group
Endocortical Raman Spectroscopy
A
M
L
P
B
Fracture Toughness Clustering with Matrix Properties (Male)
fAGEs
Median Crystallinity
Heterogeneity I1670/I1610
Median I1670/I1610
Kc_{init}
Median Mineral:Matrix
Heterogeneity Crystallinity
Gradient Crystallinity
Median Carbonate:Phosphate
Median I1670/I1640
Gradient I1670/I1610
Gradient Carbonate:Phosphate
Gradient I1670/I1640
Heterogeneity Carbonate:Phosphate
Heterogeneity I1670/I1640
Gradient Mineral:Matrix
Heterogeneity Mineral:Matrix
YL YH AL AH
Group
Group
YL = Young (5 mo) LFD
YH = Young (5 mo) HFD
AL = Aged (22 mo) LFD
AH = Aged (22 mo) HFD
Lower
Higher
0.0
1.0

PO-015 Pelumi Adedigba

Fructooligosaccharide Promotes Bone Formation and Mineralization Coincident with Alterations in PPARγ/WNT Signaling, Calcium Homeostasis and T-cell Biology

Pelumi Adedigba*1, Mariola Grez Capdeville2, Trina A. Knotts3, Gang Peng1, Edralin A. Lucas4 and Brenda J. Smith5
(1) Indiana Center for Musculoskeletal Health, Indiana University School of Medicine, Indiana University-Indianapolis, Indianapolis, IN, USA, (2) Department of Obstetrics and Gynecology, Indiana University School of Medicine, Indiana University-Indianapolis, USA, (3) Department of Surgery; Center for Alimentary and Metabolic Science, UC Davis Health, USA, (4) Department of Nutritional Sciences, College of Education and Human Sciences, Oklahoma State University, IN, USA, (5) Indiana Center for Musculoskeletal Health, Indiana University School of Medicine, Indiana University-Indianapolis, IN, USA

The gut-bone axis is a potential target for improving bone health. Short chain fructooligosaccharides (FOS) are a promising prebiotic known to alter the composition of gut microbiota, increase short chain fatty acids (SCFA) and intestinal mineral absorption (e.g., calcium and magnesium), and improve indices of cortical and trabecular bone. However, questions remain about what bone transcriptional changes are induced by FOS and the consequent alterations in bone remodeling. 8-wk-old C57BL/6 female mice (n=10/group) were acclimated for 2 weeks prior to initiating dietary treatments: AIN-93M control diet (CON) or CON diet supplemented with FOS (10%; w/w). After 4 weeks, dynamic and static bone histomorphometry was performed on femurs as well as RNA-seq on femur hard tissue and bone marrow (BM). Fecal samples were processed for microbiota profiling using 16S based amplicon sequencing. All data were analyzed using t-test except for the microbiota data which was analyzed using ANCOM-BC. FOS treated mice had higher ($P<0.05$) trabecular bone volume, number, thickness, and reduced separation ($P<0.05$) compared to CON. FOS increased endocortical and periosteal bone formation rate per bone surface (BFR/BS, $P<0.01$), endocortical mineral apposition rate (MAR, $P<0.05$) and tended to increase periosteal MAR ($P=0.09$). In trabecular bone, FOS increased MAR and BFR/BS ($P<0.0001$). Microbiota analysis revealed FOS increased the relative abundance of the Actinobacteria, Cyanobacteria, and Verrucomicrobiota phyla ($P<0.001$), as well as the SCFA-producing bacteria, Clostridia, and Lactobacillus ($P<0.001$). In the bone hard tissue, genes involved in PPARγ signaling, adipogenesis and the regulation of adipocyte lipolysis (e.g., Plin1, Slc27a1, Scd1, Fasn) ($P<0.05$) were downregulated with FOS. FOS upregulated genes involved in calcium ion transport and homeostasis (e.g., Ccl8, Cxcl9, Trpa1, Cxcl10). In the BM, genes regulating T cell apoptotic processes (Rag1, Gpam, Il7r, Pdcd1) were upregulated ($P<0.05$) with FOS as well as genes regulating the bone matrix (e.g., Col6a5, Col6a2, Col6a4) providing the scaffold for osteoblast during ossification. In both the bone hard tissue and BM, genes regulating T cells differentiation (Bach2, IL7r, Irf4, Rag1) and Wnt signaling (Sox4, Lgr5) ($P<0.05$) were upregulated. Our findings suggest that FOS increases bone formation and mineralization by downregulating PPARγ and upregulating Wnt pathway, enhancing Ca+2 transport, and modifying T-cell biology.

PO-016 Marie-Josée Bégin, MD

Histomorphometric Evaluation of TRAcP in Bone Biopsies of Patients with Renal Osteodystrophy: Assessment of Trabecular and Endocortical Surfaces

Natalie Dion, Marie-Josée Bégin* and Ste-Marie Louis-Georges, Centre hospitalier de l'Université de Montréal, Montréal, QC, Canada

Bone histomorphometric analysis of undecalcified bone specimens is the gold standard for diagnosis of complex bone disorders such as renal osteodystrophy (ROD). This analysis mainly focuses on trabecular bone (Tb) remodeling while cortical turnover is rarely evaluated. Endocortical (Ec) surface is known to be a predominant site of bone resorption, and cortical trabecularisation is a common finding in high bone turnover ROD. To facilitate osteoclasts (Oc) counting, we have validated the use of Tartrate Resistant Acid Phosphatase (TRAcP), detected by automated immunohistochemistry on undecalcified bone sections (FR-001,SUN-001, 2023 J Bone Miner Res 38 Suppl 2). In order to improve the evaluation of resorption activity, we performed Oc TRAcP counting at Tb and Ec surfaces (N.TRAcP/B.Pm) in 25 transiliac bone biopsies of ROD patients (68.8 ± 8 yo; 12 women/13 men). Ec compartment was defined as the area starting at the inner cortex and ending at a distance corresponding to a 2-fold thickness of the largest trabecula originating from the cortices. The external (e-Ec) and the internal (i-Ec) cortices were analyzed separately. External cortex was distinguished from the inner as the one with more muscle tissue adjacent to its periosteum. In trabecular compartment, N.TRAcP/B.Pm showed a strong positive correlation with eroded surfaces and bone formation rate per bone surface (rho=0.642 and rho=0.708, respectively). Trabecular N.TRAcP/B.Pm was also positively correlated with i-Ec N.TRAcP/B.Pm (rho=0.799) and in e-Ec (rho=0.628). Cortices with trabecularisation (42%) showed a lower thickness ($p<0.001$) but no significant increase in Ec N.TRAcP/B.Pm was found. Compared to biopsies with normal remodeling, Tb N.TRAcP/B.Pm was higher in high turnover biopsies ($p=0.03$) and lower in low turnover biopsies ($p=0.01$)(Table 1). For the Ec compartments, only i-Ec showed a significant difference for N.TRAcP/B.Pm when low turnover was compared to high turnover ($p=0.04$). These results highlight for the first time the use of N.TRAcP/B.Pm to evaluate bone resorption at Tb and Ec compartments in ROD biopsies and seems to be an excellent marker of bone turnover. Interestingly, in ROD, i-Ec N.TRAcP/B.Pm appears to be more associated with trabecular bone turnover than e-Ec suggesting a different behavior between the two cortices, perhaps in relation to different degree of sustained mechanical stress.

Table 1. N.TRAcP/B.Pm according to bone turnover and bone compartments

		Normal (n=8)	Low (n=11)	p-value	High (n=6)	p-value
Trabecular	Median (IQR)	0.362 (0.160)	0.072 (0.133)	0.01	0.740 (0.276)	0.03
	Mean ± SD	0.353 ± 0.148	0.127 ± 0.128		0.742 ± 0.298	
External Ec	Median (IQR)	0.407 (0.679)	0.151 (0.363)	NS	0.849 (1.124)	NS
	Mean ± SD	0.533 ± 0.566	0.313 ± 0.346		0.988 ± 0.662	
Internal Ec	Median (IQR)	0.514 (0.225)	0.106 (0.448)	NS	0.886 (0.360)	0.09*
	Mean ± SD	0.497 ± 0.255	0.293 ± 0.386		1.101 ± 0.658	

Ec: endocortical, IQR: interquartile range, SD: standard deviation, NS: not statistically significant
*p=0.04 when comparing high vs. low bone turnover

PO-017 Mohamed Hassan, DDS, PhD

The role of macrophases in the superior regenerative capacity of neural crest-derived bone_3D insights into craniofacial healing

Mohamed G. Hassan*, Anushka Gerald, Kyle Koester, Isabella Rastegar and Erica L. Scheller, Washington University in St. Louis, USA

Skeletal defects can have significant physical, psychosocial, and economic impacts on both children and adults, and the development of novel regenerative therapies are necessary to restore quality-of-life for affected individuals. Neural crest cells contribute to roughly 5% of the human skeleton, primarily forming the skull and parts of the clavicle and scapula. These bones exhibit faster regeneration compared to those formed from the mesoderm, but the underlying mechanism of accelerated healing remains unclear. Macrophages and de-novo vascularization are crucial for bone healing. Therefore, we hypothesized that early recruitment of macrophages and blood vessels contributes to the superior regenerative capacity of neural crest-derived bone. To investigate this, we created standardized 1.8 mm defects in the neural crest-derived frontal bone and mesoderm-derived parietal bone of 12-week-old mice. Micro-CT analysis confirmed prior reports of accelerated healing in neural crest-derived bone at all time points (1-, 2-, 3- and 4 weeks). Targeted depletion of macrophages using clodronate liposomes during the early stage of healing in mice prevented this accelerated healing response. We used a high-resolution 3D imaging platform to map blood vessels phenotypes and macrophages within the defects at single-cell resolution. Notably, the neural crest-derived bone defect displayed a consistently denser vascular network and ongoing de-novo vasculogenesis, surrounded by a prominent population of macrophages. These findings identify a crucial role of macrophage-lineage cells in promoting neural crest-derived bone regeneration. Our findings also highlight the close spatial relationship between blood vessels and macrophages during cranial bone healing, opening the way for future research aimed to understand the role of innate immunity in the acceleration of skeletal regeneration. Additionally, our 3D imaging technique holds promise for studying other cells types and investigating various unexplored aspects of craniofacial skeletal biology.

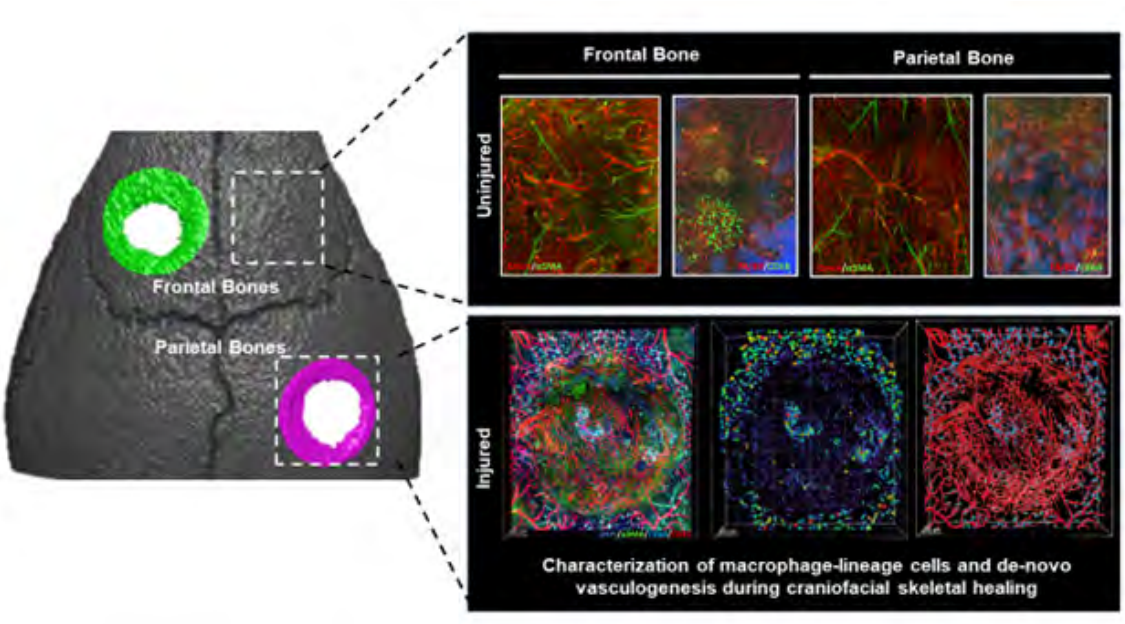

PO-018 Vishal Gokani

Automated Quantitative Histomorphometric Analysis of Osteonecrosis of the Femoral Head: A Deep Learning Approach

Vishal Gokani*1 and Harry K. W. Kim2, (1)Texas Scottish Rite Hospital, Dallas, TX, USA, (2)Scottish Rite Hospital/UTSW, dallas, TX, USA

Background: Osteonecrosis of the femoral head (ONFH) produces deformity and disability. The piglet model of ONFH involves disruption of blood flow and produces bone histomorphometric changes, which can be detected by time-consuming manual analysis that creates a bottle neck in animal studies. The purpose of this study was to assess the accuracy of computer vision (CV) models applied to bone histomorphometry. We hypothesized that automated quantitative analysis using finetuned CV models (MaskRCNN, YOLOv8, SAM) would provide accurate analysis of histomorphometric parameters with great efficiency.

Methods: 40 pigs underwent unilateral surgery to induce ONFH, providing histologic sections from 40 necrotic and 40 normal femoral head samples for analysis. Calcein and Xylenol Orange were administrated 4 days apart to generate double-labeled surfaces to analyze bone formation. Femoral heads were processed for methyl methacrylate embedding and sectioning. Slides were stained with TRAP or McNeal or left unstained for fluorochrome labeling analysis. Whole slides were imaged at 10x magnification and annotated by three observers. 50 femoral head samples were used for training and validation while 30 were used for testing. We used intersection over union (IoU), precision (positive predictive value), recall (sensitivity), and intra-class correlation (ICC) to assess the accuracy of the CV models' histomorphometric measurements compared to human observers.

Results: For TRAP-stained slides, osteoclasts were recognized as TRAP-positive cells in proximity to bone (Fig1A) with an IoU of 94%. Similarly, assessment of McNeal-stained slides showed segmentation of trabecular bone and osteoblasts, despite vague cell borders and smudged appearance (Fig 1B), with an IoU of 76%. For fluorescent double labeled slides, the CV models classified and segmented red- and green-single-labeled surfaces and adjacent double-labeled surfaces (Fig 1C) with an IoU of 83%. Precision and recall exceeded 85% and ICC exceeded 0.9 ($p < 0.01$) for cell counts, bone histomorphometry, and dynamic remodeling measurements. CV models provided a 10-fold improvement in efficiency with a whole slide processing time of 693 + 382 sec.

Conclusion: CV models segmented osteoblasts, osteoclasts, fluorescent bone labels, and trabecular bone with the accuracy of observers and greater efficiency, allowing for automated quantitation of histomorphometry.

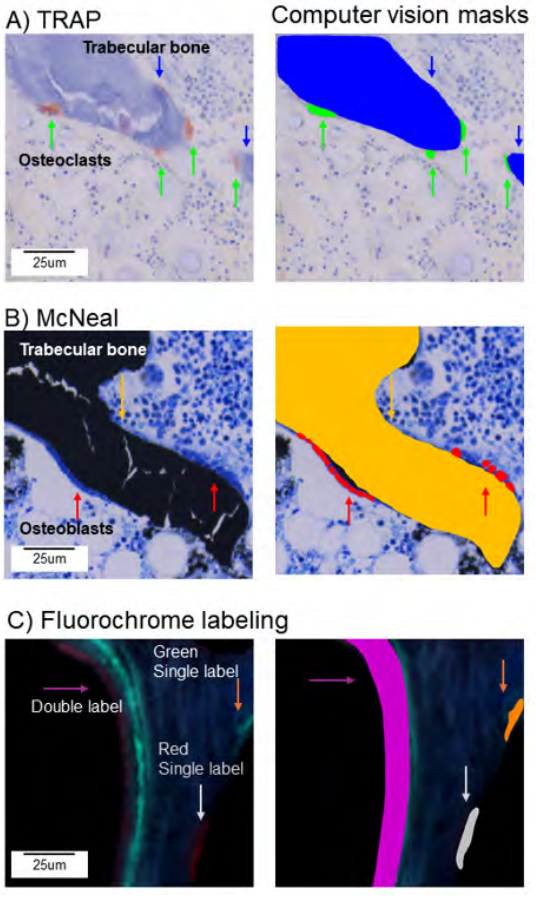

PO-019 Anastasiia Sadetskaia

The Mystery of Cement Lines in Bone Structure: Spatial Distribution of Zn and Changes in Surrounding Matrix Mapped by Synchrotron-Radiation Experiments

Anastasiia Sadetskaia*1, Jonas Palle1, Nina Kølln Wittig1, Carsten Pedersen1, Annemarie Brüel2, Maik Kahnt3, Manuel Guizar-Sicairos4,5 and Henrik Birkedal1,
(1) Department of Chemistry and iNANO, Aarhus University, Aarhus, Denmark, (2) Department of Biomedicine, Aarhus University, Aarhus, Denmark, (3) MAX IV Laboratory, Lund University, Lund, Sweden, (4) Paul Scherrer Institute, Villigen, Switzerland, (5) École Polytechnique Fédérale de Lausanne, Lausanne, Switzerland

Cement lines are one of the most mysterious bone organization units involved in the remodeling process of bone. They are ~5 µm thick densely mineralized borderlines emerging between the newly laid and old bone as a part of osteon formation. Their nanostructure, relation to the surrounding matrix, role, and function are still poorly understood. Recent studies suggest that cement lines, as well as osteocyte lacunar borders, are enriched in Zn1 and that the associated mineral matrix differs from the rest of bone2. However, the reason why Zn accumulates in these regions remains unclear and the answer to that might be linked to the form in which Zn is stored – in mineral or as part of a protein. As a first step to investigate this, we have performed 3D spatial mapping of Zn in bone regions around cement lines and osteocyte lacunae with a sub-micron step size using synchrotron-radiation nanoimaging, X-Ray fluorescence (XRF) and X-Ray diffraction (XRD) techniques. Sections of human femoral bone (male, n=4) were cut by hand under a stereomicroscope, mounted on pins and milled into ~20 µm diameter cylinders using a custom-built lathe. Between the cutting and milling stages, in-house 3D X-Ray microscopy was used to map and verify the placement of the cement line and osteocyte lacunae within the 3D sample volume3. The nanoimaging data were collected at the cSAXS beamline, SLS, Switzerland with a resolution down to 55 nm. The 3D XRF/XRD data were collected at the NanoMAX beamline, MAX IV, Sweden, with a step size down to 80 nm, allowing for mapping the Zn and Ca content, as well as mineral properties in 3D. Custom-written MATLAB code was used for analysis.

As far as we know, this is the first high resolution 3D mapping of the Zn distribution near cement lines. The reconstructed XRF maps provide excellent information on the Zn distribution in the cement line and peri-osteocyte lacuno-canalicular network regions. Both are enriched with Zn. Interestingly, the newly formed bone at the border of the cement line is deficient in Zn compared to the older matrix. The collected XRD patterns suggest the orientational effects of the mineral with both ordered and disordered motifs around cement line. The excellent sub-micron resolution allowed for more precise elemental mapping and opens the possibility of correlating the elemental distribution with nanoimaging and other techniques. This gives a strong basis for understanding the role of accumulated Zn levels and in turn the structure of cement lines.

1Pemmer B, et al. Bone. 57(1):184-93, 2013.
2Grünewald TA, et al. IUCrJ. 10(Pt 2):189-198, 2023.
3Wittig NK, et al. JTMS. 5:100027, 2024.

PO-020 Atousa Moayedi

Investingating the alterations in enthesis lacunae morphometry undermechanical loading

Atousa Moayedi 1, Katerina Karali 1, Jovana Radulovic 1, Gordon Blunn 2
(1) Department of Mechanical and Design Engineering, University of Portsmouth, UK, (2) Department of Pharmacy and Biomedical Sciences, University of Portsmouth, UK
atousa.moayedi@port.ac.uk

Introduction: The calcified fibrocartilage (CFC) of the enthesis is considered as a transitional zone where tendon collagen fibres merge with the mineralised tissue. Understanding the morphometry of CFC lacunae is crucial for elucidating its biomechanical properties, response to mechanical stimuli, and insights into underlying reasons for degeneration and inflammation progression at the tendon-bone interface. Existing research suggests that mechanical loading influences the structure of entheseal tissue [1-2]. However, the specific effects of mechanical load on CFC lacunae morphology is not understood. This study aims to investigate the full field lacunae size, shape, and angle within CFC and how these change under in-situ uniaxial tensile testing.
Method: Achilles tendon attached to the calcaneus were dissected from euthanised 8 months old male mice (ethical approval 2022-104588). In-situ μCT (Versa 610, Zeiss) tensile testing was performed with 4X optical magnification, 1.3 μm pixel size, and 1601 projection number. The tendon's tensile axis was aligned to the calcaneus axis. Samples were scanned once in unloaded condition and then at 4.5N uniaxial load corresponding to physiological range (Deben CT500, Deben Ltd, UK). Images were rigidly registered (Avizo, USA). Tomograms before and after load were scaled using HA phantom to match the intensity histograms and the lacunae network was extracted using interactive thresholding. Morphometry parameters including Lacunae Volume (Lc.V), number (Lc.N), Stretch (Lc.St), and angle (Lc.θ) were calculated (XamFlow, Lucid AG, Switzerland).
Result: μCT 3D tomograms showed the distribution of lacunae volume ranging between 50 and 1000 μm³, with higher volumes predominantly concentrated in the central areas of the CFC. Before applying the tensile load, lacunae below 300 μm³ were round with value between 0 to 0.5, and as the volume increased, the lacunae became more oval and stretched (value between 0.5 to 1). After loading, larger lacunae were mostly between 0.4 to 0.6. The angle of lacunae with respect to the coronal plane had the highest frequency between 45 and 75 degrees, which increased after loading to 55 and 90 degrees.
Conclusion: μCT tomograms, combined with morphometry analysis, were employed to capture lacunae characteristics under both unloaded and loaded conditions. The study revealed that larger lacunae within CFC undergo shape and angle alterations, highlighting the adaptation process in response to physiological loading conditions. Lacunae morphology transitioned from predominantly circular to increasingly elongated shapes as their size increased. However, after loading, the larger lacunae exhibited a transition from elongated towards spherical Furthermore, alterations in lacunae orientation after loading were observed, with a notable shift towards higher angles with respect to the coronal plane. However this is dependent on the angle of loading.
Acknowledgement: This research has been funded by Faculty of Technology University of Portsmouth and Carl Zeiss Microscopy.
Disclosures: Atousa Moayedi (N), Katerina Karali (N), Jovana Radulovic (N), Gordon Blunn (N)
References: 1- Benjamin et al., J of Anatomy, V. 208 (2006) 2- Sang et al., J Mech Behavior of Biomedical Materials, V.135 (2022)

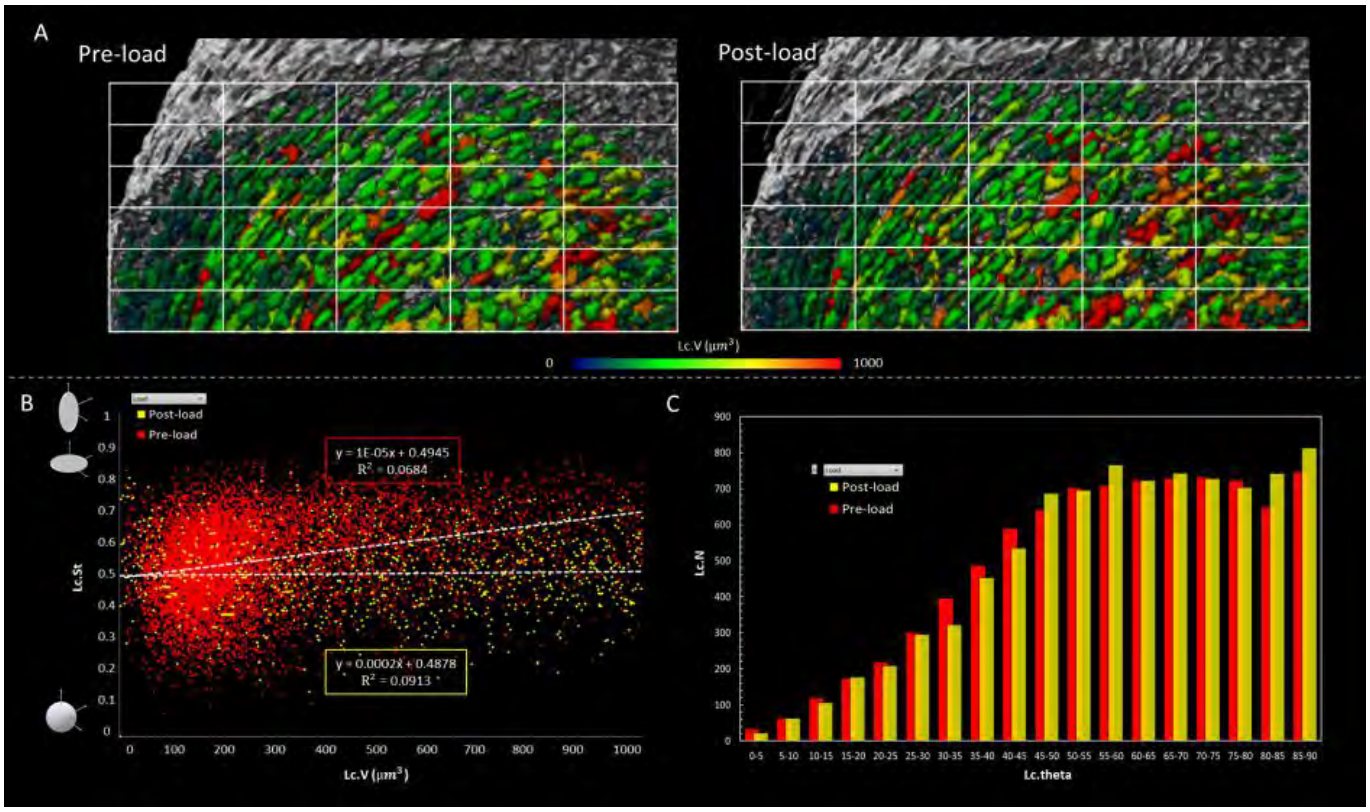

Figure 1. A) 3D representation of enthesis CFC lacunae network before and after tensile load. B) The lacunae stretch (Lc. St) as a function of lacunar volume (Lc.V) before and after tensile load. C) Lacuna angle frequency distribution before and after tensile load.

PO-021 Hongzhi Liu

Macrophages Regulate Angiogenesis-Osteogenesis Coupling Induced by Mechanical Loading through the Piezo1 Pathway

Hongzhi Liu*, Hang Zhou, Yuanhao Fan, Jiawei Li and Chao Liu, Southern University of Science and Technology, Shenzhen, Guangdong, China

Purpose: Mechanical stimuli are essential environmental factor for development, growth, maintenance, and repair of the bone. While macrophages are cells of monocytic lineage that are abundant and functional during inflammatory response after bone injury, they are also present throughout the bone repair process. How mechanical stimuli modulates macrophages during bone regeneration, particularly in intramembranous ossification, is still unclear. Here, we utilized conditional knockout of Piezo1 in LysM+ myeloid cells and in vivo mechanical loading to investigate the mechanoregulation of macrophages and their contribution to bone repair.
Methods: Bilateral monocortical tibial defect surgeries were performed on 12-week-old LysM-Cre; Piezo1fl/fl (Piezo1ΔLysM) mice. Daily mechanical loading was applied from the post-surgery day (PSD) 5 to 8. Mice were euthanized on PSD 10, and their tibiae were collected for evaluation of bone defect repair using micro-CT, and immunostaining.
Results: Micro-CT data showed that the enhancement in bone regeneration by mechanical loading was impaired in Piezo1ΔLysM mice. Immunostaining results revealed that mechanical loading promoted coupling of angiogenesis and osteogenesis in Piezo1fl/fl mice by significantly increasing the percentage of M2 macrophages and Osterix+ osteoprogenitor cells, suggesting an important role of macrophage mechanosensing during bone repair. However, all the loading-induced upregulations were abolished by Piezo1ΔLysM mice.
Conclusions: Mechanical activation of Piezo1 in macrophages significantly contributes to the regulation of bone regeneration by influencing M2 polarization and coupling of angiogenesis and osteogenesis.

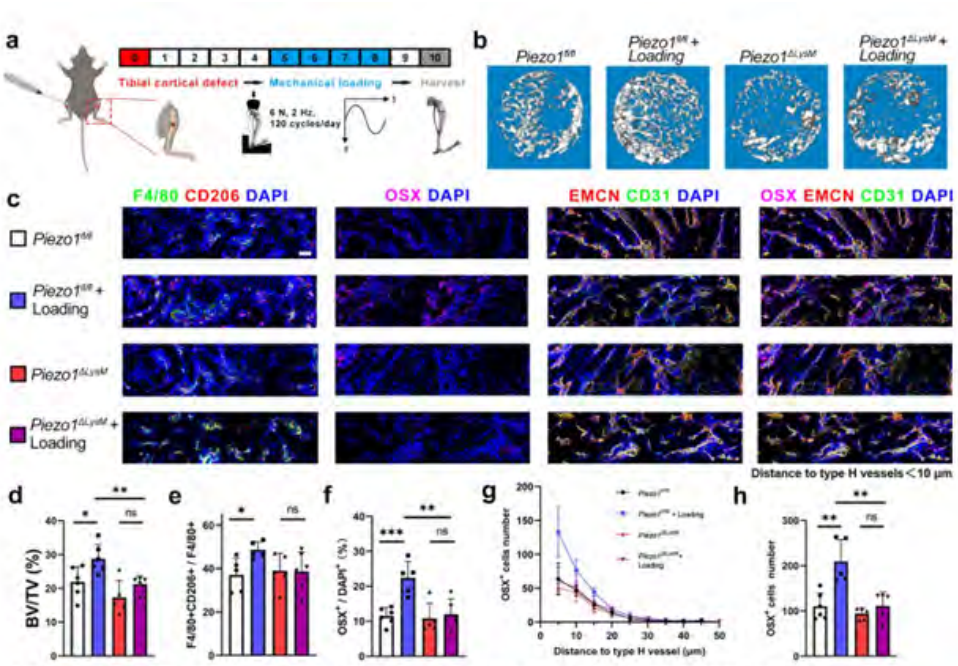

Fig.1 | (a) Schematic illustration of the design of animal experiments to test the effect of mechanical loading on bone repair. (b) Micro-CT reconstruction of cortical bone defect regions on PSD10 in female mice. (c) Fluorescent microscopy showing M2 (CD206+, red; F4/80+, green) macrophage, EMCN+(red)CD31+(green) vessels and osteoprogenitor cells (OSX+, purple) within defect region in the tibial monocortical defect model; Nuclei were counterstained with DAPI (blue); Scale bars: 50 μm. (d) Bone mass of bone defect regions on PSD10. (e) The ratio of M2 macrophages to total macrophages. (f) Percentage of OSX+ osteoprogenitor cells within defect region. (g) 3D distance analysis of OSX+ osteoprogenitor cells to type H vessels within defect region in different group. (h) The number of OSX+ osteoprogenitor cells within 10 μm next to type H vessels in different group. Data are means ± SD. *p < 0.05, **p < 0.01, ***p <0.001.

PO-022 Xuan Wei

3D Morphological Analysis of Age and Sex-Related Changes in Human Cortical Bone Remodeling Spaces Using Micro-CT

Xuan Wei*1, Lindsay Loundagin2 and David Michael Lane Cooper2
(1) Department of Anatomy Physiology and Pharmacology, College of Medicine, University of Saskatchewan, Saskatoon, SK, Canada, (2) Department of Anatomy, Physiology and Pharmacology, College of Medicine, University of Saskatchewan, Saskatoon, SK, Canada

Bone remodeling is the internal turnover process through which the demand of mineral homeostasis and tissue maintenance is met. Age-related increase in cortical porosity can be attributed to imbalance and/or uncoupling between resorption and formation. These states should be reflected in altered remodeling space morphology, with imbalance associated with larger remodeling space caused by excessive resorption, larger final canal due to incomplete infilling and uncoupling reflected by delayed or absent initiation of formation (presence of a transition zone of relatively stable diameter following resorption). We sought to determine if remodeling space morphology differs by age and sex. We hypothesized that with aging, these spaces would exhibit evidence of imbalance and/or uncoupling and this pattern would be more pronounced in women. We analyzed micro-CT scans of anterior femoral midshaft specimens from 58 human donors (22 females, 36 males; aged 20-82 yrs), which yielded 184 remodeling spaces with classically described morphology (a cutting cone followed by a closing cone and then a canal with stable diameter). They were then assessed by mapping 3D radial diameter along their lengths. Results showed a decreasing trend in remodeling space dimensions with age, but no differences in the distributions of any of the measurements between sexes. While the remodeling space length and maximal radius decreased in older individuals, the transition zone length and final canal radius did not differ, counter to our hypothesis. Longer transition zones were more common in older women, but also in younger men. Although these patterns only became significant following the removal of outliers, they may be indicative of different underlying mechanisms causing prolonged transition zones. This study demonstrated the value of 3D analysis at the level of individual remodeling spaces. Sex and age differences in morphology (or the lack thereof) indicate the intricate interplay of systemic and local controls from myriad mechanical, hormonal and cell senescence factors on remodeling dynamics, and the potential existence of seemingly normal remodeling events superimposed against the backdrop of overall progressive bone loss with age. An important limitation to consider is that our focus on classical remodeling space morphology excludes irregular patterns, particularly those that arise with interconnecting or coalescing pores and trabecularization of the cortex.

PO-023 Cindy Cruz

In Vivo Sequential MicroCT-based Radiographic Features of the Pre-Clinical Osteonecrosis of the Jaw (ONJ) prodrome in rice rats

Cindy Cruz Camacho1, Delaney Freehill1, Cynthia Castillo1, Norma Chavez Saldaña1, Christine Conover2, Jayachandra Kura2, Joshua Yarrow2, Evelyn Castillo1, Alexis Powers3, Anita Gohel3, Indraneel Bhattacharyya3, Donald B. Kimmel1 and Jose Ignacio B. Aguirre*1
(1) Department of Physiological Sciences, University of Florida, Gainesville, FL, USA, (2) VA Medical Center, Research Service, VAMC, Gainesville, FL, USA, (3) Department of Oral & Maxillofacial Diagnostic Sciences, College of Dentistry, University of Florida, Gainesville, FL, USA

Introduction: Osteonecrosis of the jaw (ONJ) is a potentially debilitating condition in patients receiving antiresorptives such as zoledronic acid (ZOL) who also have a concurrent oral risk factor (e.g. periodontitis, tooth extraction, etc.,). ONJ is clinically classified into 4-stages (0–3). Stage 0 patients have no-exposed bone with poorly-defined clinical/radiographic alveolar bone features. In contrast, stages 1-3 patients have a clinical disease with exposed bone. We have previously established a reliable model replicating clinical ONJ in ZOL-treated rice rats after 9-12 weeks. The time-window before clinical disease manifestation creates a unique scenario for investigating the ONJ prodrome/Stage-0. We hypothesize that characteristic radiologic, cellular and molecular features precede the development of clinical disease during the prodrome.

Methods: This study combined longitudinal/cross-sectional approaches. 80 rice rats with or without periodontitis received ZOL (oncology dose) or saline. All rats received oral exams, and their heads were scanned by in vivo microCT every-3wks. Groups of rats were then euthanized at 0, 3, 6, 9, and 12-weeks and jaws were processed to assess the prevalence of ONJ by histopathology, apoptosis/necroptosis, and cellular/molecular markers of inflammation. All endpoints are being correlated with the MicroCT-based radiographic data.

Results: Histopathologic ONJ developed only in the rats with periodontitis treated with ZOL, with a prevalence of 25%, 25% and 75% after 6, 9 and 12 wks of treatment, respectively. Non-ZOL-treated rats or rats with no periodontitis never had ONJ. Assessment of sequential microCT scans in the rats with periodontitis treated with ZOL identified five radiographic features (bone sequestration, crater-like defects, trabecular sclerosis, cortical-erosion, and periosteal-reaction) considered predictors of clinical ONJ in patients. However, trabecular sclerosis, cortical erosion, and bone sequestration developed during the prodrome only in the rats that ultimately had ONJ, and progressively became more apparent while clinical ONJ developed. Qualitative/quantitative microCT analyses, cellular/molecular assessments, and correlation with radiographic data are being undertaken.
Conclusion: This study represents the first multi-faceted, sequential characterization of features present in the ONJ prodrome in rats. The study suggests trabecular sclerosis, cortical erosion and bone sequestration are radiographic features developing during the prodrome of ONJ that progress toward clinical disease. Characterization and correlation of the radiographic, cellular, and molecular features of a region that eventually becomes an ONJ site are being evaluated before clinical ONJ is customarily diagnosed.

PO-024 Brett Mattingly

Conditional Loss of CaMKK2 in Osterix-Positive Osteoprogenitors Enhances Osteoblast Function in a Sex-Divergent Manner

Brett Mattingly*1,2, Anuradha Valiya Kambrath1,2, Xinchun Ding1,2, William Roy Thompson1,2,3 and Uma Sankar1,2
(1) Indiana University School of Medicine, Indianapolis, IN, USA, (2) Indiana Center for Musculoskeletal Health, Indianapolis, IN, USA, (3) Indiana University School of Health and Human Sciences, Indianapolis, IN, USA

Ca2+/calmodulin-dependent protein kinase kinase 2 (CaMKK2) is a multi-functional, serine/threonine protein kinase with predominant roles in inflammation, systemic energy metabolism, and bone remodeling. We previously reported that global ablation of CaMKK2 or its systemic pharmacological inhibition led to bone mass accrual in mice by stimulating osteoblasts and inhibiting osteoclasts. However, a direct, cell-intrinsic role for the kinase in the osteoblast lineage has not been established. Here we report that conditional deletion of CaMKK2 from osteoprogenitors, using the Osterix 1 (Osx1) - GFP::Cre (tetracycline-off) mouse line, resulted in increased trabecular bone mass due to an acute stimulation of osteoblast function in male and female mice. The acute simulation of osteoblasts and bone formation following conditional ablation of osteoprogenitor-derived CaMKK2 was sustained only in female mice. Periosteal bone formation at the cortical bone was enhanced only in male conditional knockout mice without altering cortical bone mass or strength. Prolonged deletion of CaMKK2 in early osteoblasts was accompanied by a stimulation of osteoclasts in both sexes, indicating a coupling effect. Notably, alterations in trabecular and cortical bone mass were absent in the doxycycline-removed “Cre-only” Osx1-GFP::Cre mice. Thus, the increase in osteoblast function at the trabecular and cortical bone surfaces following the conditional deletion of CaMKK2 in osteoprogenitors is indicative of a direct but sex-divergent role for the kinase in osteoblasts.

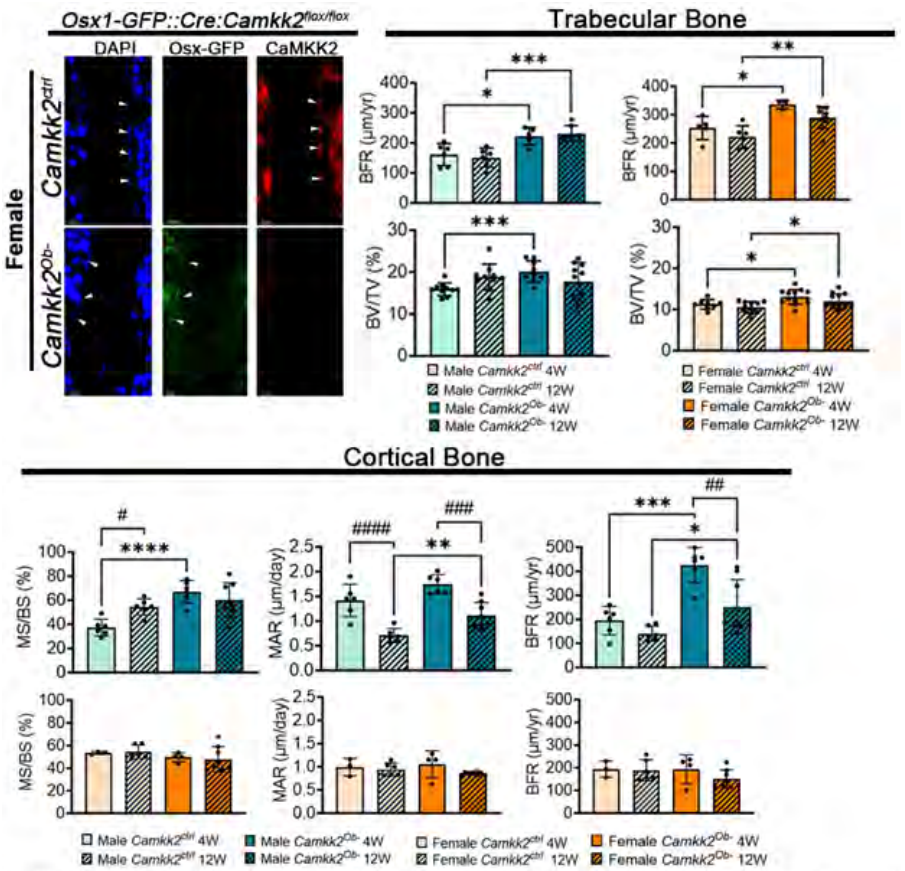

Figure 1: Representative images depicting the deletion of CaMKK2 in osteoblasts in female mice following the removal of doxycycline. Graphs depicting the acute increase in trabecular bone mass in male and female mice. Sustained trabecular bone mass seen in female but not male mice. Cortical graphs showed both accute and sustained increases in MAR and BFR in the periosteum of male but not female mice.

P-025 Ahmed Al Saedi, PhD

A novel role of CXXC Finger Protein1 in osteoblast differentiation during the early stages of bone development

Ahmed Al Saedi*1,2, Joshua Meyer1, Lijie Jiang1, Molly Persky1, David E. Maridas3, Laura Gamer3, Vicki Rosen4 and Diana L. Carlone1,2,
(1) Division of Endocrinology, Boston Children's Hospital, Boston, MA, USA, (2) Department of Pediatrics, Harvard Medical School, Boston, Boston, MA, USA, (3) Harvard School of Dental Medicine, USA, (4) Department of Developmental Biology, Harvard School of Dental Medicine, Boston, MA, USA

CXXC Finger Protein 1 (CFP1), an epigenetic regulator, is critical for skeletal stem/progenitor cell (SPC) function during development. Mice lacking CFP1 in Prx1+ cells (cKOPrx1) fail to form forelimbs, have severely abnormal hindlimbs, and display defects in calvarial bone formation. To gain insight into CFP1 regulation of calvarial bone formation we examined the effect of CFP1 loss on both calvarial stem cells (CSCs) and pre-osteoblasts (Obs) obtained from calvarial digestion fractions. Interestingly, while isolated control CSCs (CD200+CD105-) grew in culture, mutant cells failed to survive, suggesting a role for CFP1 in stem cell maintenance. In contrast, Obs from cKOPrx1 mice grew normally in culture but failed to properly differentiate, compared to controls, as assessed by qRT-PCR analysis of osteogenic marker expression (Runx2, Osx, Col1a1, Ocn) and Alizarin red staining. Consistent with this observation in primary cells, deletion of CFP1 in the calvarial-derived pre-osteoblastic murine cell line, MC3T3-E1, using CRISPR/Cas9, also resulted in a defect in osteoblast differentiation. Defects in osteoblast differentiation were also observed when CFP1 was deleted from primary murine bone marrow stromal cells and the murine bone marrow stromal cell line, W-20. Surprisingly, deletion of CFP1 using Osx-Cre (cKOOsx) had no effect on osteoblast differentiation as assessed by microcomputed tomography, histological, and cell culture analyses. cKOOsx mice did however exhibit reduced long bone length, likely due to a reduction in the proliferative zone of the growth plate. Together, our data show that CFP1 is required for both endochondral and intramembranous ossification, and that CFP1 is a crucial regulator of early osteoblast differentiation but is dispensable at later stages. Mechanistically, we observed that BMP signaling is altered in the absence of CFP1, and consistent with this finding, osteoblast differentiation was rescued upon the addition of exogenous BMP. Future studies on CFP1 will offer new insight into the epigenetic control of the skeletal system

P-026 Kim Harrison, PhD

Cortical Remodeling Dynamics in the Rabbit: Does Alendronate Reduce Longitudinal Erosion Rate?

Kim Harrison*1, Lindsay Loundagin1, Xuan Wei1, Arash Panahifar2,3, Terra Arnason4, Alain Fafard5, Peter Pivonka6 and David Cooper1,
(1) Department of Anatomy, Physiology and Pharmacology, College of Medicine, University of Saskatchewan, Saskatoon, SK, Canada, (2) BioMedical Imaging and Therapy Beamline, Canadian Light Source, Saskatoon, SK, Canada, (3) Department of Medical Imaging, College of Medicine, University of Saskatchewan, Saskatoon, SK, Canada, (4) Department of Medicine, Division of Endocrinology, Faculty of Medicine & Dentistry, University of Alberta, Edmonton, AB, Canada, (5) Animal Care and Research Support Office, Office of the Vice President of Research, University of Saskatchewan, Saskatoon, SK, Canada, (6) School of Mechanical, Medical, and Process Engineering, Queensland University of Technology, Brisbane, QLD, Australia

Basic Multicellular Units (BMUs) - fundamental units of remodeling - continuously renew bone tissue through the coupled actions of their osteoclastic removal and osteoblastic formation of bone. Increased resorption can lead to bone loss characteristic of osteoporosis (OP). Bisphosphonates, one of the most commonly used anti-resorptive drugs to treat OP, inhibit osteoclastogenesis and activity, yet, despite their efficacy, their direct effect on BMU dynamics is not well known. Understanding the influence of bisphosphonates on BMU longitudinal erosion rate (LER) in 4D (i.e., 3D over time) will provide critical insight into mechanisms of bisphosphonate modulation of BMU dynamics which may in turn lead to improvements in their use for combating OP. To test the hypothesis that alendronate would slow and/or stop active BMUs, we employed in vivo imaging using in-line phase contrast micro-CT at the Canadian Light Source (CLS) synchrotron to track cortical bone BMUs and determine their LER in female New Zealand rabbits (six-months of age). Animals were divided into an ovariohysterectomy (OVH) or OVH+Alendronate (OVH+Aln) treatment group (n=7/group). Ten weeks post OVH surgery, and two weeks after the initiation of dosing (saline 1 ml or alendronate 3.5 μg/kg twice per week), the right tibiae were scanned in vivo (voxel size=13 μm) and following an additional two weeks of dosing, ex vivo (voxel size=6 μm) postmortem. The datasets from each rabbit were co-registered in 3D and LER calculated as the distance traversed by BMU cutting-cones in the 14-day interval between scans. A total of 392 BMUs were rendered and measured. An independent t-test on mean BMU LER/rabbit was assessed and revealed that contrary to our hypothesis, LER in the OVH+Aln group (33.12 μm/day) was not significantly reduced compared to the OVH group (35.22 μm/day; p=0.40). At this clinically relevant dose and brief treatment period, alendronate did not affect LER. However, preliminary results of a high-dose (120 μg/kg twice per week) alendronate group (n=7) have revealed a marked decrease in remodeling – evidenced by little to no remodeling spaces remaining at the end of the four-week treatment period. In future studies, we will further explore bisphosphonates' effects on BMU LER through modified imaging schedules - using novel multiple sequential in vivo scans prior to initiation of/and during drug treatment which could greatly enhance our current understanding of bisphosphonates' effects on cortical remodeling.

P-027 Yixia Xie, PhD

Expression of GFP-Tagged Collagen in Craniofacial Tissues in GFP-Collagen Transgenic Mice

Yixia Xie* 1, Mark Dallas 2, Eleanor Ray 1 and Sarah L. Dallas 1
(1) University of Missouri Kansas City, Kansas City, MO, USA, (2) UMKC School of Dentistry, Kansas City, MO, USA

Type I collagen, the major bone extracellular matrix protein, is a heterotrimer of two α1(I) chains and one α2(I) chain, encoded by the COL1A1 & COL1A2 genes. As a model to study collagen assembly dynamics in living cells and intravitally in live animals, we previously generated a transgenic mouse line expressing GFP-tagged collagen in which a GFPtopaz tag was placed in the α2(I) procollagen chain to replace the N-propeptide and telopeptide. Expression of the GFP-collagen transgene is driven by the 3.6kb-COL1A1 promoter and the transgene is expressed on a background of two wild-type alleles. Here, we report on the expression of GFP-tagged type I collagen in dental and skeletal structures of the craniofacial skeleton in 3 month old GFP-collagen transgenic mice. Fluorescent imaging in cryosections of the mandible showed strong GFP-collagen expression in the periodontal ligament (PDL), alveolar bone matrix, dentin of the incisor and first molar, cellular cementum and ligaments of muscle attachments. In the calvarium, GFP-collagen was expressed in the calvarial bone matrix and coronal sutures. Fluorescent imaging of the GFP-collagen fusion protein also revealed collagen organization and detailed substructure in these collagen-rich tissues, with GFP-collagen fluorescence appearing brighter in newly deposited predentin compared to mature dentin and collagen fibers oriented radially through the dentin, parallel to dentinal tubules. In the PDL, collagen fiber directionality and organization perpendicular to the long axis of the tooth and their insertions into bone and cellular cementum could be distinguished. GFP-collagen in newly deposited alveolar bone or calvarial bone appeared brighter compared to mature bone and cement lines demarcating successive cycles of bone formation were also visible. Some osteocytes showed bright rings of collagen deposition around their lacunae, suggesting perilacunar remodeling and newly deposited collagen around vascular channels appeared brighter compared to mature bone, sometimes with concentric rings suggesting cycles of collagen deposition. GFP-collagen was also prominent in the cellular cementum, with the majority of cementocytes showing brighter GFP collagen signal around their lacunae, suggesting their ability to deposit collagen in the perilacunar matrix. These data validate that GFP-collagen transgenic mice express the GFP-collagen fusion protein in collagen-rich tissues of the craniofacial skeleton and that this fusion protein can distinguish substructure and collagen organization in these tissues. The GFP-collagen transgenic mouse is therefore a useful model to examine the dynamic processes of collagen assembly and bone and dentin formation in dental and skeletal-related cranofacial tissues in cells or organ cultures or in the whole animal under normal and pathological states.

P-028 Tor Hildebrand, PhD

Volumetric Quantification of Plates, Rods, and Junctions in Trabecular Bone with the Local SMI – A New Approach

Peter Suter1, Johannes Krug2, Tor Hildebrand1, Phil Salmon4, Björn Busse2 3, Felix von Brackel2
(1) Lucid Concepts AG, Zurich, Switzerland (2) Department of Osteology and Biomechanics, University Medical Center Hamburg-Eppendorf, Hamburg, Germany (3) Interdisciplinary Competence Center for Interface Research, University Medical Center Hamburg-Eppendorf, Hamburg, Germany (4) Bruker Micro-CT, Kontich, Belgium

Introduction: One of the most common pathologies in bone, osteoporosis, is characterized by an overall loss of bone mass, increasing the fracture risk in a large portion of the population, especially the elderly and postmenopausal women. This bone loss has been shown to be accompanied by a change in the structure of the trabecular bone by shifting from a plate-like to a more rod-like shape [1,2], negatively influencing its mechanical competence [3]. Furthermore, previous indices tend to collapse the entire structure into a single value [7], and while some methods classify the shape of individual voxels [6], their high computational demands limit their practical use for large images in clinical or research settings. Thus, a standardized method for characterizing trabecular bone structure is still needed.
Solution: We propose a method for quantifying the natural transition from cortical bone into plates and ultimately rods. It is inspired partly by the original SMI (Structure Model Index) paper, attempting to quantify the shape of trabecular bone structure, and partly by the EF (Ellipsoid Factor) [6], assigning to each point of the structure a shape index based on the local geometry of the structure. We calculate an index called the Local SMI, by evaluating the local expansion of the structure at each voxel in evenly spaced directions. To address the inherent computational costs of this approach, we implemented the method for GPU execution, reducing processing time from hours to minutes for large images (2000^3) and to seconds for smaller images (500^3). Raymarching the distance field of the bone mask helps determine surface points in all directions. The covariance matrix's eigenvalues of this point cloud indicate elongation in various directions, and a formula combines these eigenvalues into an index. This formula produces an image map that smoothly transitions across different shapes, showing the distribution of trabecular bone structure shapes. From this map, mean and variance of the shape can be derived, and structures can be classified in post-processing steps with traditional or advanced ML techniques.
Results: The method has been validated on bone images from various imaging devices at different resolutions like synchrotron micro-CT, standard micro-CT, and HR-pQCT. The results show it is possible to quantify the various structure models and the transition between them in a plausible way, see figure. In an ongoing study, the method will be used for analyzing human bone scans from HR-pQCT (SCANCO XtremeCT II) and human bone biopsies scanned with micro-CT (Bruker SkyScan 1272).
References
1. https://doi.org/10.1016/S8756-3282(99)00281-1
2. https://doi.org/10.1210/jc.2019-00843
3. 10.1016/j.bone.2014.11.006
4. 10.1080/01495739708936692
5. 10.3389/fendo.2015.00162
6. 10.3389/fendo.2015.00015
7. 10.1016/S8756-3282(92)90078-b

P-029 Elizabeth Zimmermann, PhD

Bone density and microarchitecture in ambulatory children with spastic diplegic cerebral palsy

Elizabeth A. Zimmermann* 1, Marianne Gagnon 2,3, Dominique Audet 2, Catherine Julien 2, Mahdi Hosseinitabatabaei 1,2,4, Bettina M. Willie 1,2, Alessandra Carriero 5, Louis-Nicolas Veilleux 2,3 and Jean-Pierre Farmer 2,6,
(1) Faculty of Dental Medicine and Oral Health Sciences, McGill University, Montreal, QC, Canada, (2) Research Centre, Shriners Hospital for Children, Montreal, QC, Canada, (3) Department of Surgery, McGill University, Montreal, QC, Canada (4) Department of Biomedical Engineering, McGill University, Montreal, QC, Canada (5) Department of Biomedical Engineering, The City College of New York, New York, NY, USA (6) Department of Pediatric Surgery, McGill University, Montreal, QC, Canada

Purpose: Cerebral palsy (CP) is a non-progressive neurological syndrome resulting in abnormal muscle tone, movement, and posture. Spasticity – the most common type of CP – describes stiff muscles with increased tone. Non-ambulatory children with CP are known to have deficits in bone mineral density (BMD). However, it is unclear how altered movements in ambulatory children impact their skeletal health. This study investigates bone density and microarchitecture in ambulatory children with spastic CP.

Methods: Children with spastic diplegic CP (n = 12) between the ages of 3-8 years were recruited. Areal BMD was measured with dual x-ray absorptiometry (DXA) at the proximal and distal femur and compared to normative data [1,2]. High resolution peripheral quantitative computed tomography (HR-pQCT) was performed at the distal tibia and distal radius in a subset of participants (CP group: n=5; Control group: n=7). Gait pathology in children with CP (n=10) was measured with the Gait Deviation Index (GDI) from quantitative gait analysis (GDI ≥ 100 indicates no gait pathology). Mean ± standard deviation is reported with 95% confidence interval (CI). Independent t-test or Mann-Whitney test was performed on HR-pQCT data.

Results: Even though the CP group exhibited muscle spasticity in the lower limbs and gait abnormality (GDI = 56.9 ± 10.2), DXA aBMD Z-scores at the distal femur were within a normal range. aBMD Z-scores for the CP group at the proximal femur indicated deficits in bone (Z-score = -1.4 ± 1.4, 95% CI: -2.3, -0.4). At the distal tibia, children with spastic CP had significant deficits in HR-pQCT-measured bone geometry and trabecular microarchitecture: 35% lower total area (CP: 186.6 ± 31.5, Control: 290.7 ± 46.8, $p<0.01$), 42% lower trabecular area (CP: 121.4 ± 26.5, Control: 209.8 ± 30.4, $p<0.001$), 40% lower trabecular volumetric BMD (CP: 75.9 ± 23.9, Control: 126.1 ± 25.6, $p<0.01$), and 48% lower trabecular number (CP: 0.657 ± 0.188, Control: 1.260 ± 0.210, $p<0.001$) than controls. However, there were no significant difference between groups in total and cortical volumetric BMD, cortical thickness and cortical porosity. Additionally, there were no differences between groups in HR-pQCT-measured bone geometry and microarchitecture at the distal radius.

Conclusion: Although DXA Z-scores were within the normal range at the distal femur, HR-pQCT data from a small cohort indicates that children with CP have deficits in bone geometry and trabecular microarchitecture in the lower limbs. There is conflicting evidence regarding DXA-measured bone deficits in ambulatory children with CP [3]. Future studies using HR-pQCT with larger sample sizes are needed to confirm our findings.

References: [1] Webber et al., Can J Assoc Radiol 2007. [2] Henderson et al., Am J Roentgenol 2002. [3] Mus-Peters et al., Disabil Rehabil 2019.

P-030 Yener Yeni, PhD

Textural and geometric measures derived from digital tomosynthesis discriminate patients with vertebral fracture from those without

Yener N Yeni* 1, Daniel Oravec, Ram Yadav, Joshua Drost, Michael Flynn, George Divine and Sudhaker D Rao,
(1)Henry Ford Health, Detroit, MI, USA

Digital tomosynthesis (DTS) is a limited-angle tomographic imaging modality providing a stack image of an object at high resolution and low radiation exposure. The purpose of this study was to examine the extent to which DTS derived textural and geometric properties of vertebrae discriminate patients with and without vertebral fracture.

Under IRB approval, 93 postmenopausal women (age ≥ 50 years) with no history of bone disease other than osteoporosis were enrolled. The patients with vertebral fracture (Fx, N = 39) and those without (NFx, N = 54) were not different in age (65 ± 8 vs 64 ± 7 years; $p > 0.2$), BMI (25.1 ± 3.3 vs 25.1 ± 3.7 kg/m2; $p > 0.9$) or race distribution (9\30 vs 8\46 Black\Nonblack; $p > 0.3$).
Lumbar spine bone mineral density (BMD) and trabecular bone score (TBS) were measured, and vertebral fracture assessment was performed from DXA scans.

DTS of the spine was performed using a clinical system (Sonialvision Safire II, Shimadzu Inc) with the participant in supine position and central X-ray tube fixed at the T12-L1 level. DTS images were reconstructed with a voxel spacing of 0.28 x 0.28 x 1 mm. Fractal dimension (FD, a measure of texture complexity) and lacunarity (λ, a measure of texture heterogeneity) were calculated for cancellous bone using FracLac and ImageJ software. Mean intercept length (MIL, a measure of feature size) and line fraction deviation (LFD, a measure of orientation) were measured and degree of anisotropy (DA) was calculated (maximum MIL/minimum MIL). In addition, vertebral width was calculated at the narrowest section of the mid-vertebra using coronal images.

DTS values for fractured T12 and L1 vertebrae were imputed from unfractured levels using a mixed model regression of each DTS variable by vertebral level from a superset of 131 patients with no fracture. DTS measurements of the T12 and L1 vertebrae were averaged for each subject. Differences between groups were assessed using t-tests or Wilcoxon tests based on data normality. Logistic regression models were constructed to examine the extent to which DTS predicts vertebral fracture status.

BMD and TBS were higher, while DA and width were lower, in NFx than Fx ($p < 0.02$ to $p < 0.003$). Multiple logistic regression identified BMD, FD, λ, DA and width as significant predictors ($p < 0.02$ to $p < 0.001$) with AUC of ROC = 0.79 (compared to 0.67 for BMD alone) (Figure).
These results support complementary use of DTS in assessment of bone quality and potentially of fracture risk.

P-031 Sneha Korlakunta, PhD

Tissue-specific VEGF-D overexpression induces lymphangiogenesis and heterotopic bone resorption

Neda Vishlaghi*1, Danielle Griswold-Wheeler2, Sneha Korlakunta3, Trisha Ghotra2, Alec Bancroft2, Yuxiao Sun4, Michael Dellinger5 and Benjamin Levi6,

(1)UT Southwestern Medical Center, Dallas, TX, USA, (2)Research assistant, Dallas, TX, USA, (3) Center for Organogenesis, Regeneration, and Trauma, Department of Surgery, University of Texas Southwestern, Dallas, TX, USA, (4)Research scientist, Dallas, TX, USA, (5)Professor, Dallas, TX, USA, (6)Center for Organogenesis and Trauma, Department of Surgery, University of Texas Southwestern, Dallas, TX, USA

INTRODUCTION: Heterotopic ossification (HO) is abnormal bone formation outside skeletal tissues, commonly occurring after fractures, injuries, or surgeries. Current treatments, like anti-inflammatory drugs and radiation therapy, offer limited success and side effects. Surgical resection, the standard treatment for established HO, often fails, leading to recurrence. While blood vessels are implicated in HO, the role of lymphatic vessels is unclear. We investigate lymphangiogenesis's impact on HO using Vegfd transgenic mice.

METHODS: We used our validated burn/tenotomy (B/T) model in mice. Mice aged 8 to 10 weeks underwent a dorsal burn covering 30% of their body surface area, along with transection of the left Achilles tendon, while the uninjured right leg served as a control. Using a conditional overexpression approach, we induced lymphangiogenesis in the zeugopod by crossing Hoxa11wt/CreERT2 mice with R26wt/rtTA;TetO-Vegfd mice. Hindlimb samples were collected 9 weeks post-injury, fixed in 4% paraformaldehyde (PFA) at 4°C for 24 hours, and prepared for micro-CT and histological analysis, including various staining techniques to characterize phenotypic changes.

RESULTS: We found that lymphatic vessels invade the tendon, but not heterotopic or native bone in control mice following B/T (Fig1.A). In contrast, lymphatic vessels infiltrate heterotopic and native bone in Hoxa11wt/CreERT2;R26wt/rtTA;TetO-Vegfd mice following B/T (Fig1.B). Post-injury quantification confirmed significant lymphatic vessel expansion in the Vegfd overexpression group (Fig2.A), with no significant increase in blood vessels (Fig2.B). Micro-CT analysis revealed that Hoxa11wt/CreERT2;R26wt/rtTA;TetO-Vegfd mice had significantly less HO than control mice (Fig3.A-B). Lastly, TRAP staining demonstrated a significant increase in osteoclasts within heterotopic and native bone in Hoxa11wt/CreERT2;R26wt/rtTA;TetO-Vegfd mice compared to control mice (Fig4. A-B).

DISCUSSION: Our research shows that overexpression of Vegfd in MPCs causes a significant increase in lymphatic vessel growth and invasion of bone following B/T injury. Increased lymphangiogenesis and osteoclasts can result in bone resorption offering a new potential approach to resorb existing HO.

P-031 Sneha Korlakunta, PhD

SIGNIFICANCE/CLINICAL RELEVANCE: This important study marks the foremost endeavor to comprehensively elucidate how lymphatic vessel infiltration of heterotopic bone can incite bone resorption. The identification and targeting of novel molecular pathways governing lymphatic function during injury will provide unprecedented insights into the field of musculoskeletal injury and regeneration. Furthermore, while established therapies primarily revolve around HO prevention, there exists an unmet clinical need for therapies aimed at resorbing existing HO, a need this research aims to address.

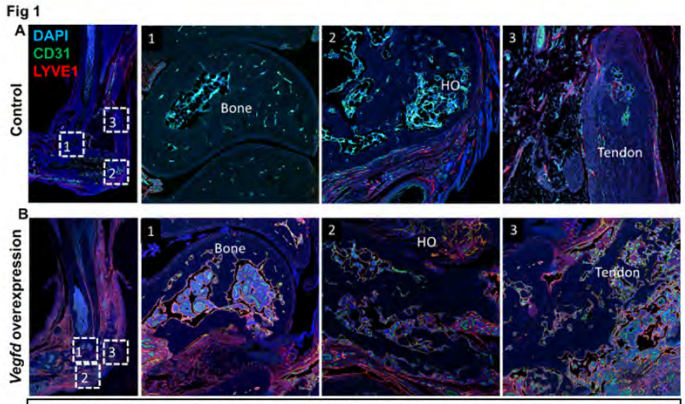

Figure 1: **Lymphatic vessel invasion into bone tissue.** (A) Confocal tile and magnified images of control and (B) *Vegfd* overexpression hindlimbs 9 weeks post injury stained for LYVE1 and CD31.

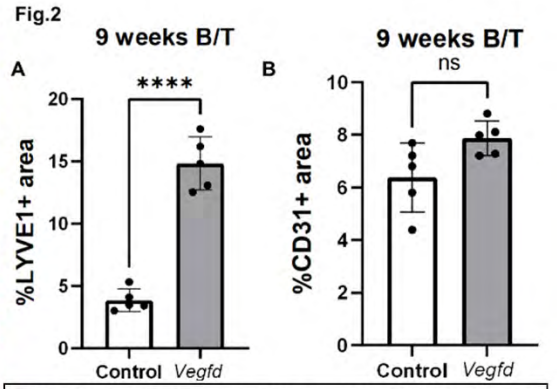

Figure 2: **Lymphatic vessels formation increased post injury.** (A) Significant increase in lymphatic vessel expansion post injury within *Vegfd* overexpressed (B) No significant differences in blood vessel expansion post injury within *Vegfd* overexpressed compared to controls.

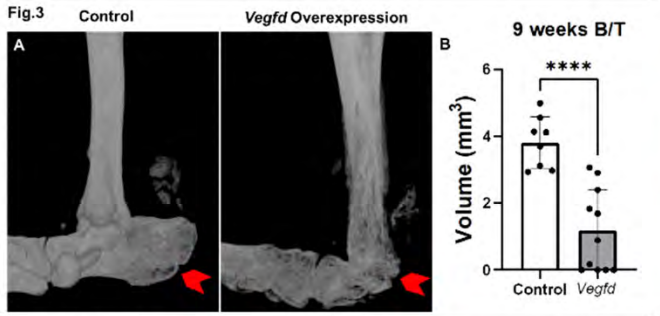

Figure 3: MPC specific Vegfd overexpression reduced HO volume. (A) µCT reconstruction and (B) quantification of HO volume 9 weeks post-B/T.

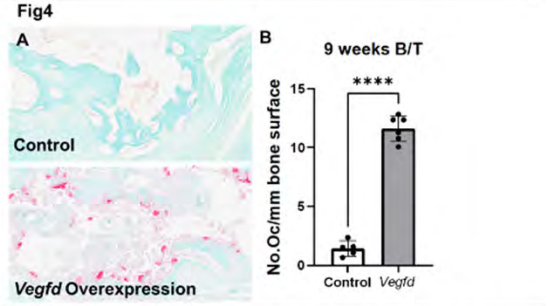

Figure 4: Increased lymphatics stimulates osteoclast mediated bone resorption. (A) TRAP staining of injured hindlimb. (B) Quantification of osteoclast cells number over the bone surface.

P-032 Jodi Dowthwaite, PhD

Circum-menarcheal Exercise Loading and gSOS Polygenic Risk Score Independently Predict Variance in Distal Radius Bone Properties in Post-menarcheal Girls

Jodi N. Dowthwaite* 1, Jonathan P. Bradfield 2, Babette S. Zemel 3, Jonathan A. Mitchell 3, Struan F.A. Grant 4 and Tamara A. Scerpella 5
(1) Department of Orthopedic Surgery, SUNY Upstate Medical University, Syracuse, NY, USA (2) Quantinuum Research, Wayne, PA, USA (3) Department of Pediatrics, Perelman School of Medicine, University of Pennsylvania, Philadelphia, PA, USA (4) Division of Endocrinology and Diabetes, Children's Hospital of Philadelphia, Philadelphia, PA, USA (5) Department of Orthopedics & Rehabilitation, School of Medicine & Public Health, University of Wisconsin - Madison, Madison, WI, USA

Purpose: Genetic and environmental factors influence bone quality and fracture risk in adolescents, but their relative, site-specific associations are poorly characterized. Exercise loading is a key modifiable environmental factor that may yield site-specific bone benefits. In girls, peak bone mineral accrual velocity is centered circum-menarche, with a large proportion of adult bone mass gained in 3 circum-menarcheal years (CIRCAMEN). In our cohort, bone properties stabilize after 2 years post-menarche (POSTMEN). Here, we explore 2 validated indices as predictors of distal radius bone properties assessed during this period of CIRCAMEN malleability leading to increasing stabilization, 1 to 2.5 years POSTMEN: 1) a polygenic risk score called gSOS; and a 3-year CIRCAMEN arm-specific bone loading index based on longitudinal exercise data (ARMBLI). We hypothesized that gSOS and ARMBLI are independent predictors of distal radius properties.

Methods: A subset of female participants from a longitudinal youth exercise study provided saliva for DNA extraction and genome-wide genotyping. Over 20,000 variants were used to calculate gSOS scores. In UK Biobank adults, high gSOS indicated high bone quality as heel ultrasound speed of sound, suggesting high BMD and low osteoporotic fracture risk. We calculated ARMBLI from longitudinal physical activity records (3-year CIRCAMEN osteogenic loading dose, as cumulative sport-specific hours and loading magnitude, velocity, & frequency). Key POSTMEN data were measured in a single session: height (cm), whole body DXA non-bone fat-free mass (WBNBFFM, kg), and non-dominant arm DXA dependent variables [ultradistal (UD) and 1/3 radius: AREA (cm2), BMC (g), BMD (g/cm2), LN-transformed as needed to improve normality]. Multiple regression assessed predictive value of gSOS and ARMBLI for radius DXA outcomes; models tested for gSOS*ARMBLI interactions and accounted for height, WBNBFFM, and POSTMEN measurement timing (GYNAGE, years). We assessed semi-partial r as effect size: small r≥0.1 to <0.3; medium r≥0.3 to <0.5; large r≥0.5.

Results: As independent model predictors, gSOS and ARMBLI both associated positively with UDAREA, LNUDBMC, LNUDBMD, & 1/3BMC (Table 1). Only gSOS associated with 1/3AREA, and only ARMBLI associated with LN1/3BMD. Interactions were not detected (gSOS*ARMBLI: excluded from final models, p=0.28 to 0.98).

Conclusion: Both gSOS and ARMBLI were independently associated with most distal radius outcomes, with small-medium and small-large effect sizes, respectively. Results suggest that both

genotype and CIRCAMEN exercise loading contribute to POSTMEN bone mineral content at both sites, while contributions to bone geometry and areal density are site and/or tissue-specific. Our findings emphasize adolescent exercise loading as a potential tool to enhance baseline adult bone status in healthy girls, regardless of gSOS score.

Table 1. Multiple Linear Regression Predictors: Semi-partial Correlation Coefficients & Significance
(Post-menarcheal girls, n=50; White n=41, Asian n=6, Mixed race n=3)¥

DXA Radius Outcome	gSOS	ARMBLI	GYNAGE (years)	HEIGHT (cm)	WBNBFFM (kg)
UD AREA (cm^2)	**+0.20** (p=0.04)	**+0.25** (p=0.01)	-0.05 (p=0.57)	**+0.22** (p=0.02)	**+0.40** (p<0.001)
LN UD BMC (g)	**+0.27** (p<0.001)	**+0.54** (p<0.001)	+0.08 (p=0.24)	+0.02 (p=0.83)	**+0.32** (p<0.001)
LN UD BMD (g/cm^2)	**+0.25** (p=0.002)	**+0.58** (p<0.001)	**+0.16** (p<0.04)	-0.14 (p=0.07)	**+0.18** (p=0.02)
1/3 AREA (cm^2)	**+0.34** (p=0.001)	+0.17 (p=0.09)	+0.06 (p=0.58)	-0.20 (p=0.05)	**+0.45** (p<0.001)
1/3 BMC (g)	**+0.28** (p=0.006)	**+0.36** (p<0.001)	+0.19 (p=0.06)	-0.08 (p=0.42)	**+0.32** (p=0.002)
LN 1/3 BMD (g/cm^2)	+0.09 (p=0.45)	**+0.42** (p=0.001)	+0.25 (p=0.05)	+0.09 (p=0.48)	+0.05 (p=0.68)

Significance: α=0.05; bolded semi-partial correlation coefficients.
Note: gSOS*3yrArmBLI interactions were entered, then excluded from all models (p=0.28 to 0.98).
gSOS = polygenic bone quality score; ARMBLI= 3-year circum-menarcheal arm bone loading index;
GYNAGE = age in years post-menarche; WBNBFFM = DXA whole body non-bone fat-free mass;
UD = Ultradistal; AREA = bone projected area; BMC = bone mineral content;
BMD = areal bone mineral density.
¥: After excluding non-White participants (White only sub-sample), similar patterns were observed. However, power (gSOS) & variance (ARMBLI) were inadequate to detect associations with UDAREA. [n=41: gSOS vs. UDAREA SPCC= +0.22, p=0.06; ARMBLI vs. UDAREA SPCC= +0.15, p=0.18]

P-033 Jodi Dowthwaite, PhD

Contrasting Physical Activity and Energy Availability Patterns from Childhood to Adulthood: A Comparison of Height, Body Composition, and Bone Mass Growth Curves Relative to Menarche

Jodi N. Dowthwaite*1, Laure Spake2 and Tamara A. Scerpella3
(1) Department of Orthopedic Surgery, SUNY Upstate Medical University, Syracuse, NY, USA, (2) Department of Anthropology, Binghamton University, Binghamton, NY, USA, (3) Department of Orthopedics & Rehabilitation, School of Medicine & Public Health, University of Wisconsin - Madison, Madison, WI, USA

Purpose: Physical activity may promote muscle & bone gains, but low energy availability may impede growth, maturation, and bone accrual. Thus, we compared growth curves for height, fat, muscle, and bone mass relative to menarche, in girls with contrasting youth activity profiles, to evaluate mechanical loading exposure and energy availability as modifiable factors in growth.
We hypothesized that gymnasts (GYM) who trained pre-menarche (PREMEN), circum-menarche (CIRCAMEN), and post-menarche (POSTMEN), would have high, early, rapid muscle & bone growth but low, late, slow fat & height growth. In contrast, we hypothesized that ex-gymnasts (EX) who quit PREMEN would have high muscle and bone mass PREMEN; however, EX muscle & bone growth would be blunted CIRCAMEN and POSTMEN due to loading withdrawal, freeing up energy for high, early, rapid growth in height & fat mass.
Methods: Female longitudinal study participants (1997-2023) were classified as GYM, EX, or non-gymnasts (NON). Annual measures included: height (cm) and whole body DXA [fat mass (WBFAT, kg), “muscle” as non-bone fat free mass (WBNBFFM, kg), and bone mineral content (WBBMC, g)]. Organized activity and menstrual function were recorded semi-annually. SuperImposition, Translation And Rotation (SITAR package: R) was used to model & compare growth curve parameters centered at menarche up to age 21yrs. GYM & EX were compared to the NON standard using this gynecological age clock (GYNAGE, years), assessing regression terms for EX & GYM SITAR parameters [size, timing, intensity: alpha ≤0.05]. We tested for group differences in mean age at menarche by ANOVA.
Results: For HEIGHT (vs. NON): GYM had lower size, and EX had higher size ($p<0.001$); GYM had lower intensity ($p<0.001$). For WBnbFFM (vs. NON): GYM trended toward earlier timing ($p=0.06$). For WBFAT (vs. NON): GYM had lower size ($p<0.001$); EX trended toward lower size ($p=0.07$). For WBBMC (vs. NON): GYM had earlier timing ($p=0.02$); NON trended toward lower INTENSITY ($p=0.08$). Order of peak growth velocity (PkV) timing was: WBNBFFM (PREMEN), HEIGHT (PREMEN), WBBMC (GYM & EX: PREMEN; NON: CIRCAMEN), WBFAT (POSTMEN). Group means for age at menarche did not differ ($p>0.46$).
Conclusions: In GYM, training through menarche may have limited energy availability while boosting loading, yielding lower fat mass, slower height growth, and lower adult height, without limiting muscle or bone mass. In fact, GYM gained bone early, likely prioritizing high muscle and bone mass gains for smaller body size and limited fat depots. In contrast, for taller height, EX fat mass was low, suggesting low energy availability, with blunted muscle and bone gains for height CIRCAMEN and POSTMEN. Small EX sample limited power to detect differences. Future work will assess time-varying exercise, nutrient intake, height, and fat mass as predictors of growth curves for musculoskeletal properties from childhood into adulthood.

P-034 Rachel Klassen

Comparing In Vivo HR-pQCT Against Ex Vivo Histological Methods to Assess Remodeling in Knee Osteoarthritis Bone Marrow Lesions

Rachel E Klassen1,5, Daphne Kaketsis1,5, Shannon Puloski2, Richard Walker1,3, Emma Billington4, Jason Werle2, Steven K Boyd1, Sarah L Manske1

1McCaig InsItute for Bone and Joint Health, Calgary, Canada
2Department of Orthopedic Surgery, University of Calgary, Calgary, Canada
3Department of Radiology, University of Calgary, Canada
4Department of Endocrinology, University of Calgary, Canada
5Biomedical Engineering Graduate Program, University of Calgary, Canada

Bone marrow lesions (BMLs) are a hallmark sign of osteoarthritis (OA) associated with clinical symptoms, namely severe pain and pain progression. Based on previous literature, BMLs are centers of increased bone turnover. Currently, there is no consensus as to what defines a BML outside of their appearance on MRI. Furthermore, the current gold standard method to assess bone turnover is histology requiring invasive bone biopsies. High resolution peripheral quantitative computed tomography (HR-pQCT) is a potential solution for this problem but has not been validated in humans. This study aims to elucidate the degree of bone remodelling and turnover characteristics in BMLs using a human knee OA model. Secondly, we aim to validate bone remodeling measures as identified by HR-pQCT against histology.

Participants were scanned with HR-pQCT and MRI six months prior to total knee arthroplasty (TKA). Participants were given tetracycline to produce fluorescent double labels signifying newly mineralized bone. Four tibial plateau explants were collected following TKA. BMLs and paired control regions were identified on previous in vivo MRI, before histological sectioning and PMMA embedding. BIOQUANTOsteo was used to measure mineral appositional rate (MAR) and formation rate (MFR) on histological sections. Statistical analyses were used to determine differences between paired BML and control regions.

Preliminary results demonstrate that BMLs exhibit higher MAR (2.89μm/day versus 1.13μm/day) and MFR (0.07μm/day versus 0.28μm/day) than non-BML tissue suggesting that BML regions are characterized by a greater amount of bone remodeling than non-BML regions. Ongoing work includes a comparison of remodeling measurements between the in vivo and ex vivo HR-pQCT scans to compare the results against the histological results. Furthermore, Bland-Altman plots will be employed to assess agreement between the results from both HRpQCT and tetracycline histology. Additionally, spatial transcriptomics will be performed to assess genetic signatures of BML versus control regions. This study could elucidate novel therapeutic targets for treatment of knee OA as well as discriminate patients at the highest risk of requiring TKAs for participatifon in future clinical trials.

P-035 Galateia Kazakia, PhD

The Effect of Laplace-Hamming Segmentation on Micro-Finite Element Bone Mechanics Estimations Is Cohort- and Skeletal Site-specific

Minhao Zhou*, Saghi Sadoughi, Gabriella Ramil, Isra Saeed, Andrew J. Burghardt and Galateia J. Kazakia, Department of Radiology and Biomedical Imaging, University of California at San Francisco, San Francisco, CA, USA

Micro-finite element models (μFE) constructed from high-resolution peripheral quantitative CT (HR-pQCT) scans estimate the mechanics of complex bone structures. We previously developed and validated a Laplace-Hamming binarization approach (LH) on second-generation HR-pQCT to capture accurate bone microarchitecture (FigA).1 However, whether LH affects μFE outputs remains unknown. Therefore, this work examines the effect of LH on μFE biomechanics metrics. We hypothesized that LH statistically alters μFE predictions.

Twenty healthy volunteers and 11 patients with chronic kidney disease (CKD) were scanned on an XtremeCT II at a single timepoint. Each scan was segmented using the manufacturer's standard evaluation (STD) and the LH approach. Model boundary and loading conditions and failure criterion were defined per published guidelines. Apparent modulus (Ea), stiffness (K), failure load (FL), and distal cortical load fraction (Loadcort,dist) were assessed. The effect of LH was determined by the Wilcoxon signed-rank test. The relationships between changes in microarchitecture (e.g. ΔTb.N=Tb.NLH-Tb.NSTD) and μFE outputs (e.g. ΔK=KLH-KSTD) with LH were explored.

In the healthy cohort, LH significantly reduced the apparent modulus, stiffness, and failure load at the tibia. However, LH did not alter the apparent modulus and significantly increased stiffness and failure load at the radius. In the CKD cohort, LH significantly reduced the apparent modulus and stiffness at the tibia but did not affect them at the radius; LH did not alter the failure load in the CKD cohort. In both cohorts, LH significantly lowered the distal cortical load fraction at both skeletal sites (FigB).

The impact of LH on μFE mechanics metrics mainly scaled with trabecular bone volume fraction (ΔTb.BV/TV) and thickness (ΔTb.Th). However, such relationships were cohort- and skeletal site-specific. For example, in the CKD cohort, changes in apparent modulus (ΔEa) were sensitive to changes in cortical porosity (ΔCt.Po) and not ΔTb.BV/TV at the tibia. Similarly, changes in stiffness (ΔK) and failure load (ΔFL) were sensitive to ΔCt.Po only at the tibia and only for the CKD cohort (FigC).

This study demonstrates that LH statistically alters μFE mechanics predictions, and this effect is cohort- and skeletal site-specific. In general, LH affects tibia metrics more than the radius. Interestingly, though LH captures significantly more cortical porosity,1 the associations between ΔCt.Po and changes in mechanics with LH were only marginal at the tibia and moderate at the radius. However, CKD amplifies the effect of ΔCt.Po at the tibia, perhaps due to the heavy cortical bone involvement in CKD pathology. Subsequent work will evaluate the effect of LH on μFE estimations for cohorts with different representative bone microarchitecture.

1. An LH Approach for 2nd-Gen HR-pQCT Rescues Fine Feature Segmentation, JBMR. 38(7), 2023

P-035 Galateia Kazakia, PhD

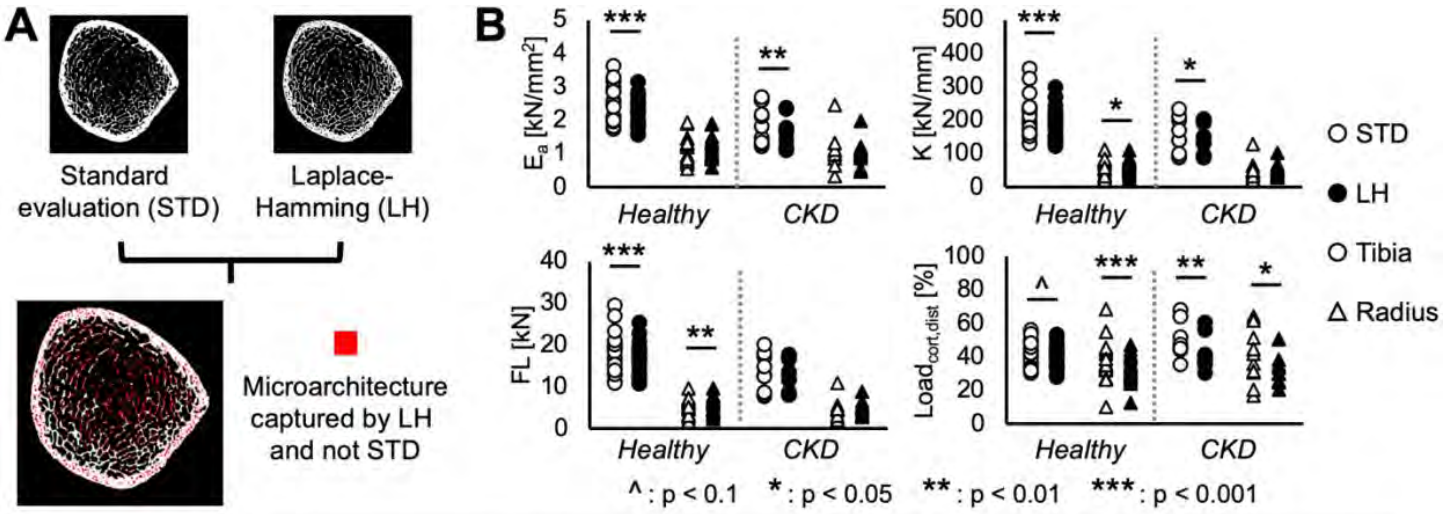

C

		Tibia						Radius					
		ΔTb. BV/TV	ΔTb.N	ΔTb.Th	ΔTb.Sp	ΔCt.Po	ΔCt. Po.Dm	ΔTb. BV/TV	ΔTb.N	ΔTb.Th	ΔTb.Sp	ΔCt.Po	ΔCt. Po.Dm
ΔE_a	*Healthy*	0.92	0.43	0.78	-0.50		0.38	0.63		0.63		-0.68	0.52
	CKD			0.34		-0.47	0.39	0.95		0.85		-0.40	0.65
ΔK	*Healthy*	0.90	0.47	0.64	-0.56		0.39	0.68		0.67		-0.69	0.46
	CKD	0.51		0.46	-0.56	-0.61	0.72	0.95		0.75		-0.52	0.61
ΔFL	*Healthy*	0.87	0.46	0.61	-0.54		0.40	0.72		0.64		-0.61	0.43
	CKD	0.52		0.45	-0.54	-0.57	0.69	0.96		0.74		-0.50	0.58
$\Delta Load_{cort,dist}$	*Healthy*	-0.86		-0.74	0.50	-0.57		-0.77	-0.35	-0.47	0.44	0.34	-0.38
	CKD	-0.67	-0.61	-0.51	0.50		-0.32	-0.64		-0.40			

Correlation strength: Weak Moderate Strong

Figure (A) Representative distal tibia images from both segmentation approaches, with LH-rescued microarchitecture superimposed on the STD mask. **(B)** Apparent modulus (E_a), stiffness (K), failure load (FL), and distal cortical load fraction ($Load_{cort,dist}$) from STD and LH micro-finite element (μFE) models. **(C)** Pearson correlation coefficients between Δmicroarchitecture and ΔμFE predictions (STD vs. LH).

P-036 Stephane Blouin, PhD

Abnormally Low Bone Matrix Mineralization in a Boy with a Pathogenic SATB2 Variant

Stephane Blouin*1, Barbara M. Misof1, Martin Munteanu2, Markus A. Hartmann3, Nadja Fratzl-Zelman3 and Corinna Grasemann2
(1) Ludwig Boltzmann Institute of Osteology, Vienna, Austria, (2) Department of Pediatrics, Division of Rare Diseases, St. Josef-Hospital, Ruhr-University Bochum, Bochum, Germany, (3) Ludwig Boltzmann Institute of Osteology at the Hanusch Hospital of OEGK and AUVA Trauma Centre Meidling, 1st Med. Department Hanusch Hospital, Vienna, Austria

Background: Special AT-rich sequence-binding protein 2 SATB2 (encoded by the SATB2-Gene; MIM* 608148) is intrinsically linked to proper development of the nervous system and the skeleton. At the molecular level, it activates Runx2 and ATF4, two critical transcription factors that regulate osteoblast differentiation. SATB2 deficiency is associated with low bone mass and early onset fragility fractures. Its role for bone microstructure and material is largely unknown.
Patient & Methods: We present bone biopsy findings from a nine year-old boy with a heterozygous pathogenic [1] (ACMG class 5) SATB2 variant (NM_001172517.1): c.1165C>T, p.(Arg389Cys) who presented with low BMD by DXA (L1-L2: 0.420 g/cm2, Z-score -3.4) and femoral and tibial bowing. We analyzed bone histomorphometric characteristics and bone mineralization density distribution (BMDD) and osteocyte lacunae sections (OLS) characteristics (by quantitative backscattered electron imaging). Outcomes were compared to pediatric reference data.
Results: The biopsy sample contained mostly cortical bone. Extensive fibrotic tissue was present in the marrow space. The few available trabeculae appeared qualitatively thin and half covered by osteoid of normal thickness (7.1mm). Cortical thickness was within normal range (Z-Score -0.2). While very few typical secondary osteons were visible, primary osteons (i.e. canals within lamellae oriented in parallel to the periosteal surface) were frequent. The BMDD revealed abnormally low calcium concentrations (Figure) with average degree of mineralization, CaMean Z-scores of -5.1 and -2.3, and highly increased area of lowly mineralized matrix, CaLow Z-scores +11.2 and +3.5 for trabecular and cortical bone respectively. OLS-density was within normal range (Z-score +1.1) but OLS had a more elongated shape (OLS-aspect ratio Z-score +2.2) and increased size (OLS-area Z-score +4.8) resulting in an elevated OLS-porosity (Z-score: +4.0).
Conclusion: Our study revealed various bone development defects in our patient: a failure of secondary remodeling of primary lamellar bone into osteonal bone, overall reduced bone matrix mineralization, and elevated bone marrow fibrosis consistent with the role of SATB2 in early stages of osteoblastic differentiation. The severe hypomineralization of the bone matrix along with the low BMD very likely contributes to the bowing of the lower limbs in our patient with SATB2 variant.

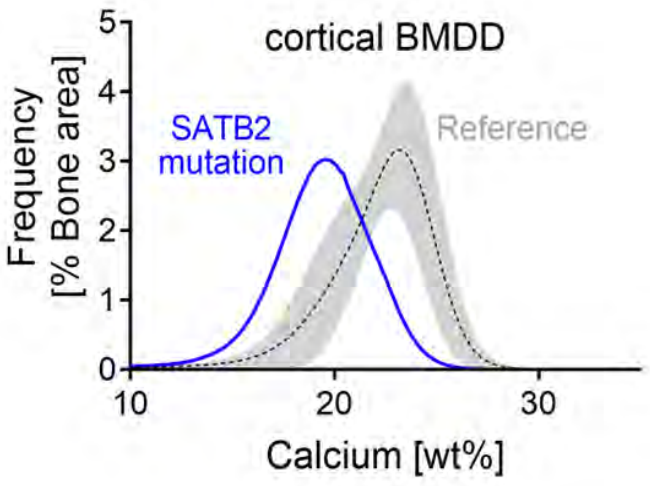

[1] https://www.ncbi.nlm.nih.gov/clinvar/variation/381575

P-037 Kaja Laursen, PhD

Development of a 7-plex Immunofluorescent Protocol for Cellular and Molecular Characterization of the Bone Marrow Microenvironment in Muliple Myeloma

Kaja S. Laursen1, Bilal El-Masri2,3, Michael T. Gundesen4, Thomas Lund4, Maja Hinge6, Megan Weivoda5, Matthew Drake5, Thomas L. Andersen1,2,3 and Marta Diaz-delCastillo1
(1) Molecular Bone Histology Team, Department of Forensic Medicine, Aarhus University, Aarhus, Denmark (2) Clinical Cell Biology, Pathology Research Unit, Department of Clinical Research and Molecular Medicine, University of Southern Denmark, Denmark (3) Department of Pathology, Odense University Hospital, Odense, Denmark (4) Department of Hematology Odense University Hospital, Odense, Denmark (5) Mayo Clinic College of Medicine and Science, Rochester, MN, USA. (6) Division of Hematology, Department of Internal Medicine, Vejle Hospital, Vejle, Denmark

Background: Multiple myeloma (MM) is an incurable cancer of the plasma cells in the bone marrow. Unlike other cancers, MM is always preceded by two asymptomatic premalignant conditions called “monoclonal gammopathy of undetermined significance” (MGUS) and “smoldering multiple myeloma” (SMM), which present a 1 to 10% yearly risk of progression to MM, respectively. Today, there is no treatment to prevent MGUS and SMM development into MM. In previous studies, we have observed increased senescence in plasma cells and their proximal bone marrow microenvironment in MGUS and SMM patients who do not progress to MM, suggesting that paracrine senescence acts as a physiological mechanism to prevent tumor progression.
Aim: To identify the cell lineage of senescent bone marrow microenvironment proximal to senescent and non-senescent plasma cells in bone biopsies from patients with MGUS and SMM with or without progression to MM, and newly diagnosed MM patients.
Methods: We have developed a 7-plex immunofluorescent (IF) protocol for cellular and senescence bone marrow characterization that can be evaluated through artificial intelligence (AI) - assisted histology. The end-goal is to quantify the density and spatial relation of plasma cells (CD138), blood vessels (CD34) stromal cells (CD271) and adipocytes (perilipin) in relation to each other and to the bone surfaces, and determine their senescent status based on loss of nuclear markers LaminB1 and HMGB1.
Results: In this project, we first optimized a panel of primary antibodies with independent visualization systems as single-plex IF. We then combined them into a 7-plex IF where we utilize the unique characteristics of each primary antibody (species, isotype or tag) to prevent cross-reactivity between them (Figure 1).
Conclusion: Multiplex IF are powerful histological techniques used to identify cell types, lineage and/or co-localize protein expression in given cell populations. In this project, we have optimized a 7-plex IF protocol to determine cell lineages and their senescent status in the bone marrow microenvironment of bone biopsies from patients with pre-malignant MGUS and SMM or malignant MM. This unique multiplex IF builds on our expertise on molecular bone histology in human samples, where each protocol is designed with a unique and specific combination of antibodies. In addition, IF can be relatively easily combined with fluorescent in Situ Hybridization (FISH) for gene expression markers, if the IF antibodies work with the FISH pretreatment. Ongoing work is focused on evaluating the spatial relationships between cell types using AI-assisted histology.

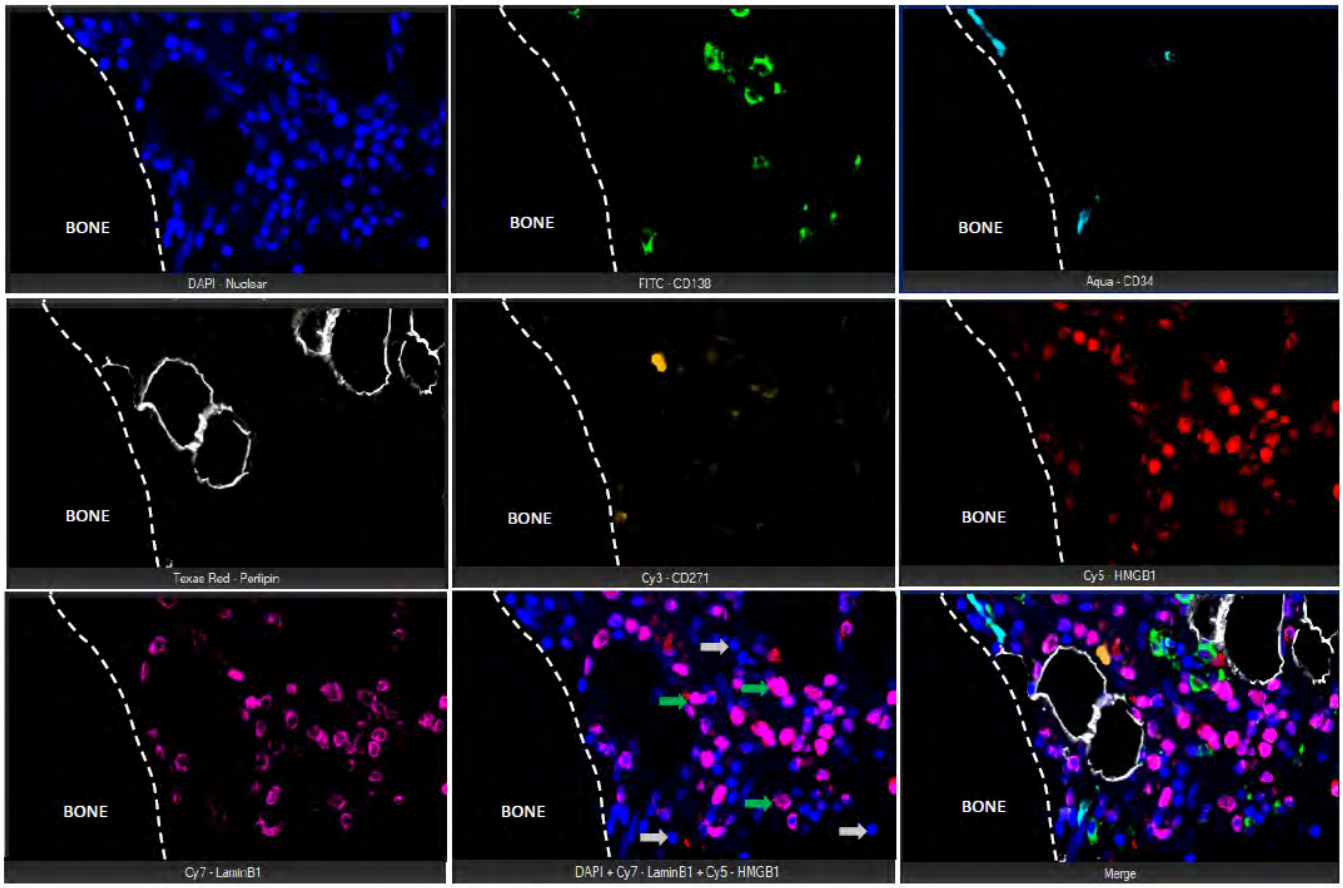

Senescent cells (negative for both)
Non-senescent cells (positive for LaminB1 and HMGB1)

P-038 Flavia Kiweewa Matovu, PhD

High Hypovitaminosis D prevalence among Women with Normal Bone Mass in an African Setting

Flavia Kiweewa Matovu*1,2, Martin Nabwana1, Esther Isingel1, Nicholas Matovu3, Mags Beksinsa4 and John M. Pettifor5
(1) Makerere University-Johns Hopkins University Research Collaboration, Kampala, Uganda, (2) Makerere University College of Health Sciences, School of Public Health, Kampala, Uganda, (3) Makerere University, Kampala, Uganda, (4) Maternal Adiolescent and Child Health Research Unit, South Africa, (5) Faculty of Health Sciences Research Office and the Department of Paediatrics, University of the Witwatersrand, South Africa

Vitamin D deficiency is considered a public health problem due to its worldwide high prevalence and adverse clinical consequences regarding musculoskeletal health. The main source of vitamin D for is ultraviolet-B (UV-B) (sunlight) which is abundant in African settings. However, there are limited data on vitamin D status and bone health in many African settings. We examined the prevalence of hypovitaminosis D and its association with low bone mineral density (BMD) among Ugandan women of reproductive age. Methods: We examined a cross-sectional sample of 152 HIV negative women aged 18 to 45 years at the Mulago National Specialized Hospital Family Planning Clinic in Uganda who had not been pregnant or breastfeeding in the last two years. Of these, 72 women were current depot medroxyprogesterone acetate (DMPA) users and 80 were on non-hormonal contraception (condoms or intra-uterine contraceptive device). Current DMPA use was defined as documented consistent use of DMPA in the last 2 years prior to study participation. Women were excluded if pregnant or breastfeeding in the last two years. 25-hydroxyvitamin D (25(OH)D) was assessed using Architect System - an Abbot platform. Hypovitaminosis D was defined as a serum 25OHD concentration < 30 ng/ml. BMD assessments of the lumbar spine, total hip and femoral neck were performed according to international densitometry guidelines using Dual-energy X-Ray absorptiometry (Hologic). Low BMD was defined as a Z score ≤−2 at any of the three sites) in accordance with the National Osteoporosis Foundation guidelines. Multiple logistic regression was used to examine the independent association of vitamin D and BMD adjusting for age and body mass index. We further assessed whether there was effect modification by contraceptive use. Results: The median (IQR) age was 31 (26, 37) years with overall median 25OHD levels of 22.6 (19.2, 27.3) ng/mL. DMPA users had significantly higher 25OHD levels compared to non-hormonal users, 24.8 (21.4, 28.9) vs. 20.6 (17.6, 24.4) ng/mL, p=0.002. The majority of women (82%) had hypovitaminosis D, 76.4% DMPA vs. 87.5 % non-hormonal users, p=0.074. Low BMD was observed in 13 (18.1%) of DMPA users compared to 00.0 (0%) of non-hormonal users using the age matched non-hormonal users as controls. There was no association between hypovitaminosis D and low BMD, p-value > 0.186, Table. This relationship was not modified by DMPA use. Conclusion: There was high prevalence of hypovitaminosis D among Ugandan women which was not associated with low BMD. Further research is needed to investigate adverse clinical implications of low vitamin D levels among Ugandan women on other health outcomes other than BMD.

Table: BMD Z-score among women with insufficient and normal hydroxyl vitamin 25(OH)D levels

25 (OH)D in ng/ml	*Lumbar Spine BMD Z-score*		*Total Hip BMD Z-score*		*Neck Femur BMD Z-score*	
	Normal	**Low**	**Normal**	**Low**	**Normal**	**Low**
Insufficient (<30 ng/ml)	118 (94.4)	7 (5.6)	122 (97.6)	3 (2.4)	122 (97.6)	3 (2.4)
Normal (≥30 ng/ml)	25 (92.6)	2 (7.4)	25 (92.6)	2 (7.4)	26 (96.3)	1 (3.7)
P-value	*0.718*		*0.186*		*0.701*	

P-039 Heithem Ben Amara, PhD

Bone regeneration around biodegradable magnesium-based biomaterials: Diferential efects on osteopromotion and adiposity accumulation as a function of material composition

H Ben Amara1, D C. Martinez2, K Iskhakova3, L Emanuelsson1, B Norlindh1, A Johansson Loo1, DC F. Wieland3, B Zeller-Plumhoff3, R Willumeit-Römer3, T Plocinski2, W Swieszkowski2, F A. Shah1, A Palmquist1, O Omar4, P Thomsen1
(1) Department of Biomaterials, University of Gothenburg, Sweden (2) Biomaterials group, Materials Design Division, Warsaw University of Technology, Poland (3) Institute of Metallic Biomaterials, Helmholtz-Zentrum Hereon, Geesthacht, Germany (4) Department of Biomedical Dental Sciences, Imam Abdulrahman bin Faisal University, Saudi Arabia

Introduction: Biodegradable metallic implants made of magnesium (Mg) are increasingly used as alternatives to nondegradable implants. Mg implants facilitate osteogenesis [1] and are widely believed to mitigate inflammation and bone resorption. However, this is hard to reconcile with the early inflammation observed around these implants [2]. Using a suite of imaging, molecular biology, and spectroscopy techniques, the present in vivo study aimed to: i) investigate bone cellular and molecular regulation during inflammation in response to Mg implants with different degradation behaviors; ii) study the subsequent reparative response at the bone–implant interface and the surrounding bone marrow.
Methods: Screws made of biodegradable pure Mg (MgP), biodegradable clinical-grade alloyed Mg (MgA; MgYREZr), and titanium (Ti) were implanted in rat tibae (n=84, Fig. 1a). After 3 and 28 d, implants and associated bone were retrieved and quantitative polymerase chain reaction (qPCR) and immunohistochemistry were performed. Histomorphometry quantified new bone deposition at the implant surfaces and the adjacent bone marrow cellular composition was determined using MarrowQuant and AdipoQuant [3] digital athology tools. Raman spectroscopy nabled compositional analysis of new bone matrix. Kruskal–Wallis test served for tatistics ($p<0.05$).
Results: Compared to Ti, cells collected at the interface with MgP and MgA implants exhibited a transient upregulation of genes related to inflammatory cytokines, proinflammatory macrophage, osteoclastogenesis, and neoangiogenesis. At 28 d, both MgP and MgA implants featured a ~50% superior bone–implant contact (Fig. 1b). However, unlike MgA, bone interfacing with the faster degrading MgP implants displayed a lower calcium to phosphorus ratio and more Mg, with Raman spectroscopy revealing a ~30% decreased mineral crystallinity (Fig. 1c) and a ~45% increased organic component, indicative of a younger bone. Consistent with adipogenesis gene upregulation, histomorphometry (Fig. 1d) showed increased density and size of bone marrow adipocytes with a persistently higher density of CD68-immunopositive inflammatory cells around MgP (Fig. 1e), but not MgA implants.
Conclusions: Using a combination of imaging, molecular biology, and spectroscopy techniques, this study demonstrated that MgP and MgA implants elicit in bone a transient proinflammatory milieu that reinforces osteogenesis. However, the faster MgP degradation causes compositional alteration in the interfacial bone. Moreover, observations of a previously unknown proadipogenic response and persistent low-grade inflammation of the bone marrow call for rigorous tailoring of Mg implants and monitoring of the adjacent bone marrow.
REFERENCES: 1Y. Zhang et al (2016) Nat Med. 2H. Ben Amara et al (2023) Bioact Mater. 3J. Tratwal et al (2020) Front Endocrinol.

P-039 Heithem Ben Amara, PhD

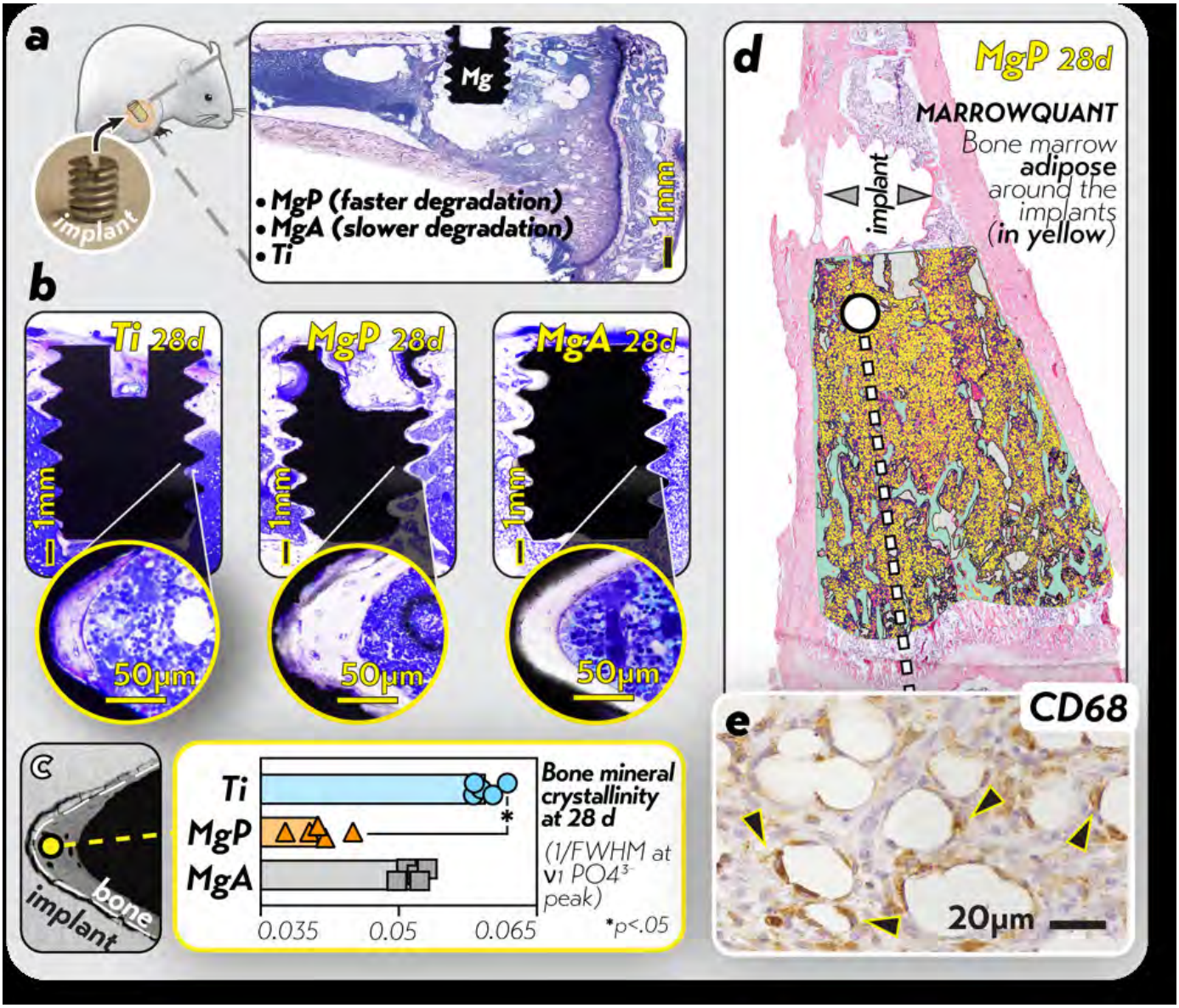

P-040 Eugenie Macfarlane, PhD

Rhythmic Circulating Glucocorticoid Levels play a Critical Role in Osteoarthritis driven by Chronic Disruption of Circadian Rhythms

Eugenie Macfarlane*, Lauryn Cavanagh, Colette Fong-Yee, Joseph Tannous, Markus J. Seibel and Hong Zhou, ANZAC Research Institute, The University of Sydney, Concord, NSW, Australia

Chronic disruption of circadian rhythms (CR) from shift work increases the risk of osteoarthritis (OA). However, the underlying mechanisms that drive joint degeneration from shift work are unknown. Endogenous glucocorticoid secretion follows a diurnal rhythm and is known to regulate CR by synchronizing the cellular clocks throughout the body. We therefore asked whether glucocorticoid signaling in chondrocytes mediates the effects of environmental CR disruption during OA development in wild-type (WT) and tamoxifen-inducible chondrocyte glucocorticoid receptor knockout mice.

Eight-week-old male Col2a1Cre/GRf/f (GRKO) mice and their WT (GRf/f) littermates were exposed to an established model of chronic CR disruption for 22 weeks. Mice were maintained on either a normal 12:12hr light-dark cycle (non-shifted) or exposed to weekly 12hr phaseshifts, equivalent to spending alternate weeks in America and Australia (shifted; Fig.1A).

Chronic disruption of CR abolished the diurnal rhythmicity of circulating glucocorticoids, characterized by a loss in the normal daily peak of serum corticosterone (upon awakening) in all shifted mice (Fig. 1B). Overall 24-hour concentrations of serum corticosterone were no different between groups. Consequently, rhythmic expression of the major clock gene Bmal1 was abrogated in femoral cartilage tissue of WT shifted mice. However, in GRKO shifted mice cartilaginous Bmal1 expression remained rhythmic, although in opposite phase to non-shifted animals. This indicates that blocking arrhythmic chondrocytic GC signaling allows a selfsustaining rhythm in Bmal1 expression to persist in cartilage tissue (Fig.1B).

Histological analysis revealed that chronic disruption of CR resulted in knee joint cartilage degradation in WT mice, but not in GRKO mice (Fig. 1C). To further investigate the effects of chronic CR disruption on joint health we studied the progression of posttraumatic OA by destabilization of the medial meniscus (DMM) four weeks prior to harvest. In WT mice, chronic disruption of CR accelerated cartilage degradation, subchondral bone sclerosis, and induced synovial mast cell infiltration during the early stages of posttraumatic OA. These features were significantly less pronounced in GRKO mice (Fig.1C).

Our results, for the first time, provide compelling in vivo evidence that glucocorticoid signaling in chondrocytes is central to the development and progression of posttraumatic OA during chronic disruption of circadian rhythm. These novel findings provide valuable insight into how chronic disruption of circadian rhythm drives detrimental effects on skeletal health in shift workers.

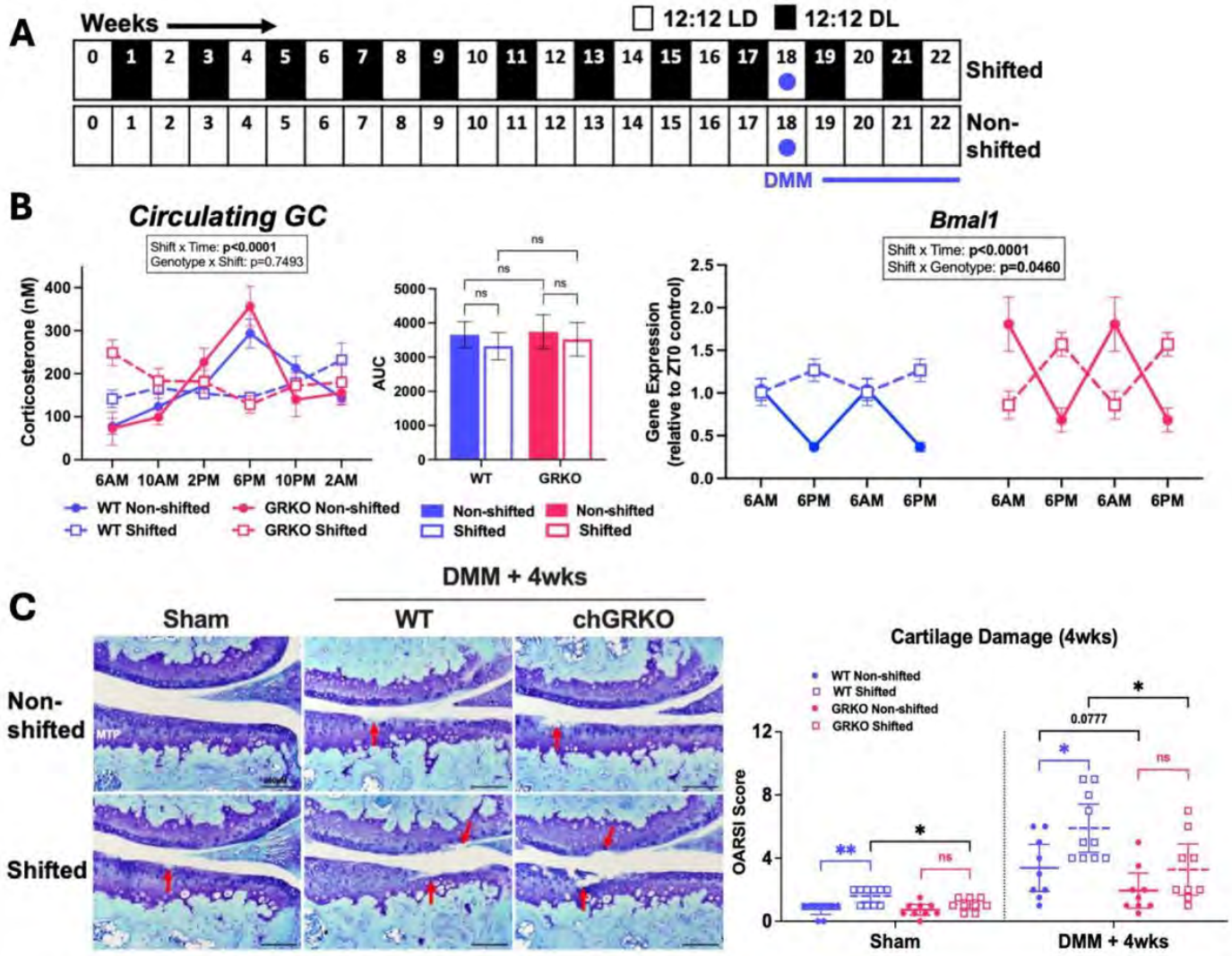

Figure 1. Phenotype induced by chronic disruption of circadian rhythm in wild-type (WT) and chondrocyte (ch) glucocorticoid receptor knockout (GRKO) mice. Destabilization of the medial meniscus (DMM) was performed at 4 weeks prior to harvest in shifted and non-shifted mice. GC, glucocorticoid; Bmal, brain and muscle ARNT-Like protein; LD, Light:Dark. OARSI, Osteoarthritis Research Society International; AUC, Area under curve (for overall GC concentration analysis). Analysed by 2- or 3-way ANOVA, n=4-10/group.

P-041 Mahdi Hosseinitabatabaei, PhD

Natural history of the peripheral bones in children with osteogenesis imperfecta and age- and sex-matched healthy controls using longitudinal HR-pQCT analysis

Mahdi Hosseinitabatabaei* 1, Samantha McCluskey 1,2,4, Carolyn Denton 1,2,3, Elizabeth A. Zimmermann 3, Francis H. Glorieux 2, Fredrick Charbonneau 2, Frank Rauch 2 and Bettina M. Willie2,

(1) Department of Biomedical Engineering, McGill University, Montreal, QC, Canada (2) Research Centre, Shriners Hospital for Children, Montreal, QC, Canada (3) Faculty of Dental Medicine and Oral Health Sciences, McGill University, Montreal, QC, Canada Department of Surgery, McGill University, Montreal, QC, Canada

Background: Osteogenesis imperfecta (OI) is characterized by increased bone fragility with frequent fractures, especially in children. So far, only one cross-sectional study has reported high-resolution peripheral QCT (HR-pQCT) data for children with OI. Their measurements were limited to the metaphysis, although long bone fractures in children with OI most often occur in the diaphysis. We compared HR-pQCT measurements and their 1-year changes between children with OI and age- and sex-matched controls.

Methods: At baseline and 1-year followup, we acquired HR-pQCT scans from 20 children with OI and 20 age- and sex-matched healthy controls at the radius and tibia. At each site, double-stack scans were acquired at the metaphysis, and single stack scans at the diaphysis. Scans were acquired using a second-generation scanner (XtremeCTII, Scanco Medical) at 60.7 µm. Scans were evaluated using manufacturer's recommended settings, without any image registration with the other timepoint. We report trabecular (Tb.) and cortical (Ct.) volumetric BMD (vBMD), Tb. volume fraction (Tb.BV/TV), Ct. thickness (Ct.Th), Tb. area (Tb.Ar), Ct.Ar, as well as failure load from microFE analysis.

Results: At the tibia metaphysis, controls had significantly larger Tb.vBMD, Ct.vBMD, Ct.Th, and failure load. Ct.Th, Ct.Ar, and failure load increased similarly over 1-year for both the OI and controls groups, while Tb.vBMD and Tb.BV/TV increased only for the control group. While Ct.vBMD increased for both groups, changes for the OI group were significantly bigger than OI. At the radius metaphysis, Tb.BV/TV and failure load were bigger for the control group, and failure load increased similarly for both groups. All cortical parameters increased for both groups, while changes in Ct.vBMD and Ct.Ar were significantly bigger for the OI and control groups, respectively. At the tibia diaphysis, Ct.vBMD was significantly bigger for the OI group and increased significantly. Marrow cavity area was significantly bigger for the controls. Ct.Ar and Ct.Th increased similarly for both groups. Failure load was significantly higher for the controls and increased for both groups. At the radius diaphysis, Ct.Ar, marrow cavity area, and failure load were bigger for the control group, and increased similarly for Ct.Ar and failure load for both groups. Ct.vBMD only increased for the OI group.

Conclusion: Our data showed that deteriorations in the OI group in cortical and trabecular measurements were more prominent at the tibia compared to the radius. The changes over the ~1-year period was mostly comparable between the OI and control groups at both the radius and tibia. At the diaphysis, we found similar results at the radius and tibia, where differences between the two groups were mainly driven by area, especially larger marrow cavity area in the control group. Failure load was lower in the OI group regardless of the anatomical site and region.

P-042 Ali Ghasem-Zadeh, PhD

Bone's Microarchitectural Spatial Configuration Determines its Own Remodelling and Susceptibility to Becoming Fragile

Ego Seeman 1, Minh Bui 2, Esther Briganti 3, Ali Ghasem-Zadeh* 1

(1) Departments of Endocrinology and Medicine, Austin Health, The University of Melbourne (2) Centre for Epidemiology and Biostatistics, Melbourne School of Population and Global Health, The University of Melbourne (3) School of Public Health and Preventive Medicine Faculty of Medicine, Nursing and Health Sciences, Monash University, Melbourne, Australia

Introduction: Identification of women at risk for fracture is challenging because bone mineral density (BMD) is insensitive; the threshold for 'osteoporosis' of ≤ -2.5 SD detects only 25% of women having fractures. Three traits bare power relationships with bone strength independent of BMD - bone microarchitecture, bone cross sectional area (CSA) and bone matrix mineral density (MMD). We hypothesised that measurement of deterioration of these traits will contribute the loss of estimated bone strength.

Methods: In 324 twin pairs aged 26-76 years, (364 premenopausal, pre-M), 255 postmenopausal, post-M) we used HR-pQCT to measure distal radial and tibial microarchitecture expressed as a Structural Fragility Score (SFS), bone CSA and MMD. An increase in SFS captures concurrent deterioration of cortical porosity and trabecular density. Bone failure load (a surrogate of bone strength) was estimated using finite element analysis (FEA). Associations are presented as correlation coefficients (SEM).

Results: As shown in the numbered rows in the table, and figures, in univariate analyses:
Row 1 Estimated Strength increased across age in pre-M but decreased in post-M (Fig. A)
Row 2 SFS was unchanged in pre-M but increased in post-M (Fig. B)
Row 3 Larger bone CSA had a higher SFS in pre- and post-M women.
Row 4 Larger CSA was associated with greater strength in pre-M (despite higher SFS) but larger CSA in post-M was not associated with greater strength (Fig. C)
Row 5 In both pre-M and post-M women, SFS was inversely associated with bone strength, the more severely deteriorated microstructure was associated with lower estimated failure load (Fig. D)
Row 6 In a multivariate associations larger CSA was associated with greater strength in both pre-MW and post-MW after accounting for SFS.
Row 7 Higher SFS was associated lower strength independent of CSA and age.
Row 8 Age remained a predictor of strength independent of SFS and CSA in pre-M, but not post-M.

Fig E: Larger total CSAs are assembled with relatively less mass so (i) total volumetric vBMD is lower in larger bones due to (ii) higher cortical porosity (more surface for remodelling) and (iii) lower MMD. Smaller bone CSAs have a higher vBMD and less surface for remodelling. Trabecular vBMD was independent of CSA (iv). Therefore, larger bones are frugally assembled and have higher SFS.

Fig F: Estimated peak strength is greatest when microarchitecture is intact (low SFS) in a larger bone, but estimated strength decreases more rapidly in larger bones as microarchitecture deteriorates (SFS increases) perhaps due to the frugal assembly of larger bones.

P-042 Ali Ghasem-Zadeh, PhD

Conclusion: Bone's microstructural design formed during growth determines its own remodelling and so, bone fragility in advanced age. A minimised mass of bone assembled during growth is adequate during young adulthood but becomes a liability as age-related bone loss sacrifices the biomechanical advantage of larger bone size.

Table. Association between bone strength and microstructural traits

Trait association Univariate	Premenopausal Women	P value	Postmenopausal Women	P value
(1) Strength vs. Age	12.08 (3.96)	0.002	- 16.26 (5.15)	0.002
(2) SFS vs. Age	-2.0 (0.13)	NS	0.85 (0.17)	<0.001
(3) SFS vs. CSA	0.147 (0.02)	<0.001	0.123 (0.03)	<0.001
(4) Strength vs. CSA	1.97 (0.60)	0.001	- 0.46 (0.80)	NS
(5) Strength vs. SFS	- 15.25 (1.3)	<0.001	- 20.29 (1.5)	<0.001
Multivariate				
(6) Strength vs. CSA	5.72 (0.38)	<0.001	2.39 (0.69)	0.001
(7) Strength vs. SFS	-24.1 (1.40)	<0.001	-21.29 (1.47)	<0.001
(8) Strength vs. Age	5.19 (2.23)	0.02	1.96 (3.96)	NS

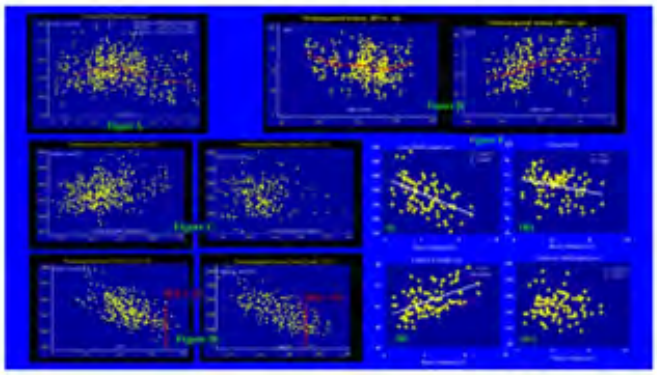

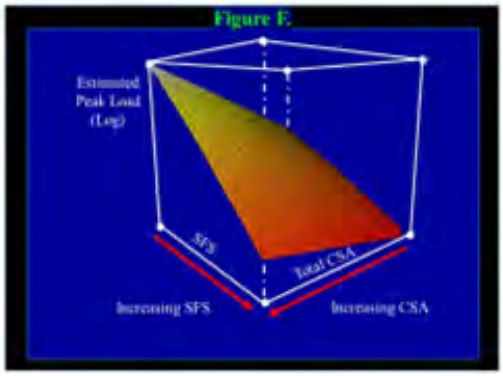

P-043 Gurpreet Baht, PhD

Targeting circulating apolipoprotein E to improve aged bone healing

Mingjian Huang, Abhi R. Balu, Kristin H. Molitoris, Gurpreet S. Baht*, Duke Molecular Physiology Institute, Department of Orthopaedic Surgery, Duke University

Bone fracture healing is impaired with advanced age. Based on our combination of parabiosis models and proteomic analyses, we hypothesized that circulating apolipoprotein E (ApoE), whose levels increase with age in patients and in mice, is an aging factor that impairs bone regeneration. As the liver is the primary source of circulating ApoE, we deleted hepatic expression of ApoE using Albumin-Cre::ApoEfl/fl mouse models and investigated tibial fracture healing in aged (24-month-old) mice. Albumin-Cre::ApoEfl/fl mice displayed a 95% reduction in circulating ApoE relative to their littermate counterparts. Micro-CT analysis demonstrated increased bone deposition within 21 days post-fracture in Albumin-Cre::ApoEfl/fl fracture calluses; however, no other hallmarks of healing were altered. In tissue culture models, treatment with recombinant ApoE inhibited osteoblast differentiation (decreased osteogenic transcripts) and inhibited osteoblast activity (decreased matrix formation and mineralization). RNA sequencing of these cultures indicated that the Wnt/beta-catenin pathway was the primary target of ApoE-based inhibition. We used osteoblastic cells in which the beta-catenin pathway was stabilized/unable to be modulated and found ApoE was unable to alter differentiation of these cultures. Furthermore, we determined Lrp4 to be the osteoblastic cell surface receptor for ApoE. Indeed, loss of Lrp4 expression in osteoblastic cells nullified ApoE's inhibitory effect. Finally, we treated aged, wildtype mice that underwent tibial fracture surgery with an ApoE-neutralizing antibody (HJ6.3) able to bind ApoE with high affinity (or with IgG control). Fracture calluses from ApoE-neutralizing antibody-treated mice contained 35% more bone tissue, effectively improving aged fracture healing (Figure). In summary, we determined that circulating ApoE increases with age to impair osteoblast function by binding to Lrp4 to inhibit Wnt/beta-catenin signaling. Administration of ApoE-neutralizing antibody blocks ApoE's inhibitory effects, improving aged fracture healing. Our work here identifies a novel target to improve bone fracture healing and provides a translatable therapeutic intervention.

P-044 Michael Wan, PhD

NOISe: Nuclei-Aware Osteoclast Instance Segmentation for Mouse-to-Human Domain Transfer

Michael Wan* 1, Sai Kumar Reddy Manne 1, Brendan Martin 1, Tyler Roy 2, Ryan Jack Neilson 2, Rebecca Peters 2,3, Meghana Chillara 1, Christine Lary 1 and Audrie Langlais 2,3,4
(1) Northeastern University, Portland, ME, USA,
(2) MaineHealth Institute for Research, Scarborough, ME, USA
(3) University of Maine, Orono, ME, USA
(4) Tufts University, Boston, MA, USA

Osteoclast cell image analysis plays a key role in osteoporosis research, but its execution typically involves extensive manual image processing and hand annotations by a trained expert. We present the first machine learning approach which fully automates the task of identifying the locations and shapes of individual osteoclasts—that is, the task of osteoclast instance segmentation—for both in vitro mouse osteoclast cells on plastic tissue culture plates and human osteoclast cells on bone chips. This goes beyond earlier efforts addressing only parts of the human-led annotation process, such as osteoclast location detection. Our method achieves a performance of 0.82 mAP@0.5 (mean average precision at intersection-over-union threshold of 0.5) in cross validation on our mouse osteoclasts dataset. The approach uses a novel nuclei-aware osteoclast instance segmentation training strategy (NOISe) based on the unique multinucleated nature of osteoclasts, to improve the model's generalizability and boost the mAP@0.5 from a baseline of 0.60 to 0.82 on human osteoclasts. The figure highlights this performance gap: it features human osteoclasts on a bone chip sample ("Input"), the baseline model predictions ("YOLOv8"), our nuclei-aware model predictions ("NOISe"), and the true osteoclast labels ("Ground Truth"). To support our machine learning model, we present a new dataset with ~20 K annotated mouse osteoclast masks. Following conventions in the field of machine learning, we will publish this dataset, together with our algorithm's model code and the pretrained model weights, to enable reproducibility and to provide a public tool to accelerate osteoporosis research.

P-045 Krittikan Chanpaisaeng, PhD

Cannabidiol does not ameliorate ovariectomy-induced bone loss in skeletally mature rats

Krittikan Chanpaisaeng* 1,2,3, Nathaporn Phonsatta 2, Atikorn Panya 2 and Narattaphol Charoenphandhu 3,4,5,6
(1) Department of Pharmacology and Physiology, Chulalongkorn University, Bangkok, Thailand (2) National Center for Genetic Engineering and Biotechnology (BIOTEC), Pathum Thani, Thailand (3) Center of Calcium and Bone Research (COCAB), Mahidol University, Bangkok, Thailand (4) Department of Physiology, Mahidol University, Bangkok, Thailand (5) Institute of Molecular Biosciences, Mahidol University, Nakorn Pathom, Thailand (6) The Academy of Science, The Royal Society of Thailand, Bangkok, Thailand

Cannabidiol (CBD) is a component of cannabis that has a variety of medicinal properties, including potential bone protective effect. Endocannabinoids produced in the body and phytocannabonoids like CBD act by binding to CB1, CB2, GPR55, and/or TRPV1 receptors. While osteoblasts and osteoclasts express these receptor genes and studies using genetically modified mice with one of these genes knocked out resulted in abnormal bone microstructure, there is no direct evidence showing whether CBD can reduce bone loss in a postmenopausal animal model. The objective of this research was to investigate the effect of CBD on bone metabolism and changes in the expression of cannabinoid receptors in the bone of skeletally mature ovariectomized rats (ovariectomized, OVX) to simulate the condition of postmenopausal women who lack estrogen. The effects of CBD (5 mg/kg/d) continuously administered through osmotic pump were compared to a placebo (vehicle, VEH) and estrogen (E2). There were five experimental groups including sham-operated rats (SHM) receiving VEH (SHM/VEH), SHM receiving CBD (SHM/CBD5), OVX receiving VEH (OVX/VEH), OVX receiving E2 (OVX/E2), and OVX receiving CBD (OVX/CBD5). Additionally, the effect of CBD on the expression of genes in the endocannabinoid system (Cnr1, Cnr2, Gpr55, and Trpv1) in rat bones were also studied. We observed that CBD administration could not ameliorate bone resorption that occurred due to the lack of estrogen. Trabecular bone mass of the rats that received CBD (OVX/CBD5) decreased continuously over the course of the 12-week intervention period, with no differences from the bone of OVX/VEH group. Bone gene expression data showed that E2 was able to significantly reduce Ctsk expression when compared to the OVX/VEH group whereas the expression of this gene in the OVX/CBD5 group was not different from OVX/VEH and had a trend (p=0.059) toward an increased expression when compared to the OVX/E2 group. Blood biomarkers indicated OVX/CBD5 rats had increased bone resorption compared to SHM/VEH and OVX/E2 rats, which could restore bone mass back to the same level as that in the SHM/VEH rats. In summary, this research demonstrates that CBD given subcutaneously for 12 weeks (blood concentrations of 1,280±89.51 ng/μL) had no effects on mitigating OVX-induced bone loss in skeletally mature rats.

P-046 Mitchell Froemming, PhD

Spatial Mapping of Senescent Cells in the Bone Microenvironment

Mitchell Froemming*1, Madison L. Doolittle1,2, David G. Monroe1 and Sundeep Khosla1,
(1) Mayo Clinic, Rochester, MN, USA, (2) UConn Health, Farmington, CT, USA

Cellular senescence has been identified as a crucial contributor to organismal aging. Although methodologies for identifying these cells have advanced, understanding their direct interactions within their microenvironments, especially in bone, remains elusive. Specifically, although next-generation sequencing and other single-cell techniques have greatly expanded our understanding of the characteristics of these cells, these techniques fall short of revealing how senescent cells interact with neighboring cells in their native environments, a particularly challenging task given the complex heterogeneity of the bone microenvironment. To address the spatial context of senescence, our study leveraged the Visium Assay by 10X Genomics. Building on our previous work (Nat Comm 14:4587, 2023), we defined senescent cells in bone from an aged mouse (24 months) using a combination of markers, specifically as Cdkn2a+ (p16+), mKi67- and Bcl2+ ("p16KB cells"), which also exhibited elevated levels of mRNAs encoding senescence-associated secretory protein (SASP) factors and evidence of increased DNA damage. While these cells have been previously detected using single-cell techniques, their spatial distribution within the bone microenvironment remains uncharted at the whole transcriptome level. In our approach, we selected a p16KB cell and analyzed its influence on the surrounding cells by drawing a series of concentric rings extending up to 400µm from the cell, creating a total of four distinct zones (Panel A). By comparing the average log2 fold-change of a validated senescence gene set (SenMayo) normalized to the selected clusters, we observed a significant decrease in SASP expression with increasing distance from the p16KB barcode (Panel B), essentially disappearing by ~350 µm from the p16KB cells. This pattern supports the hypothesis that senescent cells induce secondary senescence and/or inflammation in adjacent cells within the bone microenvironment. Further, by utilizing CellChat, we were able to delineate the interactions between cells across different regions, substantiating our observations that the p16KB cell actively interacts with its surroundings (Panel C). Collectively, our data provide proof-of-concept that senescent cells and their resulting SASP effects can be spatially mapped in the bone microenvironment. Moreover, our findings indicate that senescent cells may locally perturb surrounding cells to undergo secondary senescence and/or inflammation.

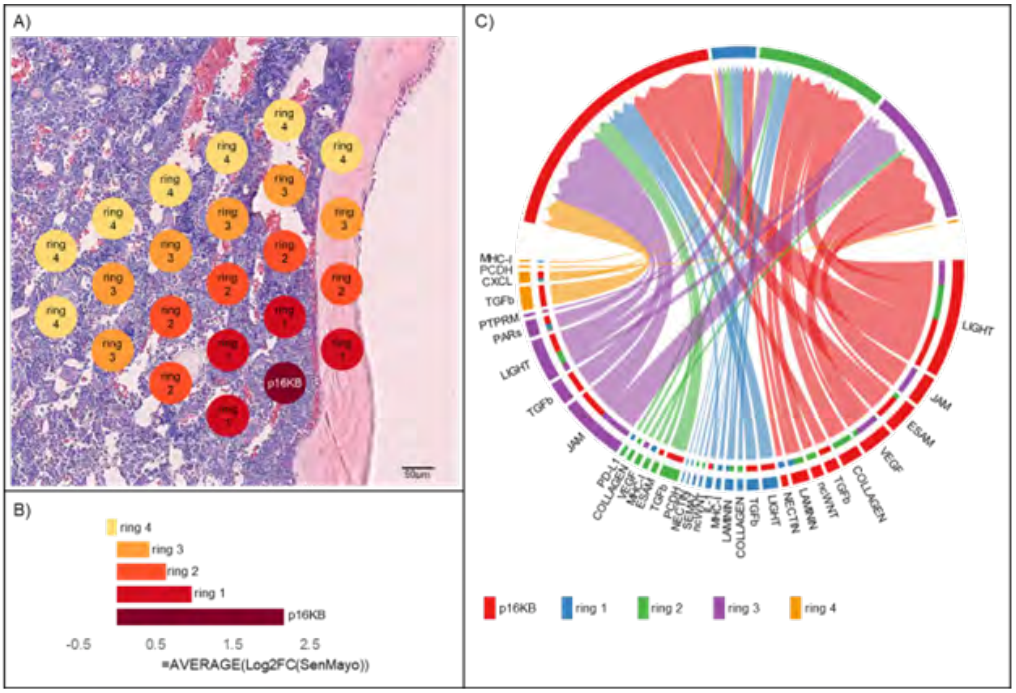

P-047 Gabriel Ramirez

Sex-Dependent Changes in Body Composition and Bone Mineral Density in Wild Type Mice and the APP-SAA Alzheimer's Disease Mouse Model

Gabriel Ramirez*1, Alix Teal1, Lakshmi Chellaganapathy1, Roquelina Pianeta1,2, Alyson Essex1, Chiaki Yamada3, Alexandru Movila3 and Lilian I. Plotkin1,2
(1) Indiana University School of Medicine, Indianapolis, IN, USA, (2) Richard L. Roudebush Veterans' Administration Medical Center, Indianapolis, IN, USA, (3) Indiana University School of Dentistry, Indianapolis, IN, USA

Alzheimer's disease (AD), a condition with cognitive decline and behavioral changes, affects more females than males, even when corrected by differences in their lifespan. Recent research has revealed intriguing connections between AD and bone biology. The skeletal system beyond the brain, may provide critical insights into disease mechanisms and potential therapies for both cognitive and skeletal deficiencies. We used genetically modified mice, APP-SAA knock-in mouse model (APP-SAA), that express humanized forms of the AD-linked mutations in the amyloid precursor protein, including the Swedish-KM670/671NL double mutation, Arctic-E693G mutation, and Austrian-T714I mutation, and wildtype (WT) C57BL/6J male and female mice. The transgene appears at high levels at 5-6 months, coinciding with development of amyloid plaques. Mice (6-13/group) were examined at 13 months of age by Dxa/Piximus. Data was analyzed by 2-way ANOVA, with sex and genotypes as the 2 independent variables, and Tukey's test to estimate the pairwise differences, $p<0.05$ was considered significant. Our findings reveal significant variations in bone mineral density (BMD) and body weight/composition depending on genotype, sex, or their interaction. Thus, WT and APP-SAA female mice show lower body weight compared to male counterparts, but no overall effect on body weight is seen when either male or female APP-SAA mice are compared to the respective WT mice. Further, no differences between sexes for either genotype or when female APP-SAA mice are compared to WT mice of the same sex in total BMD are seen, but APP-SAA male mice show higher total BMD compared to the male WT mice. However, APP-SAA female mice show lower femur BMD than APP-SAA male mice, with no other significant variations observed for this site. Further, WT females show lower lean mass compared to WT males within the femur, and both male and female APP mice display a higher femur lean mass compared to the WT mice. WT and APP-SAA female mice show increased spine BMD when compared to the respective genotype counterparts, yet no differences are seen when genotypes are compared for either sex. WT and APP-SAA male mice show higher lean body mass compared to the female counterparts and APP-SAA male mice show a greater lean body mass compared to WT male mice. An absence of differences is seen in fat mass, % lean mass or % fat mass when comparing APP-SAA male and female mice with the respective WTs or when comparing the sexes within the same genotype. These results suggest a potential sex-specific response to the APP-SAA mutations, with enhanced sex differences for femur BMD in the APP-SAA model, emphasizing the need for further exploration into its impact on musculoskeletal health.

P-047 Gabriel Ramirez

Table 1. Bone mineral density and body composition at 13 months of age					
		wildtype		APP-SAA	
	measurements	male	female	male	female
	body weight (g) £	39.5 ± 2.5	28.1 ± 2.3*	40.3 ± 4.0	31.0 ± 6.3*
bone mineral density (g/cm^2)	total £,&	0.053 ± 0.001	0.054± 0.001	0.056 ± 0.002#	0.055 ± 0.002
	femur £,&	0.072 ± 0.004	0.071 ± 0.002*	0.077 ± 0.005	0.068 ± 0.004
	spine £	0.048 ± 0.004	0.055 ± 0.002*	0.049 ± 0.005	0.054 ± 0.003*
body tissue mass (g)	lean body mass £,&	24.069 ± 0.651	18.191 ± 0.977*	25.928 ± 1.267#	19.963 ± 1.751*
	fat mass £	10.584 ± 2.323	6.219 ± 1.468	11.587 ± 3.827	8.150 ± 4.615
femur tissue mass (g)	lean femur mass $, £	0.788 ± 0.049	0.638 ± 0.074*	0.933 ± 0.126#	0.839 ± 0.083#
	fat femur mass $, £	0.382 ± 0.071	0.246 ± 0.79	0.480 ± 0.164	0.392 ± 0.159

Values indicate mean ± SD, only parameters that are significantly different are shown.
Stats: 2-way ANOVA: $= Genotype effect; £= Sex effect; &=Genotype x Sex effect interaction, Tukey's post-hoc test: $p<0.05$
*versus male of the same genotype, #versus wildtype of the same sex.

P-048 Xiao-Hua Qin, PhD

Laser-printed Hydrogel Niches to Grow 3D Cell Networks for Miniaturized Bone Organoids

Christian Gehre 1, Wanwan Qiu 1, Patrick Jäger 1, Xiaopu Wang 2, Francisco Marques 1, Bradley J. Nelson 2, Ralph Müller 1, and Xiao-Hua Qin 1
(1) Institute for Biomechanics, ETH Zurich, Zurich, Switzerland (2) Institute for Robotic Systems, ETH Zurich, Zurich, Switzerland

The inaccessible nature of osteocyte networks in bones renders fundamental research on skeletal biology a major challenge. This limit is partly due to the lack of high-resolution tools that can manipulate the pericellular environment in 3D cultures in vitro. As a result, growing human bone organoids comprising osteocytes is still largely unrealized. The goal of this study is to guide single bone cells to form a 3D network in vitro via photosensi;zed two-photon abla;on of microchannels in gelation methacryloyl (GelMA) hydrogels. A water-soluble two-photon photosensitizer (P2CK) was added to soft GelMA hydrogels to enhance the abla;on efficiency. Remarkably, adding 0.5 mM P2CK reduced the energy dosage threshold five-fold compared to untreated controls, enabling more cell-compatible ablation. By employing low-energy ablation (100 J/cm2) with a grid pattern of 1 µm wide and 30 µm deep microchannels, we induced dendritic outgrowth in human mesenchymal stem cells (hMSC). After 7 days, the cells successfully utilized the microchannels and formed a 3D network. Our findings reveal that cellular viability after low-energy ablation was comparable to unablated controls, whereas high energy ablation (500 J/cm2) resulted in 42 % cell death. Low-energy grid ablation significantly promoted network formation and >40 µm long protrusion outgrowth. While the broad-spectrum matrix metalloproteinase inhibitor (GM6001) reduced cell spreading by inhibiting matrix degradation, cells invaded the microchannel grid with long protrusions. Collectively, these results emphasize the potential of laser-printed hydrogel niches to sculpt interconnected bone cell networks as miniaturized bone organoids, opening new avenues for disease modelling and drug testing applications.

P-049 Mary Beth Cole, PhD

Preliminary Comparison of Cortical Volumes and Cortical Cross-Sections as Predictors of Human Rib Structural Bending Response

Mary E. Cole 1,2, Yun-Seok Kang 2, Amanda M. Agnew 2
(1) Division of Radiologic Sciences and Therapy, The Ohio State University (2) Injury Biomechanics Research Center, The Ohio State University

In elderly populations, rib fractures are a significant source of morbidity and mortality. Previous work has explored predictors of rib structural properties by dynamically loading ribs to failure in a simplified bending scenario representing a frontal thoracic impact. Rib structural properties were initially best explained by cross-sectional geometry adjacent to the fracture location, outperforming age, sex, body size, bone mineral density, and simple whole rib geometry. Further work strengthened cross-sectional predictors by subtracting cortical pores from the rib cortex. Compared to a solid cortex, porous cortex cross-sectional predictors explained up to 8.4% more variation in univariate analyses of rib structural properties. These previous analyses were limited to 2D histological cross-sections. The objective of this study was to evaluate whether 3D cortical volumes improved prediction of rib structural properties over 2D cortical cross-sections. An age series (n = 15, 24—97 years, mean = 58.9 years) of right sixth ribs with midshaft fractures was selected as a preliminary subset of the previously analyzed histological dataset (n = 191). Immediately adjacent to the histological section, a 10 mm length of the rib was visualized with micro-CT (voxel size = 7.9671 μm) and morphometrically characterized with the custom toolkit Pore Extractor 3D. Univariate analyses of this subset were sufficiently powered to examine peak force, total energy, and plastic energy. These structural properties were better explained by cross-sectional predictors that were averaged across 1,256 micro-CT slices, compared to the single histological slice. Micro-CT increased the variance explained in force and energy by cortical or bone area (solid cortex: +4.54—6.97%; porous cortex: +1.26—5.70%) and by second moments of inertia about the cortical bone distribution minimum (solid cortex: +6.73—8.81%; porous cortex: +8.55—9.24%) and maximum (solid cortex: +1.43—2.72%; porous cortex: +2.16—3.07%). Percent porosity also explained more variance in force and energy (+12.64—23.49%) when derived from micro-CT, compared to histology. Within the micro-CT dataset, the porous cortex further outperformed the solid cortex in variance explained in force (+0.54—1.79%) and energy (+2.61—4.42%) by cross-sectional predictors. A 3D cortical volume captures more variation in cortical geometry and porous bone loss, improving prediction of rib structural properties over a 2D cortical cross-section.

P-050 Furqan Ali Shah, PhD

Rethinking the validity of Ca/P ratio as a measure of bone mineral stoichiometry

H. Ben Amara 1, F A. Shah* 1
(1) Department of Biomaterials, University of Gothenburg, Sweden

Introduction: The mineral of bone is often incorrectly described as “hydroxy(l)apatite” (HAp)1, implying the presence of 6 phosphorus (P) atoms for every 10 calcium (Ca) atoms within the apatite crystal lattice. In bone apatite, a fraction of phosphate (PO43-) is substituted by carbonate (CO32-). Some Ca sites can be occupied bymagnesium (Mg), sodium (Na), and other cations. The calcium to phosphorus ratio (Ca/P) is taken as a measure of tissue age and/or mineral maturity2. However, P (or PO4 3-) from organic and intracellular sources can alter the measured Ca/P ratio. Additionally, since CO3 2- content increases with tissue age3, failure to account for CO3 2- results in overestimation of the cation to anion ratio (CAR). Here, we demonstrate that the Ca/P ratio of isolated bone mineral differs significantly from that of whole bone and propose alternative compositional metrics, e.g., the total cation to phosphorus ratio [Ca+Mg+Na/P], calcium to combined phosphorus and carbon ratio [Ca/P+C], and the total cation to combined phosphorus and carbon ratio [Ca+Mg+Na/P+C].

Methods: Bone fragments were obtained from fresh cadaveric bovine tibiae using a dental drill unit and deproteinised with dry heat (24h at 200 °C) or 10% NaOCl4 (3h and 3d at 4 °C). Deproteinisation was monitored using Raman spectroscopy (n=6). Energy dispersive X-ray spectroscopy (n=30) was used for elemental analysis. The Mann-Whitney U test was used for statistical analysis (all vs. whole bone).

Results and Discussion: Raman spectroscopy reveals that 3h and 3d exposures to 10% NaOCl correspond to 59% and 24% remaining organic matrix, which is also reflected in the calcium to carbon ratio (Ca/C). Initially, loss of C elevates Ca/P+C and Ca+Mg+Na/P+C ratios (Figure 1). With progressive removal of the organic matrix, the Ca/P and Ca+Mg+Na/P ratios also increase. Heating at 200 °C results in complete denaturation of collagen and elevation of Ca/P, Ca+Mg+Na/P, Ca/P+C, and Ca+Mg+Na/P+C ratios due to losses of both P and C, presumably in the form of volatile substances. Loss of the organic matrix significantly alters the elemental composition, including the Ca/P ratio. The Ca+Mg+Na/P+C ratio of isolated bone mineral reveals a more accurate picture of mineral composition by accounting for various ion substitutions. Heating denatures the collagen/organic matrix but organic C is not eliminated from the sample. NaOCl deproteinisation removes the organic C, allowing for the measurement of mainly inorganic C (i.e., CO3 2-).

Conclusions: Organic matrix removal is essential for accurate estimation of bone mineral CAR. We propose the use of Ca+Mg+Na/P+C ratio in completely deproteinised bone instead of the Ca/P ratio of whole bone, which does not reflect the chemical makeup of bone mineral.

REFERENCES:
1 Wopenka & Pasteris (2005) Mater Sci Eng C
2 P. Milovanovic et al (2013) ACS Nano
3 F. A. Shah et al (2020) Bone Rep
4 F. A. Shah et al (2016) Calcif Tissue Int

P-050 Furqan Ali Shah, PhD

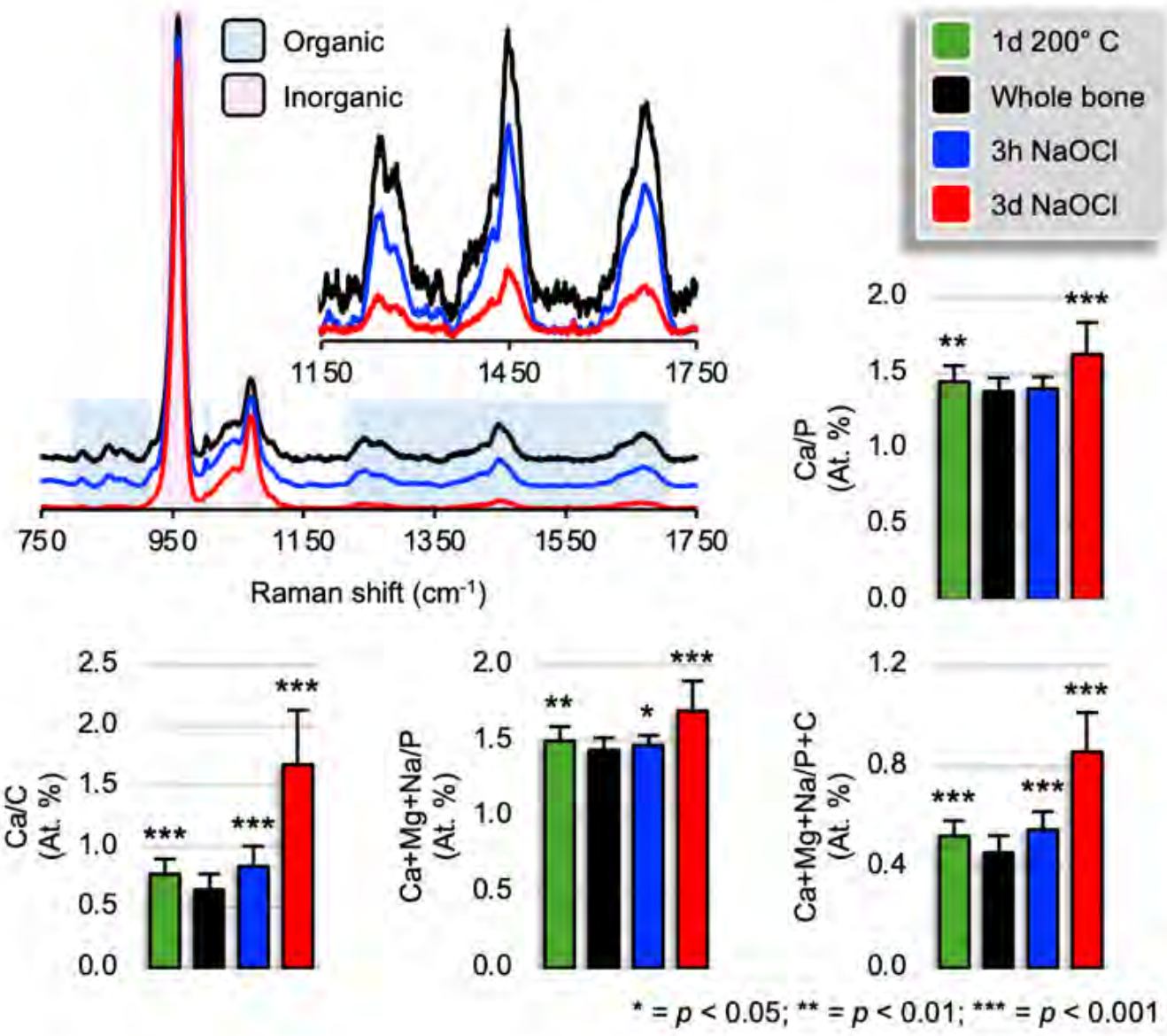

P-051 Lindsay Loundagin, PhD

Balanced Basic Multicellular Unit Activity in a Rabbit Model of Osteoporosis

Lindsay Loundagin*, Kim Harrison and David Michael Lane Cooper
Department of Anatomy, Physiology and Pharmacology, College of Medicine, University of Saskatchewan, Saskatoon, SK, Canada

Bone loss in postmenopausal osteoporosis (OP) is often attributed to elevated and/or imbalanced remodeling. The latter is considered a negative balance of basic multicellular unit (BMU) activity, in which bone resorption is greater than formation. Indeed, recent work with an ovariohysterectomy (OVH) rabbit model demonstrated a respective 2.4- and 6.4-fold increase in cortical porosity and activation frequency, but it is unclear if a negative BMU balance also contributes to OVH-induced porosity or how remodeling dynamics (e.g. rate of resorption and formation) are altered to maintain or disrupt BMU balance. This work used in vivo synchrotron imaging to investigate the spatial and temporal balance of cortical remodeling spaces in a rabbit model of OP. Ten New Zealand white rabbits (six-months old) received OVH or SHAM surgery, followed by 10-weeks recovery. The distal tibia was scanned first in vivo using in-line phase contrast microCT and again ex vivo two weeks later using desktop microCT. The distance between BMU cutting-cones in the registered datasets was used to calculate longitudinal erosion rate (LER). The radial profile of the remodeling space was derived from its 3D morphology and partitioned into a resorption and formation zone based on the maximum radius. BMU balance was assessed by the maximum radius, canal radius and wall thickness. The length of each zone and LER were used to calculate resorption and formation duration, as well as the radial infill rate. Remodeling spaces in OVH rabbits were larger than those in SHAM rabbits; however, this augmented resorption was accompanied by increased formation such that OVH BMUs remained balanced to an extent similar to SHAMs, evidenced by increased wall thickness in OVH rabbits and a similar canal radius between groups. Maintaining this balance was achieved by an extended formation duration, which was 50% longer in OVH than SHAM (21.0 vs 13.2days), while the radial infill rate was nearly identical between groups (OVH=2.1 vs SHAM=2.0μm/day). LER was not different between groups (OVH=41.3 vs SHAM=40.1μm/day) and resorption phase duration was 4.2 and 3.5 days for OVH and SHAM, respectively. These results suggest that the elevated porosity in this OVH rabbit model is predominately due to increased activation of remodeling events rather than negative BMU balance. This is in contrast to the negative BMU balance reported in human OP and may be due to the young age or earlier disease stage of these rabbits.

P-052 Lindsay Loundagin, PhD

Fusing 2D Histological and 3D Imaging Techniques: A Novel Approach to Investigate the Spatio-Temporal Organization of Basic Multicellular Units in the Rabbit

Lindsay Loundagin* 1, Kim Harrison 1, Xuan Wei 1, Malene Nielsen 2, Thomas Andersen 2, David Cooper 1
(1) Department of Anatomy, Physiology and Pharmacology, College of Medicine, University of Saskatchewan, Saskatchewan, Canada (2) Molecular Bone Histology-lab, Research Unit of Pathology, Dept. of Clinical Research, University of Southern Denmark, Denmark

Recently our lab established a microCT-based imaging pipeline to observe and track individual remodeling events over time in rabbit models of osteoporosis. The 3D and 4D data produced from this unique platform have the potential to elucidate the spatio-temporal behavior of basic multicellular units (BMUs). To assess the spatial relationship between remodeling phases, an automated approach has been developed to partition the remodeling space into three phases— resorption, reversal and formation— based on its 3D morphology. In this way changes in shape are interpreted as changes in cellular activity; however, the assumption that cellular activity corresponds to detectable shape changes is not trivial and central to the validity of this analysis. Hence, constraints of the phase segmentation need to be validated with gold-standard histological techniques. In this pilot study we use a cortical bone sample from an ovariohysterectomized New Zealand white rabbit to demonstrate the feasibility of mapping spatially resolved cellular information from fluorochrome labeled and immunostained sections of BMUs onto corresponding remodeling spaces observed in the 3D imaging data. As part of a larger cohort, the rabbit was given two calcein labels two weeks apart with the final label administered a day before euthanasia. A 5mm portion of the tibia was extracted postmortem, imaged using microCT (voxel size=5μm), decalcified and paraffin-embedded. Longitudinal serial sections (n=90) 3.5μm thick were cut, and alternating sections were stained for TRAcP enzyme activity (not included here) or immunofluorescence stained for osteopontin and nuclei. Histological slices were manually aligned and registered with the 3D data. Osteopontin was concentrated along the cement lines and highlighted packets of bone turnover from individual remodeling events with smooth or scalloped lines indicating a resting or eroded surface. The final calcein label aligned with the closing cone on the 3D remodeling space confirming a site of active formation, while flattened bone lining cells indicated a quiescent surface. These data will be used to refine the 3D morphology analysis but the preliminary results support the description of remodeling processes and structures reported in humans. From a broader perspective, the fusion of these imaging approaches provides a comprehensive view of remodeling activity and will inform the relevance of the rabbit as a preclinical model of bone remodeling in humans.

P-052 Lindsay Loundagin, PhD

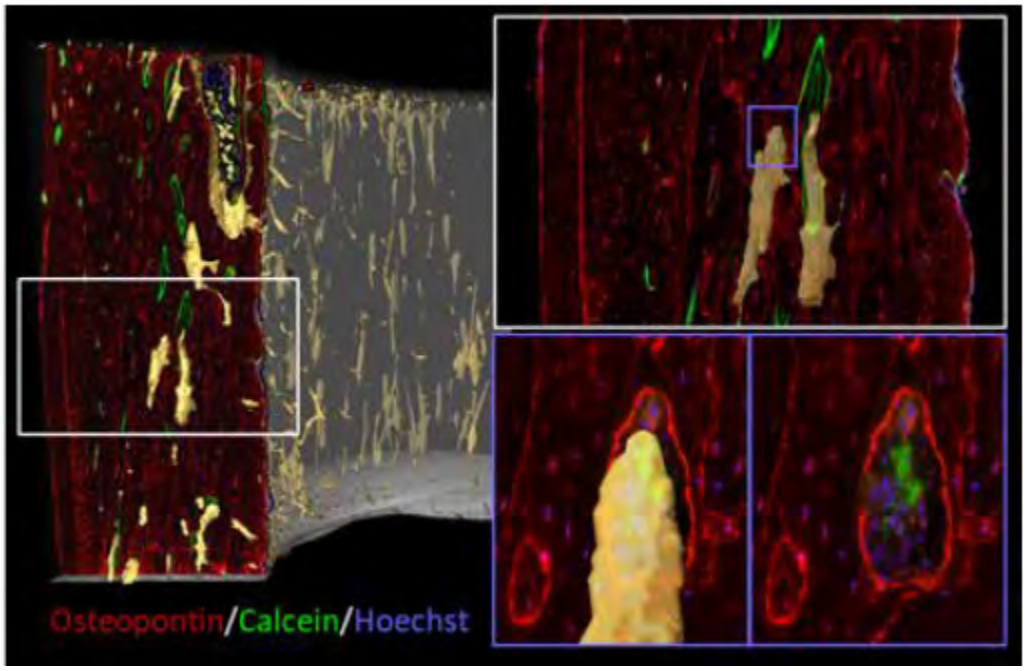

Figure: Immunofluorescence-stained section registered with the microCT render of a rabbit cortical bone sample. Calcein labels aligned with the closing cone (top right), while eroded surfaces and potential osteoclasts were observed within the cutting cone (bottom right) of the 3D remodeling space.

P-053 Maja Ostergaard, PhD

Changes in Osteocyte Lacunar Properties Are Due to New Bone Formation in Patients with Hypoparathyroidism Treated with Parathyroid Hormone

Maja Østergaard* 1, Tanja Sikjær 2, Sameera Siddiqui 1, Morten B. Nielsen 1, Lars Rejnmark 2 and Henrik Birkedal 1
(1) Department of Chemistry and iNANO, Aarhus University, Aarhus, Denmark (2) Department of Endocrinology and Internal Medicine, Aarhus University Hospital, Aarhus, Denmark

Patients suffering from hypoparathyroidism (hypoPT) have reduced parathyroid gland capacity, and hence impaired ability to make parathyroid hormone (PTH). PTH regulates the calcium and phosphate levels in the blood, thus patients lacking the hormone suffer from low blood calcium and a very low bone turnover, causing a lack of bone renewal.[1,2] Recent studies have shown promise for treating with recombinant human PTH1-84 (rhPTH), since this treatment leads to renewed bone formation.[1-6] With that we have a unique case of quiescent state bones from hypoPT patients, where treatment with rhPTH leads to renewed bone formation, we have the chance to detect lacunae during mineralization, when they are actively laying down new bone. In this situation, the shape and thus the size of the active cell lacunae are expected to change. The aim of this study is to quantify this change and gain information on how the lacunae form during bone mineralization.
Patients with hypoPT were randomized to 6 months of rhPTH (PTH6) or placebo (PLB) as add-on to conventional therapy with active vitamin D and calcium supplements when an iliac crest biopsy was collected [3]. Some patients continued in an open-label study, where former placebo patients continue with conventional treatment (CON) and the rhPTH treated patients either continued (PTH30) or switched to conventional treatment (PTHw) for the following 24 months. At 30 months in total, a biopsy was again collected. The biopsies were cut to rods with dimensions of app. 1 mm×500 µm×500 µm and measured with synchrotron radiation micro computed tomography (SR-µCT) at the TOMCAT beamline at Swiss Light Source with an isotropic voxel size of 0.325 µm to investigate the density variations in the material (new/mature bone) and quantify the lacunae morphometry.
Regions of newly formed bone are visible in the scanned biopsies from patients treated with rhPTH for 6 months. Statistical tests determined that the PTH6 group had a significantly lower mean new bone density compared to both the PLB, CON, and PTHw groups, corresponding to new bone formation in this group. In addition, significantly more new bone is formed when treating with PTH compared to PLB and more new bone is formed when treating with PTH for longer.
Lacunar volumes are significantly smaller in mature trabecular bone compared to new cortical bone. In the biopsies taken at 6 months, the change in volume is independent on group, meaning that their shape at this time point is not affected by the treatment. The lacunar density is also increased in newly formed bone.

[1] Rejnmark, L. et al., Osteoporos Int, (2013) 24, 1529-1536.
[2] Rejnmark, L. et al., Endocrinol Metab (2015) 30, 436-442.
[3] Sikjaer, T. et al., J Bone Miner Res,(2011) 26, 2358-2370.
[4] Sikjaer, T. et al., J Bone Miner Res, (2013) 28, 2232-2243.
[5] Rubin, M. R. et al., J Bone Miner Res, (2011) 26, 2727-2736.
[6] Gafni, R. I. et al., J Bone Miner Res, (2012) 27, 1811-1820.

P-054 Manabu Tsukamoto, PhD

Impact of Pulmonary Emphysema on Bone Quality

Manabu Tsukamoto* 1, Takayuki Nabeshima 1, Ke-Yong Wang 2, Yosuke Mano 1, Daisuke Arakawa 1, Eiichiro Nakamura 1, Ryosuke Ozasa 3, Takayoshi Nakano 3 and Akinori Sakai 1,
(1) Department of Orthopaedic Surgery, University of Occupational and Environmental Health, Japan, Japan (2) Shared-Use Research Center, University of Occupational and Environmental Health, Japan, Japan (3) Division of Materials and Manufacturing Science, Graduate School of Engineering, Osaka University, Japan

Introduction: The mechanism of pathogenesis on musculoskeletal disorders associated with Chronic Obstructive Pulmonary Disease (COPD) is unclear. Since COPD patients have multi factors that contribute to the development of those disorders, basic research using animal models will be needed. We demonstrated that intratracheally administered elastase (PPE) induces emphysema in a mice model (COPD mice), which exhibits trabecular bone loss with decreased bone formation, however we did not investigate the bone quality. Our study aimed to investigate the impacts of pulmonary emphysema induction on bone quality.

Methods: Twelve-week-old male C57BL/6J mice were intratracheally administered saline (Saline group) or PPE (PPE group), and every 4 weeks, food intake, water intake, urine volume, fecal volume and spontaneous activity were measured using a metabolic gauge and the EthoVision XT (Noldus, Wageningen, Netherlands), respectively. At 24 weeks after intratracheal administration, the animals were sacrificed. Lungs, femurs, and tibiae were harvested, and lungs were measured for mean inter-alveolar distance (Lm) in tissue specimens. The bone microstructure and histomorphometry were analyzed using micro-CT images and tissue specimens, and all the microbeam X-ray diffraction experiments were performed using the Rigaku R-AXIS Bone Quality system. In addition, bone marrow cells were harvested and CAGE-seq was performed.

Results: No significant differences in food intake, water intake, urine volume, feces volume, and spontaneous activity were found between the two groups at each time point. At 24 weeks after intratracheal administration, the PPE group had significantly larger Lm values than the saline group and showed pulmonary emphysema. In vivo micro-CT showed a temporary decrease in the change rate of trabecular BMD in the femur at 12 weeks after intratracheal administration, however there was no significant difference between the saline and PPE groups at 24 weeks finally. In bone histomorphometry or ex vivo micro CT, the values of BV/TV, Tb.Th, Tb.N and Ob.S/BS and Ob.N/BS were significantly lower in the PPE group. In addition, the PPE group showed lower preferential alignment of the biological apatite crystallite at the diaphysis of the femur than the saline group despite no significant decrease of cortical BMD. CAGE-seq demonstrated that most of the genes that showed change in the PPE group were mitochondria (oxidative stress)-related genes.
Conclusions: PPE-induced pulmonary emphysema mice showed deterioration of bone quality by bone microstructure and apatite orientation despite the absence of bone mineral density loss.

P-055 Nikolas Knowles, PhD

Image Based Finite Element Model Stiffness and vBMD by Single and Dual Energy CT Reconstruction Kernel

Nikolas Knowles*, Sarah Quayyum, Jonathan Ying, Chloe Stiles and Daniel Beshay, University of Waterloo, Waterloo, ON, Canada
(1) Department of Orthopaedic Surgery, University of Occupational and Environmental Health, Japan, Japan (2) Shared-Use Research Center, University of Occupational and Environmental Health, Japan, Japan(3) Division of Materials and Manufacturing Science, Graduate School of Engineering, Osaka University, Japan

Single-energy quantitative computed tomography (SEQCT) provides volumetric bone mineral density (vBMD) measures that are important to track bone changes due to injury and disease and are used as input to image based finite element models (FEMs). Clinical CT resolution limits SEQCT to distinguish material variations that alter vBMD in each voxel, such as bone marrow fat or fluid infiltration following acute trauma. Dual-energy CT (DECT) can account for voxel-specific variations utilizing scans at multiple x-ray energies and material decomposition. Image vBMD data is further altered by image reconstruction kernel that cannot be accounted for using standardized calibration phantoms. This study compared vBMD and FEM stiffness derived from SEQCT and DECT images reconstructed with two common kernels.

SEQCT and DECT images of cadaveric shoulders (n = 10) were collected using standard (STD) and boneplus (BONE) kernels. Hounsfield Units were converted to vBMD using specimen-specific calibration equations for each image. DECT STD and BONE images were generated using an established material decomposition method with 40 and 90 keV simulated monochromatic images. A proximal humerus bone section directly below the anatomic neck was used for vBMD analysis and FEM generation. FEMs were loaded to 1% apparent strain for stiffness measurements.
Between STD and BONE kernel reconstructed images, average vBMD differed 0.9 mgK2HPO4/cc and 4.1 mgK2HPO4/cc, in SEQCT and DECT images, respectively. Significant differences only occurred in DECT images (p=0.001). BONE reconstructed images consistently produced higher vBMD measures across both SEQCT and DECT images. DECT showed larger vBMD than SEQCT for both STD and BONE images. The difference between STD and BONE in both SEQCT- and DECT-based FEMs persisted, with larger estimated stiffness in BONE versus STD derived models. DECT-based models had larger stiffness values and a larger difference between STD and BONE derived models (DECT: 17.2 kN/mm; SEQCT: 13.3 kN/mm) (Table 1). Stiffness values were significanetly different within image types for both STD and BONE kernels and across reconstruction kernel images for SEQCT and DECT images.

This study shows important differences in vBMD, and FEM estimated stiffness that occur due to CT-based imaging parameters alone. These results indicate that consistent imaging parameters should be used for longitudinal monitoring of vBMD and as FEM input to avoid systematic errors in measurements.

P-056 Sirion Aksornthong

Osteoclast indices in Osteogenesis Imperfecta: systematic review and meta-analysis

Sirion Aksornthong* 1,2, Priyesh Patel 2,3 and Svetlana V. Komarova 1,2,3,4
(1) Department of Experimental Surgery, McGill University, Montreal, QC, Canada, (2) Shriners Hospital for Children – Canada, Montréal, QC, Canada, (3) Faculty of Dental Medicine and Oral Health Sciences, Montreal, QC, Canada, (4) Department of Biomedical Engineering, Faculty of Engineering, University of Alberta, Edmonton, AB, Canada

Osteogenesis imperfecta (OI) is a rare bone fragility disorder caused by mutation in genes that encode collagen type I or affect its processing. Alterations in osteoclasts were reported and suggested to contribute to OI pathophysiology. However, it is unclear if osteoclast function is similarly affected in different phenotype and severity presentations. We aimed to systematically identify studies reporting measures of osteoclast formation and function in patients and mouse models of OI, to quantify OI-induced changes. The search strategy was developed and applied for systematic search in Medline, OVID and Web of Science databases. The screening was performed using Rayyan Systematic Review Screening Software. From the full-text articles, we extracted the data describing study characteristics and osteoclast-related outcomes from OI and healthy control group for urine or serum levels of collagen degradation markers (CTX-1, NTX or urinary DPD) and osteoclast parameters from bone histomorphometric analysis (osteoclast number, osteoclast surface, resorptive surface and eroded surface). The standardized mean difference was used as the effect size. The random effects meta-analysis was performed using R-studio. The systematic search identified 798 unique studies. After the screening, we included for meta-analysis 23 studies reporting osteoclast parameters in 310 OI patients of 9 different types and 16 studies reporting osteoclast parameters in 406 animals of 11 different OI mouse models. In OI patients, collagen degradation markers were significantly higher in patients with OI compared to age-matched control with an effect size of 1.23 [Confidence interval (CI): 0.36, 2.10]. Collagen degradation markers were the most elevated in the 3 to 7-year-old age group and in patients with more severe forms of OI. Bone histomorphometry demonstrated the trends for higher osteoclast numbers, 1.16 [CI: -0.22, 2.55], and osteoclast surface, 0.43 [CI: -0.63; 1.49], and significantly higher eroded surface, 3.24 [CI: 0.51, 5.96] compared to the aged-match control. In OI mice, meta-analysis demonstrated significant increases in collagen degradation markers, 1.59 [CI: 1.07, 2.11]; osteoclast numbers, 0.94 [CI: 0.50, 1.39], osteoclast surface, 0.73 [CI:0.22, 1.23], and eroded surface 1.31 [CI: 0.54, 2.08]. The largest differences were in OI mice with the mutation in Col1a1 and Col1a2 genes. There were no differences between males and females in clinical or animal studies. In conclusion, quantitative estimates of changes in osteoclast indices and their variance for patients with OI are important for planning future studies. The increased osteoclast indices were demonstrated, especially in young OI subjects with higher phenotype severity. We confirmed that similar changes are observed in mice with OI, supporting their translational utility.

Table 1: vBMD and stiffness in SEQCT and DECT humerus models

Parameter	SEQCT		DECT	
	BONE	STD	BONE	STD
vBMD [mg_{K2HPO4}/cc]	100.8 ± 26.3	99.9 ± 28.9	104.0 ± 24.9[a]	99.9 ± 23.9[a]
Stiffness [kN/mm]	124.1 ± 70.4[b,c]	110.8 ± 67.4[b,d]	127.3 ± 72.9[d,e]	110.1 ± 63.2[c,e]

Average values sharing a common letter are significantly different (one-way RM-ANOVA a: p = 0.001; b: p = 0.002; c: p = 0.023; d: p = 0.008; e: p = 0.005)

P-057 Jianguo Tao

Multi-omics Integration Reveals Candidate Determinants of Bone Mineral Density and the Role of AZIN1 in Bone Homeostasis

Jianguo Tao* 1,2, Xiangjiao Yi 1, Yu Qian 1, Maomao Miao 1, Xin Li 1, Jiaxuan Gu 1 and Hou-Feng Zheng 1,2
(1)Diseases & Population (DaP) Geninfo Lab, School of Life Sciences, Westlake University, Hangzhou, China (2) School of Life Sciences, Zhejiang University, Hangzhou, China

Osteoporosis, a common disease diagnosed primarily by BMD, has elusive genetic determinants. In this study, we conducted genome-wide association studies (GWAS) of BMD measured using dual-energy X-ray absorptiometry at 11 skeletal sites in nearly 40,000 individuals. We identified 18 novel genetic association loci, of which 5 annotated genes have not been previously reported in bone research. Among these loci, lead SNP rs2247355, located in promoter region of AZIN1 gene, showed a significant association with head BMD. This SNP is modified by super enhancer H3K27Ac and significantly correlated with AZIN1 gene expression, as demonstrated by eQTL analysis. Gene-based and summary-data-based Mendelian randomization analyses supported a positive causal link between genetically determined AZIN1 gene expression and head BMD. By integrating head BMD GWAS and scRNA-seq data from different tissues, including bone and brain, we discerned MSCs, osteoblasts, monocytes, macrophages, astrocytes, and other cell types through which the risk variants impact head BMD. Bulk RNA-seq data analysis of BMSCs from young individuals and senile osteoporosis patients indicated that AZIN1 mRNA levels and RNA editing frequency were decreased in BMSCs from aged participants, suggesting a potential role of AZIN1 in age-related bone loss. Utilizing pseudotime results of scRNA-seq data generated from bone of WT mice, we observed a temporal pattern of AZIN1 expression during osteoblast differentiation, with its levels rising in pre-osteoblasts, peaking in osteoblasts and declining in terminal osteocytes. Importantly, AZIN1 knockdown significantly inhibited osteoblast differentiation and mineralization in MC3T3-E1 pre-osteoblast cells while promoting osteoclastogenesis in RAW264.7 cells. Although limited by current sample size (2/group), μCT analysis hinted at a decrease in bone volume in AZIN1f/f;Prx1cre and AZIN1f/f;OCNcre mice. Moreover, compared to overexpression of the WT form of AZIN1, overexpression of RNA-edited AZIN1 enhanced osteogenic differentiation and mineralization of MC3T3-E1 cells while suppressing cell proliferation, whereas non-edited AZIN1 had opposite effects in vitro. Mechanistically, CoIP-MS data revealed that RNA-edited AZIN1 exhibited an increased affinity to interact with osteoblast differentiation-related proteins, including transcriptional factors such as DDX5, suggesting that RNA-edited AZIN1 entered nucleus to promote osteogenic differentiation. Additionally, AZIN1 knockdown in MC3T3-E1 or knockout in H9 hESCs dramatically reduced PIEZO1 protein levels, which could crosstalk with osteoclasts by regulating YAP/Col-II/IX axis, thereby promoting osteoclast differentiation. Collectively, our findings unveil the candidate determinants of BMD and highlight the role of AZIN1 in regulating bone homeostasis, which may be leveraged to prevent bone loss.

P-058 Melia Matthews

Intravital Perturbation of Osteocyte Nanoparticle Uptake with Dynamin and Cholesterol Inhibitors

Melia Matthews*, Nuzhat Mukul, Alexander Saffari, Nada Naguib, Ulrich Wiesner and Karl J Lewis
Cornell University, Ithaca, NY, USA
*: Presenting author

Osteocytes use integrins to mediate mechanotransduction during physiological fluid flow stimulation and contribute to skeletal homeostasis1. Membrane-bound integrins are metabolized and maintained via endocytosis in numerous cell types in vitro2. However, to our knowledge, there has been no systematic study to understand endocytic pathways in osteocytes. We previously validated the use of ultrasmall surface-functionalizable fluorescent core-shell silica nanoparticles (C'Dots) as a novel in vivo tool for studying osteocyte uptake dynanics3. Here, we report use of this platform to test the hypothesis that pharmacological perturbation of dynamin or cholesterol, components affecting distinct endocytic mechanisms, impairs uptake and trafficking of integrin-targeted nanoparticles in osteocytes in vivo.

Isoflurane anesthetized C57BL/6J mice (16-18weeks, M/F) were injected subcutaneously above the third metatarsal (MT3) with Dyngo-4a to disrupt dynamin (Abcam), Methyl-β-cyclodextrin to disrupt cholesterol (Sigma), or PBS control for 30 minutes. PEGylated C'Dots with Cy5 dye (control), RGD functionalized (integrin-targeted), and membrane penetrating TAT-functionalized (positive control), created as previously described4, were then injected and incubated for a 45 min period. The MT3 was then surgically isolated, stabilized, and submerged in a PBS bath in preparation for imaging. Fluorescent C'Dot signal was observed using 2-photon in vivo microscopy (ThorLabs). Ten 35μm z-stacks were taken over 2.5 hours at 1090nm. Osteocyte C'Dot signal was quantified in ImageJ (NIH) using 3D segmentation. T-Tests and 2-Way ANOVAs were run on GraphPad Prism software. Dyngo4a administration impacted integrin-targeted C'Dots, but not PEG or TAT, as indicated by changes in slope. Males had a higher cell count while females had lower compared to control, suggesting a sexually dimorphic role for dynamin in integrin endocytosis. MβCD increased initial uptake across PEG and RGD C'Dots, with males and females displaying improved signal retention. Interestingly, MβCD reduced uptake and slope in TAT positive control groups, indicating that the impact of cholesterol perturbation does not depend on C'Dot functionalization. Our findings suggest nanoparticle uptake and clearance rates are modulated by small molecule endocytosis disruptors and implicates those pathways in osteocyte integrin dynamics.

1) Thi+ PNAS (2013). 2) Moreno-Layseca+ Nat Cell Bio (2019). 3) Matthews+ Bone (2023). 4) Erstling+ Adv Materials (2021).

P-059 Anika Shimonty, PhD

Mutation in CLCN7 Results in Impaired Osteoclast Resorption and Puzzle-like Bone Structural Units in ADOII Mice

Anika Shimonty* 1,2, Xenia Borggaard 3,4, Elissa Zboinski 1, Malene Hykkelbjerg Nielsen 3,4, Emily Nicole McDonald 1, Joseph Michael Wallace 5, Thomas Levin Andersen 3,4,6 and Julia F. Charles 1,2
(1) Brigham & Women's Hospital, BOSTON, MA, USA (2) Harvard Medical School, Boston, MA, USA (3) Molecular Bone Histology Lab, Research Unit of Pathology, Department of Clinical Research, University of Southern Denmark, Denmark (4) Odense University Hospital, Odense, Denmark (5) Indiana University Purdue University Indianapolis, Indianapolis, IN, USA (6) Department of Forensic Medicine, Aarhus University, Aarhus, Denmark

Autosomal Dominant Osteopetrosis Type II (ADOII) is a rare inheritable condition caused by mutations in the CLCN7 gene, encoding a Cl-/H+ exchanger necessary for osteoclastic bone resorption. ADOII patients have high bone mass yet are susceptible to fracture, suggesting impaired bone tissue quality. We hypothesized that changes in bone structural unit (BSU) composition could explain increased fragility. To examine our hypothesis, we used 12, 24, and 52-week-old female and male FVB1 wildtype (WT) and Clcn7 p.F316L heterozygous (het) mice, analogous to a mutation reported in Chinese, Italian and American ADOII patients. Vertebral µCT analysis of Clcn7 p.F316L het mice reveals significantly higher trabecular bone volume fraction (BV/TV) and bone mineral density (BMD) across all ages and sexes. This finding suggests a robust phenotype regardless of age and sex. Serum markers exhibit increased tartrate-resistant acid phosphatase (TRAP) levels with no significant difference in CTX in the het mice, suggesting richly abundant but poorly resorptive osteoclasts. Next, we performed immunostaining on vertebral sections for osteopontin-rich cement lines to determine the BSU composition. At 12 weeks, both het female and male mice had smaller BSU area, with higher BSU number per trabecular area compared to WT littermates resulting in a puzzle-like structure. Mean BSU perimeter was inversely correlated to BV/TV in both sexes. We see a similar phenotype of smaller BSUs in 24-week-old male mice, indicating a robust phenotype regardless of age (Figure). Additionally, 12 and 24-week-old het mice from both sexes had higher cartilage area per trabecular bone area compared to WTs, indicating reduced resorptive activity. Our findings suggest that while ADOII osteoclasts exhibit poor catabolic activity, bone formation continues despite reduced resorption. This combined activity of ADOII osteoclasts and osteoblasts forms a puzzle-like BSU composition, which may contribute to the bone fragility observed in ADOII. We are currently performing similar analyses on human ADO samples and age/sex matched controls to correlate mouse and human phenotypes. In the future, we plan to examine the mechanical properties of the vertebrae to correlate the puzzle-like BSU composition with bone mechanical properties.

P-059 Anika Shimonty, PhD

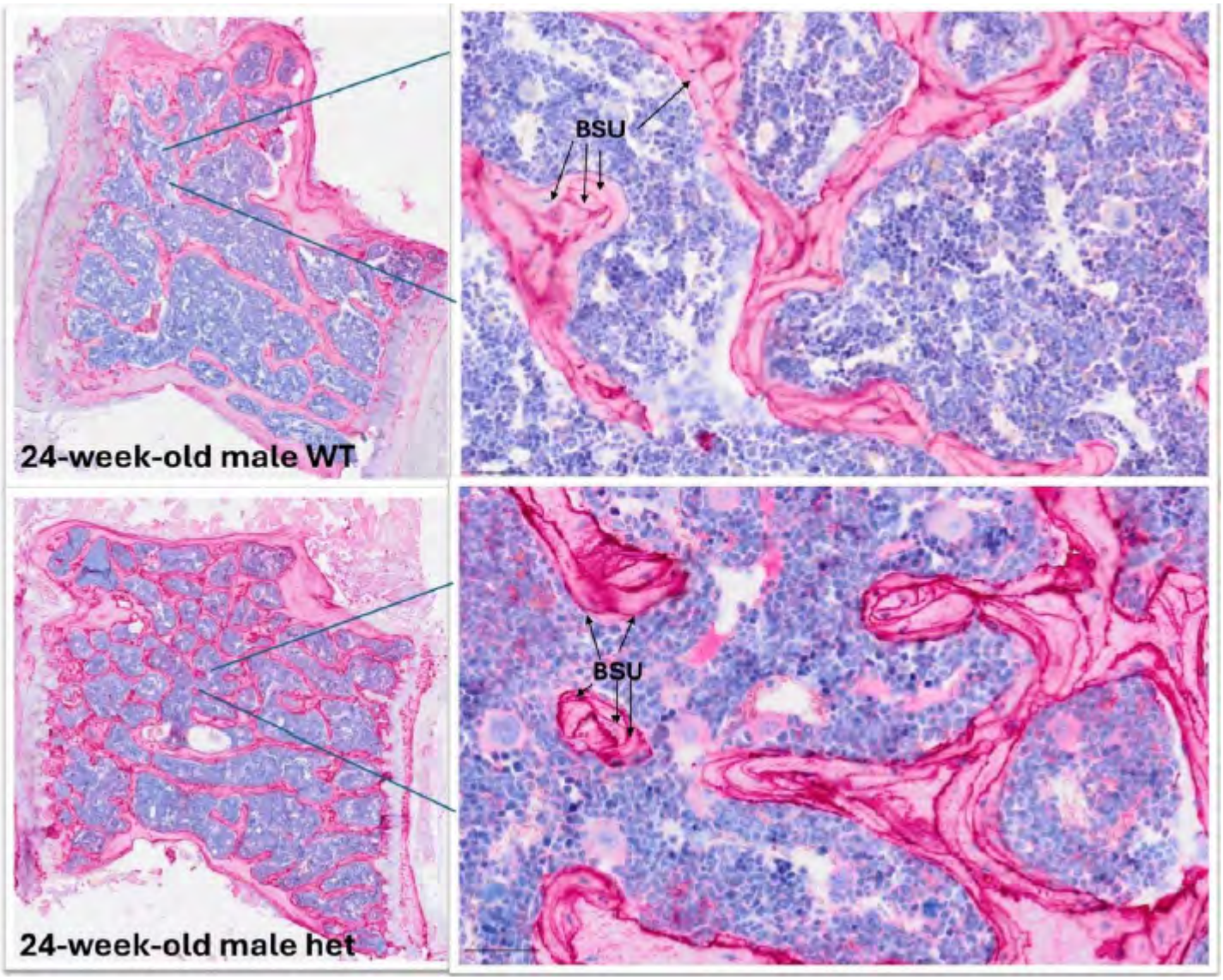

P-060 Jan Hughes-Austin, PhD

Femoral Head Bone Marrow Fat Fraction by Computed Tomography is Associated with Higher Bone Turnover in Patients Experiencing Hip Fractures

Jan M. Hughes-Austin* 1, David B. Berry 1, Madison T. Alexander1, Deborah M. Kado 2, Ronit Katz3, Lauren Claravall1, William T. Kent 1, Paul Girard 1, Alexandra K. Schwartz 1, Isidro B. Salusky 4, Renata C Pereira 4 and Joachim H. Ix 1
(1) University of California, San Diego, La Jolla, USA (2) Stanford University, CA, USA (3) University of Washington, Seattle, USA (4) University of California Los Angeles, Los Angeles, USA

Background: Bone turnover can be either high or low, leading to higher fracture risk. It should impact choice of medical treatment, but currently cannot be easily assessed, particularly when kidney function is impaired or in the acute fracture setting. However, bone marrow adiposity (BMA) has been implicated in bone loss and fracture via affecting bone turnover by inhibiting osteoblast function and promoting osteoclast differentiation. We sought to determine whether bone marrow fat fraction measured through computed tomography (CT) scans of patients undergoing surgery for hip fracture was correlated with bone turnover

Methods: This cross-sectional study included patients ages 18 or older who were admitted to our institution for surgical repair of hip fracture from January 2021 to present. Among 13 available CT scans in these patients, we measured BMA in the femoral heads. To quantify fat fraction in the femoral head, we calculated the ratio of number of voxels with a -150<Hounsfield Units (HU)<-50 (accepted range for fat) to the total number of voxels in the region of interest with HU>500 (threshold for cortical bone). Using femoral head biopsies obtained at time of surgery, we assessed bone turnover via histomorphometry, currently considered the gold standard test. Using Spearman coefficients, we tested correlations between fat fraction and bone turnover.

Results: Average age was 71 ± 14, 77% were female, 69% were non-Hispanic, and 46% were White. The mean estimated glomerular filtration rate (eGFR) was 67 ± 31 ml/min/1.73m2 and 7/13 had eGFR < 60. The mean (SD) fat fraction was 0.02 ± 0.02 %. Fat fraction was significantly and strongly correlated with osteoblast surface (Ob.S/BS) (r=0.90, p=0.01) and osteoid thickness (O.Th) (r=0.83, p=0.04). Fat fraction appeared marginally associated with osteoid volume (OV/BV) (r=0.77, p=0.07); and inversely correlated with bone sclerostin relative to tissue area (r=-0.77, p=0.07). (Table)
Discussion: Fat fraction in the femoral head assessed by CT scan is strongly correlated with osteoblast surface (a marker of high turnover). A strong inverse correlation was suggested with tissue sclerostin staining (a protein that limits bone turnover) but did not reach statistical significance. If validated, hip CT and quantification of fat percentage could provide an effective non-invasive measure of bone turnover, potentially better guiding medical treatment for osteoporosis.

	Spearman correlation coefficient	P-value
Osteoblast Surface/Bone Surface (Ob.S/BS), %	0.90	0.01
Osteoid Thickness (O.Th), um	0.83	0.04
Osteoid Volume / Bone Volume (OV/BV), %	0.77	0.07
Osteoclast Surface / Bone Surface (Oc.S/BS), %	0.52	0.29
Trabecular Separation (Tb.Sp), um	0.31	0.54
Sclerostin / Bone Area (Sclerostin / B.Ar)	-0.43	0.40
Bone Volume / Tissue Volume (BV/TV), %	-0.49	0.33
Trabecular Thickness, (Tb.Th) um	-0.49	0.33
Sclerostin / Tissue Area (Sclerostin / T.Ar)	-0.77	0.07

P-061 Adam Yiu-chung Lau, MBBS

Lower CYP27B1 Expression in Osteocytes Increases the Risk of Curve Progression in a New Mouse Model of Scoliosis

Wayne YW Lee*1, Zhang Zhe2, Gen Tang2, Kenneth Guangpu Yang2, Adam Yiu-Chung Lau3, Huanxiong Chen4, Tsz-Ping Lam5 and Jack Chun-Yiu Cheng5

(1)Department of Orthopaedics and Traumatology, the Chinese University of Hong Kong, Hong Kong, China, (2)Department of Orthopaedics and Traumatology,the Chinese University of Hong Kong, China, (3)Department of Orthopaedics and Traumatology,the Chinese University of Hong Kong, Hong Kong, (4)Department of Spine Surgery, The First Affiliated Hospital of Hainan Medical University, Haikou 571199, China, China, (5)SH Ho Scoliosis Research Lab, Joint Scoliosis Research Center of the Chinese University of Hong Kong and Nanjing University, Department of Orthopaedics & Traumatology, The Chinese University of Hong Kong, Hong Kong, China

Adolescent Idiopathic Scoliosis (AIS) is a prevalent three-dimensional spinal deformity affecting girl mostly during puberty without clear cause. Our previous RCT showed that vitamin D supplementation could improve bone quality and reduce progression risk simultaneously. In previous ASBMR meeting, we reported lower CYP27B1 expression and activity in AIS osteocytes. These prompted us to ask whether the extra-renal activity of CYP27B1, particularly in osteocytes, is impaired in AIS which contribute to curve progression. In this study, a new mouse model of scoliosis is established to address our research question.

C57BL/6 background female mice at age of 4-week-old were used to mimic rapid skeletal growth. Structural scoliosis was induced with in-house designed restrainers to introduce hypokyphosis and asymmetric loading, thus compromising vertebral rotational stability in quadrupeds and leading to progressive deformity as evidenced by weekly restrainer-free radiography, and 3D structural examination by microCT and paraspinal muscle histology at age of 10-week-old. Iliac bone tissues (N=12) were collected intra-operatively from severe AIS patients for qPCR and Western blot to verify the link between extra-renal CYP27B1 in bone and curvature. In vivo functional validation was conducted with osteocyte-specific Cyp27b1-knockout mice (cKO) and Cyp27b1-floxed mice (control) receiving various vitamin D diets (0, 1,000 or 20,000 IU/kg) (N≥6 per group). Femora were collected for bone histomorphometry and osteocyte lacunar-canalicular network (LCN) analysis. Blood samples were used to determine serum vitamin D level.

All mice with 6-weeks restrainer treatment exhibited progressive right thoracic spinal deformity associated with hypokyphosis, vertebra rotation and muscle fiber type change. CYP27B1 expression in iliac bone was negatively correlated with Cobb angle. Ablation of Cyp27b1 in osteocytes resulted in lower bone mass, poorer bone microarchitecture and deranged osteocyte LCN in cKO mice, which were more susceptible to restrainer induced scoliosis resulting in larger curvature. Restrainer induced curvature was mitigated by 20,000 IU/kg vitamin D diet, but aggravated by 0 IU/kg diet.

This is the first preclinical study showing the crucial role of Cyp27b1 expression in osteocytes on scoliosis curve progression supported by correlation analysis with clinical bone tissues. Pathogenic mechanistic study can be facilitated by this new mouse model of scoliosis.

P-061 Adam Yiu-chung Lau, MBBS

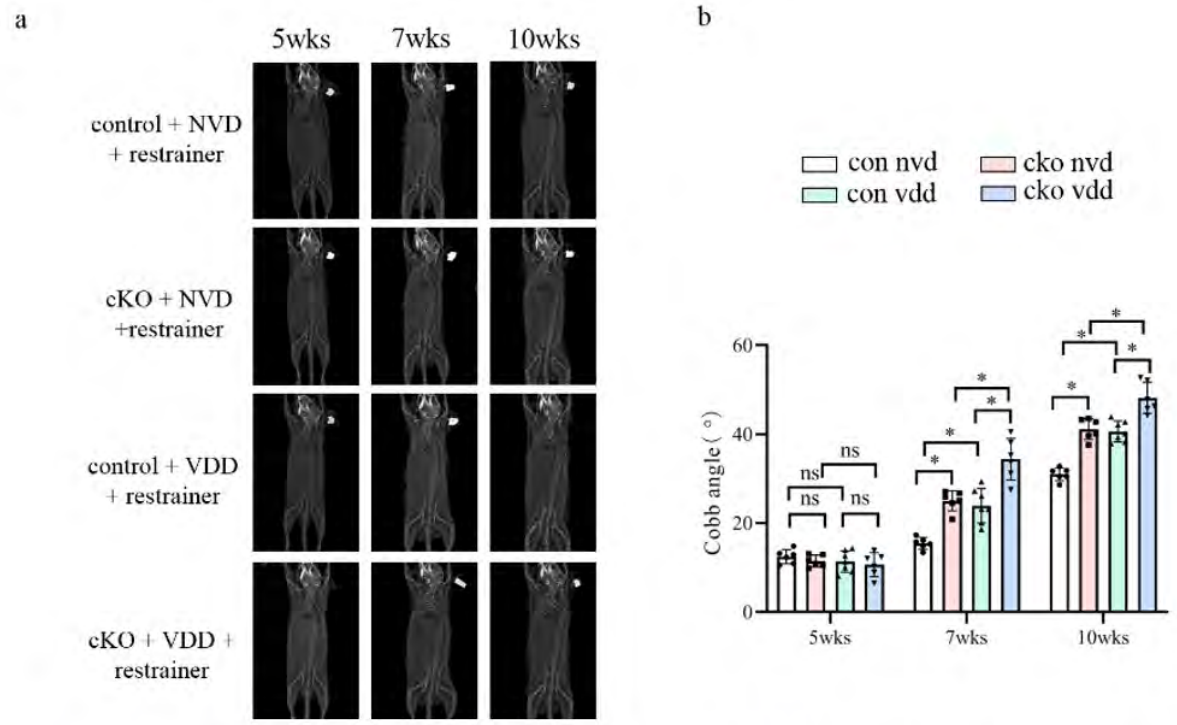

Deletion of Cyp27b1 in osteocyte and vitamin D deficiency diet aggravate curve progression in control and cKO mice in the presence of restrainer treatment from 4-week-old to 10-week-old. The mice were receiving either control diet (1,000 IU/kg (NVD)) or vitamin D deficiency diet (0 IU/kg (VDD)) during the 6 weeks treatment period. (a) Representative images of mice X-ray images without restrainer. (b) Cobb angle analysis with 5 or 6 mice per group. * $p < 0.05$.

P-062 Adam Yiu-chung Lau, MBBS

Preventing Curve Progression to Bracing Threshold in Early Adolescent diopathic Scoliosis (AIS) Using Calcium Plus Vitamin D Supplementation – An Initiated Randomized Double-blinded Placebo-controlled Trial

Tsz Ping Lam*1, Kenneth Guangpu Yang1, Wayne YW Lee2, Adam Yiu-Chung Lau1, Alec Lik-hang Hung2, Eric Cheuk-Kin Kwan1, Nelson Leung Sang Tang3 and Jack Chun-yiu Cheng1
(1) SH Ho Scoliosis Research Lab, Joint Scoliosis Research Center of the Chinese University of Hong Kong and Nanjing University, Department of Orthopaedics & Traumatology, The Chinese University of Hong Kong, Hong Kong, China, (2) SH Ho Scoliosis Research Lab, Joint Scoliosis Research Center of the Chinese University of Hong Kong and Nanjing University, Department of Orthopaedics & Traumatology, The Chinese University of Hong Kong, China, (3) Department of Chemical Pathology and Li Ka Shing Institute of Health Sciences, Faculty of Medicine, The Chinese University of Hong Kong, China

Introduction: Adolescent Idiopathic Scoliosis(AIS) is a prevalent three-dimensional spinal deformity mainly affecting pubertal girls. It can lead to serious complications including spine degeneration, cardiopulmonary compromise, grossly deformed torso and psychosocial disorders. Current treatments are far from being satisfactory, with bracing being lengthy and physically demanding and surgery being a major invasive procedure.

There is an association between AIS and low bone mass which has been reported to be a significant prognostic factor for curve progression. Given that dietary calcium(Ca) intake and serum Vitamin D(Vit-D) levels were also low in AIS, we previously reported an award-winning randomized double-blinded placebo-controlled trial showing Ca+Vit-D could prevent curve progression and improve bone health in immature AIS girls having Cobb angle mainly above 20 degrees and Z-score of areal bone mineral density(aBMD)<0. Results showed for those with low baseline serum 25(OH)Vit-D, 16.2% with treatment had curve progression≥6 degrees as compared with 48.6% in the Placebo Group(p=0.003). To translate research findings into clinical practice, it is mandatory to investigate whether Ca+Vit-D is also effective for early AIS having Cobb angle between 10-20 degrees in preventing disease progression to bracing threshold.

Objective: We therefore launched the current study to investigate if Ca plus Vit-D supplementation can prevent curve progression and improve bone health in early AIS.

Methods: This was an initiated randomized double-blinded placebo-controlled trial to evaluate if daily 600mgCa+800IUVit-D for three years could improve bone health and prevent curve progression. Immature AIS girls with Cobb angle 10-20 degrees were randomized either to the Treatment or Placebo group. The main outcome measures for evaluation at 3-year treatment timepoint were: (1) percentage of patients who required bracing and (2) Bone health measurements using High Resolution Peripheral Quantitative Computed Tomography.

Preliminary Results and Discussion: We have reached the three-year treatment timepoint at the final stage of data verification and analysis. Out of 199 subjects enrolled into the study, 99 subjects with mean age 12.0±1.0 years were in Placebo Group; 100 subjects with mean age 12.0±1.0 years were in Treatment Group. 161 subjects (80.9%) completed three-year treatment with results to be available for reporting by the first day of the ASBMR Annual Meeting. This study will carry significant impacts in that if Ca+Vit-D supplementation is proven to be useful, it can be prescribed for early AIS for preventing disease progression to avoid the need for lengthy and physically demanding bracing and invasive surgical procedures.

P-063 Xiangjiao Yi, PhD

Multi-omics Integration Uncovers Atrazine Induces Skeletal Muscle Atrophy by Disturbing Satellite Cell Fate, Energy Metabolism and Proteostasis

Jianguo Tao*1,2, Xiangjiao Yi1, Yu Qian1, Maomao Miao1, Xin Li1, Jiaxuan Gu1 and Hou-Feng Zheng1,2
(1) Diseases & Population (DaP) Geninfo Lab, School of Life Sciences, Westlake University, Hangzhou, China, (2) School of Life Sciences, Zhejiang University, Hangzhou, China

Osteoporosis, a common disease diagnosed primarily by BMD, has elusive genetic determinants. In this study, we conducted genome-wide association studies (GWAS) of BMD measured using dual-energy X-ray absorptiometry at 11 skeletal sites in nearly 40,000 individuals. We identified 18 novel genetic association loci, of which 5 annotated genes have not been previously reported in bone research. Among these loci, lead SNP rs2247355, located in promoter region of AZIN1 gene, showed a significant association with head BMD. This SNP is modified by super enhancer H3K27Ac and significantly correlated with AZIN1 gene expression, as demonstrated by eQTL analysis. Gene-based and summary-data-based Mendelian randomization analyses supported a positive causal link between genetically determined AZIN1 gene expression and head BMD. By integrating head BMD GWAS and scRNA-seq data from different tissues, including bone and brain, we discerned MSCs, osteoblasts, monocytes, macrophages, astrocytes, and other cell types through which the risk variants impact head BMD. Bulk RNA-seq data analysis of BMSCs from young individuals and senile osteoporosis patients indicated that AZIN1 mRNA levels and RNA editing frequency were decreased in BMSCs from aged participants, suggesting a potential role of AZIN1 in age-related bone loss. Utilizing pseudotime results of scRNA-seq data generated from bone of WT mice, we observed a temporal pattern of AZIN1 expression during osteoblast differentiation, with its levels rising in pre-osteoblasts, peaking in osteoblasts and declining in terminal osteocytes. Importantly, AZIN1 knockdown significantly inhibited osteoblast differentiation and mineralization in MC3T3-E1 pre-osteoblast cells while promoting osteoclastogenesis in RAW264.7 cells. Although limited by current sample size (2/group), μCT analysis hinted at a decrease in bone volume in AZIN1f/f;Prx1cre and AZIN1f/f;OCNcre mice. Moreover, compared to overexpression of the WT form of AZIN1, overexpression of RNA-edited AZIN1 enhanced osteogenic differentiation and mineralization of MC3T3-E1 cells while suppressing cell proliferation, whereas non-edited AZIN1 had opposite effects in vitro. Mechanistically, CoIP-MS data revealed that RNA-edited AZIN1 exhibited an increased affinity to interact with osteoblast differentiation-related proteins, including transcriptional factors such as DDX5, suggesting that RNA-edited AZIN1 entered nucleus to promote osteogenic differentiation. Additionally, AZIN1 knockdown in MC3T3-E1 or knockout in H9 hESCs dramatically reduced PIEZO1 protein levels, which could crosstalk with osteoclasts by regulating YAP/Col-II/IX axis, thereby promoting osteoclast differentiation. Collectively, our findings unveil the candidate determinants of BMD and highlight the role of AZIN1 in regulating bone homeostasis, which may be leveraged to prevent bone loss.

P-064 Hang Zhou

Hyperbaric oxygen promotes bone regeneration by activating the mechanosensitive Piezo1 pathway in osteogenic progenitors

Hang Zhou*, Hongzhi Liu, Minmin Lin, Hantang Wang and Chao Liu, Southern University of Science and Technology, Shenzhen, Guangdong, China

Purpose: Bone defects can greatly diminish the quality of life and increase the risk of mortality. Hyperbaric oxygen (HBO) therapy deliver high pressure and pure oxygen to promote injury repair. However, there remains a lack of research regarding the biological mechanisms underlying HBO for bone repair. To address this gap, this study aims to elucidate the impact of HBO therapy on bone regeneration. As HBO may achieve its effect through oxygen-sensitive and mechanosensitive pathways, we speculate HBO activates Piezo1 in osteogenic cells to promote bone regeneration, as Piezo1 could be modulated by oxygen and mechanical forces. Finally, we compared the therapeutic effect of HBO and anabolic mechanical stimulation.
Methods: Bilateral monocortical tibial defect surgeries were performed on 12-week-old Prrx1-Cre; Piezo1+/+ and Prrx1-Cre; Piezo1fl/+ conditional knockout mice. Daily HBO treatment was applied on the post-surgery day (PSD) 1, and daily mechanical loading on tibia was from PSD 5 to 8. The mice were euthanized on PSD 10, and their tibiae were collected for evaluation of bone defect repair using μCT and immunofluorescence imaging.
Results: Immunofluorescence staining of Prrx1-Cre; Piezo1+/+ mice on PSD 8 showed that HBO treatment significantly increased the volume of type H vessels, and Prrx1+ cells within the bone defect compared to the control group. HBO also promoted angiogenesis-osteogenesis coupling as observed by significantly shortened distance between Prrx1+ cells and type H vessels. According to the μCT data on PSD10, the volume of newly formed bone in the bone defect from HBO group was higher. The combination of HBO treatment and mechanical loading had a moderate synergistic effect. However, in Prrx1-Cre; Piezo1fl/+ mice, HBO group and mechanical loading group did not show significant increase in bone regeneration.
Conclusions: HBO therapy enhances bone defect repair by activating Piezo1 in Prrx1+ skeletal stem cells and increase angiogenesis-osteogenesis coupling. This work offered scientific evidence for the clinical use of HBO therapy in bone defect repair.

P-064 Hang Zhou

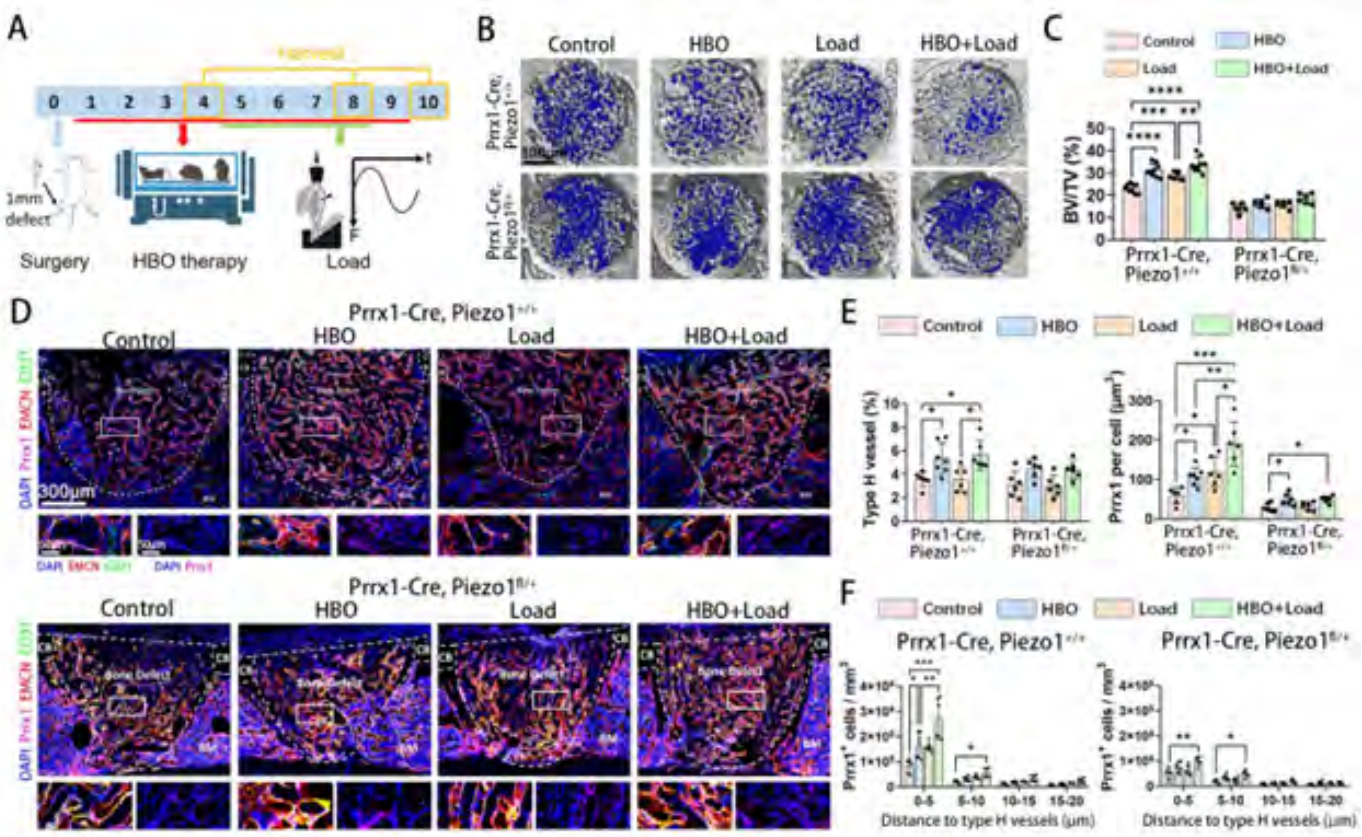

Figure 1. (A) Experimental design. (B-C) The μCT analysis of newly formed bone in bone defects on PSD10 (n ⩾ 6). (D) Confocal images of immunofluorescence signals of Prrx1, EMCN and CD31 on PSD8. (D) Volume of type H vessels and Prrx1+ cells (n ⩾ 6). (F) The number of Prrx1+ cells classified by the distance to type H vessels (n ⩾ 6). Data are presented as means ± standard deviation; *p < 0.05, **p < 0.01, ***p < 0.001, ****p < 0.0001.

P-065 Abhayavarshini Sridhar

In utero and Lactation Exposure to Dolutegravir-based Combination Antiretroviral Therapy Reduced Trabecular Bone but not Cortical Bone Mass in Rats

Abhayavarshini Sridhar*1, Jean Harry2, Helen Cunny2 and Ryan Ross3,
(1) Rush University, CHICAGO, IL, USA, (2) NIH/NIEHS, USA, (3) Rush University Medical Center, Chicago, IL, USA

Introduction: Maternal combination antiretroviral therapy (cART) use has reduced perinatal HIV transmission but increased the number of HIV-exposed but uninfected (HEU) children1. HEU children experience higher rates of co-morbidities such as reduced bone mass2. Current clinical recommendations include use of dolutegravir (DTG) anchored cART for pregnant women3. DTG readily crosses the placenta4 and is detected in breast milk5 and infant plasma5. DTG use is associated with bone mass loss in adults living with HIV6, but the long-term effects of DTG-based cART on bone development in HEU is unknown. We hypothesized that in utero exposure to DTG-based cART would lead to reduced bone mass in a rat model of HEU children.
Methods: Time-mated 10–13-week-old female Harlan Sprague Dawley rats were treated with a clinically relevant combination of DTG/ Abacavir (ABC)/ Lamivudine (3TC) or vehicle via oral gavage starting at gestational day 6, continuing until postpartum day 28. Male and female offspring were not directly dosed. At 573 days of age tissues were isolated and femoral length was measured using digital calipers. Femoral trabecular architecture and cortical geometry were evaluated using micro-computed tomography. Bone strength was measured via three-point bending. Results were analyzed using a two-way ANOVA with treatment and sex as factors.
Results: Femoral length was greater in cART treated rats, with a significant 3.4% increase in males and a non-significant 0.7% increase in females. Trabecular bone volume fraction (BV/TV) was impaired by cART treatment, with a significant 24% reduction in males and a non-significant 6.5% reduction in females. cART treatment caused a decrease in trabecular number in females and an increase in trabecular spacing in both sexes. Neither cortical bone area nor cortical porosity were affected by treatment. There were no significant treatment effects in the mechanical properties.
Conclusion: Our data suggests that exposure to DTG-based cART during early development has long-lasting negative effects on trabecular bone mass and potentially influences bone growth. It is currently unclear whether the loss of trabecular bone mass is due to impaired development or accelerated age-related loss. Importantly, impaired bone mass accrual can increase the risk for osteoporosis later in life, and therefore HEU children may be at an increased risk for osteoporosis.

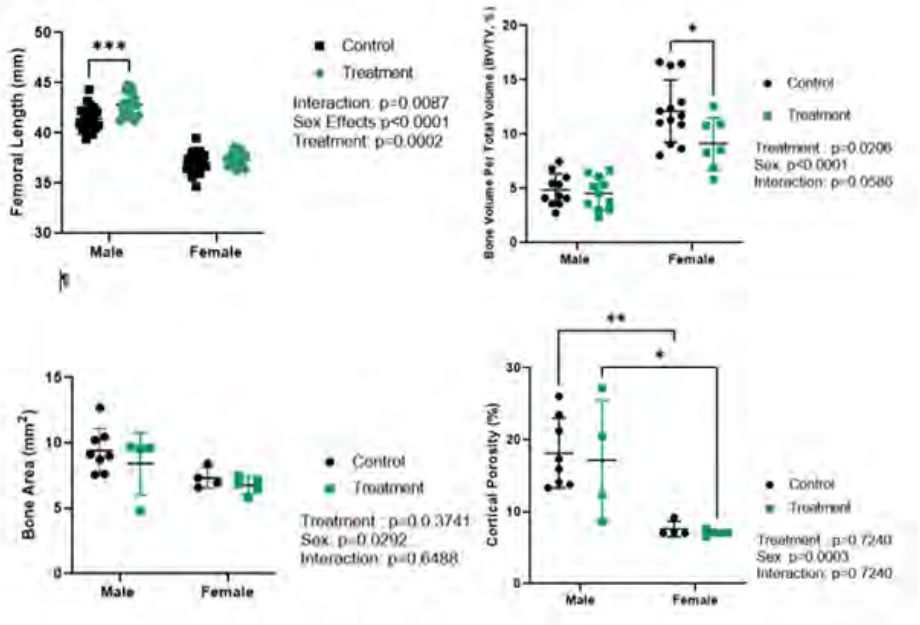

P-066 Christopher Hernandez, PhD

Staphylococcus Aureus does not use durotaxis to penetrate osteocyte canaliculi-like channels

Kelsey Defrates1, Junsung Lee1, Gissell Jimenez1,2 and Christopher J. Hernandez*1,2,3,
(1) University of California, San Francisco, CA, USA, (2) University of California, Berkeley, CA, USA,
(3) Chan Zuckerberg Biohub, San Francisco, CA, USA

Osteomyelitis causes pain and bone loss and is a risk factor for sepsis. Systemic antibiotics often do not clear osteomyelitis and surgical interventions have high rates of failure. Observations that infectious bacteria such as S. aureus can penetrate the lacunar-canalicular network during osteomyelitis suggest persistence of osteomyelitis may be caused by bacteria sequestered within the lacunar canalicular network that are protected from neutrophils and other immune cell populations and also experience lower concentrations of antibiotics delivered systemically. How S. aureus enters the lacunar canalicular system is unclear: S. aureus are non-motile organisms and are 3-4 times larger (1-1.2 μm diameter) than the diameter of osteocyte canaliculi (~0.3 μm diameter). It has been proposed that S. aureus may enter canaliculi through durotaxis, in which they preferentially divide into smaller channels, eventually forming a chain extending the length of the canaliculi and entering osteocyte lacunae1. We used a micro- nanofluidic system designed by our laboratory that traps individual bacteria within tapered channels (0.25 μm width) using a differential fluid pressure (1 to 6.5 kPa, Fig. 1A) to determine: 1) The fluid pressure required to deform S. aureus into canaliculi-sized channels; 2) The rate of division of S. aureus when deformed inside such channels; and 3) if division of S. aureus occurs preferentially into small channels. We applied a methicillin-resistant strain of S. aureus (COL strain, 1.03±0.08 μm diameter, mean±SD) to our system to determine the relationship between cell deformation and applied differential fluid pressure, then recorded the time until cell division and whether or not division occurred downstream (toward the thinner side of the tapered channel). Greater differential fluid pressure resulted in greater deformation of S. aureus and further transit down the tapered channels (Fig. 1B). A differential fluid pressure of 5 kPa was sufficient to deform S. aureus to a width of 500nm. S. aureus experiencing greater deformation showed reduced rates of division (Fig 1C). S. aureus cells that did divide, on average, migrated 93 nm ± 217nm upstream ($p < 0.001$ different than zero), indicating no evidence of growth into smaller spaces. Our findings suggest that S. aureus does not preferentially divide into smaller spaces, and when deformed more than half cell width, is unlikely to divide at all, suggesting that transit of S. aureus through canaliculi is unlikely to occur as a result of durotaxis. However, S. aureus readily deforms to sizes comparable to that of canaliculi under fluid pressure (5 kPa) much smaller than that seen at the surface of orthopaedic implants during motion (8-20 kPa2). Hence our study suggests that it is more likely that fluid pressure associated with locomotion is a more likely stimulus for the penetration of the lacunar canalicular system by S. aureus.

P-066 Christopher Hernandez, PhD

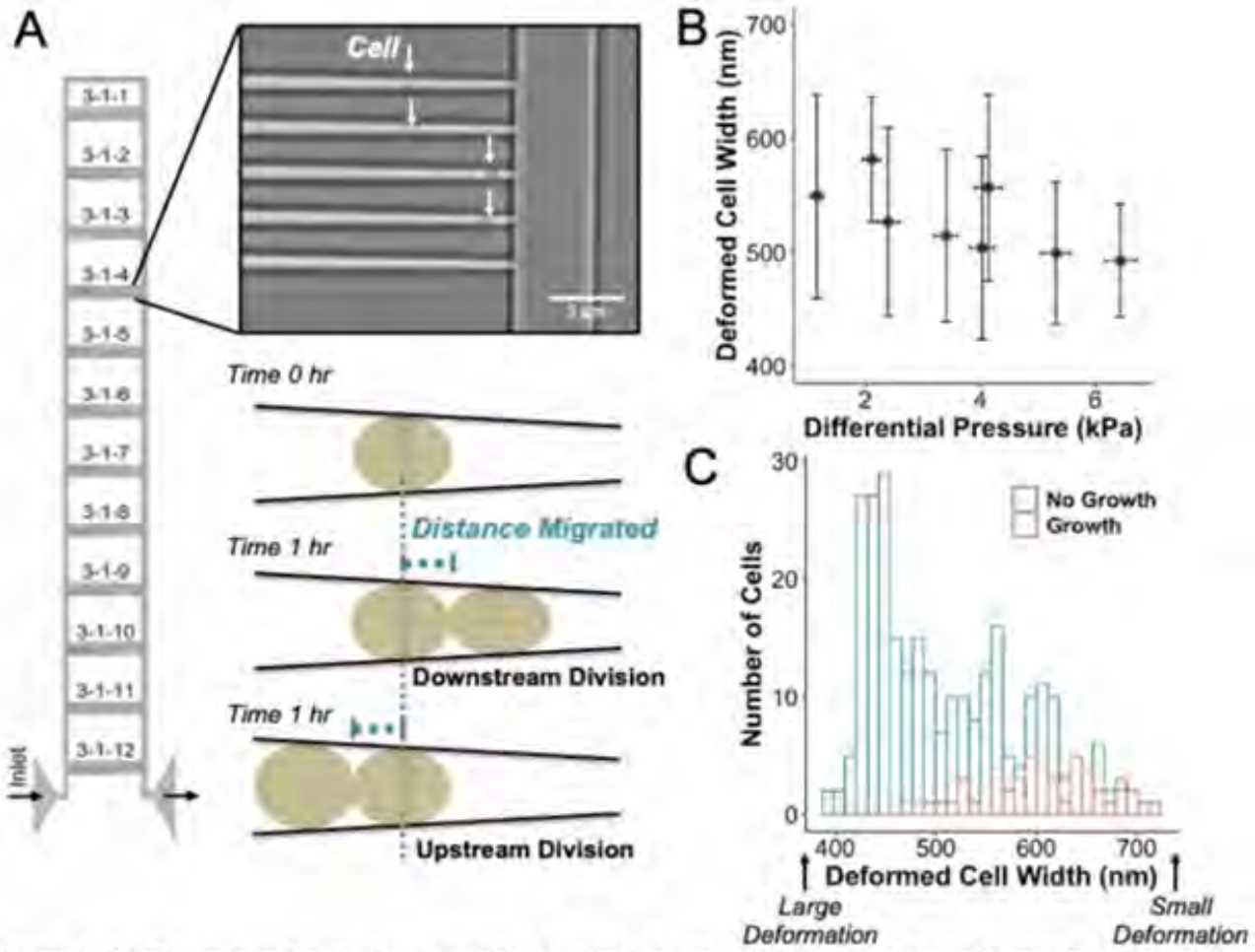

Figure 1. A) The microfluidic device includes twelve sets of tapered channels, each applying a different differential pressure. Inset: Cells within the device are trapped and their growth is observed. The distance the cell migrates during division is illustrated for downstream (smaller channel) v. upstream. B) Cells submitted to greater differential pressure underwent more deformation (smaller deformed cell width). C) Cells undergoing more deformation were less likely to divide during the experiment.

P-067 Anders Palmquist, PhD

Correlative HAADF STEM – EDX tomography of bone

A. Palmquist* 1, C. Micheletti 1,2, F.A. Shah 1, K. Grandfield 2
(1) Department of Biomaterials, Sahlgrenska Academy, University of Gothenburg, Sweden (2) Department of Materials Science and Engineering, School of Biomedical Engineering, and Brockhouse Institute for Materials Research, McMaster University, Canada.

INTRODUCTION: Bone as a highly hierarchical structure composed of mainly apatite and collagen, where the mineralized collagen fibrils serve as the fundamental units of bone on a nanoscale level. Although it's established that collagen fibrils undergo mineralization within their gaps (intra-fibrillar) and on their outer surfaces (extra-fibrillar), achieving a clear three-dimensional visualization, which combines both structural and compositional details over sizable volumes without sacrificing resolution, continues to present challenges.

The aim of the current study1 was to evaluate correlative electron tomography (ET) by High angle annular dark field – scanning transmission electron microscopy (HAADF-STEM) and energy dispersive X-ray spectroscopy (EDX) imaging on needle shaped samples to reduce artefacts in ET due to the missing wedge and explore nanoporosity.

METHODS: A human femur was chemically fixed, resin-embedded and sectioned. Various lamellar and conical samples for STEM were prepared by focused ion beam milling. STEM imaging and EDX mapping were performed on a Talos 200X (Thermo Fisher Scientific, USA) equipped with a Super-X detector at 200 kV. ET used a 180º rotation in an on-axis holder (Model 2050, Fischione Instruments, USA). Automated imaging (STEM Tomography in Velox, Thermo Fisher Scientific, USA) acquired multiple signals simultaneously from HAADF-STEM, EDX, and/or Bright Field (BF-STEM) with automated focusing and image shifting. The tilt series were aligned by cross-correlation and reconstructed by SIRT with 25 iterations in Inspect 3D (Thermo Fisher Scientific, USA), visualization and analysis were done in Dragonfly (Object Research Systems, Canada).

RESULTS: The electron tomograms were successfully reconstructed when using HAADF-STEM imaging, while some artefacts were observed using the BF-STEM imaging, with a diameter of the needle samples up to 700 nm. The views in orthogonal planes confirmed the typical banding pattern (along the collagen) and lacy pattern (perpendicular to the collagen), which is commonly observed in the lamellar samples. Previously supposed holes in the lacy pattern were probed by chemical analysis to confirm the presence of collagen.

CONCLUSIONS: Correlative ET using different signals originating from the electron-sample interaction serves as an important analytical tool enabling a greater understanding of the ultrastructure of bone, including the presence/absence of porosity.

REFERENCES: 1Micheletti et al (2023) ACS Nano, 17:24710−24

P-068 Mathieu Simon

Automatic Segmentation of Cortical Bone Microstructure: Analysis of Three Proximal Femur Sites

Mathieu Simon* 1, Silvia Owusu 2, Stefan Bracher 1, Dieter D. Bosshardt 2, Michael Pretterklieber 3, and Philippe Zysset 1
(1) ARTORG Centre for Biomedical Engineering Research, University of Bern, Switzerland (2) Department of Periodontology, School of Dental Medicine, University of Bern, Switzerland (3) Division of Macroscopical and Clinical Anatomy, Medical University of Graz, Austria

Introduction: Osteoporosis is the most common bone metabolic unbalance,leading to fragility fractures, which are known to be associated with structural changes in the bone. Cortical bone undergoes remodeling throughout life, leading to changes in its thickness and microstructure. Although many studies quantified the different cortical bone structures using CT techniques (3D), they are often realised on a small number of samples. Therefore, the work presented here proposes a method to quantify cortical bone microstructure using 2D histology, shows its application on a set of 94 samples and compares to 3D methods.

Materials and Methods: Fresh frozen human femur pairs from 47 donors aged between 57 to 96 years were obtained from the Medical University of Vienna. Bone samples were cut from 3 sites: proximal part of the diaphysis, inferior and superior segments of the neck. The samples were stained with toluidine blue and imaged under light microscopy. After manual segmentation of a few regions of interest by multiple operators, a convolutional neural network was trained in combination with a random forest for automatic segmentation. The segmentation analysis investigates morphology and structure distribution of Haversian canals, osteocyte lacunae, and cement lines. Results are compared with literature, between anatomical sites, sex, left and right sides, and related to ageing.

Results: Morphological analysis of the segmentation gives results similar to the literature. Comparison between male and female donors (sexes) shows no significant differences. There is no significant difference between left and right femur on paired samples (sides) but significant differences are observed between anatomical locations (sites). The structures' surface densities do not present significant changes with age but only weak tendencies. Nevertheless, a strong correlation was observed between osteocyte lacunae density and bone areal fraction.

Discussion: This study presents a full process to stain and automatically segment digital cortical bone images. Its application to a large sample set of proximal femora provides strong statistics on the cortical bone structures morphology and distribution. Similarities observed between sides and sexes together with differences observed between sites could indicate that mechanical loading might be a main driver for bone microstructure. Additionally, the relationship between osteocyte lacunae density and bone areal fraction could suggest that bone porosity is regulated by osteocyte survival.

Acknowledgments: The authors are highly indebted to all voluntary body donators permitting anatomical research. Special acknowledgments are dedicated to all the operators who performed the ground truth manual segmentation.
Funding: This work was funded by the Swiss National Science Foundation (SNSF), grant number 200365.
REFERENCES: 1Micheletti et al (2023) ACS Nano, 17:24710−24

P-068 Mathieu Simon

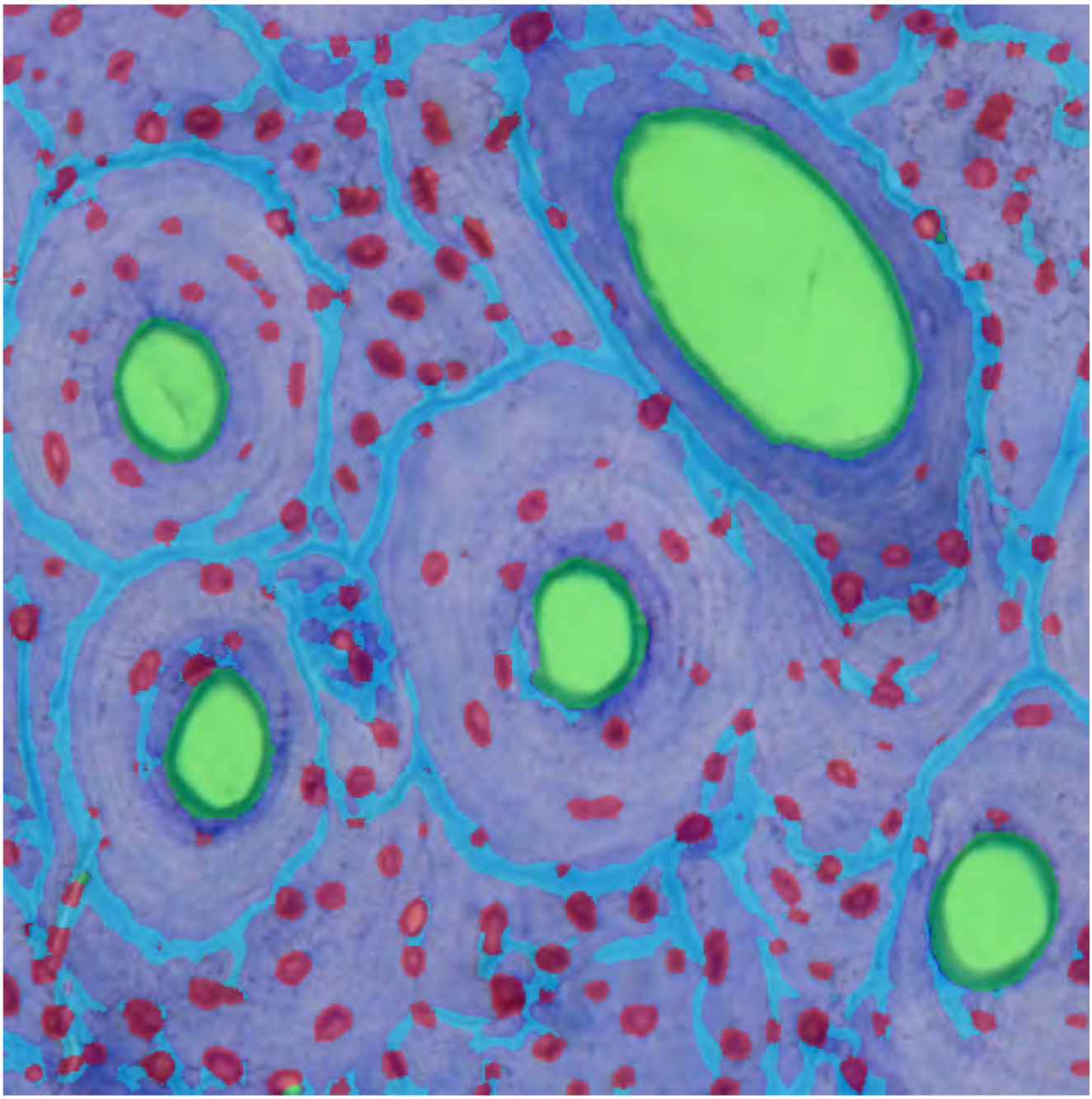

Figure: Example of automatically segmented region of interest. Haversian canals are in green, osteocyte lacunae are in red, and cement lines are in cyan.

P-069 Martina Dzubanova

Revealing a role of NADPH oxisase 4 (NOX4) in bone homeostasis and sex dimorphism

Martina Dzubanova*1,2, Jacob Bond3, Michaela Ferencakova1, Grzegorz Pyka4, Andrea Benova1,2, Adele Addington3, Greet Kerckhofs4,5,6, Tomas Cajka7, Christina Moeller Andreasen8, Thomas Levin Andersen9, Siobhan Craige3 and Michaela Tencerova1,
(1) Laboratory of Molecular Physiology of Bone, Institute of Physiology of the Czech Academy of Sciences, Prague, Czech Republic, (2) Charles University, Faculty of Sciences, Prague, Czech Republic, (3) Human Nutrition, Foods and Exercise; Virginia Tech, Blacksburg, VA, USA, (4) Biomechanics lab, Institute of Mechanics, Materials, and Civil Engineering, UCLouvain, Louvian La Neuve, Belgium, (5) Institute for Experimental and Clinical Research, UCLouvain, Brussel - Woluwe, Belgium, (6) Department of Material Science and Engineering, KU Leuven, Leuven, Belgium, (7) Laboratory of Translational Metabolomics, Institute of Physiology of the Czech Academy of Sciences, Prague, Czech Republic, (8) Department of Pathology, Odense University Hospital, Odense, Denmark, (9) Molecular Bone Histology Lab, Research Unit of Pathology, Department of Clinical Research, University of Southern Denmark, Odense, Denmark

Obesity, a prevalent metabolic disorder, is characterized by the abnormal accumulation of fat in various organs, including bones, increasing the risk of bone fragility. Recent research demonstrates that bone marrow adipose tissue (BMAT) behaves uniquely from peripheral adipose tissue, maintaining insulin signaling and inducing hyper-metabolic status in bone marrow skeletal cells (BMSCs). This leads to increased reactive oxygen species production contributing to senescent bone marrow microenvironment and bone impairment. Notably, NADPH oxidase 4 (NOX4), a major ROS producer, is highly active in bones under obesogenic conditions, affecting cellular metabolism and senescence. However, little is known about Nox4-induced ROS production in bone physiology in the context of sex dimorphism in obesity. Thus, we studied whether Nox4 deletion has a different effect on bone and fat metabolism in males and females. In our study, male and female WT and mice lacking Nox4 (Nox4-/-) were fed either chow or a high-fat diet (HFD) for 5 months and examined for metabolic (glucose tolerance test, body composition) and bone parameters (uCT, BMAT evaluation) accompanied by gene expression analysis. Interestingly, Nox4-/- males manifested less body weight gain and fat mass (-30%, $p<0.0001$; -40%, $p<0.0001$, resp.), while Nox4-/- females gained weight and exhibited increased fat mass compared to WT mice (+20%, $p<0.001$; +13%, $p<0.0001$, resp.). These changes were accompanied by worsened glucose tolerance in Nox4-/- females, and no changes in Nox4-/- males. Notably, uCT analysis, confirmed by histology, showed that Nox4-/- males had decreased BMAT in the proximal tibia (-70%, $p<0.05$), while females exhibited increased BMAT (+140%, $p<0.01$) with changes in BMAds size distribution (females: 35-40 um vs 25-30 um, $p<0.001$, Nox4-/- vs WT; males: 20-25 um vs 35-40 um, $p<0.01$, Nox4-/- vs WT). The gene expression profile of Nox4 showed, that Nox4 is highly expressed in BMSCs compared to other bone compartments in both sexes. However, NOX4 activity in BMSC was increased in HFD males compared to females under the same condition. As existing literature predominantly focuses on the implications of inhibiting NOX4 activity and expression in males for promoting bone health, an approach which, based on our results, may not be directly applicable to females. Thus, these findings suggest that NOX4 may affect BMSC metabolism and bone homeostasis differently in respect to sex dimorphism, which should be considered in future strategies in the treatment of metabolic bone diseases.

P-070 Christopher Panebianco, PhD

Maternal exercise enhances fetal bone development

Christopher Panebianco* and Joel D. Boerckel, University of Pennsylvania, Philadelphia, PA, USA

During development, fetal movement provides mechanical forces necessary for proper skeletal morphogenesis. Clinical conditions that limit fetal movement (i.e., fetal akinesia) can impair bone development and cause skeletal deformities.1 Based on this, we hypothesized that extra-embryonic mechanical stimulation could enhance fetal skeletal development.

To mechanically stimulate embryos in utero, we performed maternal wheel running exercise. Briefly, female C57BL/6 mice were individually housed and acclimated to home cage running wheels for at least 2 weeks. Acclimated female mice were mated with male C57BL/6 mice, then housed without wheels until embryonic day (E) 13.5. At E13.5, pregnant mice were either re-housed with wheels from E13.5 to E16.5, inclusive (Ad Libitum), or subjected to 1 hour of daily supervised wheel running during the same period (Supervised). Control groups with locked wheels were included for both conditions (Jammed). Pregnant mice ran more consistently using supervised running (Fig 1A); therefore, we used this approach for future analyses.

Embryos were harvested from Supervised and Jammed groups at E17.5 to quantify bone morphogenesis and placental transport efficiency. Forelimb bone morphogenesis was quantified using microcomputed tomography (voxel size = 3 μm, x-ray tube potential = 70 kVp, x-ray intensity = 145 μA, integration time = 300 ms). Embryos from exercised mothers showed increased humerus bone collar length, indicating that maternal exercise has osteogenic effects on developing embryos (Fig 1B).

Intrauterine growth is also influenced by placental transport efficiency. To assess whether maternal exercise influences placental transport, we quantified the standard measurement of fetus weight to placental weight ratio (FW:PW).2 We observed no significant differences in FW:PW in response to Supervised maternal exercise (Fig 1C).

Together, our results demonstrate that maternal wheel running exercise promotes bone formation in fetal skeletons, independent of placental transport. Future studies will elucidate the underlying cellular and molecular mechanisms. Ultimately, this research may indicate maternal exercise as a non-invasive, in utero intervention for skeletal deformities caused by limited fetal movement. Additionally, this work establishes maternal exercise as a model for studying developmental mechanobiology in vivo.

Refs: [1] Nowlan+ Eur Cell Mater 2015; [2] Brett+ Int J Mol Sci 2014

P-070 Christopher Panebianco, PhD

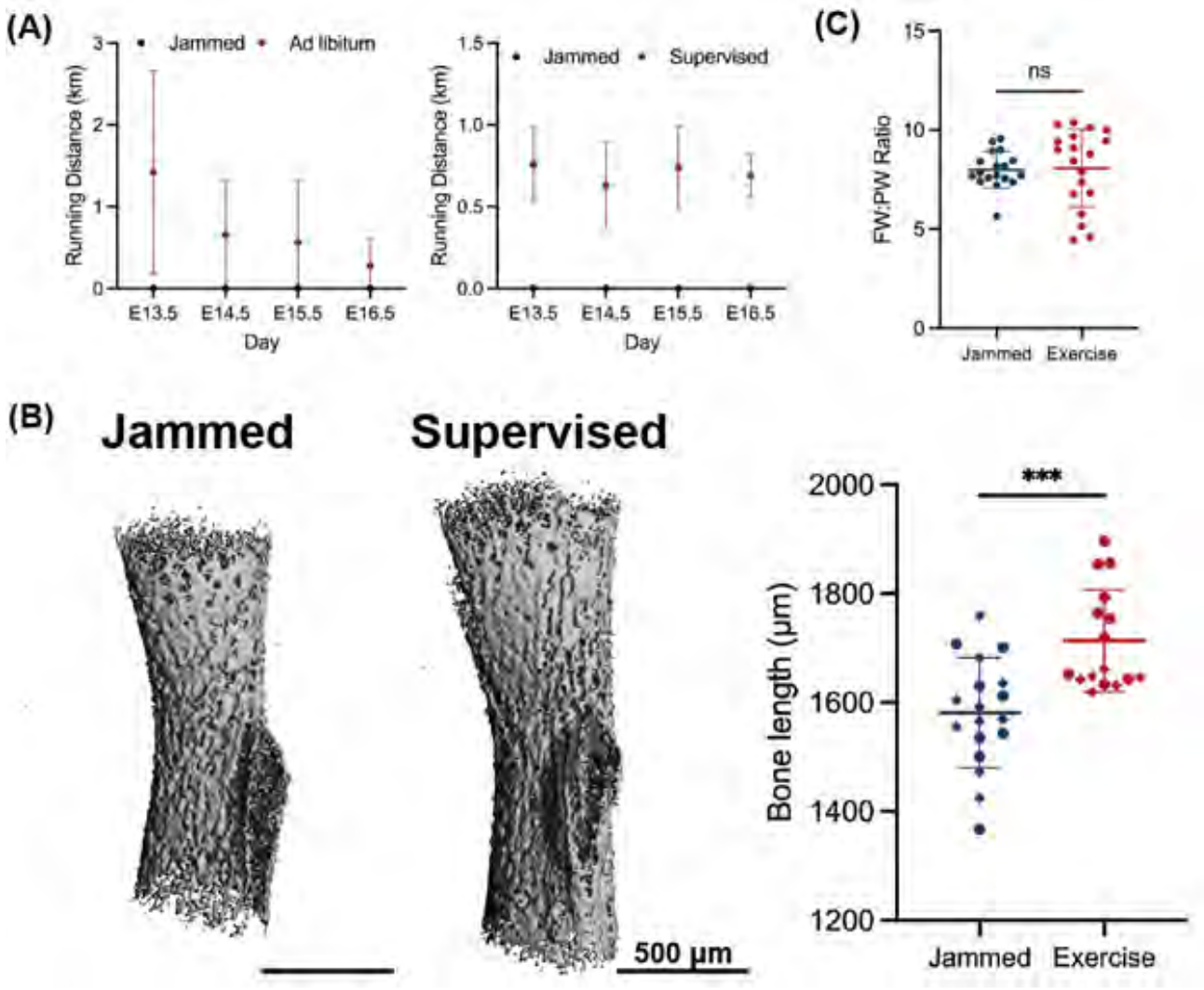

P-071 Noemy Vergara Vera

Influence of macromolecular crowding on collagen fibrillogenesis and fiber alignment in 3D printed collagen constructs

Noemy Vergara Vera*1,2, Paula Vena3, Sandra Hofmann1,2, Keita Ito1,2,3 and Miguel Castilho1,2,3, (1) Orthopaedic Biomechanics, Department of Biomedical Engineering, Eindhoven University of Technology, Eindhoven, Noord-Brabant, Netherlands, (2) Institute for Complex Molecular Systems, Eindhoven University of Technology, Eindhoven, Noord-Brabant, Netherlands, (3) Department of Orthopedics, University Medical Centre Utrecht, Utrecht, Utrecht, Netherlands

Bone tissue is an extraordinary material essential for supporting and protecting our bodies. Its composition includes both organic and inorganic components, meticulously arranged across various scales to create a sophisticated composite structure. At its core lies an organic matrix of collagen molecules, woven into microfibrils resembling ropes, which further assemble into fibrils approximately 100 nm in size before forming larger arrays. Despite advancements, accurately reproducing the intricate collagen organization seen in living tissue remains a challenge, limiting its application in tissue engineering. We propose an in vitro system that closely mimics collagen formation mechanisms in near-native environments. This system enabled us to investigate collagen organization, from microfibrils to fibrils and arrays, and to examine its correlation with macromolecular crowding (MMC). Inspired by the extracellular matrix (ECM) environment, where collagen originates, we replicated the densely-packed macromolecular setting to simulate MMC effects, known to significantly impact collagen assembly and structure.
This in vitro system uses polyethylene glycol (PEG, 20 kDa) to induce MMC and regulate collagen organization at the microscale. Additionally, we employ a suspended extrusion printing setup to align collagen macrostructure through shear forces. Two collagen precursors were tested: a tropocollagen solution (5.9 mg/mL) and a suspension of collagen fibres (10 mg/mL). We first explored the impact of PEG crowding on collagen assembly using turbidity analysis, revealing an increase in assembly rate with higher PEG concentration. To integrate PEG crowding into the printing process, we added varying concentrations of PEG to the fibrillar suspension to serve as ink. Meshes were printed into a gelatin bath (4.5% gelatin type A) supplemented with PBS 1X, followed by gelatin removal through incubation at 37°C. Scanning electron microscopy (SEM) revealed highly aligned collagen fibres within the prints, with alignment improving with increasing PEG concentration. Transmission electron microscopy (TEM) showed that the collagen arrays within the meshes retained the characteristic D-banding observed in native collagen, confirming successful preservation of structural features at the nanoscale. These findings have significant implications for understanding and optimizing collagen assembly dynamics crucial for effective bone tissue engineering strategies.

P-071 Noemy Vergara Vera

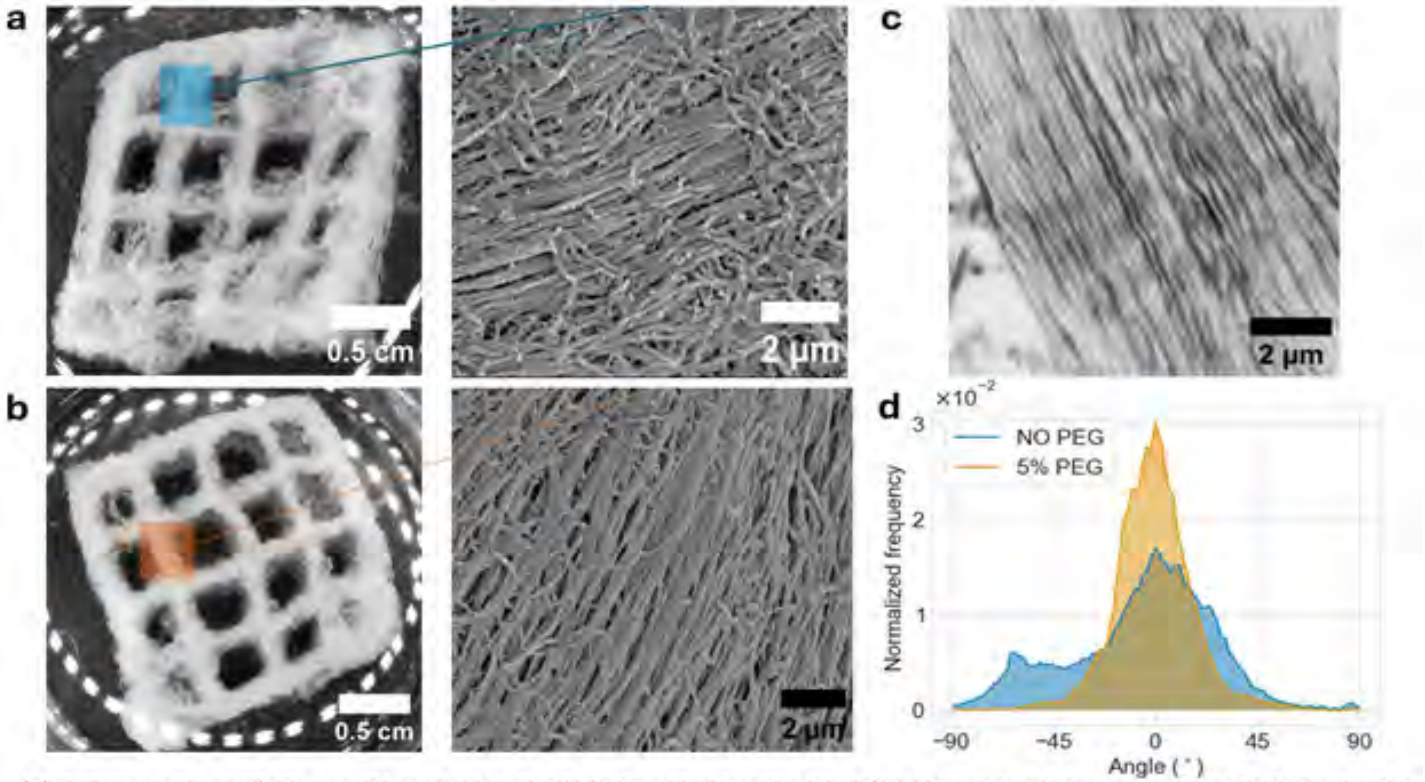

(a) Collagen-only scaffolds and **(b)** scaffolds with 5% PEG added into the ink. **(c)**TEM images of collagen-only scaffolds display the presence of *D-banding*. **(d)** Normalized frequency distribution plots comparing fiber angle distributions from the SEM images in **(a)** and **(b)**. A narrower distribution for 5% PEG samples indicates higher fiber alignment in the presence ofthe crowder.

P-072 Natasha Sanz

Assessing offspring tooth and mandibular histomorphometric parameters and bone property changes due to caffeinated beverage (Yerba Mate) consumption during gestation and lactation

Sanz Natasha1,2,, Buiatti Florencia1, De Sogos Alfonso, Tourn Nazareno, Plotkin I. Lilian3, Brun Lucas R1,2.
(1) Bone Biology Laboratory. School of Medicine, Rosario National University, Argentina. (2) National Council of Scientific and Technical Research (CONICET), Argentina. (3) Anatomy, Cell Biology & Physiology, School of Medicine, Indiana University, USA.

Caffeine consumption is widely spread all around the world. In South America the most known and popular source of caffeine is Yerba Mate (YM) obtained from ground and milled dry leaves from the species Ilex paraguariensis. YM is also known for its antioxidant capacity given by a high presence of polyphenols. YM infusions are normally consumed through pregnancy, and caffeine intake during this stage has been associated with lower weight and bone density in the offspring, meanwhile polyphenols have demonstrated to improve bone properties and oxidative stress parameters. The daily consumption of caffeine in Argentina is approximately 288 mg/day, therefore, the purpose of this study was to assess the impact of caffeine intake on offspring during pregnancy, when it is associated with high-level antioxidant beverages such as YM infusions on mandibular bone and teeth. Methods: Ten-week-old female Sprague-Dawley rats were divided in a control group consuming water ad libitum; YM and YM+ groups consuming an infusion prepared with 25g and 50 g of ground YM leaves in water at 70°C and 90°C respectively and administrated during pregnancy until the offspring reached 30 days old. BMD and morphometry measurements were assessed on digitalized radiographs with Image J 1.40 (NIH, Maryland, USA). We measured the length from the anteroinferior point of the mandible (O) to the middle of the condyle (A), the coronoid process (B) and the most posterior point of the bone (C), the area OBC and finally the length from the first to the last molar (ML). Three-point bending tests were performed to obtain stiffness, ultimate load, failure load, and absorbed energy. Bone volume fraction was determined in the alveolar socket of the first molar of histological buccolingual cross-sections. Body weight was also measured at day 30. Further analysis will be conducted for examining histological parameters of the tooth along with dynamic histomorphometric measurements. Results: Asterisks indicate significant differences vs. control. All values are reported as mean±SEM. Statistical analysis was conducted using one-way or two-way ANOVA and Tukey's test for multiple comparisons. Conclusion: Evidence suggests that exposure to YM during the embryonic stage, weaning, and youth cause changes in bone development affecting positively the biomechanical parameters on the mandible and interradicular alveolar bone, indicating a potential benefit for bone and dental health.

P-072 Natasha Sanz

		Control			YM			YM+		
	Sex	Mean	SEM	n	Mean	SEM	n	Mean	SEM	n
Body Weight (g)	Female	125.05	4.28	18	120.08	4.77	13	122.33	4.33	13
	Male	137.87	6.46	12	131.11	4.54	17	139.55	5.46	12
Molar Lenght (mm)	Female	6.95	0.21	14	6.69*	0.29	15	6.65*	0.24	9
	Male	6.75	0.13	11	6.66	0.20	13	6.71	0.18	10
Anteroinferior to condile Lenght - OA (mm)	Female	20.73	0.73	14	20.26	0.61	15	20.37	0.93	10
	Male	20.04	0.28	9	20.69	0.70	10	20.81	0.98	10
Anteroinferior to posterior lenght - OC (mm)	Female	19.45	0.84	14	19.17	0.51	15	19.55	0.89	10
	Male	19.27	0.93	11	19.65	0.79	10	19.67	0.97	10
Anteroinferior to apofisis Lenght - OB (mm)	Female	17.69	0.58	10	17.41	0.84	11	17.34	0.75	9
	Male	17.30	0.50	11	18.30*	0.34	6	17.56	0.65	9
Area Anteroposterior - Condile - Apofisis - OBC (mm)	Female	87.37	7.03	10	84.55	8.22	11	83.59	7.54	9
	Male	85.58	5.12	10	87.96	5.01	7	87.39	6.51	9
molar DMO ($mgCa^{2+}/mm$)	Female	46.69	4.99	12	46.42	1.52	10	45.32	5.46	10
	Male	47.40	4.76	11	45.17	4.48	12	42.79	3.13	10
BV/TV(%)	Male and Female	39.74	0.88	8	42.15	1.72	7	46.06*	1.90	4
Absorbed Energy (mJ)	Male and Female	7.60	0.28	11	8.20	0.55	18	10.75*	0.67	9
Ultimate Load (N)	Male and Female	25.04	0.87	13	28.49*	0.89	19	28.74*	1.17	9
Failure Load (N)	Male and Female	23.80	0.72	12	26.18*	0.60	18	26.68*	1.00	9
Stiffness (N/mm)	Male and Female	58.32	3.34	13	63.79	3.06	19	66.96	3.03	10

P-073 Ruban Dhaliwal, MD

PEN and CML Associate Differently with Bone Loss in Type 2 Diabetes: the Health, Aging, and Body Composition Study

Ruban Dhaliwal*1,2, Susan K. Ewing3, Bowen Wang4, Deepak Vashishth4,5 and Ann V. Schwartz3, (1) Center for Mineral Metabolism and Clinical Research, The University of Texas Southwestern Medical Center, Dallas, TX, USA, (2) Division of Endocrinology, Department of Internal Medicine, The University of Texas Southwestern Medical Center, Dallas, TX, USA, (3) Department of Epidemiology & Biostatistics, University of California, San Francisco, San Francisco, CA, USA, (4) Shirley Ann Jackson, PhD. Center of Biotechnology and Interdisciplinary Studies, Rensselaer Polytechnic Institute, Troy, NY, USA, (5) Rensselaer - Icahn School of Medicine at Mount Sinai Center for Engineering and Precision Medicine, New York, NY, USA

Advanced glycation end-products (AGEs) have been implicated in the pathophysiology of skeletal fragility in type 2 diabetes (T2D). We have previously shown that pentosidine (PEN), a crosslinking AGE and carboxymethyl-lysine (CML), a non-crosslinking AGE are independent risk factors for fracture in T2D. Moreover, higher levels of PEN are associated with lower baseline BMD and more rapid bone loss. However, the relationship of CML with bone loss in T2D is unknown. In a well-characterized cohort of men and women ages 70-79 years, we examined the relationship of CML with baseline BMD and changes in BMD during a 4-year follow-up. Determinants of T2D were use of hypoglycemic medication or elevated fasting glucose (≥126 mg/dl). Linear regression models were used to analyze the associations of log-transformed baseline AGE with baseline BMD and four-year changes in BMD. In the cohort of n=3,044 (T2D: n=712 and non-diabetes (NDM): n=2,332), mean age was 73.6 ± 2.9 years. At baseline, there was no association of CML with BMD at the total hip (TH) or femoral neck (FN) in T2D or NDM. Furthermore, there was no association found between CML and change in BMD at any site in either group. Among the subset with both PEN and CML available (n=928), a small negative correlation of baseline TH BMD was observed with CML (r= –0.11; p=0.01) and PEN (r= –0.14, p=0.003) among T2D. In NDM, baseline TH BMD was associated with PEN (r= –0.12; p=0.01) but not CML. There was no evidence of an association between AGEs and baseline FN BMD in either group. CML was not associated with change in BMD at the TH or FN in T2D or NDM (Table 1). Contrarily, higher PEN was associated with greater loss of TH BMD and FN BMD in T2D with minimal adjustment, however the associations were not statistically significant after multivariate adjustment. There was no evidence of interaction between AGEs and diabetes status after multivariate adjustment. In conclusion, PEN and CML have different relationships with bone loss in T2D. These different associations (or lack of association) suggest their distinct biological effects on bone. While PEN may negatively impact collagen and have some effect on bone remodeling, CML, hypothesized to bridge mineral and collagen in bone, causes qualitative defects through pathways not reflected with BMD. These findings extend our previous work highlighting that AGEs are risk factors for bone fragility in diabetes, independent of BMD.

Table 1. Adjusted mean difference in annualized percentage change in bone mineral density over 4 years for 1 SD increase in baseline log CML and log PEN

	No Diabetes (n = 427)	Diabetes (n = 501)	*P for interaction**
	Difference (95% CI)	**Difference (95% CI)**	
Serum CML			
Total hip (% per yr)			
Minimally adjusted model[a]	-0.016 (-0.138, 0.106)	-0.008 (-0.144, 0.127)	0.88
Multivariate adjusted model[b]	0.003 (-0.111, 0.117)	-0.002 (-0.125, 0.122)	0.72
Femoral neck (% per yr)			
Minimally adjusted model[a]	-0.076 (-0.221, 0.069)	0.101 (-0.071, 0.274)	0.08
Multivariate adjusted model[b]	-0.055 (-0.202, 0.092)	0.080 (-0.092, 0.252)	0.11
Urine PEN			
Total hip (% per yr)			
Minimally adjusted model[a]	-0.102 (-0.238, 0.033)	**-0.198 (-0.337, -0.060)**	0.14
Multivariate adjusted model[b]	-0.108 (-0.239, 0.022)	-0.071 (-0.200, 0.058)	0.94
Femoral neck (% per yr)			
Minimally adjusted model[a]	-0.067 (-0.229, 0.095)	**-0.279 (-0.455, -0.103)**	**0.04**
Multivariate adjusted model[b]	-0.092 (-0.260, 0.075)	-0.110 (-0.291, 0.070)	0.49

[a]Adjusted for age, race, sex, and clinical site.
[b]Adjusted for age, race, sex, clinical site, current smoking status, baseline BMD, baseline weight, weight change during 4-yr follow-up, cystatin- C, A1c, and medication use (vitamin D supplements, calcium supplements, oral steroids, osteoporosis drugs, thiazide diuretics, statins, oral estrogen and, in models with diabetes participants, use of insulin and thiazolidinediones).
Bolded differences signify $p < 0.05$.
*P for interaction: between diabetes status and baseline AGE

P-074 Patrick Bidros

Perioperative Use of Anabolic Agents in Three Young Adult Patients with Developmental Hip Dysplasia

Patrick Bidros*1, Kameron Kraus1, Yugant Patel1, Jonathan Webb1,2, Stephen Duncan3, Hartmut Malluche1,2 and Madhumathi Rao1,2
(1)University of Kentucky College of Medicine, Lexington, KY, USA, (2) Department of Medicine, Division of Nephrology, Bone and Mineral Metabolism, Lexington, KY, USA, (3) University of Kentucky Department of Orthopaedic Surgery, Lexington, KY, USA

Introduction
Developmental hip dysplasia (DHD) is a congenital disorder resulting in abnormal formation of the acetabulum resulting in lack of coverage of the femoral head. This can cause instability and pain for patients. There are different types of dysplasia with the neuromuscular variant being associated with low bone density, idiopathic scoliosis, and Charcot Marie Tooth (CMT) disease. We describe 3 female patients with DHD referred to the Bone Mineral Metabolism Clinic for management of bone disease in the setting of pelvic osteotomy surgery.
Cases:
Patients were 25, 28 and 18 years of age with DHD diagnosed at ages 22, 24, and 13, respectively. Table 1 shows the associated comorbidites in these patients. All underwent iliac crest bone biopsy with double tetracycline labeling to characterize bone turnover and guide treatment in the setting of corrective pelvic surgery (Figure 1).
Patient 1 had undergone right periacetabular osteotomy complicated by pelvic nonunion and pelvic stress fracture, when she was referred. She was started on teriparatide (Forteo®), then switched to abaloparatide (Tymlos®) due to side effects. Bone biopsy showed low turnover osteoporosis. In August 2020, she underwent right superior pubic ramus nonunion repair and in August 2021, she underwent successful left periacetabular osteotomy. She completed 2 years of anabolic therapy.
Patient 2 underwent right hip labral repair, and femoral osteochondroplasty in March 2021 and in August 2022, left hip femoroplasty and osteotomy. She was given Forteo® perioperatively based on bone biopsy findings and completed two years of treatment and had uneventful union of her osteotomy.
Patient 3 was recommended corrective surgery but was deferred for at least a year, as she had evidence of open growth plate in her iliac crest, precluding anabolic therapy at this time.
Discussion/Clinical Lesson:
Perioperative use of anabolic agents is well described in older patients with poor bone quality undergoing orthopedic procedures such as spinal fusion. We demonstrate that they are an important tool for preoperative bone health optimization in young patients with DHD.
The association of neuromuscular DHD with multiple comorbidities raises the question of a multi-system disorder that could potentially influence bone turnover. Bone biopsy in all three patients demonstrated low turnover osteoporosis. These patients should have long term follow up to ensure maintenance of their bone health.

Table 1: Clinical features and associated conditions

	Patient 1(age 25)	Patient 2 (age 28)	Patient 3 (age 18)
BMD – lowest Z- score	-1.8 left femoral neck	-2.3 left femoral neck	-2.4 both hips
Bone biopsy	Low bone turnover and volume	Low bone turnover and volume	Low bone turnover and volume
CMT disease	Yes	-	Yes
Idiopathic scoliosis	Yes	Yes	Yes
Torticollis	-	Yes	-
Cerebral palsy/Autism	-	Yes	-

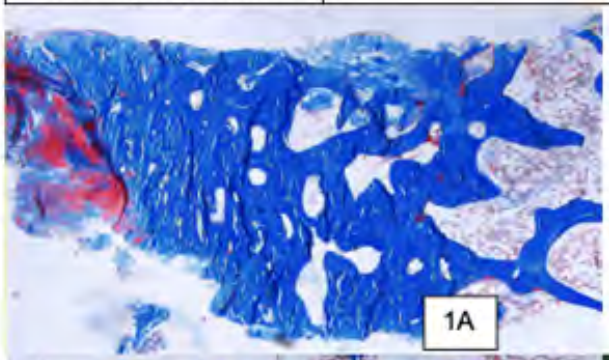

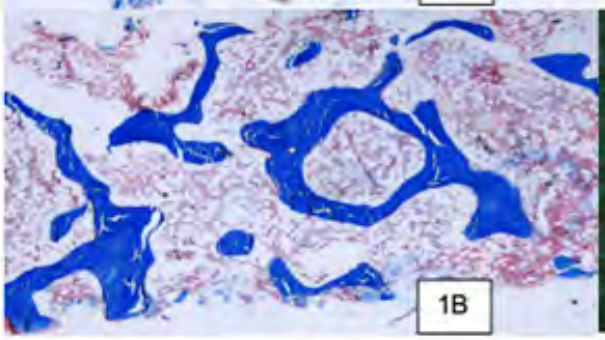

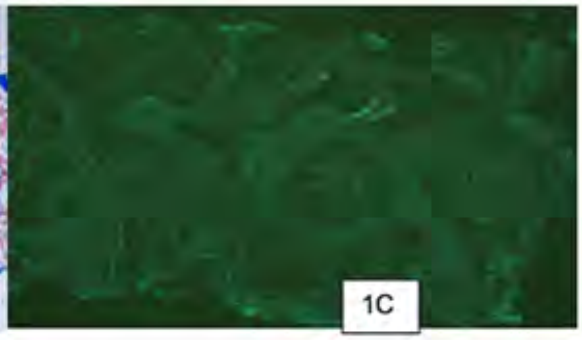

Figure 1: Undecalcified bone biopsy (Masson-Goldner trichrome, 2.5x)**1A**: Cortical porosity **1B**: Low cancellous bone volume, low trabecular thickness, high trabecular separation; very low osteoid volume and low osteoid surface. **1C**: Fluorescent microscopy 2.5x - low mineralizing surface with few double labels.

P-075 Choiselle Marius

Yolk Sac Erythromyeloid Progenitors in Fracture Healing and Regeneration

Choiselle Marius* and Benjamin A. Alman, Duke University, Durham, NC, USA

Bone fractures, especially in older individuals, can lead to delayed healing, impacting patient outcomes and healthcare costs. It is crucial to improve repair speed and prevent non-union, as these factors contribute to better patient responses and reduced expenses. Understanding the complex cellular dynamics of fracture healing, particularly the role of macrophages, is essential. Previous research, including studies from our lab and others, has identified a reservoir of yolk-sac derived monocytes generated in utero. These cells, however, reside in the spleen during adulthood and can migrate to a fracture site; however, their specific functions and mechanisms remain unclear. In pursuit of this understanding, we aim to further characterize the functions of the yolk-sac erythromyeloid progenitors and their progeny in bone healing and regeneration, capitalizing on an inducible ablation model. To deplete monocyte lineage yolk-sac erythromyeloid progenitors, we used genetically modified mice with pulse-activated cre-recombinase in monocyte lineage cells during development. Our method involved injecting pregnant females with 4-hydroxytamoxifen at E9.5 to induce cre-recombination in cre-expressing cells and their progeny, resulting in Cx3cr1CreERt;R26TdTomato;R26DTR mice. Utilizing this model, which allows us to label yolk-sac derived monocytes with fluorescent TdTomato and express Diphtheria Toxin Receptors for efficient depletion using Diphtheria Toxin, we then induce bone injuries in our mouse model through tibial osteotomies. We then evaluated the impact of yolk sac-derived monocyte ablation on fracture healing over time by collecting fractures and contralateral bones at various post-surgery intervals. To assess the effects and efficiency of the depletion, we conducted an analysis of TdTomato-positive cells using immunofluorescence. Subsequently, we employed micro computed tomography to quantify phenotypic changes in bone healing through three-dimensional assessments of bone morphology, density, and volume. Our findings at 14 days post fracture (dpf) revealed that the depleted mice exhibited lower callous density compared to controls. At 21 dpf, the depleted mice also showed an increased callous volume, yet decreased bone density compared to control limbs. Our data suggest that healing at the fracture site both suffers and slows following ablation of yolk sac-derived monocytes, and therefore suggests that this population may play a significant role in new or woven bone formation and potentially osteoblast function.

P-076 Yuwen Zheng, PhD

Early Sign of Bone Loss at Femoral Neck: Fifteen Years of Bone Accrual from Peak Bone Mass

uwen Zheng*1, Ahmed Elhakeem2,3, Stefan A. Jackowski1,4, Marta C. Erlandson1 and Adam D.G. Baxter-Jones1,
(1) University of Saskatchewan, Saskatoon, SK, Canada, (2) MRC Integrative Epidemiology Unit at the University of Bristol, Bristol, United Kingdom, (3) Population Health Sciences, Bristol Medical School, University of Bristol, Bristol, United Kingdom, (4) Children's Hospital of Eastern Ontario, Ottawa, ON, Canada

We have previously shown in a cohort of Saskatchewan children followed from 8 to 30 years (the Pediatric Bone Mineral Accrual Study (PBMAS)) that peak bone mass (PBM) occurs by the end of the second or early in the third decade of life, depending on skeletal site. However, little is known about bone accrual after PBM has occurred. The aims of this study were two-fold: (1) to develop trajectories of bone accrual (Bone Mineral Content (BMC) and areal Bone Mineral Density (aBMD)) aligned to occurrence of peak bone mass (PBM) for various anatomical sites; and (2) to identify potential changes in BMC and aBMD post PBM from the transition of emerging adulthood into young adulthood. Methods: PBMAS was initiated in 1991, when 251 children aged 8-15 years were recruited. Participants underwent up to fifteen annual DXA scans (Hologic QDR-2000, array mode; lumbar spine (LS), total hip (TH), femoral neck (FN), total body (TB)) between 1991 and 2017. 112 males and 127 females PBMAS participants with ≥1 DXA scan were included in this analysis. Super Imposition by Translation and Rotation (SITAR) models were fitted, aligning bone parameters with age from PBM at the various anatomical sites. All analyses were performed in R version 4.0.2 (R Project for Statistical Computing) and RStudio integrated development environment version 1.3.1 (RStudio Team). Results: SITAR models showed that peak BMC and aBMD velocities occurred at -4 to -6 years from attainment of PBM for LS, TH, FN, and TB respectively. At fifteen years post PBM, at the LS and TB, BMC and aBMD had increased by 6-7% and 3-10% for males and 8% and 4-12% for females respectively. At the TH and FN, males showed a 3-5% decrease in BMC and 5% decrease in aBMD, while females showed a 4% increase in TH BMC but a 2% decrease in TH aBMD. Also seen were 6% and 8% decreases in FN BMC and FN aBMD respectively. Discussion: These models graphically illustrate the nonlinear development of BMC and aBMD pre and post attainment of PBM in both sexes. Bone loss was observed in early adulthood in the hip region, but not at the LS or TB, however the trajectory of aBMD change may not be necessarily align with BMC change at LS and TB. Also, males and females may have different patterns of change in BMC at the TH and FN after attainment of PBM. Future studies should explore the role of sex-specific, body composition and lifestyle factors associated with bone change post PBM, especially at the hip region.

P-077 Yasaman Moharrer

YAP and TAZ mediate mechanical load-induced bone adaptation

Yasaman Moharrer*1, Daniel Horan2, Tala Azar1, Annemarie Lang1, Alexander G. Robling3, Xiaowei Sherry Liu1 and Joel D. Boerckel 4
(1) University of Pennsylvania, USA, (2) Indiana University, USA, (3) Indiana University, Indianpolis, IN, USA, (4) University of Pennsylvania, Philadelphia, PA, USA

Bone adapts to mechanical stimuli; however, the mechanotransductive mechanisms are poorly understood. We hypothesized that the transcriptional regulators, YAP and TAZ, mediate bone adaptation to mechanical loads. Osteocyte deletion of YAP and TAZ alters bone architecture and lacunar/canalicular networks.1 Therefore, we used pharmacologic approaches to acutely inhibit YAP/TAZ signaling in mice with normal developmental history.

We selected two orthogonal inhibitors: verteporfin (VP), which blocks YAP/TAZ co-activation, and MGH-CP1 (CP1), which prevents TEAD binding to YAP and TAZ. We performed i.p. injections of either inhibitor (or DMSO) to 14-wk-old male C57BL/6 mice for 2 weeks. Concurrently, the left tibiae of each mouse underwent in vivo cyclic compressive loading with a 4 Hz sinusoidal waveform, at 1200 cycles per day, for 5 d/wk over 2 weeks . The peak load induced 1200 με at the location of maximal strain in the tibial shaft (37%), calibrated by strain gage. Contralateral tibiae served as non-loaded controls. MicroCT and dynamic fluorochrome labeling (calcein and alizarin complexone) were used to quantify cortical bone formation at the site of maximal cortical strain and of trabecular bone in the proximal tibia metaphysis.

Cyclic compressive tibial loading increased tibial cortical thickness in the DMSO group; however, either VP or CP1 treatment abrogated the effect of loading (Fig1A and B). Neither loading nor YAP/TAZ inhibition significantly altered trabecular bone morphometry (BV/TV, Tb.Th, Tb.N, Tb.Sp). Cyclic loading increased periosteal bone formation, and neither CP1 nor VP treatment significantly blunted periosteal MS/BS, MAR, or BFR/BS. In contrast, at the endocortex, both VP and CP1 treatment abrogated the significant effect of loading on MS/BS, MAR, and BFR/BS (Fig 1C and D).
These data provide the first in vivo evidence that YAP and TAZ mediate mechanotransduction of anabolic loading. In the tibial cortex, both VP and CP1 blocked load-induced cortical bone gains by blunting endosteal rather than periosteal bone formation. Previously, we found that VP alters osteocyte network density and perilacunar dynamics differently in endosteal- compared to periosteal-adjacent osteocytes, suggesting differential drug transport or spatial mechanotransduction. Together, these findings reveal new insights in bone mechanotransduction and identify risks of cancer-treatment-induced osteoporosis by pharmacologic targeting of YAP and TAZ as oncogenes.
1 Kegelman+ JBMR 2019

P-077 Yasaman Moharrer

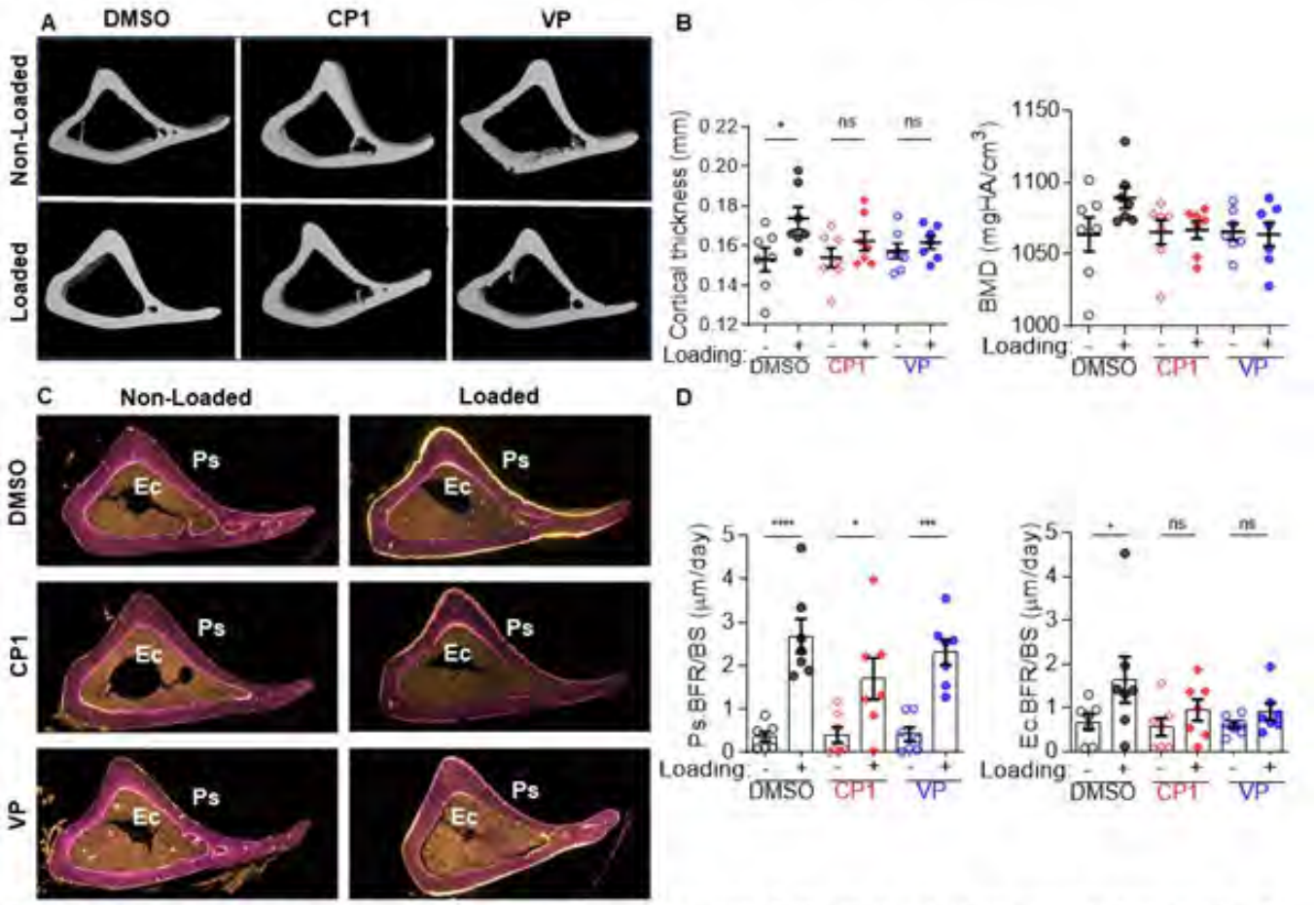

Fig. 1. A. Representative micro-CT reconstructions of diaphyseal cross section in tibia. **B.** Quantification of cortical microarchitectural properties. **C.** Representative transverse sections of fluorochrome-labeled tibias. **D.** Quantification of periosteal and endosteal bone formation properties. BMD= Bone Mineral Density, Ps=Periosteum, Ec=Endosteum. * $p< 0.05$, *** $p< 0.0005$, **** $p< 0.0001$.

P-078 Annabel Bugbird

Quantifying morphometric defects in clinical computed tomography

Annabel R. Bugbird1,3, Nathan J. Neeteson1,3, Steven K. Boyd1,2,3
(1) McCaig Institute for Bone and Joint Health, University of Calgary, Calgary, Canada (2) Department of Radiology, Cumming School of Medicine, University of Calgary, Calgary, Canada (3) Department of Biomedical Engineering, Schulich School of Engineering, University of Calgary, Calgary, Canada

Background: Fragility fractures play a major role in morbidity, mortality, and quality of life among the aging population [1, 2]. A recent study in our lab [3] developed a new metric for quantifying localized morphometric defects, known as void space, using high resolution peripheral quantitative computed tomography (HR-pQCT), providing new insight into the assessment of bone fragility.
However, physical limitations of HR-pQCT gantry size mean void space can only be investigated at peripheral sites (e.g. radius), therefore other osteoporotic sites of interest have not yet been investigated. Understanding the systemic impacts of void space at osteoporotic sites in a clinically available imaging modality will provide insight into the impact of structural defects on bone fragility. The aim of this study is to develop and validate the measurement of void space using clinical CT.

Methods: The cohort used for this study consisted of (n = 10) individuals, who had bilateral knees scanned using both HR-pQCT and clinical CT. In the HR-pQCT scans, the femur and tibia were segmented using a semi-automatic approach [4], and the void space masks were generated using our previously developed algorithm [3].
For clinical CT the tibia and femur were segmented using a trained UNet for semantic segmentation. A range of thresholds (5-80 mg/cc) created initial void space masks and connected component analysis was applied to remove voids of less than 16.5 mm3 [3].
To validate the clinical CT void space masks against HR-pQCT, the masks were registered and the void space volume (VS) and the ratio of void space to bone volume (VS/TV) were compared across the modalities using Pearson (r) correlation coefficient.

Results: Across the dataset, a threshold of 5 mg/cc was observed to be optimal for maximizing the similarity between the VS and VS/TV between the imaging modalities. The r coefficients were 0.84 and 0.76 for VS and VS/TV respectively across all sites.

Discussion: The newly developed approach for measuring void space in clinical CT showed qualitative similarity (Figure 1) and a strong quantitative correlation in void space metric compared to HR-pQCT. The spatial location of void space was consistent across modalities, particularly for larger voids (Fig 1). Developing a workflow for identifying void space in clinical CT provides a clinically relevant metric for quantifying structural defects that are important for bone strength. Future studies will investigate the systemic impact of void space and its relationship with bone fragility.

P-078 Annabel Bugbird

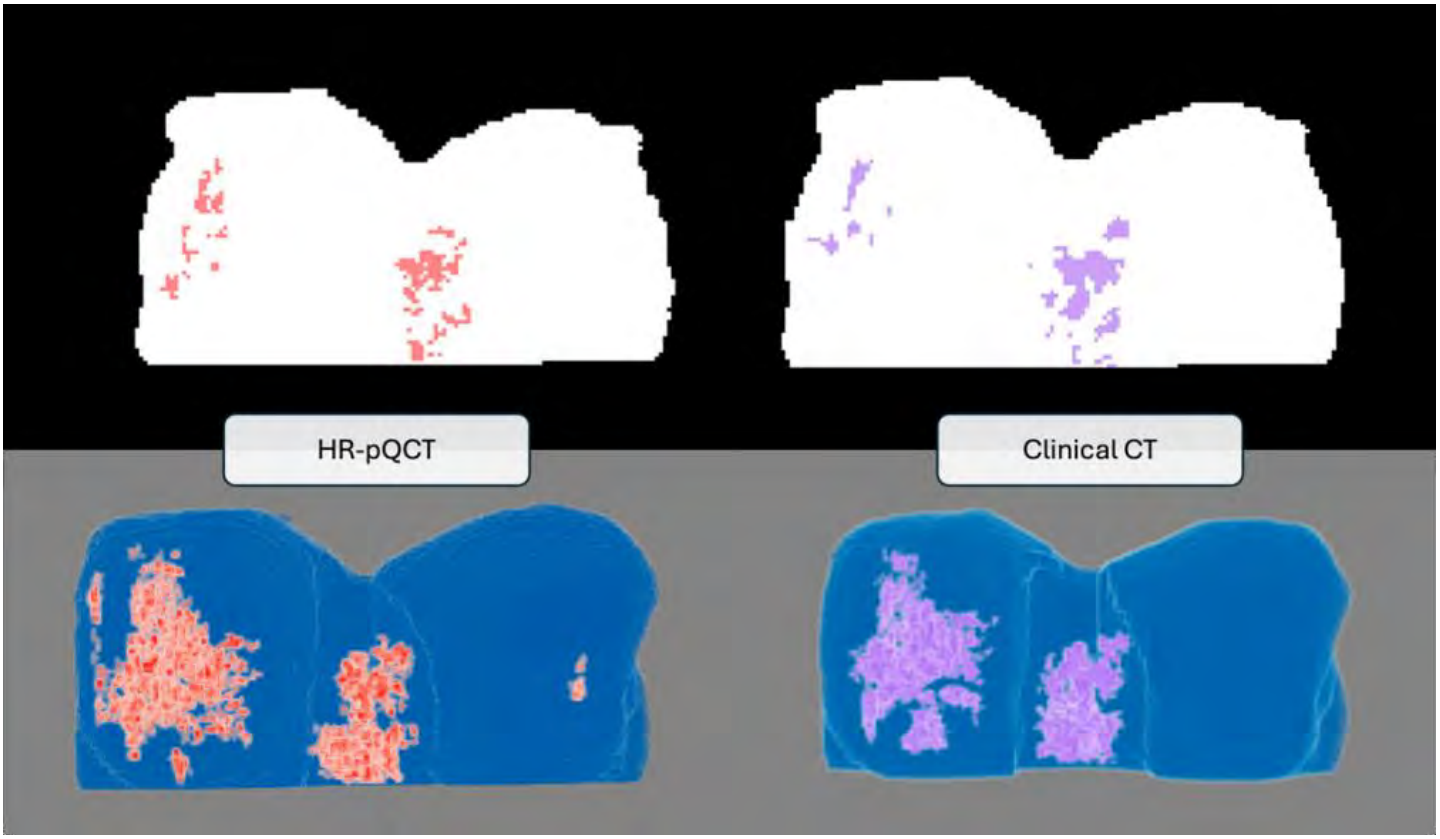

Figure 1: Segmented slice (top) and volume render (bottom) of void space mask for HR-pQCT (red) and clinical CT (purple).

P-079 Malene Nielsen, PhD

Combined cyro and paraffin bone histomorphometry: a quick and novel approach opening new opportunities

Malene H. Nielsen1,2,5, Jeanette K. Petersen2, Ditte Hansen3, Thomas L. Andersen1,2,4,5
(1) Molecular Bone Histology (MBH) lab, Department of Clinical Research, University of Southern Denmark, Denmark, (2) Department of Pathology, Odense University Hospital, Odense, Denmark, (3) Department of Nephrology, Copenhagen University Hospital, Herlev and Gentofte, Denmark, (4) Molecular Bone Histology (MBH) lab, Department of Forensic Medicine, Aarhus University, Aarhus, Denmark, (5) Danish Spatial Imaging Consortium (DanSIC)

Background: Histomorphometry have for decades been performed on sections from undecalcified methylmethacrylate embedded bone biopsies. However, this procedure is slow and prevent that the bone biopsies can be easily used for immunostainings, and exclude any in situ RNA and DNA studies. This study focus on a novel bone histomorphometric procedure combining the analysis of undecalcified cryo-sections and decalcified paraffin sections from the same biopsy. This provide a faster bone histomorphometry on human bone specimens, while making it possible to perform advanced in situ protein, RNA and DNA analysis.

Aim: To provide a faster bone histomorphometry on human bone specimens, while making it possible to perform advanced in situ protein, RNA and DNA analysis.

Methods: The methodology have been applied to 3 mm Jamshidi transiliac human bone biopsies. The dynamics of the mineralization are labelled using tetracycline that are taken at day -17,-16,-15 and -6,-5,-4 (2 x 500mg per day). The biopsies are fixed for 24 hours in 10% neutral buffered formalin (NBF) using pulses of vacuum to improve penetration. Upon arrival, the biopsy is pretreated in 30% sucrose in PBS before it is undecalcified cryo-embedded in a cryo-embedding compound (Milestone). Six µm cryo-sections are obtained using the Kawamoto tape method, and either unstained fluorescence microscopic scanned to analyze tetracycline labels (mineralization), or Von Kossa stained and light microscopic scanned to analyze osteoid surfaces. Upon approval of the cryo-sections, the bone biopsy is thawed, decalcified in formic acid for 6 hours at 37 0C and embedded in paraffin. Three and a half µm paraffin sections are Masson trichrome stained to analyze erosion, bone structure and cortical pore histomorphometry, as well as immunohistochemistry stained for TRAcP to analyze osteoclasts, and if needed H&E stained to analyze bone marrow morphology. All scans are performed on an Olympus VS200 fluorescence slide scanner and all analysis are performed digitally using VS200 Desktop software.

Results: From the arrival of the bone specimen, the cryo- and paraffin-sections are stained and ready for digital analysis within 5 workdays, which is 10-12 days shorter than with the classical MMA-method. The quality of the cryo-sections is challenging, but suitable for the analysis mineralization and osteoid, while the cellular analysis should only be performed in the paraffin sections. As the tetracycline was more visible in the cryo-sections, we expect to reduce the labelling from three to one day per time point. Furthermore, this novel methodology renders the biopsies suitable for advanced immunostaining and in situ RNA/DNA analysis, including novel spatially resolved transcriptomics.

Conclusion: This combined cryo and paraffin bone histomorphometry method provide a faster result, and opens up to a completely new world of opportunities.

P-080 Amirreza Haghighi, PhD

A Genome-Wide Association Study on Patients with Atypical Femur Fractures

Amirreza Haghighi*1,2,3, Hamideh Ghazizadeh4, Lianne Tile4,5, Aliya Khan6, David L. Kendler7, Adrian Lau5,8, Rowena Ridout4,5, Robert G. Josse5,9, Jonathan D. Adachi6 and Angela M. Cheung10,11,
(1) Harvard Medical School, Boston, MA, USA, (2) Brigham and Women's Hospital, Bostom, MA, USA, (3) University Health Network, Toronto, ON, Canada, (4) University Health Network, Canada, (5)University of Toronto, Canada, (6)McMaster University, Canada, (7) University of British Columbia, Vancouver, BC, Canada, (8) Women's College Hospital, Canada, (9) Unity Health, Canada, (10) Department of Medicine and Joint Department of Medical Imaging,University of Toronto, Toronto, ON, Canada, (11) Osteoporosis Program, Schroeder's Arthritis Institute, University Health Network (UHN), Toronto, ON, Canada

Purpose: Atypical femur fractures (AFFs) are rare but can occur in postmenopausal women on prolonged potent antiresorptive (AR) therapy, especially among those of Asian descent. Although the underlying mechanism of atypical femur fractures remains uncertain, genetic predisposition have been suggested to play a role. Thus, we conducted a genome-wide association study (GWAS) on patients with AFFs to identify potential genetic risk factors involved in the development of these unusual fractures.

Methods: 359 patients were included from the Ontario AFF Cohort and matched (on age, sex, and ethnicity) with 11,146 healthy controls from the Canadian Longitudinal Study on Aging (CLSA). All the patients met the 2014 ASBMR AFF Task Force criteria. The UK Biobank Axiom Array by Thermo Fisher (Affymetrix) was used to genotype all AFF and CLSA samples at the same centre. Principal component analysis was performed to assess population structure. Among the 298 AFF samples that past quality control, 130 were inferred to be of European (EUR), 131 East Asian (EAS) and 33 South Asian (SAS) descent. TopMed genotype imputation was conducted, followed by conducting genome-wide association analyses in each ethnic group separately.

Results: In our GWAS study, 6 single nucleotide polymorphisms (2 SNPs in EAS and 4 SNPs in SAS) reached significance at the genome-wide level ($p < 5 \times 10\text{-}8$). This includes 3 SNPs located in the intronic regions within IGF2BP3 (involved in bone density regulation and skeletal repair processes) and NLRP11genes (a modulator of osteoclast differentiation and activity), and 3 SNPs located in the intergenic regions in AFG1L<>FOXO3 and ETV3<>FCRL5 genes. Employing the candidate gene approach, which involves compiling genes that might be associated with bone-related disorders from existing literature (n=549), we also identified 2 SNPs in SAS and 4 SNPs in EAS ($p < 1\times 10\text{-}5$) located within or close to SV2C, EYA2, and AGTR1; although none reached genome-wide significance level.

Conclusion: Our findings indicate potential genetic diversity among individuals with AFFs across various ethnic groups. Further investigations are needed to validate and replicate these findings and unravel their functional significance. Studies employing whole-exome or whole-genome sequencing would be particularly useful for uncovering rare genetic variants that may contribute to the risk of developing AFFs.

P-081 Darrah Condino

Maternal Supplementation of Red Rooibos Tea on Mandible Bone Mineral Following Pregnancy and Lactation

Darrah Condino*1, Matthew Goncharow1, Jenalyn Yumol1, Michael McAlpine2 and Wendy E. Ward3
(1) Brock University, St. Catharines, ON, Canada, (2) Brock University, St. Catherines, ON, Canada, (3) Brock University, Department of Health Sciences, St. Catharines, ON, Canada

In rats, some studies have shown sustained detriments in long bones and vertebrae up to 4 months post-lactation while other skeletal sites such as mandible have been less studied. It is possible that the mandible may be protected through pregnancy and lactation due to increased food intake and the resultant mechanical load from chewing food. Red rooibos (RR) supplementation to Sprague-Dawley rats was previously shown to support the partial recovery of tibia bone mineral density (BMD) and structure at 4 months post-lactation. The objective of this study was to determine if RR supplementation supported mandible bone mineral when provided from pre-pregnancy through to 4 months post-lactation. A secondary objective was to determine if mandible responded similarly to pregnancy and lactation and RR supplementation as other skeletal sites. Six-week-old female Sprague-Dawley rats (n=42) were randomized to one of three groups: PREG TEA (pregnancy and lactation; ~2.6 g/kg body weight/day RR through drinking water), PREG WAT (pregnancy and lactation; water), GROWTH CON (age matched non-pregnant control; water). RR was provided from 6-weeks-old through to 4 months post-lactation. Rats were bred at 8 weeks of age and maintained until 4 months post-lactation when mandibles were excised. Ex vivo measurements of BMD, bone mineral content (BMC) and area for right hemimandible were obtained using dual X-ray absorptiometry (Scintica InSiGHT). There were no differences in BMD or BMC between PREG TEA and PREG WAT ($p>0.05$), showing no effect of RR intervention. There were also no differences in BMD or BMC between GROWTH CON and either pregnancy group ($p>0.05$). This demonstrated that there were no sustained effects of pregnancy and lactation in mandible by 4 months post-lactation. This contrasts with other sites, as sustained detriments in tibia, femur, and lumbar vertebrae BMD and BMC ($p<0.05$) were observed through to 4 months post-lactation in these same rats. Of note is that food intake was significantly higher in PREG TEA and PREG WAT than GROWTH CON ($p<0.05$). This finding provides evidence that the higher food intake may have stimulated a mechanical load that maintained mandible BMD. In conclusion, no significant effects of maternal RR supplementation on mandible bone mineral were observed. Moreover, pregnancy and lactation did not influence mandible bone mineral at 4 months post-lactation.

P-082 Fatima Sandmann-Afonso, MD and Carolina Aguiar Moreira, MD, PhD

Bone histomorphometry in female Wistar rats treated with different doses of Melatonin

Fatima Correa Sandmann-Afonso*1,2,3, Rafaela Ceron1, Angela Reck4, Leticia Capote dos Santos1, Lorena Bavia5, Maritana Mela Prodocimo5, Liliane Roskamp6, Thais Andrade Costa Casagrande4, Vicente Florentino Castaldo Andrade1,2,3 and Carolina Aguiar Moreira1,2,3
(1) Academic Research Center, Pro Renal Institute, Curitiba, Brazil, (2) Postgraduate in Internal Medicine and Health Sciences at Federal University of Parana, Curitiba, Brazil, (3) Endocrine Division (SEMPR), Department of Internal Medicine Federal University of Parana, Curitiba, Brazil, (4) College of Veterinary Medicine at Positivo University, Curitiba, Brazil, (5) Laboratory of Cellular Toxicology at Federal University of Parana, Curitiba, Brazil, (6) Tuiuti University of Parana School of Dentistry, Curitiba, Brazil

Hypoestrogenism during menopause is associated with decreased melatonin (Melt) production by the pineal gland, a decline that also occurs with aging. Melatonin interacts with bone receptors, particularly in the bone marrow where bone cell precursors are located. This hormone plays a protective role in the skeleton mainly by reducing bone resorption. The objective of this study was to evaluate, in an animal model of osteoporosis, the structural and remodeling parameters in tibias of female Wistar rats treated with different doses of Melt by the Bone Histomorphometry (BH). This study is a cross-sectional observational and analytical study. The project was approved by the Committee on Ethics in the Use of Animals (CEUA) under number 550. Sixty female Wistar rats underwent ovariectomy (OVX, n = 30) and SHAM surgery (SHAM, n = 30) at 20 weeks of life. They were subdivided into 6 groups (n=10), and after 11 weeks, received doses of 20 mg, 50 mg/kg of Melt or placebo by gavage, for eight weeks. Euthanasia was performed at the 41st week of life, and the tibias were collected for analysis. The OVX group showed an increase in bone volume ([BV/TV], $p < 0.001$), in the number of trabeculae ([Tb. N], $p = 0.035$) with 50 mg/kg compared to the control group (CG). There was an increase in erosion surface ([ES/B], $p = 0.002$) and trabecular separation ([Tb. Sp], $p = 0.020$) in the CG compared to the OVX group 50 mg/kg. In the SHAM animals, the Melt 20 and 50 mg/kg groups showed an increase in BV/TV ($p = 0.001$) and in the Tb. N ($p = 0.005$), with less spacing between trabeculae Tb. Sp ($p = 0.002$) compared to the CG. There was no difference between the doses in the SHAM group, and there was no significant increase in erosion surface ([ES/BS], $p = 0.080$) in the CG compared to the SHAM 20 and 50 mg/kg groups. The animals were weighed every fifteen days after the start of Melt administration. Anova showed that there was no significant interaction between the moments of weight assessment and the groups, indicating that the weight progressions of the 3 SHAM groups ($p=0.448$) and the 3 OVX groups ($p=0.591$) were not different. Furthermore, there was no significant correlation between weight and bone histomorphometry parameters in both groups. The use of Melt was linked to enhancements in structural and bone microarchitecture parameters, suggesting that this hormone could play a key role in reducing bone loss associated with estrogen deficiency and aging.

P-083 Haydee Torres, PhD

PHLPP inhibitors reduce sensory neuron joint knee innervation during OA progression in mice

Haydee Magdalena Torres*1, Elizabeth W. Bradley2, Xiaodong Li1, Elizabeth Zars1, Samantha Weaver1, Eduardo Peralta-Herrera1, Christopher Peters3, Nathan Staff4 and Jennifer J. Westendorf1,5
(1) Department of Orthopedic Surgery, Mayo Clinic, Rochester, MN, USA, (2) Department of Orthopedics, School of Medicine, Minneapolis, MN, USA, (3) Department of Anesthesiology, Wake Forest University Medical School, Winston-Salem, NC, USA, (4) Department of Neurology, Mayo Clinic, USA, (5) Department of Biochemistry & Molecular Biology, Mayo Clinic, Rochester, MN, USA

Osteoarthritis (OA) is a progressive and debilitating disease that affects 7.6% of the world's population. Despite its prevalence, there are currently no disease modifying medications available or long-term solutions to alleviate pain. OA is characterized by articular cartilage deterioration, subchondral bone sclerosis, joint stiffness and pain. We previously reported that PH domain leucine-rich repeat protein phosphatases (PHLPPs) are suppressors of chondrocyte regeneration and pain-related behaviors in OA models. Intra-articular injection of PHLPP inhibitors (PHLPPi, NSC117079) prevents joint hypersensitivity and cartilage degradation following a surgery that destabilizes the medial meniscus (DMM), a murine model of post-traumatic OA. Our central hypothesis is that PHLPP activity in sensory neurons contributes to pain-related behaviors in OA and that PHLPPi prevents sensory nerve innervation of injured joints. Nociceptive neurons cell bodies reside in dorsal root ganglia (DRG). Publicly available single cell RNA sequencing data indicates that Phlpp1 is highly expressed in satellite glial cells. We performed bulk RNA seq of L3-5 DRG from Phlpp1-/- and wildtype mice and found that fibroblast (Lum, Dcn, Mmp2) and inflammatory genes (Caf2ra, Nup210, Chil3, Ccdc88c) are significantly downregulated in Phlpp1-/- DRGs. In vitro, NSC117079 reduced neurite outgrowth from dissociated rat DRG and expression of markers of small/medium sensory neurons (e.g., NTrk1) and neurotransmitters (e.g., Cgrp), but not the broadly expressed neuronal gene, Uchl1. Immunohistochemistry for neurofilament 200 (NF200) and substance P (SubP) was performed on destabilized joints where NSC117079 reduced allodynia and preserved cartilage 12 weeks post-surgery. Less SubP was present in the subchondral bone of mice injected with the PHLPPi. NF200 was lower in the periosteal region of joints injected with NSC117079. Finally, we performed DMM surgery on reporter mice expressing tdTomato-Cre from the Nav1.8 promoter, which is active in approximately 80% of sensory neurons. Sprouting of NaV1.8-tdTomato positive neuron tracks within the subchondral bone region was significantly reduced in mice injected with the PHLPPi versus saline at 12 weeks post-surgery. Together these data demonstrate that PHLPPi can prevent sensory nerve growth within injured joints and this may be a mechanism by which PHLPPi alleviate joint pain-related behaviors in mice.

P-084 Erica Clinkenbeard, PhD

Interplay of polyamines on mineralization during iron deficiency and CKD-MBD

Erica Clinkenbeard*1, Christopher Ashley Miller1, Huda Maria Mahmood1,2, Jordan Ashley Matz1 and Katharina Maria Kirschner1,
(1) Indiana University School of Medicine, Indianapolis, IN, USA, (2) Marian College of Medicine, Indianapolis, IN, USA

Chronic Kidney Disease (CKD) affects 800 million worldwide. CKD-mineral and bone disorder (CKD-MBD) independently leads to vascular calcification, fracture risk, and mortality. Mice placed on CKD-inducing 0.2% adenine diet (AD) for 8 weeks parallels human disease phenotypes along with incidence of iron deficiency. As iron deficiency of CKD is independently associated with morbidity and mortality, we tested effects of chronic iron chelation in vitro. Introduction of iron chelator deferoxamine (DFO) suppressed osteoblast differentiation and mineralization; however, the underlying mechanism remained unclear. Reports showed iron deficiency altered polyamine homeostasis, small cationic compounds used for various biological functions, by promoting the catabolism pathway thereby reducing spermine levels. In human CKD subjects, serum spermine decreased and was further reduced with disease severity correlating with increased catabolic oxidase activity. Finally, spermine is important for osteoblast differentiation and mineralization with supplementation in vivo improving bone strength and blunting OVX-mediated bone loss. Thus, we hypothesize spermine treatment negates CKD-iron deficiency bone loss and improves mineral metabolism. We first tested the hypothesis with mouse progenitor clone 2 cell line (MPC2) undergoing osteogenic differentiation with iron chelation (DFO) with or without spermine supplementation (Spm; 1 mM or 2 mM). During mild iron deficiency, Spm significantly improved osteocalcin (Bglap; $p<0.05$) and alkaline phosphatase (Alpl; $p<0.05$) mRNA levels vs DFO alone and enhanced mineralized nodule formation. Next, we tested Spm in vivo using male and female C57Bl6J mice placed on adenine diet (AD) receiving water with either 0.3mM (low) or 3 mM (high) Spm or water control. We also maintained a cohort on casein control for baseline. After 8 weeks of treatment, both male and females on AD exhibited body weight reductions and serum blood urea nitrogen (BUN) increased versus casein without any significant influences from Spm. Intact Fibroblast Growth Factor 23 (iFGF23) showed a significant Spm dose dependent decrease (AD veh: 86,933+9,000; low: 62,675+6,996; high: 15,840+2,289 pg/mL) with no changes in serum phosphate. Bone RNA from high Spm group demonstrated enhanced reductions of Bglap ($p<0.05$ vs AD veh) males and females compared to all other groups, as well as a further induction of inflammatory marker Serpina3n ($p<0.05$ vs AD veh). Importantly, mice with high Spm exhibited heart calcifications suggesting Spm may promote extraskeletal transitions to osteoblast-like cells. Thus, further characterization of polyamine homeostasis and effects of spermine could have critical implications for patients with CKD-MBD.

P-085 Michael Friedman, PhD

Genetics, sex, and body weight affect the musculoskeletal response to disuse in mice

Michael Friedman*1, Jessica Williamson2, Yaaminata Koroma2, Zofia Bosowska3, Saikat Bandyopadhyay3, John McKean2, Jennifer Coulombe4, Charles R. Farber3 and Henry J. Donahue1
(1) Virginia Commonwealth University, Richmond, VA, USA, (2) Virginia Commonwealth University, USA, (3) University of Virginia, USA, (4) Harvard University, USA

Disuse causes extensive bone and muscle loss, increasing the risk of bone fractures. The gene pathways involved in regulating the musculoskeletal response to disuse are mostly unclear. Additionally, it remains unclear what role genetics, sex, and body weight have on this response. To study these effects, we used the diversity outbred (DO) mouse population. DO mice are genetically unique and have a high variance for biological traits like body weight. We hypothesized that the magnitude of bone and muscle loss from disuse is affected by genetics and sex. Also, by using an outbred mouse, we would uncover novel gene pathways regulating these effects that have not been uncovered in studies using inbred mice. The right leg of 16-wk old DO mice was immobilized in a cast for 3 weeks (n=30 mice/sex). Bone and muscle morphology was evaluated using in vivo μCT. Scans on day 21 were compared versus day 1 scans to measure bone resorption, bone formation, and muscle volume. Bulk RNAseq was done on tibia and gastrocnemius samples. We measured the correlations of all genes and properties with each other. Disuse increased cortical bone resorption while also decreasing trabecular BV/TV, bone strength, muscle mass and muscle strength. Genetics and sex influenced the magnitude of these changes. RNAseq identified 1,124 and 1,200 significant differentially expressed genes in female and male tibias, respectively. There were 190 and 493 significant genes in female and male gastrocnemius muscles, respectively. Pathways affecting extracellular matrix composition and organization were upregulated in tibias and gastrocnemius muscles. MAPK signaling, lipid metabolism, immune function, and cytoskeleton organization were downregulated in tibias. Mitochondrial function and fat oxidation were downregulated in gastrocnemius muscles. Males and mice with body weight above 30g had greater bone resorption volume and different gene pathways affected than females and lower-weight mice. Broad-sense heritability was higher in the properties of the immobilized legs than in the untreated contralateral limbs, indicating genetics has a strong influence on the response to disuse. Overall, bone and muscle responses to disuse are influenced by genetics, sex, and body weight. Several biological functions that are disrupted by disuse were identified. Particularly, MAPK signaling, mitochondrial function, and fat metabolism may be of interest, given that body weight affected the response to disuse.

P-085 Michael Friedman, PhD

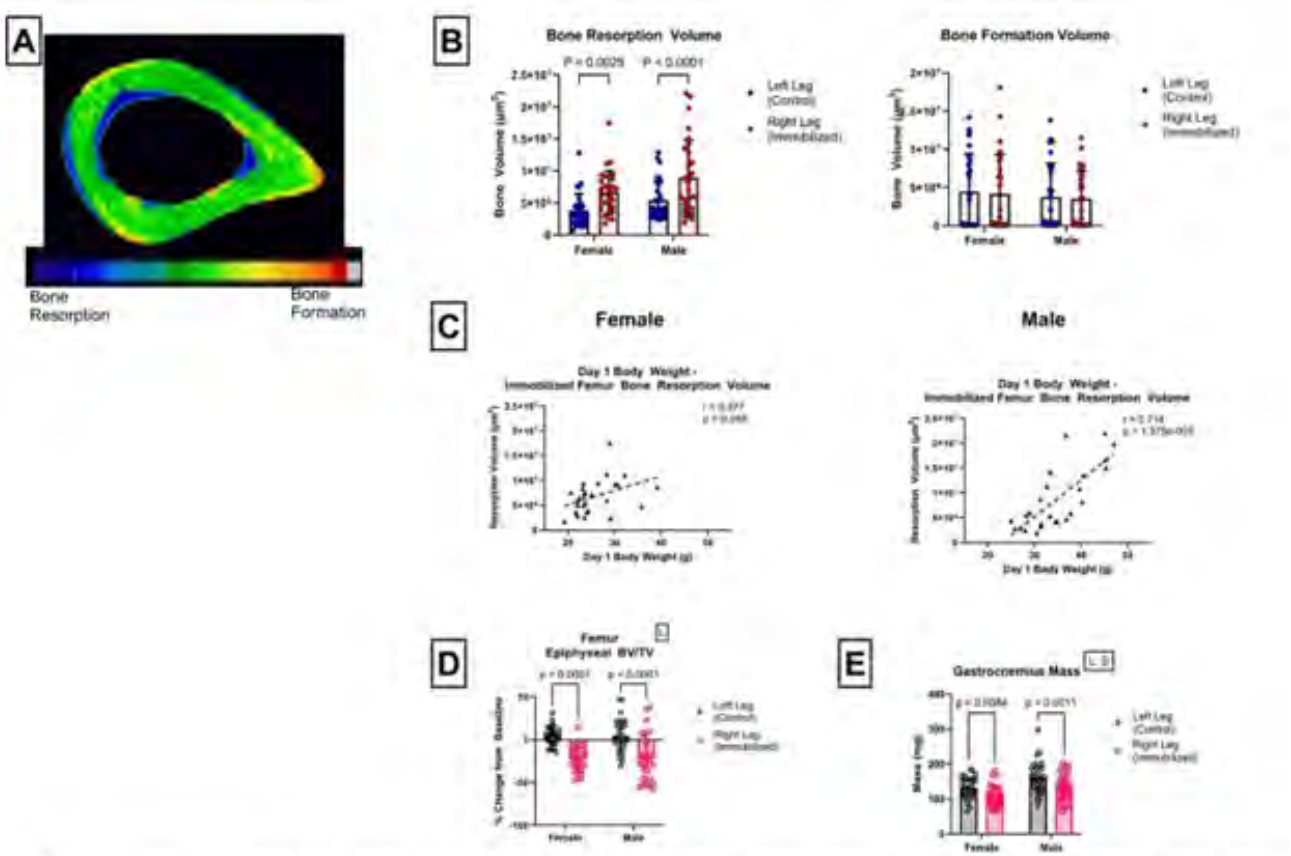

Figure 1. (A) Micro-CT image of a male immobilized femur, indicating regions of bone resorption and bone formation. (B) Bone resorption and formation volume of immobilized and contralateral control femurs. Resorption was higher in immobilized legs and in male mice. (C) Correlations between initial body weight and immobilized femur resorption volume. Initial body weight was highly predictive of how much bone loss would occur from disuse, especially in males. (D) Change in distal femur epiphyseal trabecular BV/TV from baseline. Immobilized limbs had more bone loss than contralateral limbs. (E) Gastrocnemius mass after 3 weeks of immobilization was lower in immobilized limbs.

P-086 Miryoung Lee, PhD

Adverse Effects of Metabolic Dysfunction-Associated Steatotic Liver Disease on Skeletal Health in Mexican Americans

Miryoung Lee*1, Akshata Moghe2, Catherine G. Ambrose3, Jude des Bordes4, Robert Tsai5, Jennifer Below6, Susan Fisher-Hoch1, Joseph McCormick1 and Nahid J. Rianon4, (1) University of Texas Health Science Center at Houston, School of Public Health, Department of Epidemiology, Brownsville, TX, USA, (2) University of Texas Health Science Center at Houston, McGovern Medical School, Department of Internal Medicine, Division of Gastroenterology, Hepatology, and Nutrition, Houston, TX, USA, (3) University of Texas Health Science Center at Houston, McGovern Medical School, Department of Orthopaedic Surgery, Houston, TX, USA, (4) University of Texas Health Science Center at Houston, McGovern Medical School, Department of Internal Medicine, Division of Geriatric and Palliative Medicine, Houston, TX, USA, (5) Texas A&M Health Science Center, School of Medicine, Department of Translational Medical Sciences, Houston, TX, USA, (6) Vanderbilt University Medical Center, Division of Genetic Medicine, Nashville, TN, USA

Metabolic complications such as type 2 diabetes (T2D) are associated with an increased risk of osteoporosis and fragility fractures. The association between metabolic dysfunction-associated steatotic liver disease (MASLD), a combination of hepatic steatosis, obesity, or any components of metabolic syndrome (MetS), with bone health has not been well explored. Mexican Americans (MA) are a large, poorly studied minority population with high rates of osteoporosis, disproportionately affected by MASLD. Our cross-sectional study aimed to examine the associations between MASLD and lumbar spine bone mineral density (LSBMD) and trabecular bone score (TBS), a surrogate for bone microarchitecture, in a sample of MA in South Texas.

Demographics, hepatic steatosis, T2D, and BMD/TBS data were included from 500 participants aged over 50 (60.7% females, mean age [SE], 64.1±1.0 yrs) from the community-based Cameron County Hispanic Cohort study. Participants reporting alcohol consumption or a history of hepatitis were excluded from the analysis. LSBMD and TBS were measured using dual-energy X-ray absorptiometry. Steatosis was determined by transient elastography (FibroScan, controlled attenuation parameter ≥ 268 dB/m). MASLD was determined by steatosis and at least one of the following conditions (obesity, T2D, or MetS). The effect of MASLD on LSBMD and TBS was measured by survey-sampling weighted analyses (chi-square test, linear and logistic regression) adjusted for risk factors for osteoporosis.

The weighted mean LSBMD was 1.003±0.013 g/cm2, and the mean TBS was 1.25± 0.01. Men have higher LSBMD (1.095±0.022 vs 0.946±0.012, p<0.001), TBS (1.28±0.01 vs 1.23±0.01, p<0.001) than women. Weighted overall prevalence of osteoporosis was 11.3±1.8%, having degraded microarchitecture (TBS<1.2) was 29.7±2.8%, and women had a higher prevalence of both than men. Hepatic steatosis (61.3±3.2%), obesity (50.2±3.5%), T2D (34.9±3.0%), MetS (43.6±3.4%) and MASLD (52.3±3.4%) were high in our sample, but the prevalence of each was not significantly different between genders (p>0.05). Having MASLD was not significantly associated with either osteoporosis or degraded microarchitecture in men. In women, MASLD was associated with lower odds of having osteoporosis (adjOR=0.31, 95%CI:0.14-0.68) but higher odds of having degraded microarchitecture (adjOR=2.13, 1.11-4.06) than men. Likewise, hepatic steatosis alone showed similar associations with osteoporosis and degraded microarchitecture regardless of gender.

There is a high prevalence of osteoporosis, poor bone quality, and MASLD among MA. Paradoxical relationships of MASLD with TBS and BMD in women need further investigation to explore determinants of MASLD by gender in this cohort that may help target intervention accordingly.

P-087 Kimberly Denman

Ablation of Discoidin Domain Receptor 1 (Ddr1) Alters Collagen and Mineral in Murine Bone Matrix

Kimberly Denman*1, Angela Blissett1, Christina Zachariadou2, Beth S. Lee1, Joseph Orgel3, James John Cray2, Ed Calomeni1, Brian Lee Foster1 and Gunjan Agarwal1
(1) The Ohio State University, Columbus, OH, USA, (2) The Ohio State University, USA, (3) Illinois Tech, USA

Purpose: Age related bone diseases, such as osteoporosis, are the cause of millions of fragility fractures each year. Most bone loss during aging is caused by dysregulation of bone remodeling. Bone remodeling is a dynamic process where osteoclasts resorb old bone material and osteoblasts deposit new bone material. These two steps must remain balanced for bone to remain in homeostasis. Discoidin domain receptor 1 (DDR1) is a receptor tyrosine kinase which binds to collagen and has been shown to be important for bone development. Previous studies have elucidated how the deficiency of DDR1 in osteoblasts leads to shorter bones with reduced microarchitectural features. In our recent study we elucidated how DDR1, modulates age related bone remodeling in an osteoclast dependent manner. In particular, lack of DDR1 impaired osteoclast count in murine femurs in-vitro osteoclastogenesis and bone resorption. Since both cell proliferation as well as microarchitecture are dictated by the underlying matrix environment, in this study we are aiming to investigate how DDR1 affects the bone material quality.

Methods: DDR1 knockout (KO) mice and their wild-type (WT) counterparts were utilized to evaluate the collagen and mineral content in long bones. Femurs from 2-, 6- and 12-month-old female mice were analyzed by picrosirius red staining, transmission electron microscopy and X-ray diffraction (XRD) to examine collagen at the fiber, fibril and subfibrillar levels. Thermogravimetric analysis (TGA), inductively coupled plasma optical emission spectrometry (ICP-OES), and Raman spectroscopy was used to analyze the mineral composition.

Preliminary results: Our investigations have currently revealed that the DDR1 KO mice had increased amounts of immature collagen as compared to WT mice. The fibril diameter was enhanced in KO mice while the D-periodicity exhibited no change across genotypes. However, there were differences in the intensity profile in sub-fibrillar XRD studies, indicating a change in the content of the D-periods. Mineral analysis showed a higher mineral to matrix ratio and percentage of Ca for DDR1 KO femurs although the results were not statistically significant. Taken together, our results indicate how DDR1 modulates the underlying bone material quality which in turn could dictate both osteoblast and osteoclast proliferation as well as bone resorption.

P-088 Shilpa Shree Kuduva Ramesh Babu, DDS

Establishing Age-related Normative Bone Strength Data for C3 vertebra using Cone Beam Computed Tomography

Shilpa Shree Kuduva Ramesh Babu*1, Winnie Xu1, Dan Del Collo1, Denis Lattanzi1, Michael Chang1, Elaina Truong1, Sally Farhnam1, Lily Chen1, Min-Keun (Kevin) Song1, McKenna Sun1, Austin Dai1, Lihini Ranaweera1, Steven Wang2, Anh D Le2, David Casper3, Gregory Chang4 and Chamith S. Rajapakse1
(1) Departments of Radiology and Orthopaedic Surgery, Perelman School of Medicine, University of Pennsylvania, Philadelphia, PA, USA, (2) Department of Oral and Maxillofacial Surgery, University of Pennsylvania School of Dental Medicine, Philadelphia, PA, USA, (3) Department of Clinical Orthopaedic Surgery,Perelman School of Medicine, Philadelphia, PA, USA, (4) Division of Muskuloskeletal Imaging, NYU Langone, NYC, NY, USA

Background: Osteoporosis, a disease characterized by low bone mass and reduced bone strength, leads to an increased risk of fracture. There are numerous studies describing the age-related trends of bone mineral density (BMD). However, how bone strength changes with age has not yet been studied. Using cone beam computed tomography (CBCT) with a reduced radiation dose, we aimed to assess the bone strength of the C3 vertebral body of the cervical spine among a diverse female population.
Methodology: We performed a cross-sectional, retrospective study. Ten female CBCT DICOM files from each decade of the age group of 11–100 years were randomly selected (n = 90). CBCT scans of patients with impaired bone metabolism, vitamin D deficiency, breastfeeding, pregnancy, steroid use, or smoking were excluded. BoneHealth software (Precision Radiomics, University of Pennsylvania, and NYU), a finite element analysis tool, was used to estimate the Hounsfield Unit (HU), BMD, and bone strength of the trabecular part of the C3 vertebral body of the cervical spine. Two standard deviations (SD) above and below the mean bone strength were determined and correlated with age to establish the bone strength percentiles across the population.
Results: There was a highly significant negative correlation between females' C3 cervical spine bone strength and age ($p<0.001$, $r = -0.62$). The bone strength, BMD, and HU peaked in the 21–30 years age group, with a mean ± SD of 1.69 ± 0.33 GPa, 97.5 ± 0.31 mg/cm³, and 311.3 ± 0.29, respectively. There was a significant reduction in bone strength, BMD, and HU by the mean age of 54.6 ± 2.5 years ($p<0.001$), with a mean ± SD of 1.26 ± 0.25 GPa, 76 ± 0.22 mg/cm³, and 242.2 ± 0.25, respectively. Around the age of menopause (~50 years), the bone strength at the 99th, 75th, 50th, 25th, and 1st percentiles were 2.25 GPa, 1.6 GPa, 1.48 GPa, 1.18 GPa, and 0.59 GPa, respectively. (Figure)
Conclusion: This is the first kind of study in the literature to establish bone strength evaluation and its normative data using a low radiation dose, and easily accessible imaging modality, CBCT. These study results further warrant comparison with the standard of care, the DXA modality, for achieving the diagnostic cutoffs for osteopenia and osteoporosis through CBCT.

P-088 Shilpa Shree Kuduva Ramesh Babu, DDS

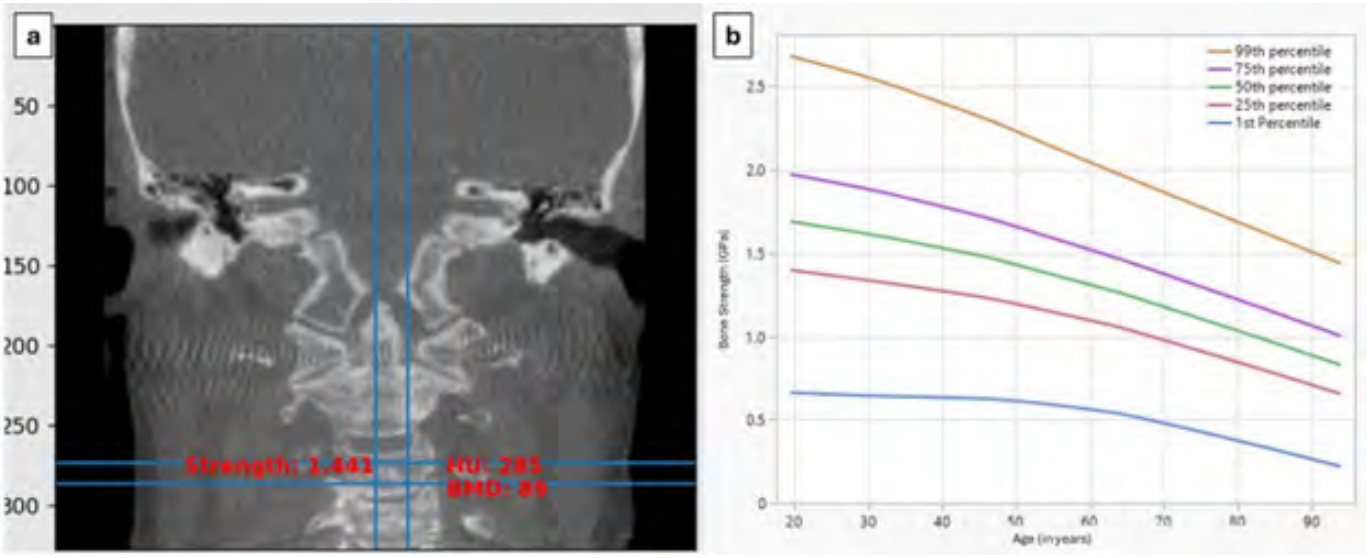

Figure: (a) Region of interest selection in the trabecula of C3 vertebra in coronal slice of CBCT scan and the simultaneous HU, BMD and Strength assessment in the BoneHealth Software (b) Bone Strength percentile (smoothened) graph among females 11-100 years.

P-089 Jing Zhang, PhD

Exploring collagen mineralization by liquid-phase transmission electron microscopy

J. Zhang1, L.-A. DiCecco1, R. X. Gao2, , E. D. Sone2,3,4, K. Grandfield1
(1) Department of Materials Science and Engineering, McMaster University, Hamilton, ON, Canada, (2) Institute of Biomedical Engineering, University of Toronto, Toronto, ON, Canada, (3) Faculty of Dentistry, University of Toronto, Toronto, ON, Canada, (4) Materials Science and Engineering, University of Toronto, Toronto, ON, Canada

Over the last several years, significant progress has been made toward understanding the mechanisms involved in the mineralization of hard collagenous tissues, such as bone. In native mineralization, hydroxyapatite minerals are formed within the collagen fibrils and are aligned with the fibril long axis.1 Although several in vitro models have been developed to mimic collagen biomineralization, the details of the mechanism of intrafibrillar collagen mineralization are still unknown. The emergence of in situ characterization methods, such as liquid-phase transmission electron microscopy (LP-TEM), provides the possibility to dynamically study the mechanisms behind collagen mineralization and in the future used elemental analysis to quantify mineralization. Recent research from our group has demonstrated a facile method for visualizing various stages of collagen mineralization in LP-TEM.2 However, this method fails to capture the dynamic formation mechanisms of calcium phosphate (CaP) precursors and their subsequent transformation into oriented crystals of HAP within the collagen fibrils.
In this work, a Poseidon Select holder (Protochips, Inc.) was used for fluidic LP-TEM with a Talos 200X (Thermo Fisher Scientific) TEM. It is imperative to note that collagen fibrils, being a biological material and matrix polymer, are sensitive to the electron beam. Similarly, CaP minerals, composed of lighter elements, are also beam sensitive. These factors render in situ repeatability exceptionally challenging, with beam-induced instability leading to observable signs of degradation within short timeframes. To circumvent this issue, several approaches were explored. First, a very thin layer (3-5 nm) of carbon sputtered on the liquid enclousure was used to mitigate some of the beam-induced radicals (Fig. 1A). In this experiment, we successfully observed nano-sized spherical amorphous CaP particles agglomerating to form a large agglomerate, with minimal beam-induced products formed observed at low-electron beam doses (Fig. 1B). However, despite this precaution, in situ observation of long-term collagen mineralization reactions
was impeded by electron beam irradiation, which still led to severe damage to our collagen fibrils over time (Fig. 1C). To address these challenges, further experiments will explore the introduction of graphene as an additional scavenger for reactive radical species to effectively neutralize them within our solution. Through these endeavours, we aim to optimize collagen mineralization and dynamic imaging within liquid cells, thereby enhancing the repeatability and potential for quantification of LP-TEM studies.

[1] M. J. Olszta, “Bone structure and formation: A new perspective”, Materials Science and Engineering: R: Reports, vol. 58, no. 3–5, pp. 77–116, 2007.
[2] L. DiCecco, R. Gao, J.L. Gray, D.F. Kelly, E. D. Sone, and K, Grandfield, Liquid Transmission Electron Microscopy for Probing Collagen Biomineralization, Nano Letters, vol. 23, no. 21, pp. 9760-9768, 2023.
[3] S. Merkens, G. D. Salvo, J. Kruse, E. Modin, C. Tollan, M. Grzelczak, and A. Chuvilin, Quantification of reagent mixing in liquid flow cells for Liquid Phase-TEM, Ultramicroscopy, vol. 245, no. 0304-3991, pp. 113654, 2023

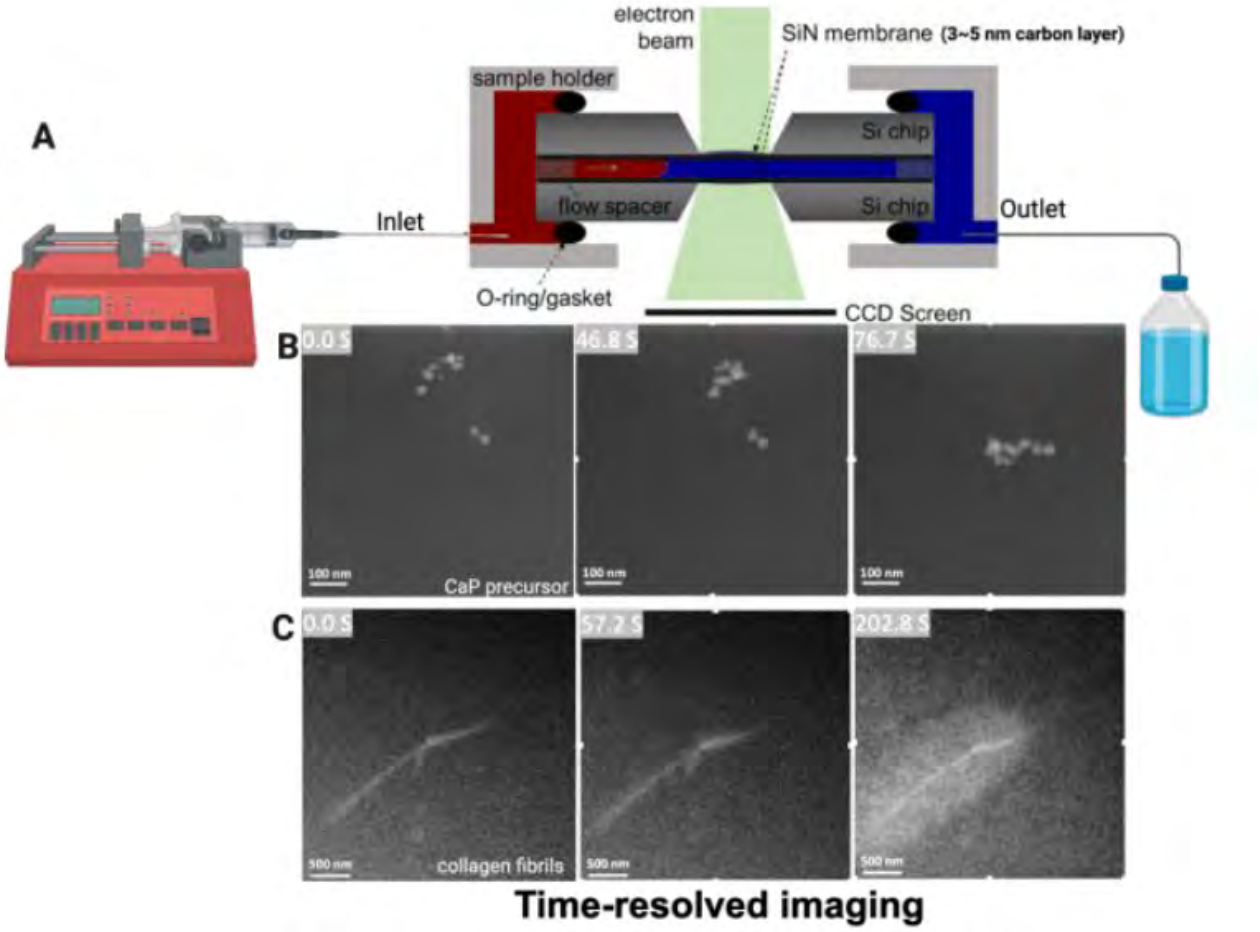

Figure 1. Overview of fluidic LP-TEM enclosures used to capture mineralization dynamics. (A) Schematic representation of LP-TEM flow system3 (created with Biorender.com). (B) In situ time-resolved liquid STEM imaging of dynamic hydrated CaP precursor agglomerates. (C) In situ time-resolved liquid STEM imaging of beam-dose related damage of hydrated collagen fibrils.

P-090 Farzin Takyar, MD, PhD

Differential Effect of High Versus Moderate Intensity Statin Therapy on Bone Density: A Substudy of a Randomized Controlled Trial

Farzin M. Takyar 1, Paolo Raggi2, Varuna Gadiyaram3, Chao Zhang4 5, Arthur E. Stillman3, and Amir H Davarpanah3

(1) Endocrine Research Center, Research Institute for Endocrine Sciences, Tehran-Iran, (2) Division of Cardiology, Department of Medicine, University of Alberta, Edmonton, Alberta, Canad(3) -Department of Radiology and Imaging Sciences, Emory University School of Medicine, Atlanta, Georgia-USA, (4) Pediatric Biostatistics Core, Department of Pediatrics, Emory University School of Medicine, Atlanta, Georgia-USA, (5) Present affiliation: General Dynamics Information Technology, Falls Church, VA.

Statins reduce cardiovascular events and may improve bone mineral density (BMD). We conducted a sub-analysis of a randomized trial that investigated the differential effect of moderate vs intensive low-density lipoprotein cholesterol (LDL-C) lowering therapy on coronary artery calcium (CAC) scores and used acquired imaging data as an opportunistic radiology source to assess how this intervention affected radiological bone attenuation loss as a marker of bone loss in thoracic vertebrae. Baseline and 12-month unenhanced chest CT scans were performed in 420 hyperlipidemic, postmenopausal women randomized in the Beyond Endorsed Lipid Lowering with Electron Beam Tomography Scanning (BELLES) trial to atorvastatin (ATV) 80 mg/day or pravastatin (PRV) 40 mg/day. Radiological bone attenuation (abbreviate as BMD) in the vertebrae was measured and averaged over three consecutive thoracic spine vertebrae. There were no differences in baseline demographic and clinical characteristics between treatment arms. The median percent lowering (range) in LDL-C was significantly greater for the ATV than the PRV group [-53(-69 to 20)% vs -28(-55 to 74)%, p<0.001], although the CAC change was similar [12(-63 to 208)% vs 13(-75 to 358)%; p= 0.44]. At follow-up, the median bone attenuation loss was significantly greater in the PRV group compared to the ATV group [-2.6(-27 to 11)% vs 0(-11 to 25)%; p < 0.001]. The absolute bone attenuation loss in the PRV group was comparable to that of an untreated general population. In the entire cohort, the LDL-C and total cholesterol relative changes were negatively correlated with that of bone attenuation (P<0.01). In adjusted multivariable linear regression analyses, race and percent change in LDL-C were independent predictors of bone attenuation loss which can be a surrogate of BMD change, albeit not comprehensively proven so far. Age, body mass index, history of smoking, diabetes mellitus, hypertension, peripheral vascular disease, or hormone replacement therapy did not affect percent change in BMD. These findings support the hypothesis that there is an interaction between bone and cardiometabolic health and that intensive statin therapy has a beneficial effect on bone health.

P-091 Sami Alsabri

Role of DNA methylation on 15-Lipoxygenase-1 gene expression in osteoarthritis

Sami Alsabri*1, Mehdi Najar1, Gadid Guedi1, Frédéric Lavoie2, Detlev Grabs3, Julio Fernandes4, Jean-Pierre Pelletier1, Johanne Martel-Pelletier5, Mohamed Benderdour4 and Hassan Fahmi1
(1) Osteoarthritis Research Unit Centre de Recherche du Centre Hospitalier de l'Université de Montréal (CRCHUM), Montreal, QC, Canada, (2) Departement of Orthopedic Surgery, Centre Hospitalier de L'Université de Montréal (CHUM), Montréal, Québec, Canada., Montreal, QC, Canada, (3) Department of anatomy, Research Unit in Clinical and Functional Anatomy, Université du Québec à Trois-Rivières, Trois-Rivières, QC, Canada, Trois-Rivières, QC, Canada, (4) Orthopedics Research Laboratory, Research Center, Hôpital du Sacré-Cœur de Montréal, Université de Montréal, Montréal, Québec, H4J 1C5, Canada, Montreal, QC, Canada, (5) Osteoarthritis Research Unit Centre de Recherche du Centre Hospitalier de l'Université de Montréal (CRCHUM), Montral, QC, Canada

Objective and design. Osteoarthritis (OA) is the most prevalent type of arthritis and a major contributor to physical impairment with a significant financial impact. OA. Pain, stiffness, and a restricted range of motion are the primary signs and symptoms of OA. Genetics, age, obesity, joint damage, and knee malalignment are risk factors for OA. Numerous anti-inflammatory and immunomodulatory lipid mediators are produced by 15-lipoxygenase-1 (15-LOX-1), which has been shown to have protective effects against a number of inflammatory diseases, including OA. The purpose of this study was to assess the expression of 15-LOX-1 in the cartilage of OA patients and normal donors, as well as to ascertain whether DNA methylation controls this expression.

Methods. Cartilage samples were collected from both OA-affected at the time of total knee replacement surgery, and normal knee joints during autopsy. Real-time polymerase chain reaction (PCR) was used to assess the expression of 15-LOX-1. Using 5-Aza-2'-desoxycytidine (5-Aza-dC), a DNA methyltransferase inhibitor, the significance of DNA methylation in 15-LOX-1 expression was evaluated. Using a CpG-free luciferase vector, the impact of CpG methylation on the activity of the 15-LOX-1 promoter was assessed. Pyrosequencing was used to ascertain the 15-LOX-1 promoter's DNA methylation status.

Results. Compared to healthy cartilage, OA showed increased expression of 15-LOX-1. 15-LOX-1 mRNA levels were upregulated in chondrocytes treated with 5-Aza-dc, and 15-LOX-1 promoter activity was downregulated in vitro through methylation. The methylation status of the 15-LOX-1 gene promoter did not differ between cartilage from normal and OA cartilage.
Conclusion. In OA cartilage, there was an increased expression level of 15-LOX-1, which might be related to a healing process. The methylation status of 15-LOX-1's promoter was not linked to its upregulation in OA cartilage, indicating that alternative mechanisms may be at play.

P-092 Sarah Ford

Bone formation by osteoid-osteocytes and osteocytes in C57Bl/6 mice

Sarah Ford*1, Kerstin Tiedemann 1, Katharina Jaehn-Rickert 2, Svetlana Komarova 1, Elizabeth Zimmermann 1
(1) Faculty of Dental Medicine and Oral Health Sciences, McGill University, (2)Department of Osteology and Biomechanics, University Medical Centre, Hamburg-Eppendorf

Purpose: Bone formation is described as occurring on bone surfaces by osteoblasts. However, as bone forming osteoblasts become entrapped in the bone matrix, these so-called osteoid-osteocytes may continue to produce bone matrix while differentiating into osteocytes [1]. Mature osteocytes deeply embedded in the bone have also been observed to remodel their surrounding bone matrix in lactation and hibernation: a process termed perilacunar remodeling [2]. The contribution of osteocyte-driven bone remodeling in the regulation of healthy bone tissue is currently unknown.

Methods: 26-week-old female C57Bl/6 mice (n=6) received two calcein injections at 10 and 3 days before euthanasia. Methylmethacrylate-embedded undecalcified L3-L5 vertebrae and femur sections were prepared. A region of interest (ROI) was identified in each section. The ROI in vertebrae consisted of trabecular bone and excluded growth plates. The ROI in femurs consisted of mid-diaphyseal cortical bone on anterior and posterior quadrants. Osteocyte lacunae with calcein labels were imaged using confocal microscopy (Leica SP8). Lacunae in or adjacent to the line of osteoblast bone formation were classified (Fig. 1) as osteoid-osteocytes, while lacunae >3 μm from a label marking osteoblast bone formation were classified as mature osteocytes. Bone formation rate at lacunae was measured by extending classic bone morphometry principles.

Results: Bone formation was observed at lacunae in trabecular (327 ± 122 # lacunae/mm2) and cortical bone (351 ± 156 # lacunae/mm2). Of the lacunae with bone formation in trabecular bone, 32% are associated with mature osteocyte lacunae and 68% with osteoid-osteocyte lacunae. Whereas in cortical bone, 87% of lacunae with bone formation are associated with mature osteocyte lacunae and 13% with osteoid-osteocyte lacunae. The osteoblast BFR was 0.60 ± 0.080 μm/day and 0.84 ± 0.80 μm/day for trabecular and cortical bone, respectively. The BFR associated with bone forming mature osteocytes is estimated to be 0.0027 ± 0.0010 μm/day and 0.021 ± 0.0078 μm/day for trabecular and cortical bone, respectively.

Conclusion: Here, we observed that a majority of vertebral bone formation at lacunae occurs at osteoid-osteocytes, which should be distinguished from mature osteocytes. Whereas in cortical bone, the majority of bone formation at lacunae occurs at mature osteocytes. The BFR due to osteocyte activity may seem small, but perilacunar remodeling is an emerging phenomenon for which the spatially dependent implications on bone quality and bone fragility are not fully understood.

References:
1. C. Palumbo, et al. Cells Tissues Organs. 137:350–358, 1990.
2. K.Jähn-Rickert & E.A. Zimmermann, Curr. Osteoporos. Rep. 19:391–402, 2021.

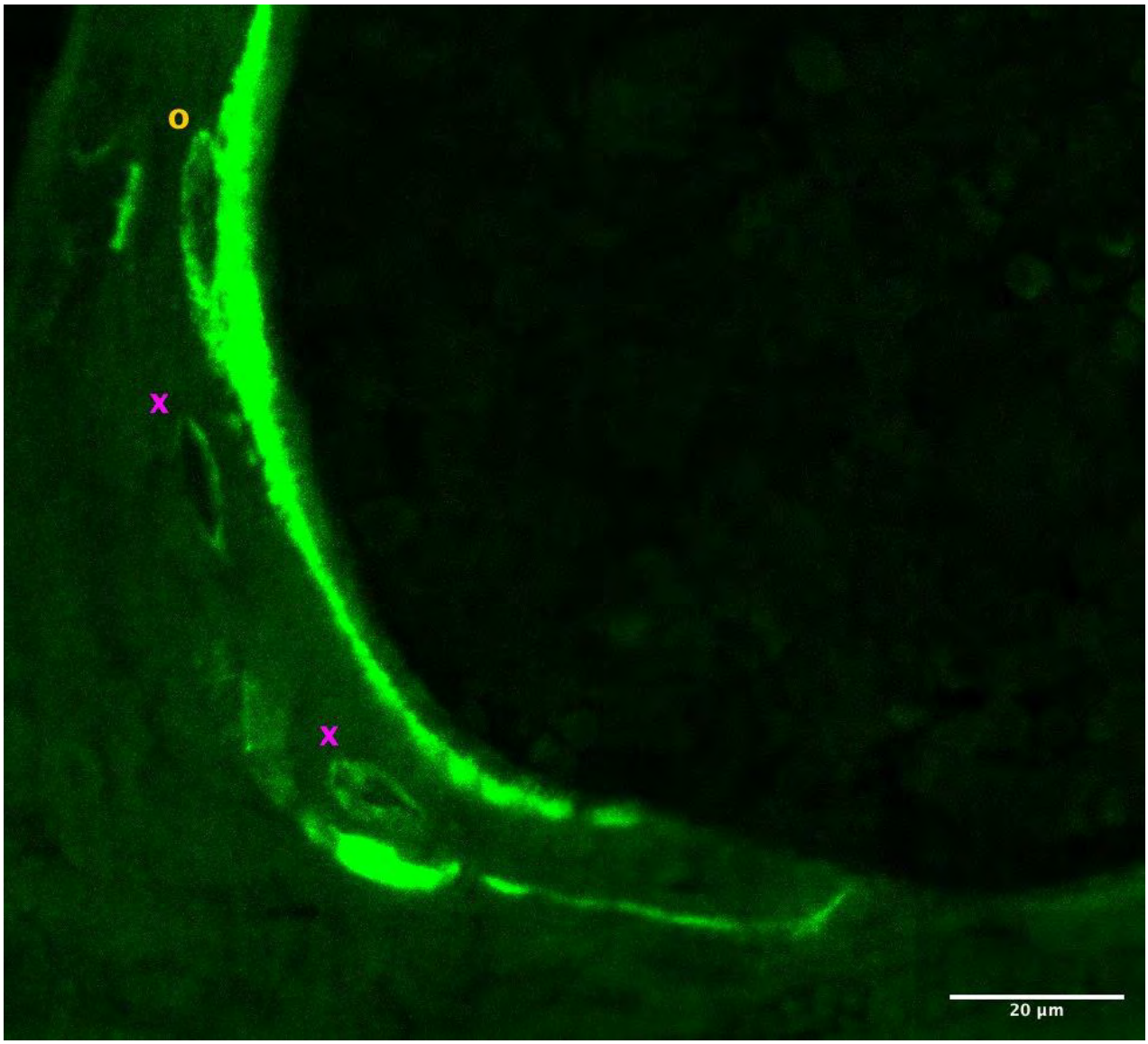

Fig. 1: Confocal visualization of the bone formation at bone forming osteocytes (pink ‘x’) and osteoid-osteocytes (orange ‘o’).

P-093 Rachana Vaidya, PhD

Impact Microindentation Accurately Predicts Hip and Wrist Fracture Susceptibility in Aging Females

Rachana Vaidya*1, Babak Jahani2, James Jin2, Christian Gonzalez3 and Simon Yue-Cheong Tang4
(1) Washington University In St.Louis, St.Louis, MO, USA, (2) Washington University in St.Louis, St Louis, MO, USA, (3) Washington University in St Louis, St.Louis, MO, USA, (4)USA, St Louis, MO, USA

Introduction: Post-menopausal women experience a significant incidence of fractures, two-thirds of which occur in those without osteoporosis, as determined by Dual-energy X-ray absorptiometry (DXA)(Ruiz-Esteves, 2022). While bone mineral density (BMD) is used to diagnose osteoporosis and evaluate fracture risk, it does not account for the tissue level material properties that contribute to bone strength (El Miedany, 2022). Impact microindentation (IMI) evaluates bone quality and can be a surrogate of bone fracture toughness (Jahani, 2024). We thus hypothesized that IMI is independently associated with bone strength and can accurately predict individual susceptibility to fractures.

Methods: We obtained 67 femurs, 65 radii, and 67 tibiae from elderly female cadavers (71±13yo). DXA was used for the BMD T-scores of the hip. IMI was performed at the FDA approved site, tibia mid-diaphysis. The femurs and radii were mechanically loaded in fall configurations to measure the ultimate fracture forces (FFracture). We calculated the individuals' impact forces on the hip (Kroonenberg, 1995) and wrist (Chiu, 1998) using a 2-link jack-knife model during a sideways fall (FFall) considering factors such as their respective body weights and body mass indices. An individual was considered susceptible to fracture when their impact force during fall was equal or greater than their ultimate fracture force i.e FFall ≥ FFracture. Receiver Operating Characteristic (ROC) curves were constructed to assess the predictive accuracy of IMI and DXA in identifying individuals susceptible to fractures. Stepwise Multivariate regression was used to assess relationships between bone strength and T-scores and/or IMI.

Results: Tibia IMI accurately predicted femur fracture susceptibility (AUC=0.75, $p<0.05$) but hip T-score did not (AUC=NS) (FigA.1). Both Tibia IMI (AUC=0.77, $p<0.01$) and hip T-scores (AUC=0.78, $p<0.01$) accurately predicted wrist fracture susceptibility (Fig B.1). Both Tibia IMI and hip T-scores were strongly correlated to bone strength at the femur and radius. Multivariate regression shows incorporating IMI measurement along with BMD improves prediction of bone strength at both femur and radius (FigA.2,B.2).

Significance/Conclusion: Our study is the first to directly address the predictive accuracy of IMI towards fracture susceptibility. Tibia IMI significantly correlates with bone strength at both the hip and wrist, and it accurately predicts fracture susceptibility in aging female cadavers. Cadaver studies facilitate the direct measurement of bone strength, allowing for comparisons across various clinically relevant modalities. While the circumstances that lead to a fracture event are complex, the findings here suggest that IMI can accurately identify individuals susceptible to fractures.

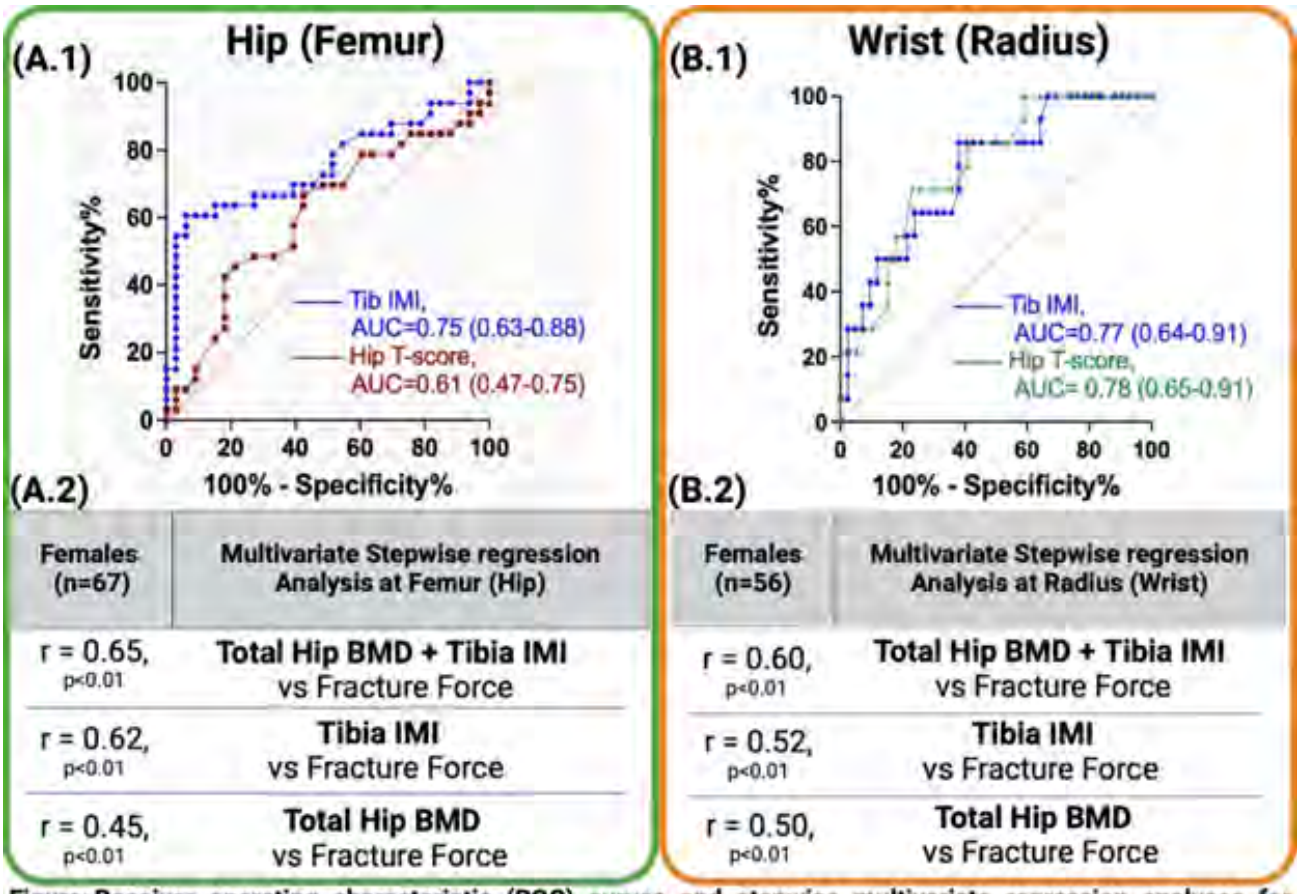

(A.2)

Females (n=67)	Multivariate Stepwise regression Analysis at Femur (Hip)
r = 0.65, p<0.01	**Total Hip BMD + Tibia IMI** vs Fracture Force
r = 0.62, p<0.01	**Tibia IMI** vs Fracture Force
r = 0.45, p<0.01	**Total Hip BMD** vs Fracture Force

(B.2)

Females (n=56)	Multivariate Stepwise regression Analysis at Radius (Wrist)
r = 0.60, p<0.01	**Total Hip BMD + Tibia IMI** vs Fracture Force
r = 0.52, p<0.01	**Tibia IMI** vs Fracture Force
r = 0.50, p<0.01	**Total Hip BMD** vs Fracture Force

Figure: Receiver operating characteristic (ROC) curves and stepwise multivariate regression analyses for fracture susceptibility. (A.1) Depicts ROC curve for the hip (femur) indicating that Tibia Impact Microindentation (IMI) has a higher accuracy than Hip T-scores in predicting fracture susceptibility during a sideways fall. **(A.2)** Presents a stepwise multivariate regression analysis table showing the correlation coefficients for femur fracture force as the dependent variable and Tibia IMI and Total Hip Bone Mineral Density (BMD) as independent variables. **(B.1)** Depicts the ROC curve for the wrist (radius), showing Tibia IMI and Hip T-score as accurate predictors of fracture susceptibility during sideways fall with an outstretched hand. **(B.2)** Displays a stepwise multivariate regression analysis table with the radius fracture force as the dependent variable, and Tibia IMI and Total Hip BMD as independent variables.

P-094 Patricia Clark, MD, PhD

Effect Of Tibolone On Cortical and Trabecular Bone In Postmenopausal Women Compared With Estrogen Therapy

Griselda-Adriana Cruz-Priego1, Patricia Clark*1, Miguel-Angel Guagnelli2, Ludovic Humbert3, Sergio Ortiz-Santiago2, Lizeth Castrejón-Delgado4 and Martha A Sánchez-Rodriguez4,
(1) Hospital Infantil de México Federico Gómez - Universidad Nacional Autónoma de México, Mexico City, DF, Mexico, (2) Hospital Infantil de México Federico Gómez - Universidad Nacional Autónoma de México, DF, Mexico, (3) 3D-Shaper Medical, Barcelona, Spain, (4)Facultad de Estudios Superiores Zaragoza UNAM, DF, Mexico

Objectives: To evaluate the effect of therapy with 2.5 mg/d of tibolone compared to 0.625 mg/d of estrogen and placebo on cortical and trabecular bone in postmenopausal women, at 6 and 12 months of treatment.

Methodology: Randomized controlled clinical trial in postmenopausal women from Mexico City.
3 groups were formed: A. Tibolone 2.5 mg/day of tibolone, B. Conjugated estrogens 0.625mg/day5mg/10d of medroxyprogesterone and C. Placebo.
Hip BMD was measured at 6 and 12 months. For measurements of the cortical and trabecular bone, 3D modeling based on DXA (3D-SHAPER v2.10.1, Galgo Medical, Spain) was performed. Cortical 3D-DXA measurements included cortical vBMD, cortical thickness and its cortical surface BMD product, as well as trabecular and trabecular vBMD. Comparisons were made between groups in the different measurements.

Results: In the tibolone group there were 22 patients, 27 with estrogens and 22 in the placebo group. There were changes in hip aBMD with increases of 0.34% for the tibolone group and a decrease of 0.47% and 0.31% for the estrogen and placebo groups respectively at 6 months of intervention. Comprehensive vBMD increased in the tibolone and estrogen group (0.77% and 0.11%, respectively), while it decreased 1.04% in control. Trabecular vBMD increased in the tibolone and estrogen group (1.51% and 0.65% respectively), but decreased 1.5% in the placebo. Cortical thickness increased 1.69% in the tibolone group, the estrogen group decreased 2.17%, while the placebo group decreased 2.75%.
3D modeling using DXA images provides a unique opportunity to review 2D-DXA data to predict whether changes in DXA aBMD were driven by effects in the trabecular or cortical compartments. The results show the trend of increase or decrease of the different parameters in both compartments, with a greater change in the group that received tibolone. The results are consistent with the literature where it is said that it can be used as an alternative to hormonal therapy with similar results in BMD and with fewer adverse effects.

Conclusions: The findings suggest that therapy with 2.5 mg/day of tibolone presents a tendency to growth in the different parameters, reaching increases of 2% in the 6-month follow-up. It can be expected that at 12 months this increase in values will be more marked in the group that received doses of tibolone.

P-095 MD Selim Reza, PhD

A Multi-Task Learning Framework Discovers Potential Drug-Repurposing Targets for Sarcopenia

Md Selim Reza*, Kuan-Jui Su, Anqi Liu, Xiao Zhang, Yun Gong, Zhe Luo, Qing Tian, Chuan Qiu, Hui Shen and Hong-Wen Deng, Tulane Center for Biomedical Informatics and Genomics, Deming Department of Medicine, School of Medicine, Tulane University, New Orleans, LA, USA

Recent advancements in deep learning methods identified numerous potential genes associated with sarcopenia. However, despite these developments, the successful identification of high-confidence, druggable targets for developing new therapies for sarcopenia using deep learning techniques and multi-omics data has remained elusive. To address this challenge, we developed a novel approach called attention-aware multi-task learning (MTA-MO), which can integrate multi-omics data to accurately identify drug targets and discover new therapies. This approach integrates multi-omics data, including transcriptome, methylome, and genome, from individuals (n=1010) aged 20-50, as well as human protein-protein interaction networks, drug-target networks, and absorption, distribution, metabolism, excretion, and toxicity (ADMET) properties. Based on our method, we identified 639 gene targets for sarcopenia. Among those gene targets, we identified seven potential genes associated with sarcopenia, including ESR1, ATM, CDC42, EP300, PIK3CA, EGF, and PTK2B, through the network analyses. The validation of these results was extended by utilizing diverse levels of pathobiological evidence associated with sarcopenia. The Gene Ontology enrichment analysis revealed some important functions such as ‘positive regulation of cell migration’, ‘epidermal growth factor receptor signaling pathway’, ‘apoptotic process’, ‘cellular response to lipid’, and ‘regulation of actin cytoskeleton organization’ that were significantly associated with skeletal muscle. The interaction network analysis identified three transcriptional factors (TFs) as the key transcriptional regulators of seven potential genes. Furthermore, our computational analysis also indicated that canagliflozin could be a beneficial therapy for sarcopenia, consistent with other research highlighting canagliflozin’s positive effects on muscle function. Canagliflozin exhibited a high inhibition constant of 6.97 μM with the PTK2B target protein, complied with drug-likeness rules, and demonstrated high human intestinal absorption (98.46%). Last, the MTA-MO method enables the integration of multi-omics data to identify genes related to lean mass and suggests that canagliflozin could be a promising therapeutic option for addressing sarcopenia.

P-096 Yi-An Hsieh, MS

A Deep Learning Pipeline for Bullet Fragment Detection in Gunshot Wound Patients for Enhanced Orthopaedic Assessment in Emergency Care

Yi-An Hsieh*1, Rashad Madi2, Winnie Xu2, Min-Keun (Kevin) Song2, Enrie Gan3, Yuanyuan Chen4, Elena Taratuta5, Jeremy Cannon6, Kristen Chreiman6, Hannah Rosenblatt3, Rasleen Grewal5, Christiana Cottrell5 and Chamith S. Rajapakse5,
(1) Department of Bioengineering, School of Engineering and Applied Sciences, University of Pennsylvania, Philadelphia, PA, USA, (2) Departments of Radiology and Orthopaedic Surgery, Perelman School of Medicine, University of Pennsylvania, Philadelphia, PA, USA, (3) Perelman School of Medicine, Philadelphia, PA, USA, (4) Boston University, Boston, MA, USA, (5)Department of Radiology, Perelman School of Medicine, University of Pennsylvania, Philadelphia, PA, USA, (6) Department of Surgery, Division of Trauma, Surgical Critical Care and Emergency Surgery, Perelman School of Medicine, University of Pennsylvania, Philadelphia, PA, USA

Introduction: Gun violence is a public health issue in the United States, with over 48,000 deaths per year from related injuries[1]. For patients with gunshot wounds (GSW), computed tomography (CT) scans are crucial for identifying injuries sustained from ballistic trauma, including solid organ injuries, acute hemorrhage, penetrating fractures, and retained bullet fragments. However, a rapid assessment of multiple GSWs in emergency settings is clinically difficult and risks treatment delays and complications. This work aims to build and assess the capabilities of machine learning pipelines to identify bullet fragments in CT scans quickly, accurately, and precisely for orthopaedic surgical planning.

Methods: Using CT scout view images and manual annotations from 1335 patients treated for GSW injuries at Penn Medicine, an urban Level 1 trauma center, from 2019 to 2022, three pipelines built upon pre-existing architectures were trained for bullet detection and segmentation (Figure 1). Pipeline 1 employed a Mask R-CNN model [2] trained on bullet fragment annotations to detect and segment bullet fragments. Pipeline 2 employed a Mask R-CNN [2] model trained on high-density annotations to detect high-density regions of interest (ROIs) then classify and segment bullet fragments. Pipeline 3 used a Faster R-CNN model [3] to detect high-density ROIs, two ResNet50 models [4] to classify images as coronal or sagittal and determine if they contain the patient's head, three ResNet50 models [4] to classify ROIs as bullet fragments, and a FCN model [5] for segmentation
.
Results & Conclusions: Pipeline 3 identified the most bullet fragments at 89-91% prediction intersection of bullet annotations across varying non-maximum suppression intersection over union thresholds (76-79% for pipeline 1, 62-66% for pipeline 2), yielded 88-91% accuracy in ROI classification (63%-71% for pipeline 1, 48-59% for pipeline 2), and also provided the greatest overlap of predicted masks and annotations with a Dice coefficient of 0.488 (0.336 for pipeline 1, 0.247 for pipeline 2). Intermediate models in pipeline 3 classified images as coronal vs sagittal with 98.8% accuracy and containing the head or not with 99.3% accuracy. Further fine-tuning could enhance bullet fragment detection, potentially matching the performance of radiologists and facilitating the calculation of additional metrics, such as bullet movement over time relative to major arteries, to improve clinical decision-making and expedite treatment in orthopaedic settings.

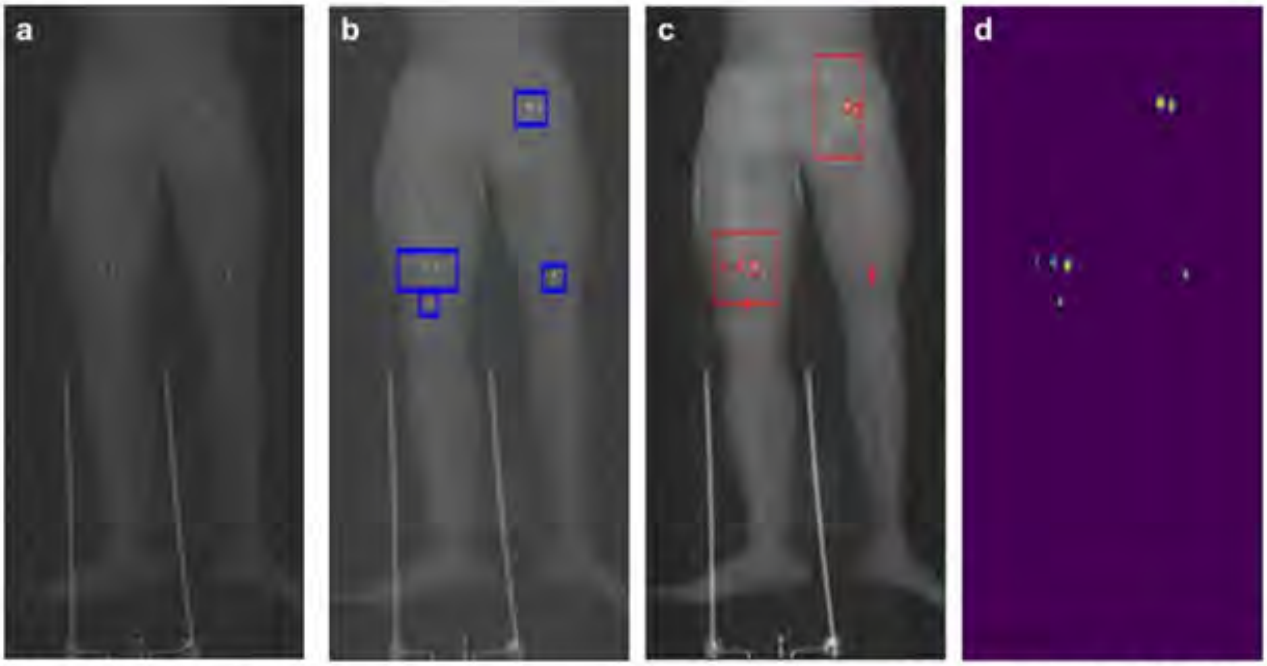

Figure 1. Bullet fragment detection and segmentation. a) The CT scout view image on the left is the original image. b) In the normalized image in the left center, the blue boxes are the ground truth manual annotation. c) In the preprocessed image in the right center, the red boxes are the bounding boxes predicted by the model. d) The segmentation mask contains bullet fragments predicted by the model.

P-097 Naoki Tsuji, PhD

Functional Bone Organoids Unveil Osteoblast-Driven Engulfment of Apoptotic Osteoclasts as a Key Contributor to Bone Remodeling

Naoki Tsuji* and Atsuhiko Hikita, The University of Tokyo, Japan

Introduction: Bone remodeling is regulated by cell-cell interactions within the basic multicellular unit (BMU) over periods ranging from weeks to months. The analysis of intercellular interactions over extended periods using traditional histological analyses and in vivo imaging is challenging. Our group has developed functional bone organoids (FBOs) that mimic BMU structures and allow observation of bone resorption by osteoclasts and the subsequent refilling of the resorption pits by osteoblasts. Osteoclasts within the BMU undergo apoptosis after bone resorption, and resulting apoptotic bodies (ABs) have shown to stimulate osteogenic differentiation of mesenchymal stem cells. However, the roles of osteoclast apoptosis on bone remodeling have not been examined in a cellular level. This study utilized the FBO to analyze the effects of inhibition of osteoclast apoptosis on osteoblasts and matrix in the bone remodeling microenvironment.

Methods: Primary osteoblasts isolated from CAG-EGFP mice were cultured in osteogenic media to form bone nodules. 1. To determine the effect of osteoclast-derived ABs on differentiated osteoblasts, DiI-labeled ABs were added, and nodules were observed continuously over three weeks. 2. To examine the effects of inhibition of osteoclast apoptosis, FBOs were prepared as follows. The nodules were co-cultured with bone marrow macrophages from Cathepsin K or RANK cre; R26-tdTomato mice. During 2-week bone resorption phase and 3-week formation phase created by different culture conditions, the nodules were observed weekly using two-photon microscopy, which enabled label-free imaging of collagen fibers in the bone matrix. The caspase inhibitor Z-VAD was added to the culture media during the transition from resorption to formation.

Results: 1. During a continuous observation of differentiated osteoblasts, cellular movement were minimal in the untreated group. On the other hand, osteoblasts in the ABs-treated group showed a morphological change from spindle-shaped to spherical and increased motility. 2. In the untreated group, the resorption pits created by osteoclasts were filled with osteoblasts, and a strong correlation was observed between the amount of bone resorption and formation in these areas. Osteoclasts decreased by apoptosis as the process transitioned from resorption to formation, and osteoblasts in the pits contained tdTomato-positive particles from osteoclasts. On the other hand, inhibition of osteoclast apoptosis by Z-VAD resulted in the persistence of resorption pits which were refilled in the control group.

Conclusion: The findings of this study indicate that ABs are indispensable for the refilling of bone resorption pits by facilitating the reactivation of differentiated osteoblasts within the bone remodeling microenvironment, thereby contributing to the maintenance of bone homeostasis.

P-098 Eun Jung Lee, PhD

Enhancing the Responsiveness of Immune Checkpoint Inhibitors in Breast Cancer Through PTHrP Blockade

Eun Jung Lee*, A-ram Kang, Da Hyeon Yun and Serk in PARK, Korea University College of Medicine, Seoul, Korea, Republic of (South)

Immune checkpoint inhibitors (ICIs), such as anti-PD-1 and -CTLA-4 antibodies, are effective in many types of cancers, yet their efficacy on breast cancer is comparatively modest due to the immunouppressive ‘cold’ tumor microenvironment (TME). We have previously shown that parathyroid hormone-related peptide (PTHrP) from breast cancer contribute to the mobilization of myeloid-derived suppressor cells (MDSC) from the bone marrow via activation of osteoblasts, contributing to the immunosuppressive TME of breaset cancer. Accordingly, we hypothesized that blockade of PTHrP enhances the efficacy of ICI. We employed the CRISPR/Cas9 system to generate PTHrP knockout cell lines from 4T1 murine triple-negative breast cancer cells. After genotyping and Pthlh mRNA levels, we selected both heterozygous and homozygous PTHrP knockout 4T1 cell lines, which maintained the morphological characteristics and proliferation rates of the parental lines in vitro. In a subcutaneous tumor model, PTHrP knockout in 4T1 cells, previously non-responsive to PD-1 inhibitors, demonstrated a marked reduction in tumor growth following anti-PD-1 antibody treatment. Notably, tumor reduction was less significant in heterozygous knockdown cells compared to those with homozygous deletions. Furthermore, while the anti-PD-1 antibody did not significantly increase CD8-positive T cell counts in the TME of the 4T1 breast tumor model, the PTHrP knockout led to a decreased MDSC count and an increase in CD8-positive T cells within the TME. In conclusion, our study demonstrates that PTHrP plays a critical role in diminishing ICI efficacy in breast cancer by facilitating MDSC migration into the TME. Consequently, we propose a new therapeutic strategy involving integrating PTHrP neutralization with other chemotherapeutic agents in combination therapy, aiming to achieve greater treatment benefits for PTHrP-expressing cold tumors non-responsive to ICIs.

P-099 Kazette Yuen Yu Chan

Characterization of Two Novel KIF22 Variants and Their Association with A Rare Neonatal-Onset Disease

Kazette Yuen Yu Chan*1, Karina da Costa Silveira2, Jason Stumpff3, Denise Cavalcanti4 and Peter Kannu2,
(1) Unversity of Alberta, Edmonton, AB, Canada, (2) University of Alberta, Canada, (3) University of Vermont, USA, (4) Grupo de Displasias Esqueléticas, Brazil

Spondyloepimetaphyseal dysplasia with joint laxity type 2 (SEMDJL2) is a rare skeletal disease, characterized by short stature, generalized ligament laxity with multiple dislocations, slender fingers, and mild spinal deformity. There is currently no cure for SEMDJL2. Our mission is to elucidate disease mechanisms to facilitate accurate diagnoses, enabling informed management strategies and ultimately leading to better patient outcomes.
Heterozygous missense variants in exon 4 of the KIF22 genes, leading to substitutions of either amino acid 148 or 149, have been identified in most SEMDJL2 patients. KIF22 encodes a protein that is essential in cellular transport and division. It has been shown that KIF22 variants lead to failure in chromosome segregation in mitosis.
Our collaborator in Brazil and we have identified two patients with phenotypes resembling SEMDJL2. Molecular tests revealed a variant of uncertain significance (VUS) in KIF22 (p.(E222Q)) and in KIF22 (p.(P144T)), respectively. VUS is a genetic variant that has been identified in genetic tests, but its impact on the health of an organism is unknown. It hinders an accurate diagnosis and management plan.
Given that the two identified patients have SMEJDL2-like phenotypes, I hypothesize that the KIF22 (p.(P144T)) and KIF22 (p.(E222Q)) variants are likely pathogenic. Since the patient with the KIF22 (p.(E222Q)) variant has a more severe phenotype, I hypothesize a more detrimental impairment in chromosomal segregation in mitosis in the KIF22 (p.(E222Q)) cells than in the KIF22 (p.(P144T)) cells.
My first aim is to establish stable cell lines with the variants KIF22 (p.(P144T)) and KIF22 (p.(E222Q)). I have successfully engineered our two novel variants using a commercial mutagenesis kit into a cell line. The mutagenesis was verified with Sanger Sequencing.
My second aim is to observe and compare the chromosome segregation in mitosis between wild-type, known pathogenic variants and our two VUSs in KIF22. I will culture the cells that harbour our two novel variants, a known pathogenic variant and the wild type and stain the cells using a live cell marker for chromosomal segregation. I expect normal chromosome segregation in wild-type cells and various degrees of chromosomal segregation impairment in variant cells in proportion to the severity of the patients' phenotypes.
In summary, this project aims to further the understanding of a rare neonatal-onset disease, SEMDJL2, classifying two novel VUSs in the KIF22 gene. It presents a replicable cell-based approach to reclassify VUSs in diseases with similar defects in mitosis, such as Seckel syndrome. This contribution is significant as rare diseases often have limited evidence base due to small patient pools. Our project holds the potential to transform clinical care for patients while adding value to basic science.

P-100 Andrew Jayarajah

Clinical Impact of New AI Tool that Predicts Low Bone Mineral Density from X-Ray: Experience at Sunnybrook Health Sciences Centre

Andrew Nishanthan Jayarajah*1, Anastasia Oikonomou2 and Tanesha Thirukkumar2,
(1) Sunnybrook Health Sciences Centre, Markham, ON, Canada, (2) Sunnybrook Health Sciences Centre, Toronto, ON, Canada

Background: Osteoporosis leads to debilitating fractures. Early detection can improve treatment and reduce associated fractures and their healthcare costs. Fracture risk is assessed by clinical review of a patient's history and refined after a dual-energy x-ray absorptiometry (DXA) exam if warranted. However, screening rates are low. We aimed to investigate the clinical adoption and perceived value of an artificial intelligence (AI) tool called Rho that opportunistically identifies patients at risk for low bone mineral density (BMD) when they undergo an x-ray for any clinical indication.
Methods: Patients aged 50 years and above (n=1142) were prospectively recruited and included if they underwent an x-ray for any clinical indication of a body part eligible for Rho screening. Questionnaires were administered to patients at baseline and at the end of the study. Family physicians of patients flagged as at-risk for low BMD were asked to provide feedback on the AI-screening tool.

Results: Of 1142 patients screened, 589 were flagged by Rho as likely to have low BMD. Of these, 67% reported they had not previously discussed osteoporosis or fracture risk with their doctor prior to the study. We expected that when these results were included in the x-ray report, a family physician might conduct a clinical risk assessment, and a portion would subsequently be referred for DXA. Within 6 months of the AI screen, 187 underwent DXA. Positive predictive value (PPV) for low BMD was 87%, 19% had high fracture risk (FR) and 41% had moderate FR. The family physician survey yielded 51 responses; 78% agreed that Rho would be beneficial for patient care and 74% would use the information in their standard of care. Of patients who reported they had not discussed osteoporosis with their physician in the pre-study questionnaire, 29% had newly discussed osteoporosis with their physician by the post-study questionnaire, and 25% had newly prescribed osteoporosis medication.

Discussion: Rho can identify patients at risk of low BMD in a clinical setting. Radiologists incorporate the positive Rho results in their reports, and family physicians find these results useful for supporting the standard of care in osteoporosis management. Rho screening leads to additional DXA referrals. Opportunistic screening for low BMD with Rho has the potential to help address low screening rates for fracture risk and osteoporosis.

P-101 Kyra Hunsberger

The Relationship Between Age at Menarche and Osteoporosis: A Systematic Review and Meta-Analysis

Kyra Hunsberger*1, Sara Kisiel1, Alma Jukic1 and Elizabeth Hauser, MD2
(1) University of Arizona, College of Medicine - Phoenix, USA, (2) Department of Obstetrics and Gynecology, Riverside Community Hospital, USA

Objective: While literature has validated risk factors associated with osteoporosis, the specific effect of menstrual history could be better defined. The present study aims to evaluate the relationship between age at menarche and the development of osteoporosis.

Methods: This systematic review and meta-analysis was performed per the Preferred Reporting Items for Systematic Reviews and Meta-Analyses (PRISMA) 2020 guidelines. Literature was evaluated from three databases including PubMed, Cochrane, and Ovid. Each search consisted of MeSH terms: ((menarche) AND (osteoporosis)). There were 655 articles identified including randomized controlled trials, meta-analyses, systematic reviews, cohort studies, and case series. Inclusion criteria consisted of randomized controlled trials written in the English language between 1994-2024 assessing a statistical relationship between age at menarche and bone mineral density among postmenopausal women. A subset meta-analysis was performed using the random effects model of DerSimonian and Laird for studies with a correlation coefficient for menarcheal age and bone mineral density, evaluating the effect size. To obtain standardized effect sizes for each correlation coefficient, we applied Fisher's r-to-z transformation. Risk of bias and quality assessment were performed using the ROBINS-I and GRADE tools, respectively.

Results: Of the articles identified, three met inclusion criteria and were subsequently analyzed. A total of 3,223 postmenopausal women were included. All three studies (n=3,223) found that bone mineral density was negatively correlated with age at menarche on a statistically significant level ($p<0.05$). One study (n=217) also found that bone mineral density in the forearm, spine, neck, and Ward's triangle was significantly higher in subjects with early menarche ($p<0.05$), adjusted for age and years since menopause. A subset meta-analysis of two studies (n=3,006) found that bone mineral density and age at menarche had a correlation coefficient of -0.110 (95% confidence interval: -0.203, -0.015) (Figure 1). Between study variance ($\tau 2$) was 0.0027.

Conclusions: Age at menarche is negatively associated with bone mineral density. It is difficult to ascertain whether late menarche potentiates risks for bone health due to hormonal dynamics, or if confounding lifestyle factors exist. Despite these challenges, the findings of this study underscore the importance of considering menarcheal age as a potential risk factor in osteoporosis prevention and management strategies. Future longitudinal studies with large, diverse cohorts and standardized assessments of bone health are warranted to establish a clearer understanding of the impact of menstrual history on the development of osteoporosis. Studies should also evaluate the use of menarcheal age as a screening tool for osteoporosis prevention.

Grant Support From:
National Institutes of Health (USA) - R13-AR084338
Canadian Institutes of Health Research - CIHR PCS-190957
Co-sponsored by ASBMR and in affiliation with the ASBMR 2024 Annual Meeting

XVIth Congress of the International Society of Bone Morphometry
September 30th - October 3rd, 2024